Doctoral Dissertation

Synthesis of Large Area Bilayer-hybrid Gels and Exploration of Novel Functions

（大面積二分子膜ハイブリッドゲルの合成とその新機能探索）

Submitted By:

MUHAMMAD ILYAS

Submitted to Supervisor:

Professor Dr. Jian Ping GONG

Laboratory of Soft & Wet Matter (LSW),

Graduate School of Life Science, Hokkaido University

Sapporo 060-0810, Japan

March 2018

Contents

CHAPTER 1

General Introduction

1.1 Overview

Hydrogels, composed of three dimensional hydrophilic polymer strands swollen in large amount of water 50-99%, are novel soft and wet materials.[1] As a hybrid of solid and liquid constituents, hydrogels have a high permeability to water including small molecules and experience reversible volume change by intake and release of water and if functionalize response to a wide variety of stimuli, such as light, temperature, pH, ionic strength, chemical reactions.[2–6] The elasticity of hydrogels is because of polymer strands, that help compliant under applied mechanical force, and recovers its most probable original shape after the removal of applied mechanical force.[7]

Because of their soft and wet nature hydrogels are gaining tremendous attention in wide range of applicability as contact lenses, superabsorbent, microfluidic devices, tissue regeneration, ionic conductivity, muscle-like actuators, skin-like sensors, stretchable soft touchpad, stretchable electroluminescent displays, transparent triboelectric generators, and stretchable liquid crystal devices, and air stable gels as smart textile.[6,8–13] Beside numerous application conventional hydrogels are poor in mechanical properties that limited the scope of their applications. This stimulated efforts to discover tough hydrogels for artificial cartilages replacement, tissue adhesives, and soft robotics.[14–17] For that purpose tough hydrogels have been developed by researchers such as tetra-PEG gel, sliding ring gel, polymer-clay nanocomposite gel, polyampholyte gel, alginate-acrylamide gel and double network hydrogels, respectively.[18–23] Besides their improved mechanical properties they are amorphous in

structure and far beyond to mimic the real structure of natural biological system.[24–27] The precise design of biological system as hierarchical multifarious hybrid structures self-assembled from nano to macro length scales in large area provide diverse functions, are model systems are often difficult to achieve in synthetic soft and wet materials.

Therefore, creation of novel hydrogels with a flexible, dynamic hierarchical structure in similar to biological systems, and discovery of its unprecedented functions are among the most fundamental but challenging topics in the research of soft matter. The challenge is to acquire bonds that are both strong and reversible similar to variety of tough, biological materials. As biological system have well-defined hierarchy structure from molecular level to macroscopic scale arranged in large area. Inducing the long range ordered hierarchical structures in hydrogel to impart structural color in addition to toughness is important for wide range of application. The resultant hydrogels known as photonic hydrogels act as visual indicator to verities of stimuli. Some researcher developed a method to prepare color tuning soft matter such as photonic gel based on colloidal crystals, inverse opal, and photonic rubber sheet.[28–31] They have limited application due to irreversible color tuning and small dimension.

Amphiphilic molecules, which have both hydrophilic head group and hydrophobic tail, self-assemble in aqueous media into various hierarchical structures.[32] Inducing such hierarchical structure composed of amphiphilic molecules into amorphous hydrogels is a promising approach to meet the above-mentioned challenges. Recently, macro-scale bilayer hybrid hydrogels (PDGI/PAAm), based on amphiphilic polymer PDGI poly(dodecyl glyceryl itaconate), have been developed.[33] The gels exhibited excellent functions, such as structure color, high mechanical toughness, and stimuli responsive properties.[34–37] This promises great potential of the bilayer-based hydrogels for diversified application. Developing large area

bilayer-hybrid hydrogels with the supramolecular self-assembled structure is indispensable for these potential applications.

This thesis aims to establish a method to fabricate high quality bilayer-based hydrogels thin films and explore novel functions of bilayer-hybrid gels.

1.2 Outline of this dissertation

The research finding in this dissertation mainly emphases, first, on the synthesis and anisotropic functions of a hydrogel by developing method to induce large area several tens of centimeter scale supramolecular self-assembled macroscopic mono-domain bilayer structure inside in polyacrylamide polymer matrix. Furthermore, we report here the drying induced functions of bilayer-hybrid gels.

Chapter 2 is a review about the self-assembly approach of amphiphilic polymerizable surfactant DGI: dodecyl-glyceryl-itaconate. The unique iridescence phenomena as a result of self-assembled liquid crystalline lamellar phases in aqueous media, polymerization in polymer network, hybrid hydrogel of bilayer membrane and polymer network, and the limitations of the hybrid hydrogel with randomly aligned lamellar bilayer domains in different application.

In chapter 3, establish a method to fabricate high quality bilayer-based hydrogels thin films. The large area anisotropic hydrogel, macroscopic size ordered arrangement of lipid bilayer structure is developed. The synthesis is performed in a single step polymerization reaction of a precursor solution containing polymerizable amphiphilic surfactant dodecyl glyceryl itaconate along with acrylamide in presence of a cross-linker, initiator, and co-surfactant. Before polymerization, using automatic pump suction method and applying shear flow to the precursor solution, several thousands of bilayers of self-assembled DGI are aligned in one direction parallel to the substrate surface. By polymerization the bilayers self-assembled

periodically and fixed in the polyacrylamide network to give a mechanically strong bilayer hybrid hydrogel thin films PDGI/PAAm. The hybrid gel thin film showed ID swelling, beautiful structural color by satisfying the Bragg's law of diffraction of visible light on the bilayer normal. The color of the gel further can be selectively altered by writing and erasing with water that could guide the gel to be used as water based colorful display devices.

In chapter 4, the detailed investigation of the effect of water content, temperature, solvent, configuration of monomers, on the structure and properties of bilayer-hybrid gels are explored. It is concluded that by slowly reducing water content the layered microstructure is unperturbed, and ductile-brittle transition of the PAAm gel layers occurs at much higher water content (58 wt%) as compared to the water content (26 wt%) of bulk PAAm hydrogels. At this transition point, the thickness of PAAm gel layers is 52 nm, much higher than the reported literature of water confined at several nanometer length scale. Accompanied with such a transition, the free water in the lamellar gels disappeared. These results indicate the long-range ordering of water in the lamellar hydrogels, which is observed for the first time.

In co-solvent, the adaptive mechanical behavior of gels at various concentration is studied. Drying water from co-solvent produced air stable, soft, tough and stretchable ion gel based on bilayers. The hybrid gel synthesized by adding small amount of ionic liquid that perturb the structure of water shows self-healing. The ion gel exhibited an ultra-fast self-healing behavior due to multiple reversible interactions.

The hybrid-gels synthesized using amphiphilic racemic and chiral monomers significantly altered the packing of bilayers that showed different yielding criteria and deformation under mechanical test.

In chapter 5, we report the effect of different types of drying and functions related to drying of bilayer-hybrid gel thin film. It is found that by free air drying, the gel shows rainbow like patterning, uniform color stimulation, nacre mimetic iridescence metallic luster. Based on these results, beetle cuticle mimetic water-based rewritable photonic paper, micro patterning with butterfly wing mimetic iridescence, and jelly fish mimetic photoluminescence, are developed. These findings might open new way to create functional devices for various application.

In chapter 6, the solvent free fabrication of soft elastomers based on amphiphilic PDGI polymer is performed. As a result, the elastomer shows malleability by roll pressing, high birefringence, high stiffness and toughness. The elastomer is also useful to understand various properties of rigid bilayers.

In chapter 7, we successfully develop glucose-responsive photonic hydrogels. To induce the glucose responsibility, poly(3-acrylamidopheylboronic acid) is introduced in the photonic PDGI/PAAm gel. The obtained hydrogel reversibly changes color in response to glucose and small deformation. The photonic hydrogel has potential application as non-invasive visual glucose sensor.

In chapter 8, the concluding remarks are included based on the overall work.

1.3 References

[1] N. A. Peppas, B. V. Slaughter, M. A. Kanzelberger, In *Polymer Science: A Comprehensive Reference, 10 Volume Set*; Elsevier, 2012; Vol. 9, pp. 385–395.

[2] T. Boyaci, N. Orakdogen, *RSC Adv.* **2015**, *5*, 77235.

[3] C. Zhu, C. J. Bettinger, *Journal of Materials Chemistry B* **2014**, *2*, 1613.

[4] A. Fiumefreddo, M. Utz, *Macromolecules* **2010**, *43*, 5814.

[5] H. Zhou, Y. Wang, Z. Zheng, X. Ding, Y. Peng, *Chemical communications (Cambridge, England)* **2014**, *50*, 6372.

[6] L. D. Zarzar, J. Aizenberg, *Accounts of Chemical Research* **2014**, *47*, 530.

[7] T. Sakai, M. Kurakazu, Y. Akagi, M. Shibayama, U. Chung, *Soft Matter* **2012**, *8*, 2730.

[8] N. Efron, N. A. Brennan, K. A. O'Brien, P. J. Murphy, *Clinical and Experimental Optometry* **1986**, *69*, 219.

[9] D. Shi, Y. Gao, L. Sun, M. Chen, *Polymer Science Series A* **2014**, *56*, 275.

[10] D. Morales, E. Palleau, M. D. Dickey, O. D. Velev, **2014**, *10*, 1235.

[11] H.-H. Chou, A. Nguyen, A. Chortos, J. W. F. To, C. Lu, J. Mei, T. Kurosawa, W.-G. Bae, J. B.-H. Tok, Z. Bao, *Nature Communications* **2015**, *6*, 8011.

[12] C. Ohm, M. Brehmer, R. Zentel, Liquid crystalline elastomers as actuators and sensors. *Advanced Materials* **2010**, *22*, 3366–3387.

[13] N. Kameta, M. Masuda, T. Shimizu, *Chem. Commun.* **2015**, *51*, 6816.

[14] D. Rus, M. T. Tolley, Design, fabrication and control of soft robots. *Nature* **2015**, *521*, 467–475.

[15] C. K. Roy, H. L. Guo, T. L. Sun, A. Bin Ihsan, T. Kurokawa, M. Takahata, T. Nonoyama, T. Nakajima, J. P. Gong, *Advanced materials (Deerfield Beach, Fla.)* **2015**, *27*, 7344.

[16] M. Ogawa, N. Kitamura, T. Kurokawa, K. Arakaki, Y. Tanaka, J. P. Gong, K. Yasuda, *Journal of biomedical materials research. Part A* **2012**, *100*, 2244.

[17] J. Li, A. D. Celiz, J. Yang, Q. Yang, I. Wamala, W. Whyte, B. R. Seo, N. V. Vasilyev, J. J. Vlassak, Z. Suo, D. J. Mooney, *Science* **2017**, *357*, 378.

[18] T. L. Sun, T. Kurokawa, S. Kuroda, A. Bin Ihsan, T. Akasaki, K. Sato, M. A. Haque, T. Nakajima, J. P. Gong, *Nature Materials* **2013**, *12*, 932.

[19] K. Haraguchi, T. Takehisa, *Advanced Materials* **2002**, *14*, 1120.

[20] Y. Okumura, K. Ito, *Advanced Materials* **2001**, *13*, 485.

[21] J. P. Gong, Y. Katsuyama, T. Kurokawa, Y. Osada, *Advanced Materials* **2003**, *15*, 1155.

[22] T. Karino, M. Shibayama, K. Ito, *Physica B: Condensed Matter* **2006**, *385–386 I*, 692.

[23] J.-Y. Sun, X. Zhao, W. R. K. Illeperuma, O. Chaudhuri, K. H. Oh, D. J. Mooney, J. J. Vlassak, Z. Suo, Highly stretchable and tough hydrogels. *Nature* **2012**, *489*, 133–136.

[24] M. A. Meyers, P.-Y. Chen, A. Y.-M. Lin, Y. Seki, *Progress in Materials Science* **2008**, *53*, 1.

[25] G. Mayer, *Science* **2005**, *310*.

[26] P.-G. De Gennes, K. Okamura, *C. R. Acad. Sci. Paris, t. 1, Série IV,: Solids, fluids: mechanical and thermal properties* **2000**, *2147*, 257.

[27] Y.-C. Fung, *Biomechanics : Mechanical Properties of Living Tissues*; Springer New York, 1993.

[28] Y.-J. Lee, P. V. Braun, *Advanced Materials* **2003**, *15*, 563.

[29] C. Liu, H. Ding, Z. Wu, B. Gao, F. Fu, L. Shang, Z. Gu, Y. Zhao, *Advanced Functional Materials* **2016**.

[30] M. Ben-Moshe, V. L. Alexeev, S. A. Asher, *Analytical chemistry* **2006**, *78*, 5149.

[31] T. Ding, G. Cao, C. G. Schäfer, Q. Zhao, M. Gallei, S. K. Smoukov, J. J. Baumberg, *ACS applied materials & interfaces* **2015**, *7*, 13497.

[32] K. Naitoh, Y. Ishii, K. Tsujii, *The Journal of Physical Chemistry* **1991**, *95*, 7915.

[33] M. A. Haque, G. Kamita, T. Kurokawa, K. Tsujii, J. P. Gong, *Advanced Materials* **2010**, *22*, 5110.

[34] M. A. Haque, T. Kurokawa, J. P. Gong, *Soft Matter* **2012**, *8*, 8008.

[35] M. A. Haque, J. P. Gong, *Reactive and Functional Polymers* **2013**, *73*, 929.

[36] Y. Yue, T. Kurokawa, M. A. Haque, T. Nakajima, T. Nonoyama, X. Li, I. Kajiwara, J. P. Gong, *Nature communications* **2014**, *5*, 4659.

[37] Y. F. Yue, M. A. Haque, T. Kurokawa, T. Nakajima, J. P. Gong, *Advanced Materials* **2013**, *25*, 3106.

CHAPTER 2

Literature review

2.1 Surfactants

Surfactant are known for their adsorption on various surfaces/interfaces leading to alteration of their free energy. The boundary region of any two non-miscible phases is called interface and the surface is an interface of existing gases/air.[1] Surfactant are also known as surface active agents that lower the surface tension of a liquid, letting easier dispersion, and reduces the interfacial tension of two interfaces. Surfactants are organic amphiphilic molecules that composed of hydrophobic tails (oil loving) and hydrophilic (water loving) head groups, are soluble in both aqueous and non-aqueous solvent. On the basis of like dissolve like phenomena, the term hydrophilic and hydrophobic mean affinity towards water (goes away from oil/fats/non-aqueous solvents) and affinity towards oil (away from water). The head group of amphiphilic is denoted by circles and tail by straight line or wavy-tail.

2.2 Monomeric amphiphilic surfactants

Dodecyl glyceryl itaconate (*n*-$C_{12}H_{25}$-$OCOCH_2C(=CH_2)COOCH_2CH(OH)CH_2$- OH), abbreviated as DGI is an amphiphilic or surfactant molecule that has a hydrophilic (water-loving) head group with a polymerizing vinyl double bond and hydrophobic tail (water-hating) containing long hydrocarbon chain of twelve carbons (**Figure 2.1**). Based on the amphiphilic behavior and long C_{12} carbon chain the solubility of DGI monomer is very low. The solid crystals to liquid crystal phase transition temperature is 32°C. The Krafft point of the DGI is 43°C.[2] Above the krafft temperature as the concentration of DGI molecules increases from the critical micelle concentration, CMC, DGI molecule self-assemble into aggregated structures in aqueous media.[2]

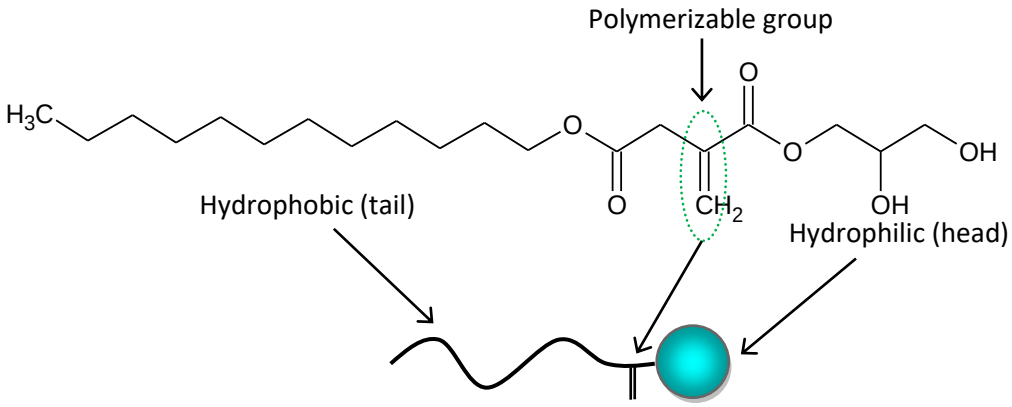

Figure 2.1: Chemical structure of amphiphilic surfactant DGI (dodecyl glyceryl itaconate) molecule.

2.3 Preparation of monomeric amphiphilic surfactant (DGI)[3]

Because of commercial unavailability the functional monomer Dodecyl-glyceryl-itaconate DGI was synthesized in laboratory described in the **Figure 2.2**. Briefly, itaconic acid anhydride (IAA) was mixed and reacted with dodecanol at 110-120 °C for 50 min to obtain the product of dodecyl itaconate (DI). By the completion of reaction, addition of *n-hexane* to the reaction vessel was performed at 70 °C, vigorously stirred, and the raw materials of white crystals was obtained. Then ethanol was used to re-crystallize DI and obtain the pure crystals of DI. The melting temperature of pure DI was 76-78 °C. The resultant product of DI was then dissolved in solvent toluene, and reacted with racemic glycidol at 100 °C in the presence of *PPTS pyridnium-para-toluene-sulfonate*. This was followed by five hours of re-fluxing and stirring process of mixture on hundred degree Celsius temperature. Then by rotary evaporator at low pressure evaporation of toluene was performed. The raw material containing DGI was added to a column of silica-gel and eluted-by a 1:1 ratio by volume of hexane/ethyl acetate mix solvent. The collected eluent contained DGI fraction of different purity was allowed to remove solvent

by rotary evaporator. The solid DGI fractions purification was performed by double re-crystallization using acetone-hexane mix-solvent (1:1 volume ratio). The final product was checked for melting and recrystallization using Differential scanning calorimeter with mp. 62-63 °C and was proven to be more than 99% pure by NMR analysis.

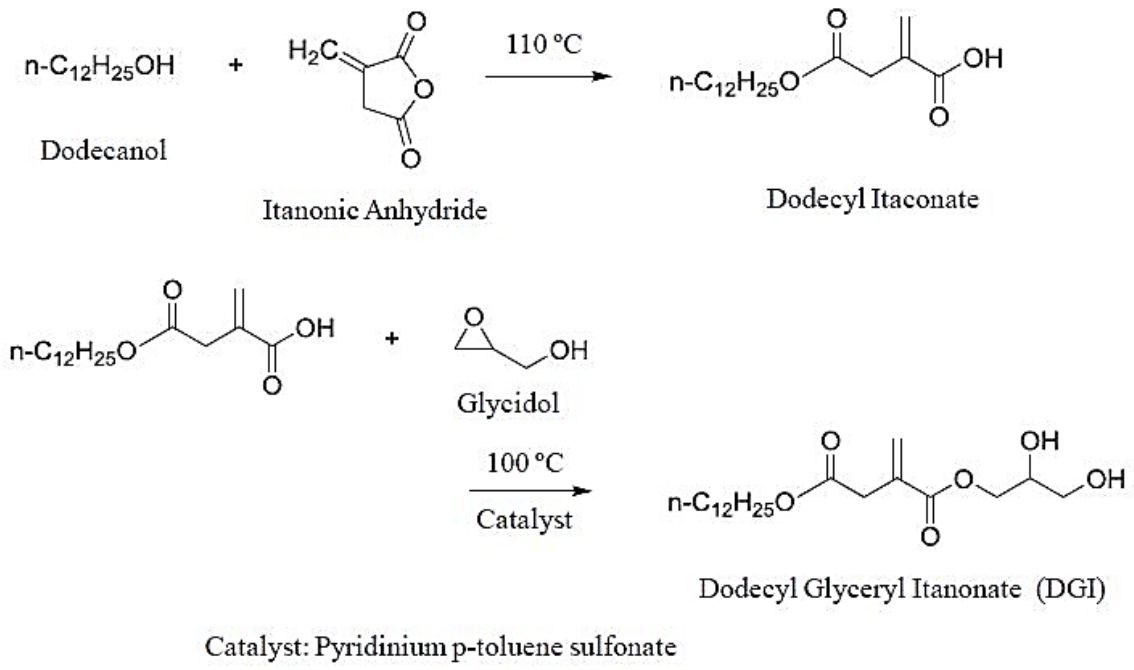

Figure 2.2: Synthesis procedure of DGI

2.4 Liquid crystalline behavior of DGI-surfactant hybrid[3]

Liquid crystals, exhibit the properties between liquid and solid crystals. For instance, a liquid crystal LC may flow like a liquid, but the molecules in the liquid organized and/or oriented as a crystal. Liquid crystals have different forms, which can be distinguished based on their different optical properties such as birefringence. There are two major classes of liquid such as thermotropic and lyotropic liquid crystals.[4] The thermotropic LCs show temperature dependent phase transition into the LC phase, whereas lyotropic LCs exhibit phase transformation as function of concentration as well as temperature.[5] Typical amphiphilic

molecules such as surfactant are lyotropic liquid crystals. Liquid crystals of surfactants are assembled of micelles that are arranged periodically in long-range order in the entire solution. The structure of the liquid crystals is directed mainly by the structure of the micelle itself: Globular, cylindrical and plate-like structurers of micelles result in cubic, hexagonal and lamellar structures of liquid crystalline phases of surfactant molecules. One typical phase structure of liquid crystals is shown in **Figure 2.3**.[6]

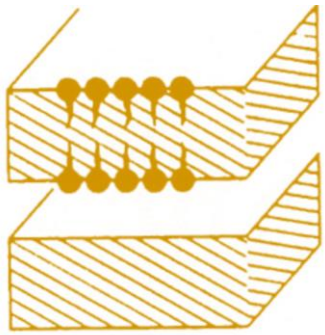

Figure 2.3: Schematics representation typical liquid crystal of surfactant in water: lamellar phase.[6]

The lamellar phase will be the most important one discussed in this thesis. The amphiphilic DGI packs into a lamellar array to form bilayer sheets with the hydrophobic tails inside, and the hydrophilic head groups facing the water. The lamellar phase can appear in two forms, continuous or as separate units. The continuous phase consists of large stacks of bilayer, recognizable by light microscopy between crossed polars as so-called oily streaks or mosaic structure.[7] Separate units appear when the bilayer sheets have closed to form vesicles.[8] Multi-lamellar vesicles appear when several bilayers pack around one another to form an “onion”. Sometime these are referred as lamellar droplets, spherulites, liposomes or onion phases. These droplets appear as so-called Maltese crosses between crossed polars and are also able to be well characterized by electron microscopy.

DGI has a very low solubility in water and the Krafft point is about 43°C.[9] When the concentration exceeds its CMC, DGI molecules tend to self-assemble into aggregated structures in aqueous phase at the temperature above the Krafft point.[10] Pure DGI itself will self-assemble into onion-like bilayer membrane structures. The interlayer distance between these bilayer membranes is several nanometers. These onion-like bilayer membrane structures or multi-lamellar vesicles can be observed under crossed polarizer with a typical texture of Maltese Cross **(Figure 2.4)**. Although the interlayer space contains water phase, the short distance cannot be expanded, and consequently a phase separation into pure water phase and these onion-like liquid crystals occurs.

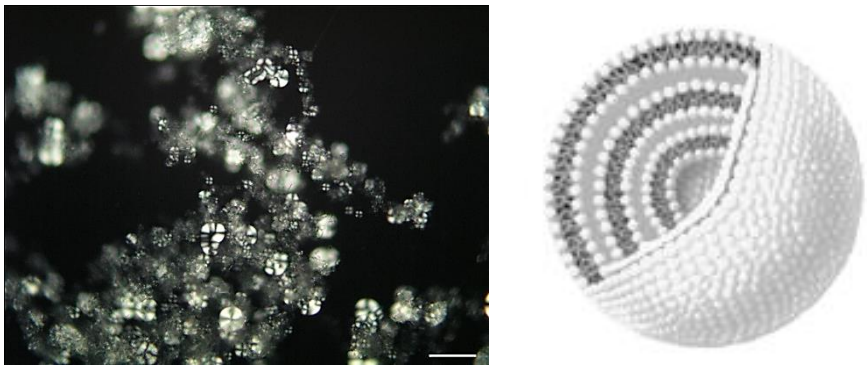

Figure 2.4: Polarized microscopic image of the lamellar liquid crystalline droplets (multi-lamellar vesicle) of pure DGI (left). The scale bar is 20 µm. An illustration of lamellar vesicle (right).[9]

In the presence of ionic surfactants, these bilayer membranes can be changed into lamellar structures depending on the concentrations of the surfactants. When DGI is in low concentration range, in the presence of some ionic surfactants, DGI bilayer membranes will be separated away from each other because of the repulsive force provided by the charges of ionic surfactants absorbed in the bilayer membranes. Since the net force between the bilayer membranes is only the repulsive force, the bilayer membranes will be separated from each other as far as the force can act. However, the volume of the surfactant solution is limited, accordingly, the interlayer

distance between the bilayer membranes is determined only by the concentration of the surfactants, which is also known as the "dilution theory". With the dilution by water, the bilayer membranes will be swollen up, and the interlayer distance increases. When the concentration of surfactants is in the range of 1- 4 wt %, the interlayer distance between the bilayer membranes is in 170-350 nm and the solution shows iridescent color. The DGI lamellar bilayer membrane structures is moldable into other structures. According to the packing theory first proposed by Tanford [11,12], the bilayer membranes changes into lamellar vesicles by increasing the ratio of ionic surfactant, whose hydrophilic head group is much larger than the hydrophobic one. In further higher concentration of ionic surfactant, DGI will form spherical micelles. With increasing the total concentration of surfactants, the spherical micellar structures can also be changed to worm-like ones and hexagonal liquid crystals with very high viscosity. The DGI lamellar phase, especially the iridescent lamellar bilayer membrane structure, is very unique, which provides an ideal compound for various studies. The large interlayer distance, which differentiates DGI from other lamellar liquid crystalline phase, is one of the characteristic properties. On the other hand, DGI has a vinylic double bond in its structure, which provides the other property of polymerizable nature. The DGI bilayer membranes can also be incorporated into polymer gels due to its polymerizable property.

2.5 How to stabilize lamellar liquid crystalline phase of surfactant

2.5.1 Theory of DLVO[13]

This theory was proposed by Derjaguin-Landau-Verwey-Overbeek (DLVO) in 1941 and 1948 respectively. It explain the balance of attractive and repulsive potential energy of interacting colloidal system. The repulsion occurs either by same charge electrical dual layers that are around the suspended particle or interaction of particle with solvent. However, vander-waals

forces are responsible for the inter-particle attraction. For the good dispersion repulsive forces must be higher than attraction while for the self-aggregation on the other way around must be performed. Moreover, surfactant effect for stabilizing lyophobic dispersion is because of surface potentiality, hamaker constant and ionic-strength of liquid for dispersion. The adsorption of surfactant on particles of same charges in disperse media as that of surfactant increases the stability. However, for the opposite sign particles in media the stability will be decreased. For the non-ionic type surfactants DLVO theory uses change of effective hamaker-constant and predict well the effect caused by ionic-surfactants that do not aggregate. To further know surfactant-effect on the stability of dispersion, some useful suggestion have been given such as: firstly, surfactant adsorption behavior over dispersing particulates of large dimension than colloids, which alters contact-angle. Increase and decrease of contact-angle cause flocculation and dispersion respectively (Parfitt 1972).

Secondly, in the absence/low level of electrical-barrier, the stability of dispersion media enhances due to the non-electrical steric-barrier to self-aggregation caused by long chain of polymeric surfactant. However, such factor is not explained by this theory. Thirdly, though for the low-dielectric-constant, the electric-barrier to self-aggregation is equal to absent. Still it is possible to use surfactants utilizing steric-barrier to self-aggregation. Fourthly, experimental protocols are not available for the measurement of stern-layer dispersant. The measurement of zeta-potential indicates electric-potential parallel to shear.

2.5.2 The theory of Helfrich thermal undulation[14]

The lyotropic liquid crystalline phases, the lamellar type structure of long range unidirectional translational is possible to achieve by critical level of tuning temperature and composition of the system. Aqueous dilution is useful for the preservation of lamellar-phases, which was in the

beginning proposed to be because of repulsive interaction of charged surfaces created by ionic-surfactants. It was given that the lamellar-morphology hyper-swollen state in large-quantity of surfactant-oil mixed-system, where the electrostatic interaction is absent.

Hyper-swelling in aqueous media was observed for the nonionic-surfactants. Helfrich proposed the swelling of lipid-bilayers in aqueous media is because of the repulsive forces that are acting at wide range. A schematic representation is shown in **Figure 2.5**.

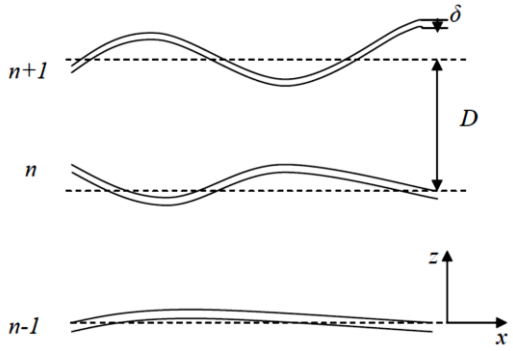

Figure 2.5: Geometry of the stack of undulating membranes. The *y* axis points into the figure.[14]

Because of the thermal undulation, the projected surface area of fluid layers decreases, compared to that of a flat base. Meanwhile, the rigidity and spontaneous curvature change.

2.5.3 Stable DGI liquid crystalline phases

DGI is a nonionic amphiphilic monomer, the DLVO theory suggests that the DGI bilayer membranes self-assemble in aqueous phase to form liquid crystalline droplets having a spacing distance of several nanometers. On adding some ionic surfactants, the bilayer membranes can be separated to occupy the whole solution space. In the latter case, the electrostatic repulsive force and the steric thermal undulation serve as the repulsion to stabilize the lamellar system. This lamellar phase, especially for the iridescent solution, is very fragile and very sensitive to the external environments. When agitated by ultrasonic action, for example, the organized

bilayer membrane structures are broken down and the iridescent color will disappear; once the temperature is lower than the Krafft point, the iridescent color disappears and a phase separation into water and DGI crystals occurs. In the presence of ionic surfactants, the bilayer membrane structures can be stabilized by the repulsive force provided by the electronic charge of ionic surfactants. When electrolyte salts is added, the repulsive force between bilayer membranes is reduced and the iridescent color disappears.

2.6 The Bragg's law of diffraction[15]

Bragg-law of diffraction given by Lawrence Bragg and Henry Bragg in 1913 in response to discovered by Lawrence and henry Braggs that crystalline solids reflect X-rays and give nice diffraction patterns and proposed Braggs-law of diffraction in 1913. Also they discovered the crystals, at some-specific light wavelength and angle of incident give highly intensive peaks for the radiation reflected also called Braggs-peak.

They explain their results by modeling of crystals as set of distinct adjacent lines separated by certain distance *d*. moreover, the constructive-interference of reflected radiation of x-rays results in Bragg peak. This happen when in-phase-shift is the multiple of 2π and is written as;

$$m\lambda = 2d\sin\theta$$

Where, *m*, λ , *d* and θ are respectively the order of diffraction, incident-wavelength, distance of adjacent atomic planes and angle of incident or reflected radiations from planes or Braggs angle (**Figure 2.6**).

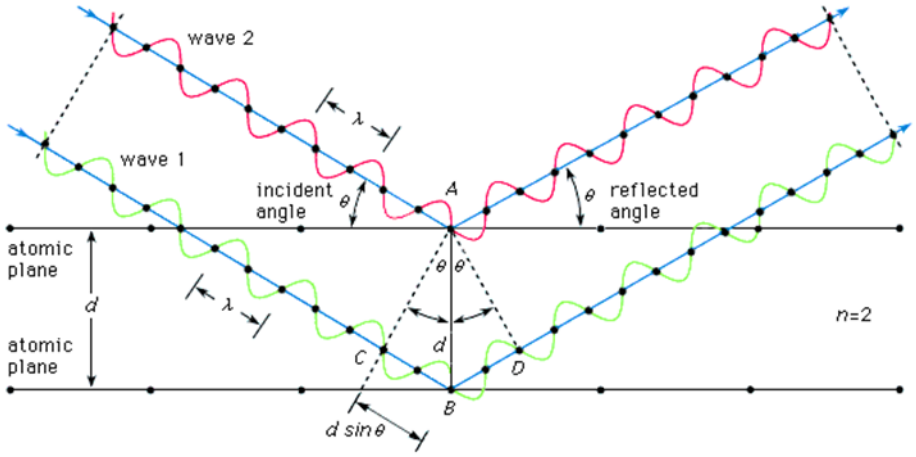

Figure 2.6: Reflection of visible light on the periodic atomic plane to satisfy the Bragg's diffraction.
(*http://www.britannica.com/EBchecked/media/17859/Bragg-diffraction*)

In DGI lamellar bilayer system, Bragg's law is satisfied when the light waves incident upon the lamellar liquid crystalline phases of DGI have same wavelength as that of the bilayer spacing, as a results of constructively interference diffraction or reflection. It happens in DGI lamellar bilayer system, because the waves are scattered from lamellar bilayer planes separated by the interplanar distance, *d*. Where the scattered waves interfere constructively in visible region; they remain in phase since the path-spacing of individual light-wave equals to integer-multiple of visible range of light waves. The space-difference of waves which interfere-constructively is shown as $2d\sin\theta$, here θ represents angle of incident and reflection with lamellar planes. When $2d\sin\theta$ is equal to the wavelength of visible light, diffraction pattern of visible color is observed. This leads to Bragg's law of diffraction for the visible light which describes the condition for constructive interference of visible light from successive lamellar bilayer planes in the DGI aqueous system and the system appears as color. For the DGI aqueous system the Bragg's law is expressed with an additional term *n* as follows[16,17]

$$m\lambda = 2nd\sin\theta$$

where n is the refractive index of water, m is an integer determined by the order of reflection, d is the interplanar distance between two nearest DGI lamellar bilayer, θ is the angle between lamellar plane and the incident visible light, and λ is the wavelength of the incident visible light. A reflection spectrum is obtained by measuring the intensity of reflected waves as a function of the wavelength of the incident light. Very strong intensities known as Bragg's reflection peaks are obtained in the reflection spectrum within visible region when satisfy the Bragg's condition.

2.6.1 The Effect of ionic surfactant on DGI bilayer structure and iridescence[2]

Above CMC, pure DGI itself will self-assemble into onion-like bilayer membrane structures in aqueous phase at the temperature above the Krafft point. The interplanar distance between these bilayer membranes is several nanometers. In the presence of small amounts of ionic surfactants, sodium dodecyl sulfate (SDS), DGI shows beautiful iridescent color. SDS have strong effects on this iridescent system. These are (i) the iridescent color changes with time after mixing DGI and SDS, (ii) the kinetic process of the above color change depends highly upon the concentration of SDS, and (iii) the iridescent color in equilibrium state changes greatly with changing concentration of SDS (**Figure 2.7a**). The time-dependent color change results from the transformation of DGI aggregate structure after being mixed with SDS. The penetration of SDS into DGI bilayer membranes is a diffusion-dominated process and depends highly upon the concentration of SDS. The iridescent color of this nonionic system can be changed from red to deep blue by altering the concentration of SDS added even though the total concentration of surfactant is almost constant. When the concentration of SDS is low, DGI bilayers are separated apart to form lamellar sheets (**Figure 2.7b**). In this lamellar sheet structure, the thermal undulation plays an important role for the solution to shift to the blue side. Helfrich thermal undulation theory can only explain a blue shift of about 20 nm as mentioned before. [18–20] The

blue shift of 70 nm in the iridescent color at equilibrium state cannot be well explained only by this thermal undulation effect. The flat lamellar sheets tend to curve by increasing the concentration of SDS to form separated onion-like and/or myelin-like structures (**Figure 2.7c**). These separated structures of lamellar system result in the decrease of spacing distance between bilayer membranes because some vacant spaces necessarily appear among these structures. [17]

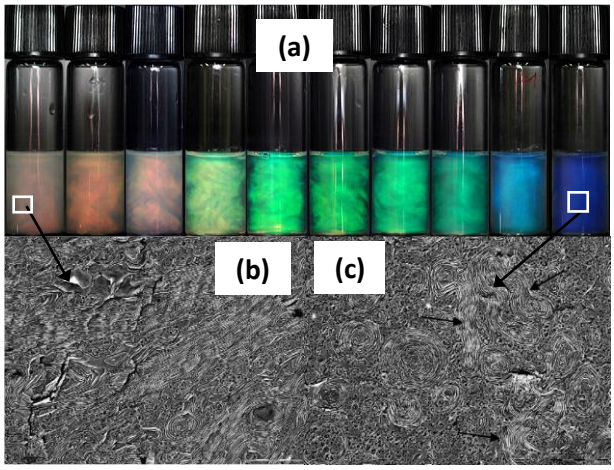

Figure 2.7: (a) Color change from pink to deep blue with increasing molar ratio of SDS to DGI observed at 3 h after mixing SDS and DGI (from left to right, the molar ratios of SDS to DGI are 1:4000, 1:2500, 1:1000, 1:600, 1:400, 1:200, 1:100, 1:75, 1:50, 1:40, respectively). **(b, c)** Freeze-fracture transmission electron microscope images of 1.63 wt% DGI aqueous solution with a SDS ratio of 1:4000 (a) and 1:40 (b). The scale bar is 10 um. When the molar ratio of SDS is 1:4000, lamellar sheets occupy the whole space. While the molar ratio of SDS is 1:40, DGI lamellae tend to curve to form onion-like and/or myelin-like structures which are separated in the water phase. Myelin structures are shown in the figure by the arrows.[2]

2.7 The Effect of configuration on DGI lamellar assembly

Amphiphilic molecules self-assemble in aqueous solutions in the form of lamellar bilayer membranes, hexagonal and spherical micelles by changing the concentrations of surfactant and/or co-surfactant.[17] The distance between the molecules in the aggregates varies when these self-assembled structures change. The distance between the two neighboring monomers is a

key factor which greatly affects the polymerization behaviors. Several methods have been taken to change the distance among the neighboring monomers. By changing the ratio of non-polymerizable co-surfactant added, the polymerization behaviors in various lyotropic liquid crystalline phases have been studied.[21] Differences in polymerization rate among lamellar, hexagonal and bicontinuous cubic phases have been ascribed to the significant differences in interfacial curvatures (an indirect way to change the distance between monomer molecules) which result in the decrease in termination. The distance between the monomer molecules can be shortened by using chiral S-DGI instead of racemic DGI, which is found to accelerate the polymerization rate. The highly ordered lamellar phase exhibits the fastest conversion rate (**Figure 2.8**), while the slowest one occurs in the hexagonal phase. By changing the position of butadiyne moiety in amphiphilic diacetylenes, the distance between monomer molecules is varied owing to the change of the tilt angle of butadiyne moiety, which leads to different polymerization behaviors in these lamellar phases.[22] The DGI bilayer membrane can be induced inside polymers gels because of its polymerizing group.

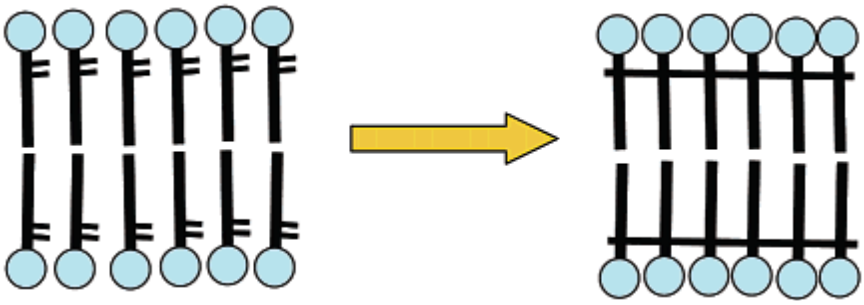

Figure 2.8: Schematic illustration of polymerization process of DGI in organized molecular assembly of bilayer membranes. A DGI molecule polymerizes preferentially with a neighbored same molecule and forms a homopolymer of DGI.

2.8 Self assembled Bilayers formation

DGI form homopolymer and is expected to be induced into ordinary gel sytem as a hybrid. The novel hybrid gels containing DGI bilayer membranes will show some unique and interesting properties which cannot be obtained from the individual polymer gels and the bilayer membranes. DGI monomer molecules form an iridescent lamellar liquid crystal in water in the presence of a small amount of ionic surfactant such as SDS.[2]

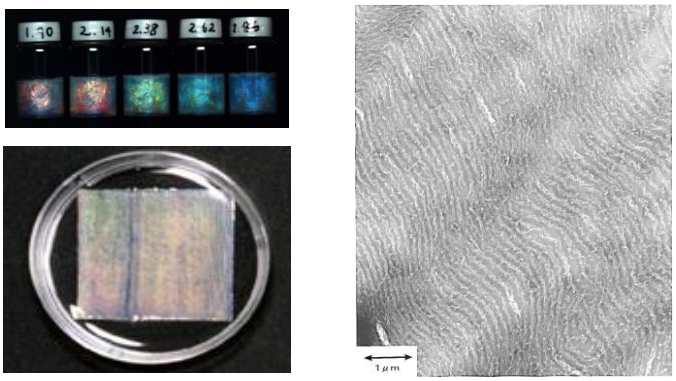

Figure 2.9: The photographs of the PDGI/PAAm gel prepared without shear flow (left-top) and at a shear flow of 0.5 mm/s (shear rate~1 s^{-1}) (left-bottom). Freeze-fracture transmission

Iridescent structure of DGI is stable even in the aqueous solution of the monomers of acrylamide (AAm), *N*,*N*-methylenebis(acrylamide) as a cross-linker, and irgacure as an initiator. The iridescent solution of DGI containing above monomers and cross linkers was photopolymerized by UV light. After polymerization, the lamellar structure of the polymeric-DGI (PDGI) was immobilized inside the PAAm network structure. The iridescent color shifts to red during the above polymerization process, since the surface area of the bilayer membranes decreases due to the bond formation between the DGI molecules, thus leading to the increase of the intermembrane distance[2]. Molecular weight of the DGI polymer was estimated by gel permeation chromatography to be about 100,000 when the DGI was homo-polymerized.[23] The hybrid material must show some coupling effects in its properties of the bilayer membranes and the polymer gels. The iridescent color controlled by the gel shrinking is a typical example of

the above coupling effect. Bilayer membrane systems are essentially anisotropic in their microstructure. But the microscopic anisotropic domains are randomly oriented in bulk, and the entire gel in a vessel shows isotropic properties (**Figure 2.9; left-top**). Although the bilayer membranes are aligned in the bulk phase and immobilized the anisotropic structure within the polymer gel networks, the poor shear flow (velocity: 0.5 mm/s, shear rate: ~1 s^{-1}) could not able to form macroscopically oriented lamellar bilayer (**Figure 2.9; left-bottom and right**). Anisotropic gels are in crucial importance for practical application of polymer gels. For example, one dimensional swelling-shrinking behavior is essential in the applications for artificial muscles. However, the hybrid gels obtained from the procedure, that developed by Tsujii *et. al*., are still far from perfect anisotropy.[23,24] Typical myelin structures grow from the interface when the concentrated DGI lamellar phase is in contact with water containing acrylamide (AAm) monomer and a cross-linker. These myelin structures can be immobilized with no structural change in poly(acrylamide) (PAAm) gels by utilizing the polymerizable property of DGI. The myelin figures thus immobilized in the gel should be stable for a long time.[17]

2.9 Bilayers-hybrid gel formation of DGI amphiphilic molecules[23]

Dodecyl glyceryl itaconate DGI, is an amphiphilic monomer, forms an iridescent lamellar liquid crystalline phase in water in the presence of small amount of ionic surfactant, SDS, and can be polymerized in this bilayer membrane system. Furthermore, this iridescent liquid crystalline structure can be immobilized in hydrogels by means of polymerization of DGI together with gel-forming monomers such as acrylamide (AAm) and methylenebis- (acrylamide). It is quite interesting question in this polymerization process whether the DGI molecules are linked with the gel-forming monomers, AAm, residing in the aqueous phase of the liquid crystal. It has been found that separated homopolymerization of DGI, and AAm takes place even in one-pot

radical reaction. The DGI molecules form a lamellar liquid crystal of bilayer membranes having the spacing distance of submicrometer and show the iridescent color in the presence of small amount of ionic surfactant. This colored bilayer system can be polymerized together with acrylamide and methylenebis(acrylamide) by photopolymerization to form a hydrogel containing the lamellar structure inside. In this polymerization process, the DGI molecules polymerize alone to form its homopolymer without reacting with any acrylamide and/or methylenebis(acrylamide) molecules. This novel phenomenon has been substantiated by the experimental techniques of SDS-PAAm gel electrophoresis, 1H NMR, and IR spectroscopy. This novel homopolymerization of DGI resulted from the preferential bond formation between DGI molecules in their organized molecular assembly. The homopolymerization process is represented in **Figure 2.10**.

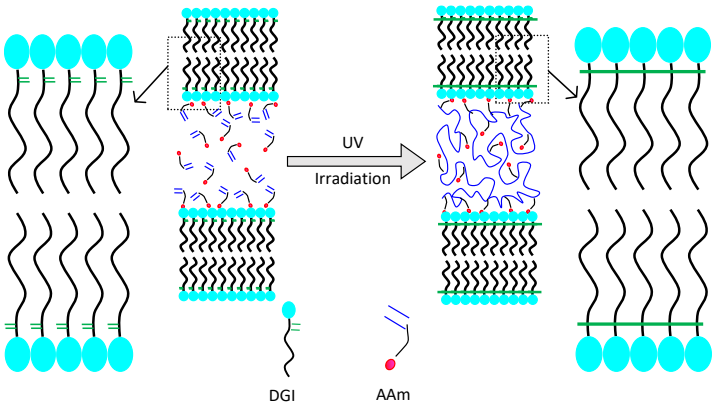

Figure 2.10: Schematic illustration of polymerization process of DGI and AAm in organized molecular assembly of bilayer membranes. A DGI molecule polymerizes preferentially with a neighbored same molecule and forms a homopolymer of DGI.

2.10 Application as soft and wet intelligent sensors

On the basis of literature survey, utilizing the concept of self-assembly in nature (**Figure 2.11a)** such as bilayers membrane, applying on ordinary hydrogels that has poor mechanical property and limited application (**Figure 2.11b)** for example PAAm gel. Therefore, our group has established a method that combine the isotropic (gel)-anisotropic (bilayer) structures together into a distinct type of gel (gel-bilayer hybrid) that greatly improved the applicability of ordinary PAAm hydrogel. The system contains 1D aligned multilayered structure along the rectangular direction.[25–31] with repeating layers of uniaxially oriented poly(dodecyl glyceryl itaconate)(PDGI) bilayer membrane (4.7 nm thick) and the chemically crosslinked or non-crosslinked polyacrylamide (PAAm) hydrogel layer (several hundred nm thick).[25,31] The bilayers are rigid, impermeable to water, while the PAAm hydrogel layers are soft and stretchable. The hybrid gel exhibited various functions (**Figure 2.11c**) such as color, one dimensional drying/swelling[26,32], mechanical anisotropy, quasi-unidirectional shrinkage upon uniaxial stretching and confined drying[27,32], high toughness and self-healing.[28] The structure color of the gels respond to external stimuli such as by small stress/strain, temperature, and pH.[29,30] Because of anisotropic structure, lamellar hydrogel closely resemble to that of natural hybrid materials. Therefore, a model system to mimic the various functions of natural anisotropic materials.[25,27,29,30,33]

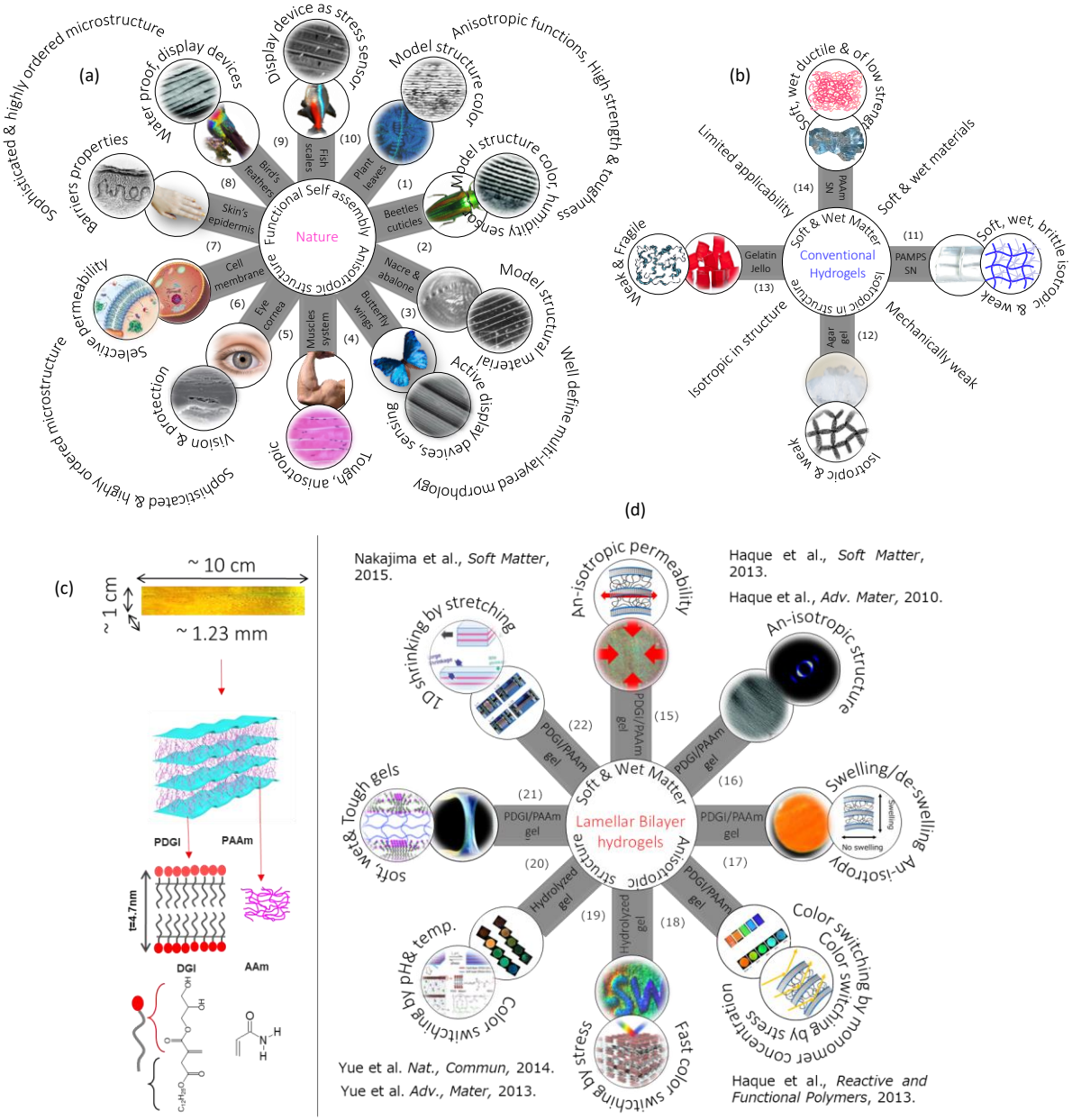

Figure 2.11 (a) the schematics of self-assembly, anisotropic, ordered structure and functions. (b) Ordinary hydrogels of isotropic structures. (c) PDGI/PAAm gel and structure. (d) PDGI/PAAm gel functions so far.

2.11 References

[1] E. D. Goddard, *Colloids and Surfaces* **1989**, *40*, 347.

[2] K. Naitoh, Y. Ishii, K. Tsujii, *The Journal of Physical Chemistry* **1991**, *95*, 7915.

[3] K. Naitoh, Y. Ishii, K. Tsujii, *The Journal of Physical Chemistry* **1991**, *95*, 7915.

[4] M.-R. Puica, *Romanian Reports in Physics* **2006**, *58*, 491.

[5] M. Knaapila, K. Kisko, B. P. Lyons, R. Stepanyan, J. P. Foreman, O. H. Seeck, U. Vainio, L. O. Pålsson, R. Serimaa, M. Torkkeli, A. P. Monkman, *Journal of Physical Chemistry B* **2004**, *108*, 10711.

[6] W. J. Gordon-Kamm, P. L. Steponkus, *Proceedings of the National Academy of Sciences of the United States of America* **1984**, *81*, 6373.

[7] C. R. López-Barrón, M. G. Basavaraj, L. Derita, N. J. Wagner, *Journal of Physical Chemistry B* **2012**, *116*, 813.

[8] Y. Uchida, T. Nishizawa, T. Omiya, Y. Hirota, N. Nishiyama, *Journal of the American Chemical Society* **2016**, *138*, 1103.

[9] H. Kunleda, T. Krafft, E. Section, **1976**, *80*, 2468.

[10] K. Tsujii, N. Saito, T. Takeuchi, **1980**, 2287.

[11] C. Tanford, *The Journal of Physical Chemistry* **1972**, *76*, 3020.

[12] C. Tanford, J. Wiley, *Journal of Chemical Education* **1980**, 232.

[13] M. J. Rosen, J. T. Kunjappu, *Surfactants and Interfacial Phenomena: Fourth Edition*; 2012.

[14] W. Helfrich, *Journal de Physique* **1985**, *46*, 1263.

[15] C. J. Humphreys, *Acta Crystallographica Section A: Foundations of Crystallography* **2013**, *69*, 45.

[16] N. Satoh, K. Tsujii, *Journal of Physical Chemistry* **1987**, *18*, 6629.

[17] X. Chen, H. Mayama, G. Matsuo, T. Torimoto, B. Ohtani, K. Tsujii, *Journal of Colloid and Interface Science* **2007**, *305*, 308.

[18] R. Schomaecker, R. Strey, *The Journal of Physical Chemistry* **1994**, *98*, 3908.

[19] M. Jonstroemer, R. Strey, *The Journal of Physical Chemistry* **1992**, *96*, 5993.

[20] R. de Vries, *Physical Review E* **1997**, *56*, 1879.

[21] X. Chen, G. Matsuo, B. Ohtani, K. Tsujii, *Journal of Polymer Science Part A: Polymer Chemistry* **2007**, *45*, 4891.

[22] H. Tachibana, Y. Yamanaka, H. Sakai, M. Abe, M. Matsumoto, *Macromolecules* **1999**, *32*, 8306.

[23] K. Tsujii, M. Hayakawa, T. Onda, T. Tanaka, *Macromolecules* **1997**, *30*, 7397.

[24] M. Hayakawa, T. Onda, T. Tanaka, K. Tsujii, *Langmuir* **1997**, *7463*, 3595.

[25] M. A. Haque, G. Kamita, T. Kurokawa, K. Tsujii, J. P. Gong, *Advanced Materials* **2010**, *22*, 5110.

[26] K. Mito, M. A. Haque, T. Nakajima, M. Uchiumi, T. Kurokawa, T. Nonoyama, J. P. Gong, *Polymer* **2017**, 1.

[27] T. Nakajima, C. Durand, X. F. Li, M. A. Haque, T. Kurokawa, J. P. Gong, *Soft matter* **2015**, *11*, 237.

[28] M. A. Haque, T. Kurokawa, G. Kamita, J. P. Gong, *Macromolecules* **2011**, *44*, 8916.

[29] Y. Yue, T. Kurokawa, M. A. Haque, T. Nakajima, T. Nonoyama, X. Li, I. Kajiwara, J. P. Gong, *Nature communications* **2014**, *5*, 4659.

[30] Y. F. Yue, M. A. Haque, T. Kurokawa, T. Nakajima, J. P. Gong, *Advanced Materials* **2013**, *25*, 3106.

[31] X. Li, T. Kurokawa, R. Takahashi, M. A. Haque, Y. Yue, T. Nakajima, J. P. Gong, *Macromolecules* **2015**, *48*, 2277.

[32] M. Ilyas, M. A. Haque, Y. Yue, T. Kurokawa, T. Nakajima, T. Nonoyama, J. P. Gong, *Macromolecules* **2017**, acs. macromol.7b01438.

[33] M. A. Haque, T. Kurokawa, J. P. Gong, *Soft Matter* **2012**, *8*, 8008.

CHAPTER 3

Synthesis and Optimization of Large Area Bilayer-hybrid Gel Thin Film

3.1 Introduction

In nature, materials both soft and hard exhibit fascinating functions such as photonic display devices (chameleon skin, butterfly wings, beetles cuticle, birds feather), water proof (feathers), barrier (Skin), selective permeability (lipid bilayer), strength & toughness (muscles & nacre) and vision (eye cornea) so on. All these functions are due to the presence of well organized, self-assembled and sophisticated microstructure.[1–4] Therefore, gaining tremendous attention and are model system for the fabrication of biomimetic materials in the field of materials science and technology. In addition, gaining the real structure similar to natural materials is of troublesome. On the contrary conventional hydrogels are isotropic in structure and do not exhibit high function.[5] To make hydrogels functional, therefore, inspired of nature our group developed a method to reinforce bilayers in conventional PAAm hydrogel. The bulk lamellar bilayer hydrogels (T ~1.23 mm) thus showed various biomimetic functions such as structure color, anisotropic diffusion, response to external stimuli such as pH, stress, strain, temperature, quasi unidirectional shrinkage upon stretching, one dimensional drug delivery, high toughness and self-recovery etc.[6–11] However, the current protocol has limitation for the uniform alignment of bilayers in gel matrix because of manual shear to precursor solution, gels of small dimensions and time consuming that restrict the gel usage for the real application where the large area bilayers-hybrid gels are required as well the mass production of bilayer based photonic gels. For example the detection of complicated dislocation of bone that fractures by accident, replacement or support of pericardial membrane, barrier coating for the skin injury

and so on require anisotropic gels of large area. To overcome the problem and widen the applicability of bilayer-hybrid gels, in this chapter the establishment of facile and optimized protocol to induce amphiphilic polymer PDGI in polyacrylamide PAAm gel is given. The production of long range ordered structure in hydrogels regardless dimension is given. It is expected that the amphiphilic molecules are lyotropic liquid crystals, their self-assembly in aqueous media has sensitivity to various parameters such as temperature, pressure, shear flow and confinement etc. Among these the shear flow, temperature and confinement are discussed and possible solution is given.

3.2 Experimental

3.2.1 Materials and method

Amphiphilic monomer, DGI; *n*-$C_{12}H_{25}$-$OCOCH_2C(=CH_2)COOCH_2CH(OH)CH_2OH$) was synthesized according to the procedure reported by Tsuji *et al*.[12] Briefly, the crude product after the synthesis was purified by passing from column packed with silica-gel, with eluting mix-solvent of ethyl acetate-hexane of 1:1 volume-ratio. For purifying raw-DGI, eluted solvent contained the fractions of DGI monomer was re-crystallize using hexane-acetone mix-solvent 1:1 weight ratio. The collected DGI is again doubly re-crystalized using hexane-acetone mixture solvent 1:1 weight-ratio. The melting and recrystallization temperature of DGI monomer were 63°C and 32°C, respectively confirmed by Differential scanning calorimetry DSC. *N*,*N*′-methylenebisacrylamide MBAA (Wako Pure Chemical Industries, Ltd., Japan) was recrystallized from ethanol, acrylamide AAm (Junsei Chemical Co., Ltd., Japan) was recrystallized from chloroform, Irgacure 2959 (BASF SE, Germany), and sodium dodecyl sulfate SDS (MP Biomedicals Inc., USA) were of commercial grade. Millipore deionized water was used for the reparation of monomer solutions and equilibrium swelling of gel.

3.2.2 Bilayer-hybrid gel synthesis

In the first set of experiment, the bilayer hybrid hydrogel, PDGI/PAAm, of large dimension (100×30-60 ×0.05-0.5 mm^3) was prepared by modifying the previous method.[6] Briefly, the conditions of shear flow, temperature and thickness optimization are discussed.

Step 1. The precursor solution, composed of 0.1 M dodecyl glyceryl itaconate (DGI), 0.025 mol % sodium dodecyl sulfate SDS (with respect to DGI monomer), 2.0 M acrylamide (AAm), 0.1 mol% *N*,*N*'-methylenebisacrylamide (MBAA) as chemical crosslinker of AAm, and 0.1 mol % Irgacure 2959 as initiator (both in relative to AAm monomers), were mixed in aqueous media and flush with Ar gas for 1 min.

Step 2. The aforementioned precursor solution was incubated in a temperature controlled water bath for ~5 h at 55°C since the krafft temperature of DGI monomer is 43°C, to dissolve amphiphilic monomer DGI powders and stabilize lyotropic liquid crystalline phases of DGI[13], it is worth to mention that after 15 min incubation the precursor solution was shake well to avoid the self-aggregation of DGI liquid crystalline domains, then at each 30 min interval the precursor solution was sheared by shake and flow for 50 times. This method allow the domains of amphiphilic molecules to self-assemble at the micrometer length scale.

Step 3. Before polymerization, a reaction cell of 100-200 mm in length (*L*), 30-60 mm in width (*W*), and 0.05-0.5 mm in thickness (*T*) was prepared by sandwiching a 0.05-0.5 mm–thickness of silicone rubber spacer sandwiched between two pre-cleaned glass plates (NaOH/Ethanol 200g/6L). The glass plates cleaning is essential step to get hydrophilic glass surface which is good for the orientation of amphiphilic domains.

Step 4. In previous method, the shear flow was applied manually to induce bilayer orientation by injecting the precursor solution manually to the reaction cell inside glove box.[6] In current

method, automatic suction method is used to apply the uniform and strong shear flow under the controlled incubation temperature using incubator with temperature console (model EYELA NTI 400E). This step is very crucial for the lyotropic liquid crystalline domains of DGI amphiphilic because the gel to liquid crystalline phase transition temperature is 43°C. Briefly, one end of the preheated reaction cell was connected to a suction pump (model Harvard PHD 4400 programmable), and through the other end, the precursor solution containing amphiphilic domains was suctioned vertically to the reaction cell against the gravity at a high suction rate to induce a strong shear flow (~133 s^{-1}) at 50°C to align the DGI domains between glass plates at controlled temperature inside incubator**.** This method permitted us to obtain a uniform DGI lamellar phase, even with 3 times the sample area of the previous method, oriented uni-axially along the glass walls.

Step 5. This was followed by a co-current homo-polymerization of the DGI and AAm using UV light irradiation for 8 hours at 50°C inside incubator. This step is very important to fix the already oriented domains in conventional polymer matrix. In case of delayed UV irradiation the gel might have un-oriented domains.

Step 6. After the polymerization, the gel was removed from the reaction cell either by peeling from glass plate or soaking in water in the case of thin gel. Then immersed in a large amount of water for 7 days to reach equilibrium swelling state and to wash away the residual chemicals. PAAm hydrogels were synthesized by UV irradiation from a precursor solution containing 2.0 M AAm, 0.1 mol% MBAA, and 0.1 mol% Irgacure 2959 as initiator using the same technique. In the second set of experiment the effect of gelation temperature above and below the krafft temperature of liquid crystalline phase transition was studied. On purpose slight modification in experimental condition was performed. Step 1, step 3 and step 6 were exactly the same. However, at the end of step 2 the incubator temperature such as water bath and oven was set

for 24h at specific temperature above and below the krafft point of DGI. Then at the same temperature conditions the suction and gelation was performed.

3.3 Characterization

3.3.1 Polarized optical microscopy (POM)

The bilayer hybrid gels were swollen in water for at least 1 week and cut into 1 cm long pieces. The thickness of gel T_S measured by polarized optical microscopy (POM). The orientation of bilayers in hybrid system is confirmed.

3.3.2 Measurement of mechanical properties

The dumb-bell shaped gel specimens, standard dimension (length, L_s = 12 mm width, W_s = 2 mm and thickness swollen gel, T_s) were cut with commercial standard gel cutter (model JIS-K6251-7). The uniaxial tensile and cyclic tests were performed using commercial tensile tester (Instron Anton Paar 5965) with tensile velocity 100 $mm.min^{-1}$ & stretching rate 0.14 s^{-1}. The modulus (stiffness) was calculated from the initial slope of the tensile stress-stretch curves within 5% deformation. The tensile tests were performed three times and average values with error bar were adopted.

3.3.3 Measurement of reflection spectrum

The structure color of PDGI/PAAm gels synthesized with different temperature was characterized by the electromagnetic spectrum of light, using moveable angle reflection measurement optics (Hamamatsu Photonics KK, C10027A10687) coupled with photonic multichannel analyzer (Hamamatsu Photonics KK, C10027). White light from Xe source was used to irradiate the gel. Reflection spectrum was acquired by keeping both the angles of incident (Bragg's angle) and reflection at 60°. The wavelength at maximum reflection intensity,

λ_{max}, was obtained from the reflection spectrum. The inter-lamellar distance (d) was estimated by using the Bragg's law of diffraction,

$$\lambda_{max} = 2nd\sin\theta \qquad (5)$$

Here n is the refractive index of water (1.33) and θ is the Bragg's angle (60°).

3.3.4 Diffusion test

Different thickness PDGI/PAAm gels and bulk PAAm gels were pre-soaked in 0.1 mg/mL aqueous neutral red dye solution for 5s. The release of dye from gel to pure water was observed at different time interval.

3.4 Results and discussion

3.4.1 Optimize shear flow

The bilayer-hybrid gels preparation under different conditions of shear flow such as automatic shear and manual shear is described. The precursor solution mentioned in the experimental section was heated in water bath for 5h at 55°C above the krafft temperature of DGI monomer.[13] After 5h of sufficient dissolution of amphiphilic monomer, the inside the glove box hot plate is placed nearby the two UV lamps at the distance of about 10 cm. The temperature is set 200°C so that the surrounding area was sufficient heated to attain 50°C reported in our previous work. Herein two sort of polymerization cells were placed in between the two UV lamps. One cell consist of two glass plates (10 x 10 cm) separated by silicone rubber spacer of thickness 0.5 mm. The silicone rubber spacer was cut at 4 places of length and width of 1 x 9 cm, respectively. The space was used for the injection of 500 microliter precursor solution by hand with high shear rate of approximately 190 s^{-1}. In the second device, two large size glass plates were used that were separated by silicone rubber spacer. In upper glass plate two holes

of ~0.5 mm inner diameter were made at the extreme upper and lower edges using glass borer machine. Then silicone rubber spacer was cut for the specific test dimension. The device was assembled as glass plate, silicone rubber spacer (already cut is specified dimension) and upper glass plate with holes. The device lower hole was connected to the bottle contained precursor solution by polyethylene tube while upper side with automatic pump. In this way the precursor solution was suctioned between two glass plates separated by silicone rubber (L 18 cm, W 40 cm, T 0.05 cm) (new device) with hand manually as well as automatic pump by that utilizes shear rate of $130s^{-1}$ as in **Scheme 3.1**. All devices were placed between two UV lamps for 8h of UV irradiation to accelerate polymerization and fix bilayers in gel matrix. After completion of polymerization times, gels were peeled out from the glass plates. The as prepared gels were transparent T_0 0.5 mm easily removed from glass plates and soaked in water to attain equilibrated swelling.

The results indicated that the gels prepared by manual hand injection of separated volume of precursor solution in small dimension columns with shear rate of ~190 s^{-1} were bluish color. The injection lines pattern indicate that this method is not repeatable and uncontrolled to repeat the same shear rate. Since the time of precursor solution incubation and injection takes long time. Therefore the gel color after swelling could not reached the desired gel color (**Figure 3.2a**). Then bulk volume of precursor solution was injected manually by applying strong shear rate the precursor solution and the gel color was found different at each batch of synthesis at equilibrium swollen condition (**Figure 3.2b**). That suggested manual shear perturb the solution flow behavior and causes difficulty to orient bilayers in hybrid gels. Therefore, the strategy of automatic pump suction and shear to precursor solution was performed. Variation in color at each synthesis batch. However, the individual gels prepared by automatic pump shear method were homogenous and three times larger than the manual shear method gels (**Figure 3.2c**). The

possible reason is the bilayer orientation require homogenous pressure with uniform flow behavior that compel the self-assembly of bilayer at long range rather than self-aggregation as a consequence of random non uniform manual shear. However, the different color of each batch suggested that there is another parameter that hinder the reproducibility of gel orientation and resultant color. One possible reason might be the fluctuation of temperature inside the glove box. The hot plate might not control the temperature of the surrounding place where the devices were placed. This suggest that problem associated with difference in each batch is not only due to shear rate because shear rate of manual method was quite higher than automatic pump method. Therefore in addition to shear flow, it is speculated that the possible parameter that restrict the reproducibility was temperature.

3.4.2 Optimize temperature

To support and confirm the speculations, various gel samples were synthesized at control temperature of 55°C, from precursor solution to polymerization using incubator with temperature console that keep temperature constant automatically. After 5h heating of precursor solution. Prior to shear flow a device was assembled from two large size glass plates separated by silicone rubber spacer and incubated for 30 min at 50°C. In upper glass plate two holes of ~0.5 mm inner diameter were made at the extreme upper and lower edges using glass borer machine. Then silicone rubber spacer was cut for the specific test dimension. The device was assembled as glass plate, silicone rubber spacer (already cut is specified dimension) and upper glass plate with holes. The device lower hole was connected to the bottle contained precursor solution by polyethylene tube while upper side with automatic pump. In order to orient bilayers in gel, the precursor solution was suctioned between two glass plates separated by silicone rubber (L 18 cm, W 40 cm, T 0.05 cm) (new device) with automatic pump with shear rate of $130s^{-1}$. This step was performed inside incubator with controlled temperature. In this way

temperature was controlled by incubator and flow by automatic pump. The devices were placed between two UV lamps already placed inside incubator for 8h of irradiation to accelerate polymerization and fix bilayers in gel matrix. After completion of polymerization times, gels were peeled out from the glass plates. The as prepared gels were transparent T_0 0.5 mm easily removed from glass plates and soaked in water to attain equilibrated swelling. The results suggested that, a series of gel samples synthesized under the same conditions of shear flow and incubation temperature after swelling displayed iridescence structural color by satisfying the Braggs law of diffraction **[Figure 3.2(d)]**. Equilibrium swollen gels structural color was quantified using reflection spectrometer that showed an average bright orange/red structural color (λ max, ~600-670 nm) **[Figure 3.3(b), (c)]** with narrow and intense peaks. The average distance between bilayers for series of batches was ~300 nm much higher than the uncontrolled temperature synthesis gels which was ~250 **[Figure 3.3(c)]**. The average value of full width at half maxima (FWHM) was ~50 and ~80 for controlled and uncontrolled condition synthesis gels, respectively **[Figure 3.3(c)]**. The lower value of FWHM, higher value of the distance between bilayers indicated that amphiphilic domains of PDGI were well aligned at long range ordered in one dimension under controlled conditions. The structural color strictly followed the recipe of precursor solution. Which was not well understood using uncontrolled method inside glove box due to uncontrolled temperature. Next the effect of bilayers reinforcement on the swelling behavior of hybrid gels was determined. As the anisotropic structure incorporation inside gels can have influence in the swelling behavior of gel dimension.[14] The bilayers are being impermeable to transport of water along the orientation axis of domains. So the gels must have property of one dimension swelling. The one dimension swelling behavior must be higher for the controlled condition as compared to gels prepared under uncontrolled conditions. Therefore, the bilayers hybrid gels swelling ratio along the three dimensions such as in

thickness T/T_0, width W/W_0 and length L/L_0 as a function of gel synthesis conditions are given **[Figure 3.2(e)],** where T, W, L were swollen and T_0, W_0, L_0 the as prepared length width thickness, respectively. The results revealed that, the swelling behavior of bilayer hybrid gels in thickness direction was higher than the length and width, showing 1D swelling. However, the overall 1D swelling of gels prepared under controlled conditions of incubation temperature and constant uniform shear flow was much higher than the uncontrolled condition, respectively **[Figure 3.2(e)]**. The 1D swelling is related to the permeability of the alternating layers; the PDGI bilayers are impermeable to the transport of water because of the large hydrophobic dodecyl chain.[15] While the PAAm gel layers are permeable as they are hydrophilic polymer strands. These results confirmed that incubation temperature and uniform shear flow are important parameters for the synthesis of high quality large area bilayer hybrid gels.

How about the effect of confinement on the orientation of bilayers and its effect on gel quality. The question arises will the gel colors and quality maintain if we change the thickness of as prepared gels and allow them to swell what kind of color might we have? Whether the controlled parameter work well for dimension change or not? To test such speculation thickness optimization were performed.

3.4.3 Optimize thickness

After the shear flow and temperature optimization the next challenge was to optimize the thickness effect by changing the spacer thickness that corresponds to the as prepared thickness of gels. The precursor solution stated in the experimental part was incubated in water bath for 5h at 55°C above the krafft temperature of DGI monomer.[13] Before shear flow of solution a polymerization device was assembled from two large size glass plates separated by silicone rubber spacer and incubated for 30 min at 50°C. In upper glass plate two holes of ~0.5 mm

inner diameter were made at the extreme upper and lower edges using glass borer machine. Then silicone rubber spacer was cut for the specific test dimension. The device was assembled as glass plate, silicone rubber spacer (already cut is specified dimension) and upper glass plate with holes. The device lower hole was connected to the bottle contained precursor solution by polyethylene tube while upper side with automatic pump. In order to orient bilayers in gel, the precursor solution was suctioned between two glass plates separated by silicone rubber of thickness T_0 (0.5 mm, 100 μm, 50 μm) Length L_0 (20 cm, 10 cm, 10 cm) and width W_0 (3 cm, 6 cm, 10 cm) using automatic pump with shear rate of $130s^{-1}$. This step was performed inside incubator with controlled temperature. In this way temperature was controlled by incubator and flow by automatic pump. The devices were placed between two UV lamps already placed inside incubator for 8h of irradiation to accelerate polymerization and fix bilayers in gel matrix. After completion of polymerization times, gels were peeled out from the glass plates.

The results indicated that, the as prepared PDGI/PAAm bilayer hybrid gel of different thickness T (0.5 mm, 100 μm, 50 μm) were transparent, respectively because they were invisible wavelength range**.** The gels showed increased in thicknesses 1.29 mm, 187 μm and 80 μm, respectively in equilibrium swollen conditions as compared to the length and width **[Figure 3.4(a)-(d)]**. The gels prepared under controlled condition showed higher swelling behavior even by changing the dimension of gels. The equilibrium swollen gels satisfying the Braggs law of diffraction[16] of visible wavelength of light waves and shifted to visual iridescence structural color in the visible light wavelength range of ~600 nm with the corresponding distance between bilayers of ~290 nm of the gels prepared under controlled conditions **[Figure 3.3(a)-(c)]** and **[Figure 3.4(a)-(c)],** and green structural color for the gel under uncontrolled condition λ ~500 nm d ~195 nm **[Figure 3.3(d)].** The gels synthesized were of sufficiently large area in which the bilayers were oriented homogenously at a long range several tens of centimeter scale that

diffract light waves in the visible spectrum of electromagnetic radiation of light, as a result the same structural color under the same preparation conditions can be observed regarding dimension **[Figure 3.3(a)-(c)]** and **[Figure 3.4(a)-(c)]**. However, the gel surface morphology changed at critical thickness (T<100 um) of preparation, the surface of bilayer-hybrid gel changed from flat/smooth to rough and porous **[Figure 3.3(a)-(d)]**. Therefore gels of different morphology from smooth surface to porous surface gels were obtained. The reason for the change in gel morphology by changing the confinement thickness is because of the possible pinning mechanism of the solution contained amphiphilic domains.[17] Furthermore, if we compare the gels under controlled conditions such as thick gel 1.29 mm and thin gel 170 μm in term of structural color both showed narrow peak in the reflection spectra as a result of good packing and orientation of bilayers inside gels. Therefore they exhibited perfect 1D swelling **[Figure 3.4(a), (b)]**, **[Figure 3.5(a-b)]** and **[Figure 3.6(a), (b)].** The thin gels prepared from same thickness cell of 50 μm but different conditions showed different structural color, swelling ratio and surface morphology**. [Figure 3.4(c), (d)]**, **[Figure 3.5(c)-(d)]** and **[Figure 3.6(c), (d)].** Therefore, the control of temperature and flow behavior are extremely important for the bilayers orientation and over all gel quality. Knowing the parameters such shear flow, incubation temperature and thickness effect one can high quality anisotropic hydrogels that contain well align lipid like bilayers at large area several centimeter length scale. The next question will be how the microscopic view of gels well the aligned bilayer are homogenously aligned or random. To support the speculations polarized optical microscopy was performed and discussed in the next step.

3.4.4 Bilayers orientation in hybrid gel

Polarized light microscopy is a powerful tool in material science to observe the orientation of crystals and their plan of orientation.[6,18,19] Homogenous orientation give uniform color birefringence. Therefore, the orientation of bilayers in equilibrium swollen hybrid-gel thick and thin film were confirmed by observing the gel under polarized optical microscopy (POM). A small piece of gels were cut from original equilibrium swollen gels using gel cutter. The observation were performed perpendicular to bilayers orientation (top view) and parallel to orientation (cross sectional view) at -45° and +45° , with 532 *nm* tint plate and cross Nicole as shown in **Figure 3.7**. The top view POM images of thick- and thin-gels showed no sign of birefringence that means the bilayers are oriented in uniaxial direction, which transmitted light homogenously across the gel samples **[Figure 3.7(a)-(d)]**. The cross section images of thick and thin-gels with tint plate exhibited very intense yellow and blue interference images under POM at crossing angles of -45° and +45°, respectively **[Figure 3.7(e)-(h)]**. The gel bright birefringence between cross Nicole without tint plate, indicating the unidirectional alignment of the PDGI bilayers **[Figure 3.7(i)-(l)]**. The bright birefringence clearly indicated that the bilayers were uniformly induced inside the PAAm gels by strong shear flow. The homogenous birefringence also suggested that the automatic flow and incubation temperature are important parameters for the well-ordered structure of bilayers in conventional hydrogels.

3.4.5 Mechanical behavior of thin and thick gel

The dumb-bell shaped thin- and thick-PAAm gels are given in **Figure 3.8(a).** The tensile stress-strain curves of PDGI/PAAm thin-gel, thick-gel and pure PAAm gel, respectively are and results are shown in **Figure 3.8(b)** and **(c)**. The results of s-s curves revealed that the thin gel was of high toughness, stiffness, deformation and strength as compared to thick-PDGI/PAAm

and pure PAAm gel which is very weak [**Figure 3.8(b) and (c)].** The thin-gel and thick-gels both initially region of s-s curve showed clear yielding behavior which is due to the presence few hundreds (~700) and few thousands (~5000) of rigid/stiffer bilayers, respectively, that act as sacrificial layers to dissipate energy during gel deformation.[9] Then the stress is transferred to the PAAm matrix that showed strain hardening at large deformation. In this way the bilayer hybrid gels not only shows high stiffness but also high toughness that dominated the pure PAAm gel which is very soft weak and ductile. However, the stiffness of thin-PDGI/PAAm gel is higher than the thick-PDGI/PAAm and PAAm gels, respectively [**Figure 3.8(b) and (c)].** Second the PAAm gel layer adsorbed on the surface of bilayers that give additional energy dissipation.[9] Further, the amount of energy dissipation and self-recoverable property of thin gel was estimated from the cyclic loading-unloading curve as in **Figure 3.8(c)**. The gel showed large hysteresis loop under the cyclic loading-unloading curve indicating large energy dissipation by the presence of bilayers regardless numbers. The time dependent self-recovery was observed. After certain time full recovery was noted **Figure 3.8(d)**. One possible reason for the high mechanical behavior of thin bilayer-hybrid gel will be the well aligned long range ordered structure. That promoted the good packing and orientation of bilayers in PAAm matrix indicating that confinement is very important to obtained highly ordered structure whenever the conditions such flow behavior and incubation temperature are under controlled. As a result the high quality bilayer hybrid gels with enhanced mechanical properties were obtained regardless dimension and numbers of bilayers.

3.4.6 Dye release test of thick- and thin-gels

The anisotropic bilayer hybrid gels were subjected to diffusion test for the understanding of release behavior as a function of different thickness gels (**Figure 3.9)**. Briefly, the thick PAAm gel, thick PDGI/PAAm gel and thin PDGI/PAAm gels were pre-soaked in aqueous neutral red

dye solution of concentration 0.1 mg/mL for 5s [**Figure 3.9 (a), (b), (c)]**. Then slightly washed the surface with distilled water to remove extraneous dye and placed in pure water for release study. After certain time the gel was took out from water and photographs were captured as under white background to have better understanding of dye concentration and release as shown in **Figure 3.9**. After very longer time the thin gel color turned transparent as compared to thick gels almost same as original state. The result suggested that the thin gel release dye into water relatively faster than that of the thick PDGI/PAAm and PAAm bulk gels. The results also indicated that, the dimension can have effect on release properties of the gels. Changing the gel dimension and number of bilayers the drug release properties could be altered. Being faster for thin gel and slower for thick gels, respectively.

3.4.7 Effect of different incubation temperature

3.4.7.1 On photonic properties

This section explain various batches of bilayer-hybrid gels preparation at different incubation temperature 50°C, 40°C, 35°C and 30°C under controlled condition from precursor solution to gelation step using incubator. The purpose was to understand how at different temperature the DGI liquid crystal behave and their long range self-assembly behavior on gel quality. Briefly, at the beginning, the precursor solution was heated in water bath for 5h at 55°C (above krafft point).[20] Then after sufficient dissolution of amphiphilic monomer the temperature of water bath is decreased to specific temperature of interest such as 50°C, 40°C, 35°C and 30°C, respectively. To achieve the equilibrated temperature, the precursor solution was left for at least 24h inside water bath under controlled temperature. Similarly the incubator oven temperature was set to the particular batch synthesis temperature in advanced. The device was already placed prior to suction inside oven at the same temperature of gelation. One side of the device

was connected to the vial consist of precursor solution via tube while other side with automatic machine pump. As the desired temperature approached after sufficient incubation such as 50°C, 40°C, 35°C and 30°C, precursor solution was suctioned between two glass plates separated by silicone rubber (L 18 cm, W 40 cm, T 0.05 cm) (new device) as in **Figure 3.1**. The solution was placed between two UV lamps for 8h of irradiation for polymerization and gelation. In this way the bilayer were fixed at each batch synthesis temperature. After the 8h of polymerization the gels were peeled out from the glass plates. The as prepared gels were transparent T_0 0.5 mm easily removed from glass plates and kept in water to attain equilibrated swelling. The bilayer hybrid gels synthesized at various temperatures of incubation 50°C, 40°C, 35°C and 30°C were orange, yellow, green and mixture of transparent-green, respectively as given in the inset of **Figure 3.10(b)**. The gels at 50°C, 40°C, 35°C were homogenous colored while at 30°C gel showed phase separation. The gels resulted in a blue shift at the equilibrium swollen conditions. The wavelength maxima changed from red (λ_{max} 630 nm, *d* 287 nm) to yellow (λ_{max} 560 nm, *d* 260 nm) and then green color (λmax 520 nm, *d* 240 nm) even in phases separated gel at each batch of synthesis temperature. However, the peak broadening was observed that indicated the PDGI head group packing distorted by reducing the temperature [**Figure 3.10(a) and (b)**]. As DGI form lyotropic lamellar liquid crystals at 55°C temperature.[20] By reducing the temperature below 43°C (krafft point) differences in interfacial curvatures might have resulted change in lamellar phases to hexagonal and somewhat cubic phases at different temperature of synthesis.[21] Therefore the difference in the rate of polymerization altered the side wise packing of bilayers molecules. The literature suggested that at higher temperature in the lamellar phases the conversion is faster while slower by reducing temperature.[22] The lamellar phases provide good packing of head group and reduces the surface area of bilayers as a results the gel showed highly one dimensional swelling at high temperature of synthesis. The gel swollen more in

thickness direction as compared to the width and length [**Figure 3.10(a) and (b)**]. However, for the phase separated sample the other directions also slightly swelled. Overall the thickness wise swelling behavior decreases as the gelation temperature decreased. This also suggested that there is rearrangement of amphiphilic molecules at different temperature. Other reason is that, at high temperature the precursor solution viscosity reduces almost same as water. There is maximum chances of amphiphilic molecules to interact with one another and self-assemble at long range order structure by applying shear force. However, reducing temperature might have perturb the structure as there are already self-aggregation at relatively high viscosity that resulted to phase separation.

3.4.7.2 On mechanical properties

To decipher the effect of batch synthesis temperature on the bilayers hybrid gel quality which greatly might have impact on mechanical properties of PDGI/PAAm gels. Therefore uniaxial tensile test along the bilayer packing direction was performed. The photographs of the dumbbell-shaped samples at different batch synthesis temperature of incubation are shown in **[Figure 3.11(a)].** The stress-strain curves of the PDGI/PAAm samples with varied synthesis batch temperature are shown in **Figure 3.11(b)**. The modulus, fracture strain, fracture stress, toughness and yield stress of these samples are summarized in **Figure 3.12 a**,**b**,**c**,**d**, respectively.

The bilayer hybrid hydrogel showed change of the mechanical properties with respect to batch synthesis or incubation temperature. The gels of stiff/tough and soft/stretchable behavior upon decreasing gelation temperature were obtained (**Figure 3.11a,b**). The modulus of gel decreased with decreasing temperature of gelation (**Figure 3.12a**,**b**). At higher temperature of synthesis the gel was stiffer as compared to low temperature. However, the fracture stress, fracture strain and toughness slightly increased by decreasing batch synthesis temperature then sharply

decreased below 35°C sample. Another feature of the lamellar hydrogel is that the yielding stress monotonously decreased with the changing temperature of gelation (**Figure 3.12e**). The yielding phenomenon was very clear at 50°C, 40°C and 35°C samples, respectively. At 30°C the phase separated gel was soft and ductile with no pronounce yielding. Which is an indication of the decreased packing of DGI head group by reducing batch synthesis temperature. The higher the temperature the more chances for the domains to interact with one another at long range. At 35°C the gels were of low modulus but high strength, stretchable and toughness. The phase separated gels lack long range interaction of bilayers and remains in cubic gel-liquid crystal hybrid state.[21,23] Therefore, is of low mechanical behavior. The higher temperature provide good gel with enhanced packing and brilliant structural color. The Mooney Rivlin curve obtained from the data of stress-strain curve also indicated stress relaxation at low deformation with the decreasing reduced stress for reducing batch synthesis temperature. However, at high deformation ratio the strain hardening was observed (**Figure 3.11c)**.

3.5 Conclusion

In conclusion, we successfully developed a method to induce bilayers in PAAm gels matrix and synthesized large area bilayer-hybrid photonic gel with alternating layered structure. The parameters such as shear flow and temperature of incubation were found to affect the orientation behavior of bilayers that largely impact the quality of bilayer-hybrid gels. Under optimized condition gels repeatability was observed and hybrid gels regarding dimension and thickness were obtained. The thin gel and thick gels contained few hundreds (~700) to few thousand (~6000) of well oriented bilayers, showed visible structural coloration. In addition to high toughness, stiffness, strength and stretchibility, and the release of small molecules was observed to be tuned by changing dimensions of gels. This method might open new ways to explore various novel function of bilayer hybrid gels where large dimension are necessary.

3.6 References

[1] J. Sun, B. Bhushan, J. Tong, *RSC Advances* **2013**, *3*, 14862.

[2] P. Fratzl, R. Weinkamer, *Progress in Materials Science* **2007**, *52*, 1263.

[3] W. Yang, V. R. Sherman, B. Gludovatz, E. Schaible, P. Stewart, R. O. Ritchie, M. A. Meyers, *Nature Communications* **2015**, *6*, 1.

[4] E. Munch, M. E. Launey, D. H. Alsem, E. Saiz, A. P. Tomsia, R. O. Ritchie, *Science (New York, N.Y.)* **2008**, *322*, 1516.

[5] J. Itagaki, Hiroko.; Kurokawa, Takayki.; Furukawa, Hidemitsu.; Nakajima, Tasuku.; Katsumoto, Yukitru and Gong, *Macromolecules* **2010**, 9495.

[6] M. A. Haque, G. Kamita, T. Kurokawa, K. Tsujii, J. P. Gong, *Advanced Materials* **2010**, *22*, 5110.

[7] Y. F. Yue, M. A. Haque, T. Kurokawa, T. Nakajima, J. P. Gong, *Advanced Materials* **2013**, *25*, 3106.

[8] Y. Yue, T. Kurokawa, M. A. Haque, T. Nakajima, T. Nonoyama, X. Li, I. Kajiwara, J. P. Gong, *Nature communications* **2014**, *5*, 4659.

[9] X. Li, T. Kurokawa, R. Takahashi, M. A. Haque, Y. Yue, T. Nakajima, J. P. Gong, *Macromolecules* **2015**, *48*, 2277.

[10] T. Nakajima, C. Durand, X. F. Li, M. A. Haque, T. Kurokawa, J. P. Gong, *Soft matter* **2015**, *11*, 237.

[11] K. Mito, M. A. Haque, T. Nakajima, M. Uchiumi, T. Kurokawa, T. Nonoyama, J. P. Gong, *Polymer* **2017**, 1.

[12] K. Tsujii, N. Saito, T. Takeuchi, **1980**, 2287.

[13] K. Naitoh, Y. Ishii, K. Tsujii, *Journal of Physical Chemistry* **1991**, *95*, 7915.

[14] and J. P. G. Md. Anamul Haque , Gen Kamita , Takayuki Kurokawa , Kaoru Tsujii, *Uma ética para quantos?* **2012**, *XXXIII*, 81.

[15] M. A. Haque, J. P. Gong, *Reactive and Functional Polymers* **2013**, *73*, 929.

[16] C. J. Humphreys, *Acta Crystallographica Section A: Foundations of Crystallography* **2013**, *69*, 45.

[17] C. Antoine, J. Irvoas, K. Schwarzenberger, K. Eckert, F. Wodlei, V. Pimienta, **2016**.

[18] R. Oldenbourg, *Cold Spring Harbor Protocols* **2013**, *2013*, 1023.

[19] D. B. Murphy, M. W. Davidson, *Fundamentals of Light Microscopy and Electronic Imaging: Second Edition*; 2012.

[20] K. Naitoh, Y. Ishii, K. Tsujii, *The Journal of Physical Chemistry* **1991**, *95*, 7915.

[21] W. J. Gordon-Kamm, P. L. Steponkus, *Proceedings of the National Academy of Sciences of the United States of America* **1984**, *81*, 6373.

[22] X. Chen, G. Matsuo, B. Ohtani, K. Tsujii, *Journal of Polymer Science Part A: Polymer Chemistry* **2007**, *45*, 4891.

[23] J. Gustafsson, H. Ljusberg-Wahren, M. Almgren, K. Larsson, *Langmuir* **1997**, *13*, 6964.

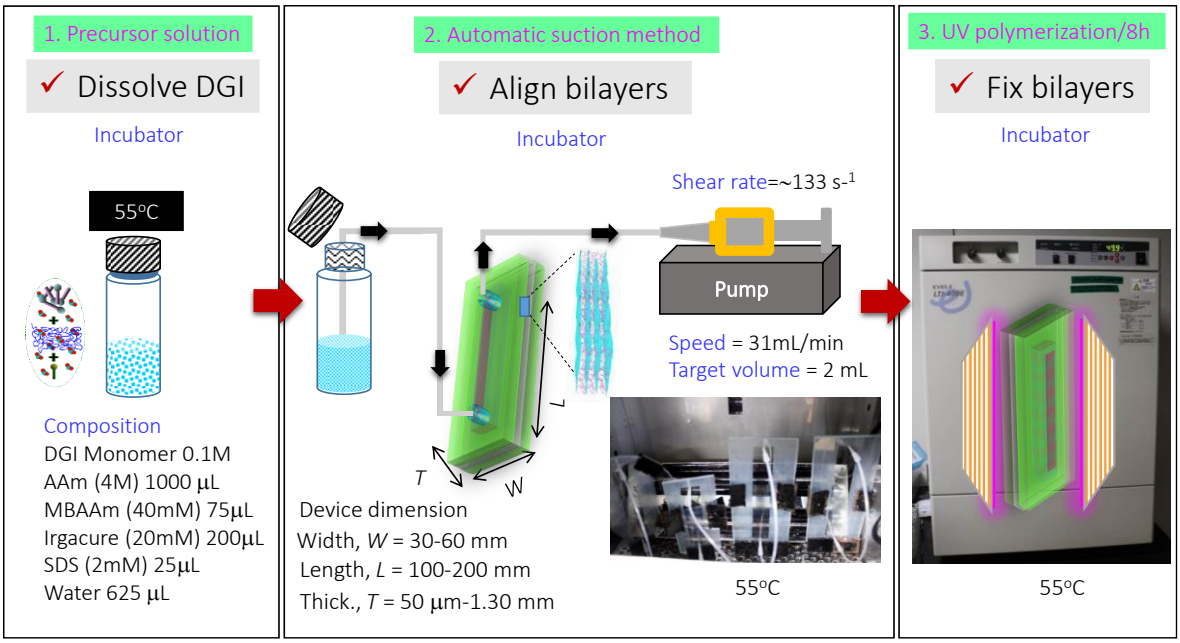

Figure 3.1 Schematics representation of anisotropic lamellar hydrogel. The method is comprise of three major steps. (a) Precursor solution preparation. (b) Applying suction to induce bilayer alignment by shear flow. (c) Polymerization by UV to start gelation for the bilayers fixing in hybrid gel. Temperature from solution to polymerization is constant.

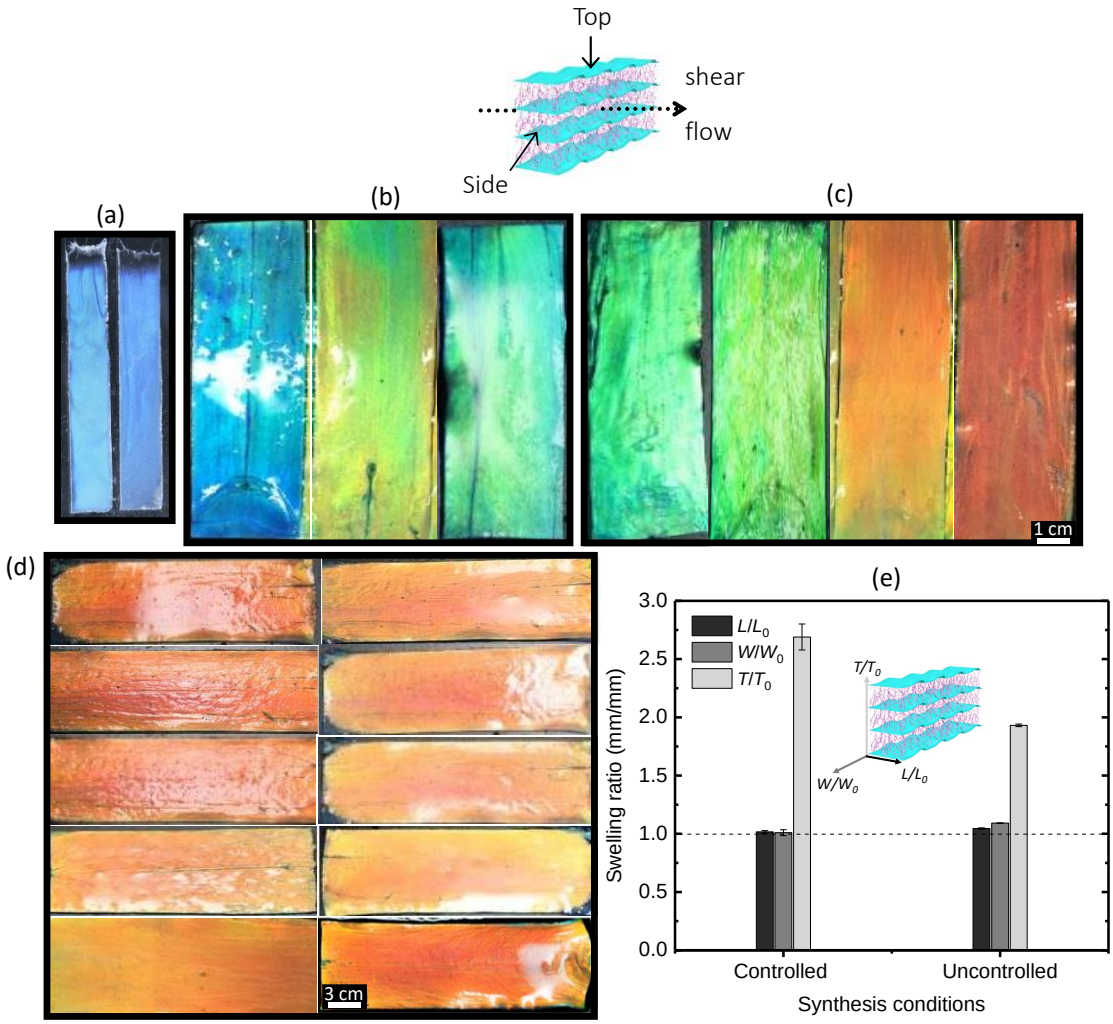

Figure 3.2 PDGI/PAAm bilayer hybrid gels from same recipe of precursor solution containing 0.1M DGI amphiphilic monomer. (a) Hybrid gels of small dimension prepared by manual shear method. The polymerization cell dimension was length L_0, width W_0, and thickness T_0, of 10 cm, 1 cm and 0.05 cm respectively. (b) Large dimension gels such as length L_0, width W_0, and thickness T_0, of 10 cm, 3 cm and 0.05 cm respectively. In this case the gels were prepared by manual shear method. The gels color were inhomogeneous and different from each batch of preparation. (c) Gels synthesized using same dimension as of "b", however the shear flow was performed by automatic pump at shear rate of $130s^{-1}$. The gels were homogenous color but difference in color at each batch of synthesis. It is worth mentioning that (a), (b) and (c) were synthesized in glove box in the presence of hot plate that control the temperature of surrounding.

(d) Gels synthesized in controlled incubation temperature from precursor solution preparation to gelation steps. In this case the color is reproducible. The scale bar is 1 cm for (a), (b) and (c). While the scale bar for (d) is 3 cm due to low magnification. (e) The comparison of swelling ratio between gels prepared under controlled and uncontrolled conditions. Where L, W, T and L_0, W_0, T_0 are the length, width and thickness of gels at the equilibrium swollen and the as prepared condition, respectively.

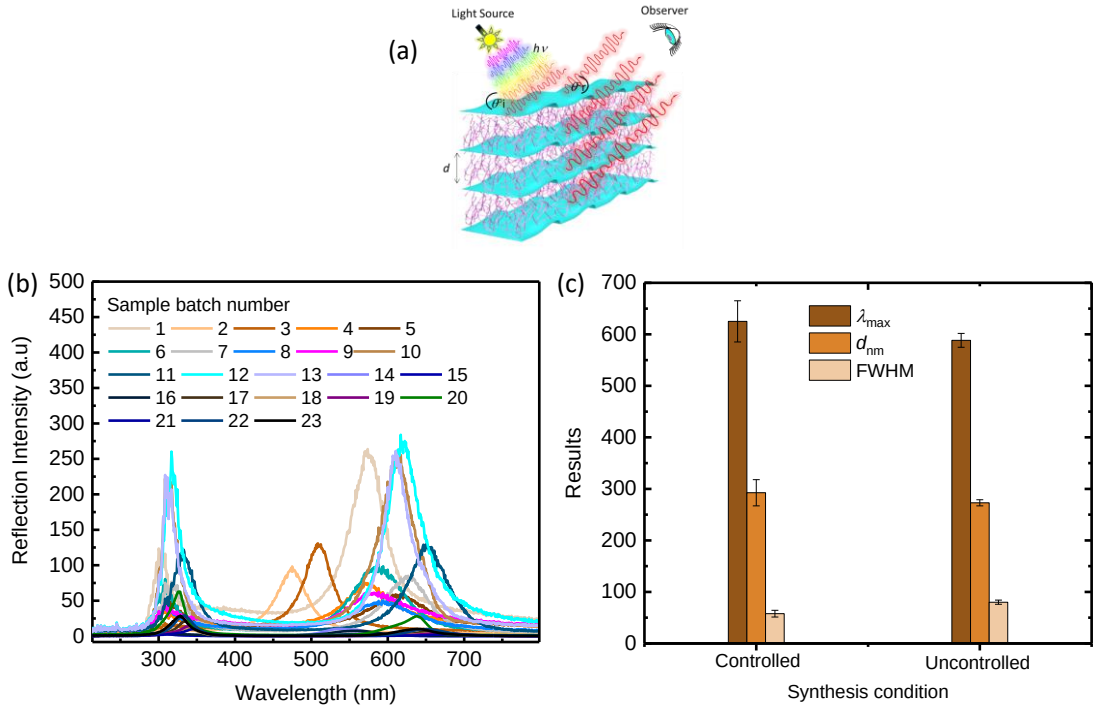

Figure 3.3 (a) Schematics of bilayer hybrid gel illuminated with high intensity white light for the collection of reflection spectra. The light was shined on surface of gel samples keeping Braggs angle of 60°.(b) The gels reflection intensity as a function of wavelength *nm* in visible region of electromagnetic spectrum of light. (c) The average value of maximum wavelength of reflected color λ_{max}, the distance between bilayers d nm and full width at half maxima FWHM of the reflected color peaks of the controlled and uncontrolled condition gel synthesis, respectively.

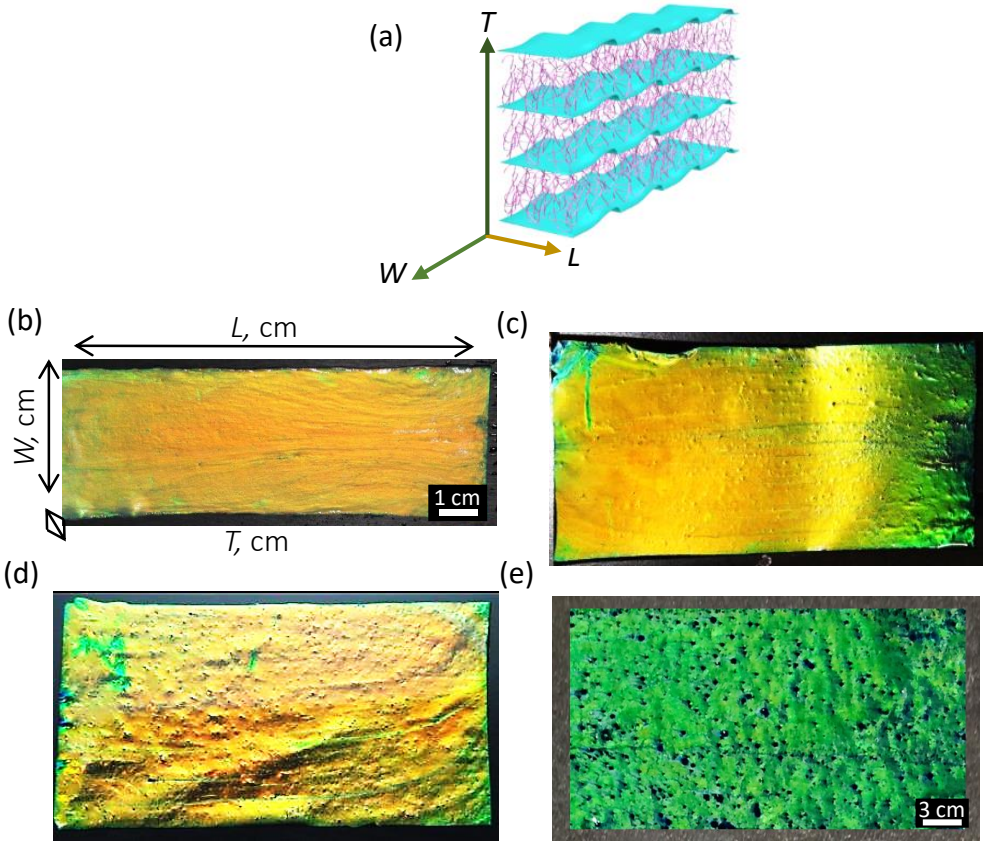

Figure 3.4 PDGI/PAAm bilayer hybrid gel thick and thin gels prepared under controlled condition using different thickness of polymerization cell (a) alternating layer structure of gels. (b), (c), (d) and (e) are, respectively the equilibrium swollen gels synthesized using different spacer thickness. After equilibrium swelling the thicknesses were 1.29 mm, 170 um and 90 μm and 80 μm, respectively. The gels showed visual structural color satisfying the Braggs law of diffraction. Despite of the change in thickness at the preparation state, the samples (b), (c) and (d) exhibited homogenous orange color because of controlled incubation temperature while, (d) showed green color as the incubation temperature was uncontrolled. Sample (d) and (e) have porous morphology.

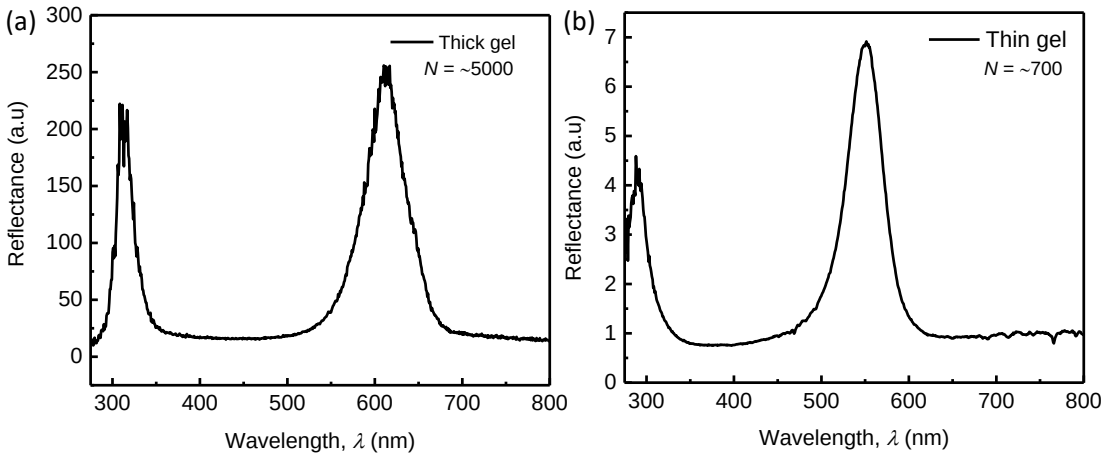

(c)

Code	*T*	λ_{max}	$d_{(nm)}$	*FWHM*	*N*
Thick gel	1.29 mm	610	300	50	5000
Thin gel	170 μm	550	270	48	700

Figure 3.5 Reflection spectra comparison of PDGI/PAAm bilayer hybrid gels synthesized using different spacer thickness under controlled condition. (a) Thick PDGI/PAAm gel of thickness 1.29 mm in equilibrium swollen state. (b) Thin PDGI/PAAm gel of thickness 170 μm in equilibrium swollen conditions. (c) Comparison of results such as obtained from reflection spectra maximum wavelength of reflected color λ_{max}, the distance between bilayers *d* nm and full width at half maxima FWHM of the reflected color peaks and *N* numbers of bilayers in gels.

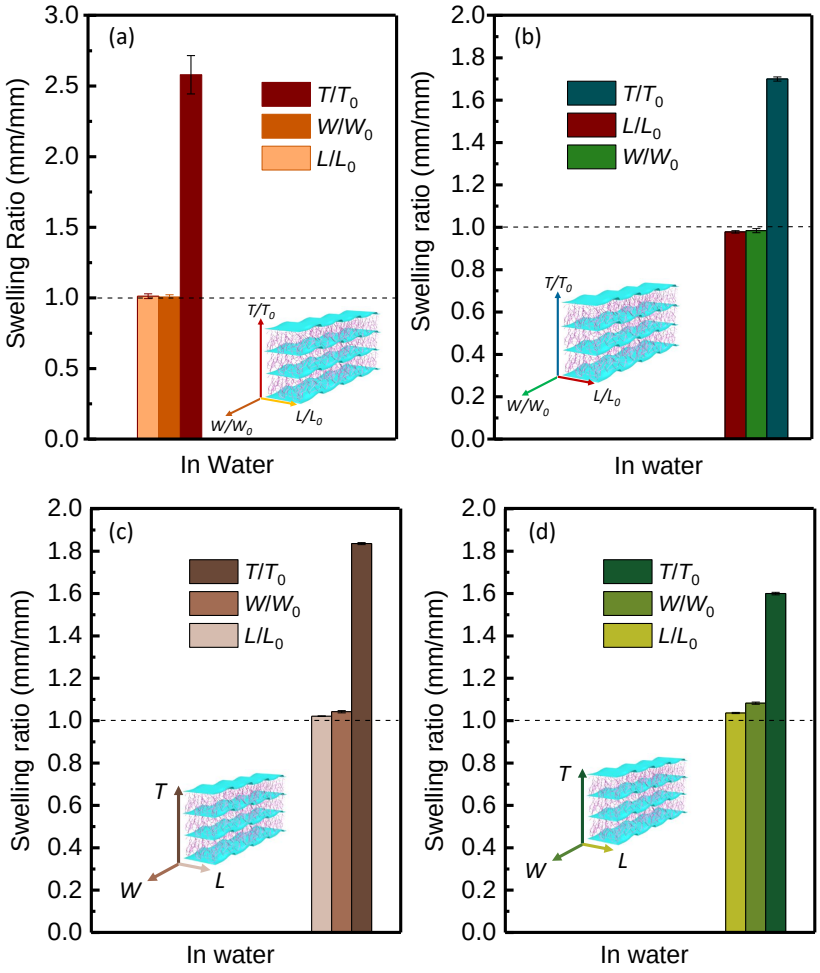

Figure 3.6 The swelling behavior of PDGI/PAAm bilayer hybrid gel thin film. The gel were synthesized using different space thicknesses (a) to (d) 0.5 mm, 100 μm, 50 μm, respectively. The gels thickness reaches in equilibrium condition as 1.29 mm, 170 μm and 90 μm and 80 μm, respectively. Along thickness axis (perpendicular to the bilayers) increases while it remains constant along the length axis (parallel to the bilayers), *i.e.*, no swelling at all, which indicates the superb anisotropic swelling. Where, L_0, T_0, W_0; and L, T, W are the length, thickness and width of the bilayer hybrid gels at as prepared state; and water swollen state, respectively.

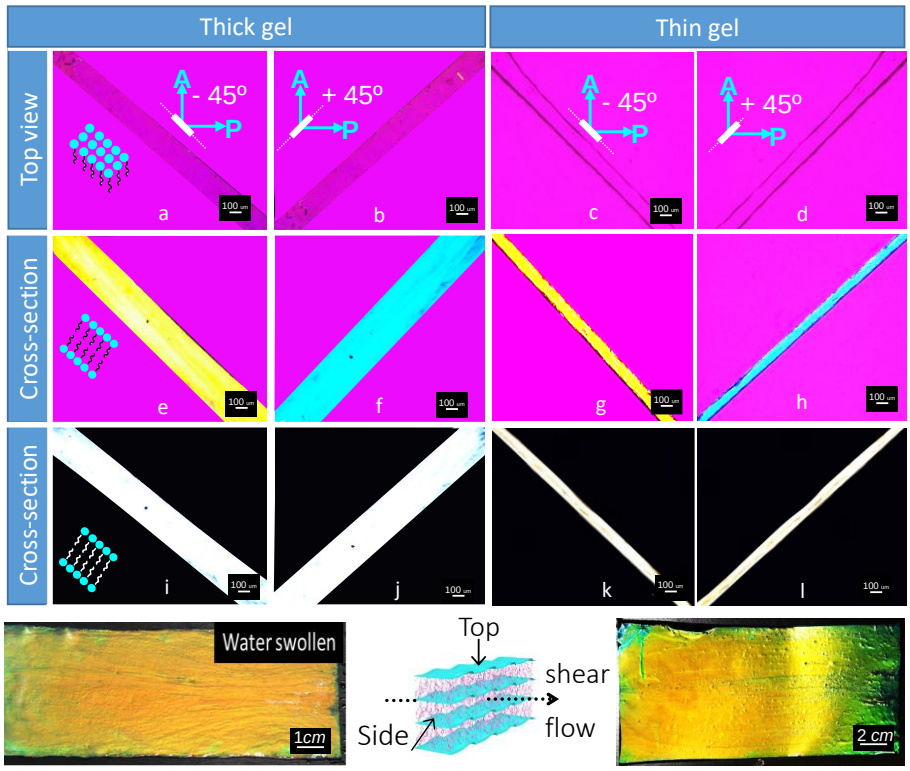

Figure 3.7 Polarizing optical microscopic analysis of thick- and thin-gel prepared with uniform shear flow (~10 cm/s) and controlled incubation temperature. The POM Images "a", "b" (thick gel) , "c" and "d" (thin gel) were taken under crossed polarizers with 532 nm tint plate at a crossing angle of -45°, and +45°, respectively. The gels, top view images revealed same colour as that of background with no sign of interference colour or birefringence. From the cross-section, the intense yellow and blue interference colour in images "e", "f" (thick gel) and "g", "h" (thin gel) respectively, taken at right angles to each other using a tint plate further confirmed the ID alignment of bilayers in hybrid gels. The gel shows bright birefringence between cross Nicole without tint plate "i", "j" (thick gel) and "k", "l" (thin gel) respectively, indicating the unidirectional alignment of the PDGI bilayers. The top view images indicates that the in-plane structure of the bilayer is amorphous. The gel were prepared from a 0.1 M DGI concentration using a 0.5 mm- and 0.1 mm-thick reaction cells, respectively. A: analyzer and P: polarizer. The scale bar in all images is 100 μm.

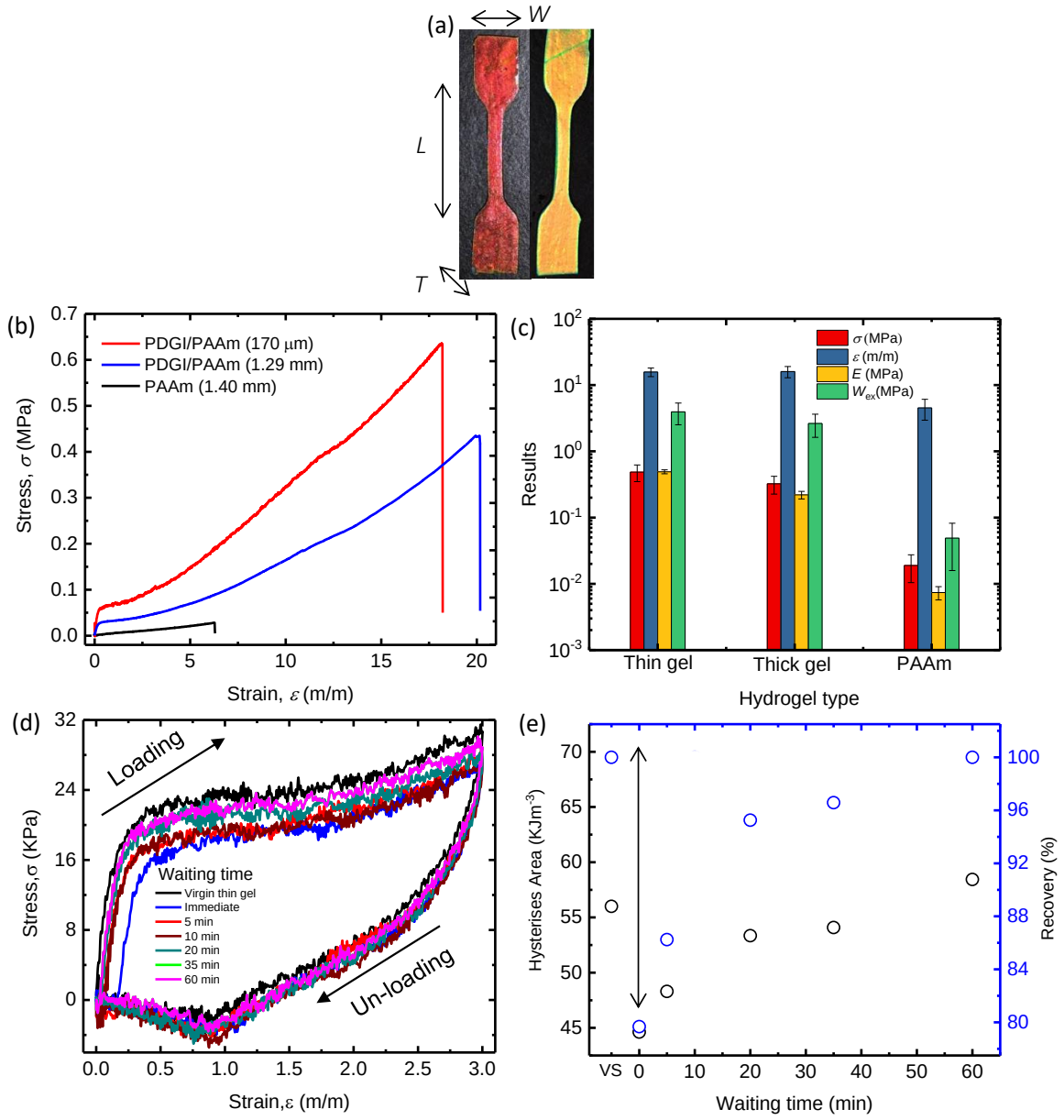

Figure 3.8 (a) Photographs of standard dumbbell shaped tensile test specimens cut out from gels synthesized at different thickness synthesized gels. The gauge length (L), width (w) and thickness (t) are 12 mm, 2 mm and thickness (thick PDGI/PAAm 1.29 mm, thin PDGI/PAAm 170 μm, bulk PAAm), respectively. (b) Stress-strain curves of PDGI/PAAm gels at different thickness and PAAm gel obtained from uniaxial tension tests. (c) Comparison of results obtained from S-S curves for different gels. The results are shown in semi log plot for clarity.

(d) The cyclic loading unloading curve on thin gel showing the recovery behavior. (e) Hysteresis area and self-recovery as a function of waiting time.

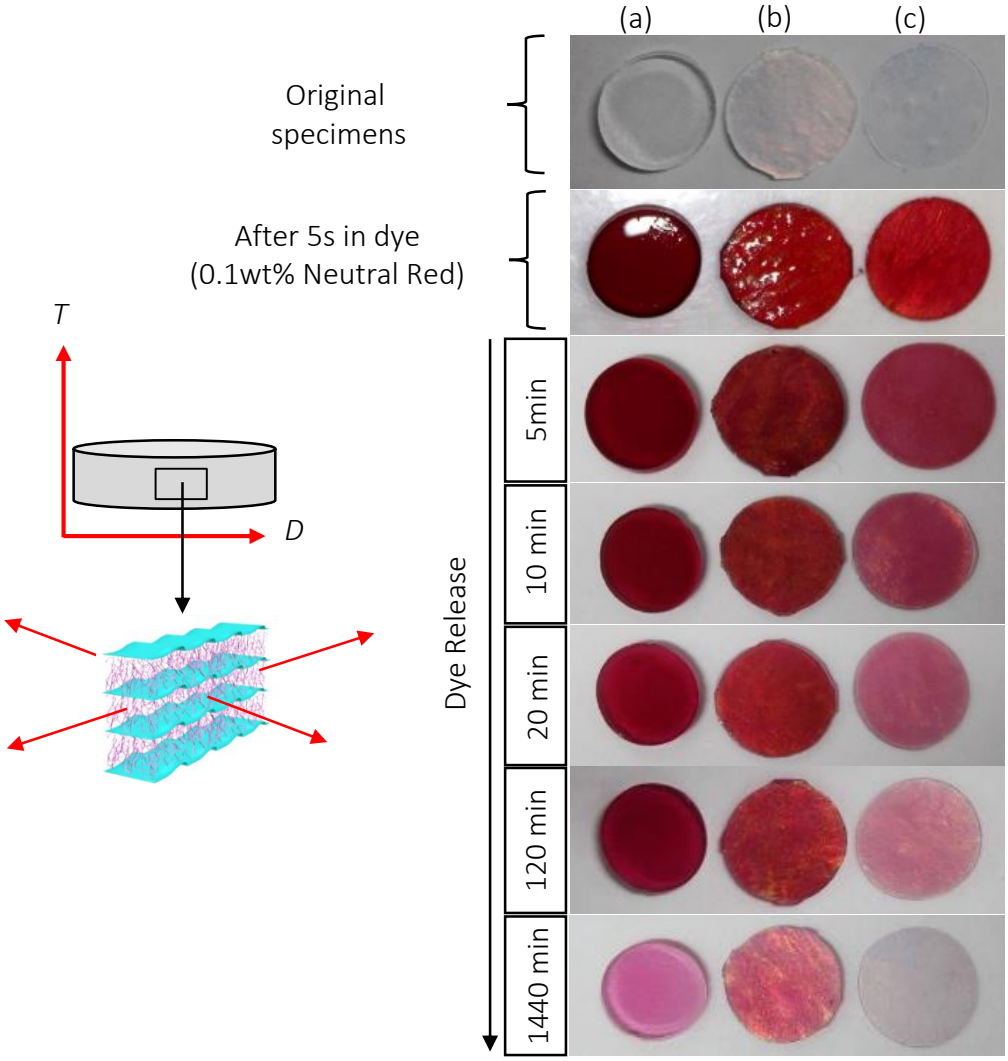

Figure 3.9 Photographs showing release of dye from different dimension gels (a) PAAm gel; (b) Thick PDGI/PAAm gel; (c) Thin PDGI/PAAm gel, respectively. The thickness were 1.41 mm, 1.29 mm and 170 μm, respectively. While the diameter of gels was 15 mm. The gels were presoaked in aqueous dye solution of 0.1mg/mL concentration. The release behavior of dye from gel to water was observed by taking photographs after certain time.

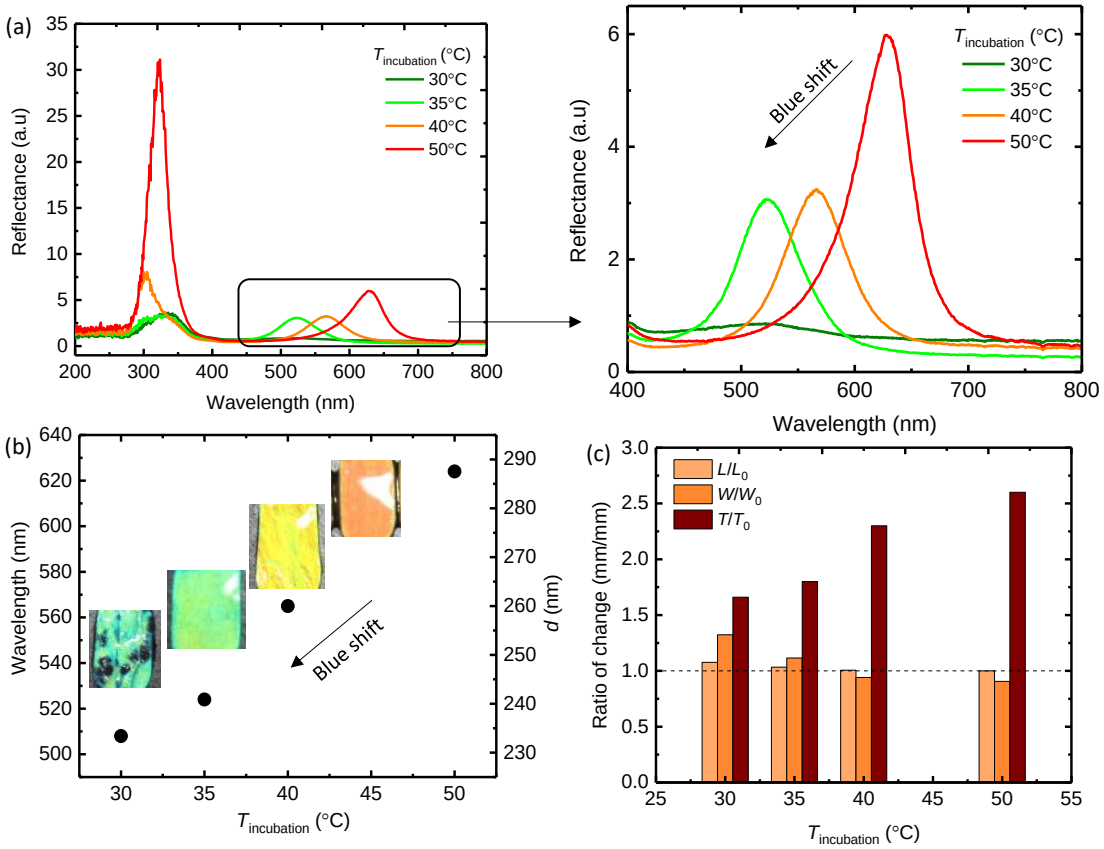

Figure 3.10 Bilayer hybrid gel thin films synthesized at different incubation temperature under controlled conditions (a) The optical reflectance of PDGI/PAAm hydrogel as a function of wavelength, taken from gels synthesized at different incubation temperature with enlarged view between 400 nm to 800 nm range of wavelength. (b) Wavelength maximum and distance between bilayers as a function of temperature of synthesis. The visual color change can be perceived from the images given inside the graph. The gels exhibited blue shift with decreasing gel synthesis incubation temperature. (c) Swelling anisotropy as a function of decreasing gel synthesis incubation temperature. Where, L_0, T_0, W_0; and L, T, W are the length, thickness and width of the bilayer hybrid gels at as prepared state; and water swollen state, respectively.

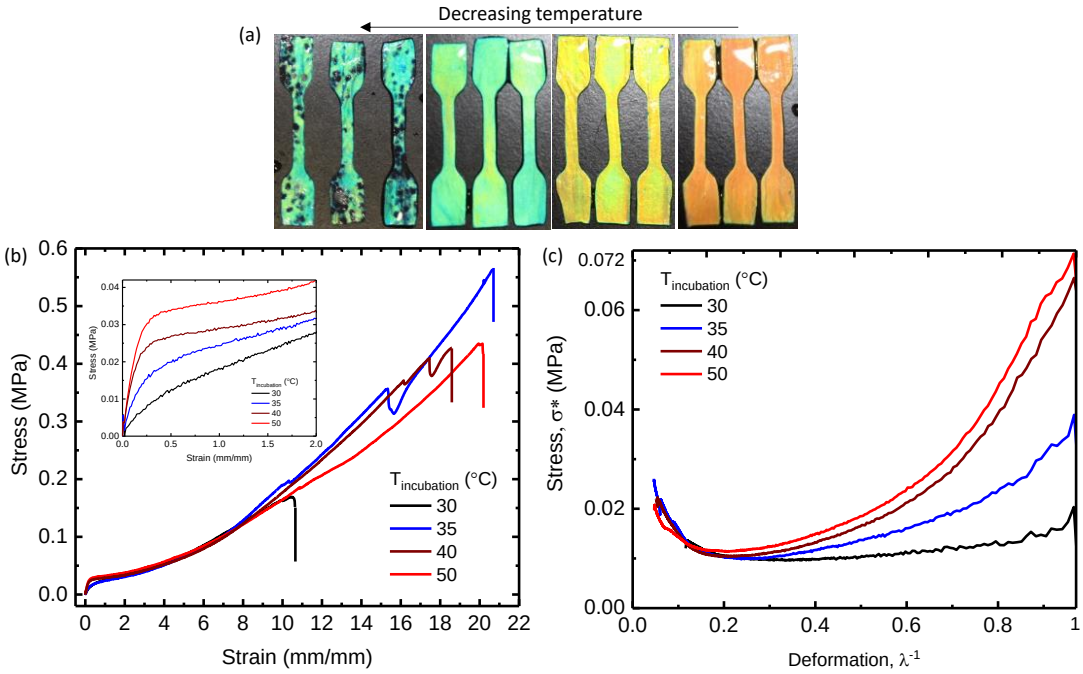

Figure 3.11 (a) Photographs of standard dumbbell shaped tensile test specimens cut out from gels synthesized at different incubation temperature. The gauge length (L), width (w) and thickness (t) are 12 mm, 2 mm and thickness dependent on gels synthesized at different temperature, respectively. (b) Stress-strain curves of PDGI/PAAm gels at different incubation temperature obtained from uniaxial tension tests. The inset figure is the enlarge region of yielding and stiffness area. (c) Mooney-Rivlin plot of the tensile result, where $\sigma^*=\sigma/(\lambda-\lambda^{-2})$ is the reduced stress and $\lambda=\varepsilon+1$ is the elongation ratio. The tests were performed for three times on each specimen, for clarity only the representative curves are shown.

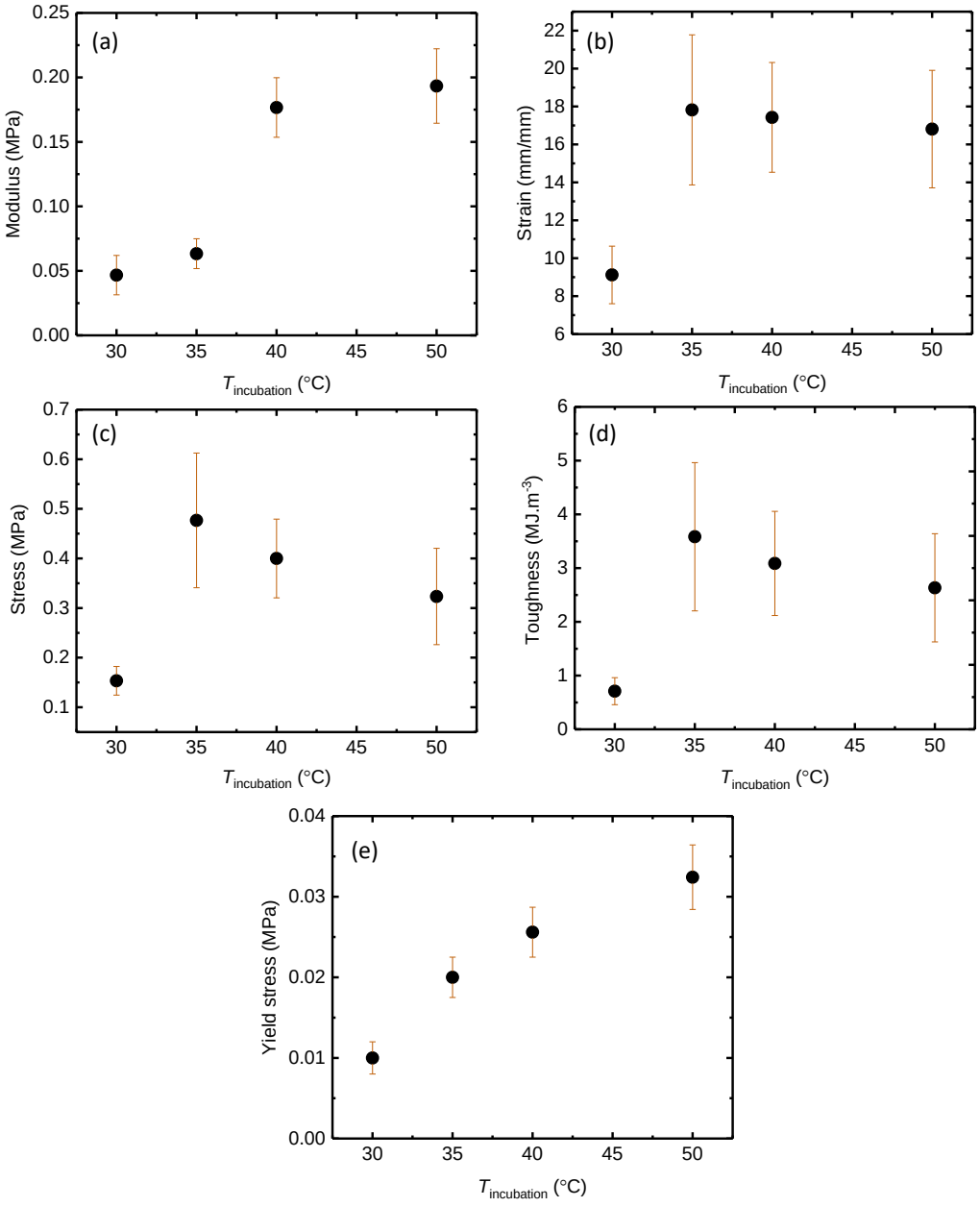

Figure 3.12 Summary of uniaxial tensile test results as a function of gels synthesis incubation temperature. (a) Young's modulus; (b) Fracture strain; (c) Fracture stress; (d) Toughness; (e) Yield stress of PDGI/PAAm gel. Where, $T_{incubation}$ is different incubation temperature for gel synthesis such as 50°C, 40°C, 35°C and 30°C, respectively.

CHAPTER 4

Structure and Properties Relationships

4.1 Water Triggered Ductile-Brittle Transition of Anisotropic Lamellar Hydrogels and Effect of Confinement on Polymer Dynamics

4.1.1 Introduction

Biological soft tissues, such as muscles and cartilages, containing 50-80 wt% of water, are soft and wet materials. The hydration plays important role in the dynamics and mechanical properties of the bio-tissues. The soft tissues usually become rigid upon dehydration to some critical water contents.[1–6] The mechanical transition behavior upon dehydration is quite similar to the glass transition of non-crystalline polymers.

Polymer hydrogels, consisting of three-dimensional cross-linked networks and a large amount of water (50–90%), are also soft and wet materials. Due to the substantial progresses in the development of highly strong and tough hydrogels in recent decade, hydrogels become promising materials for various applications, especially as biomaterials such as cartilages.[7–14]

In similar to biological tissues, polymer hydrogels also experience abrupt soft-rigid transitions upon dehydration.[15–17] Below a critical water content, the modulus of the polymer hydrogels dramatically increases. In accompany with the modulus change, the strength and toughness of the hydrogels also dramatically changes. Studies on the dehydration-induced mechanical transition of polymer hydrogels have been limited to isotropic, amorphous hydrogels from hydrophilic single or double networks.[16,17] Considering that the biological soft tissues have anisotropic, ordered microstructure of multi-components, it is an interesting topic to study the

dehydration-induced mechanical transition of hydrogels possessing ordered microstructures from hydrophobic and hydrophilic components.

We have developed anisotropic hydrogels with uniaxially aligned lamellar structure along the sheet-shaped sample direction (**Figure 4.1.1**).[18–24] This class of anisotropic hydrogels PDGI/PAAm consist of alternative stacking of uniaxially oriented poly(dodecyl glyceryl itaconate)(PDGI) bilayer membrane (4.7 nm thick) and the chemically crosslinked or non-crosslinked polyacrylamide (PAAm) hydrogel layer (several hundred nm thick).[18,24] The bilayers are rigid, impermeable to water, while the PAAm hydrogel layers are soft and stretchable. The lamellar hydrogels exhibit many unique behaviors, such as bright structure color, one dimensional diffusion and swelling[19], anisotropic mechanical properties, quasi-unidirectional shrinkage upon uniaxial stretching[20], high toughness and self-healing.[21] The structure color of the gels is tunable by small stress/strain, temperature, and pH.[22,23] Because of the structural anisotropy lamellar hydrogel closely resemble to that of natural bio-tissues such as skin and muscles. Therefore, a model system to mimic the various functions of natural bio-tissues.

In this part of chapter, the effect of water content on the structure and tensile behaviors of the PDGI/PAAm lamellar gels. The bilayers, being more rigid and brittle than the soft hydrogel layers, rupture at loading and reform at unloading, serving as reversible sacrificial bonds to dissipate energy, while the hydrogel layers maintain the elasticity. Therefore, the bilayer structures not only impart various anisotropic properties, but also serve as reversible sacrificial bonds to impart the soft materials toughness and self-healing.[21,24] Previous studies have shown that bulk PAAm hydrogels exhibit an abrupt mechanical transition, from soft rubbery state to rigid glassy-like state at ~20 wt% water content.[16] In the glassy-like state, no free water exists in the hydrated polymer. Therefore, tuning the water content in the PAAm layers are expected

to dramatically change the polymer dynamics of the PAAm and therefore, the mechanical properties of the lamellar hydrogels. One can expect that the water-impermeable bilayers act as rigid but viscoelastic component and the hydrophilic PAAm layers in rubbery state act as soft but elastic component in the highly-hydrated state. Upon dehydration to a level below the critical water content, the PAAm layers, in glassy state, act as hard and brittle component and the bilayers act as soft viscoelastic component. Such changes in the mechanical properties of the individual layers with dehydration will change the mechanical behaviors of the lamellar material and the energy dissipation mechanism. Furthermore, it is interesting to examine the effect of dehydration on the sub-microscale PAAm hydrogel layers intercalated between bilayers. In addition, given the water-impermeable nature of the bilayers and hydrophilic nature of the hydrogel layers, it is interesting to see the effect of dehydration on the swelling mismatching and the interaction at the interface between the two components, which are expected to strongly influence the stability and mechanical properties of the bilayer membranes. In this part of chapter, first the structure of the PDGI/PAAm lamellar gels at different water content obtained by using a slow dehydration method is studied. Then, the tensile behavior of these lamellar gels at different content is studied. Finally, the thermal behavior of water in these gels is studied by DSC. To understand the effect of dehydration on the PAAm hydrogel layers confined between the bilayers, the behavior of the bulk PAAm hydrogels at varied water content is also studied. The specific dehydration and mechanical behaviors of the PDGI/PAAm lamellar hydrogel are analyzed and discussed.

4.1.2 Experimental

4.1.2.1 Sample preparation

The multi-lamellar hydrogel, PDGI/PAAm, of large dimension (100×30×0.5 mm^3) was fabricated by modifying the method that described previously.[18] The precursor solution, composed of 0.1 M dodecyl glyceryl itaconate (DGI), 0.025 mol % sodium dodecyl sulfate (with respect to DGI monomer), 2.0 M acrylamide (AAm), 0.1 mol% *N*,*N*'-methylenebisacrylamide (MBAA) as chemical crosslinker of AAm, and 0.1 mol % Irgacure 2959 as initiator (both in relative to AAm monomers), was prepared in aqueous media (**Figure 4.1.2a**). The aforementioned precursor solution was kept in a temperature controlled water bath for ~5 h at 55°C to dissolve monomeric DGI powders and stabilize lyotropic liquid crystalline phases of DGI.[25] Then the precursor solution was moved to a glove box purged with argon gas to eliminate the dissolved oxygen. Before polymerization, a reaction cell of 100 mm in length (*L*), 30 mm in width (*W*), and 0.5 mm in thickness (*T*) was prepared by sandwiching a 0.5 mm –thick silicone rubber spacer between two glass plates. In the previous method we applied a shear flow to induce bilayer orientation by injecting the precursor solution manually to the reaction cell.[18] In this work we used a suction method to apply the shear flow. One end of the reaction cell was connected to a suction pump (model Harvard PHD 4400 programmable), and through the other end, the precursor solution was suctioned vertically to the reaction cell against the gravity at a high suction rate to induce a strong shear flow (~133 s^{-1}) (**Figure 4.1.2b).** This method permitted us to obtain a uniform DGI lamellar phase, even with 3 times the sample area of the previous method, oriented uni-axially along the glass walls. This was followed by a co-current homo-polymerization of the DGI and AAm using UV light irradiation for 8 hours at 50°C (**Figure 4.1.2c**). After the polymerization, the gel was removed from the reaction cell and was immersed in a large amount of water for 7 days to reach equilibrium swelling state and to

wash away the residual chemicals. PAAm hydrogels were synthesized by UV irradiation from a precursor solution containing 2.0 M AAm, 0.1 mol% MBAA, and 0.1 mol% Irgacure 2959 as initiator.

4.1.2.2 Dehydration experiment

For the dehydration experiment, the swollen gels were sandwiched between two glass plates separated by a silicone spacer and sealed in plastic with zipper bags at 25˚C. It was confirmed that the samples were not adhered on the glass plates. Under such confinement condition, dehydration of the PAAm hydrogel layers occurs homogeneously through slow evaporation of water from the periphery of the samples.

Two series of experiments were performed. In the first series of the experiment, a sample, cut into a disc of diameter D_0 = 6 mm with a weight of W_0 = 0.0540g, was sealed in the zipper bag. The sample was taken out from the zipper bag at various time intervals and its weight (W), diameter (D), and thickness (T) were measured, respectively, using a digital balance (Shimazu Co., Kyoto, Japan) and a caliper. The reflection spectrum was also measured. After the measurements, the sample was returned back to the zipper bag for further dehydration.

In the second series of the experiment, many samples were prepared and dehydrated to different water content by storage in the zipper bags for different periods of times. After certain period of drying, one sample was selected and cut into required sizes for determining the water content, the thermal property of water, and mechanical behavior.

4.1.2.3 Water content measurement

For determining the water content, ~10 mg piece of the gel was cut out from the large sample and was placed in aluminum pan, and quickly transferred to Thermogravimetric Analyzer (TGA, Thermo *plus* EVO II TG 8120). The measurement was performed by heating sample from 25°C

to 500°C at heating rate of 5°C/min. From the weight change as a function of temperature, the water content C_w of the gel is calculated at the initial regime (25-200°C) of weight change by using the following expression;

$$C_w(\%) = \frac{(m_s - m_d)}{m_s} x100\% \qquad (1)$$

Where, m_s and m_d are the mass of swollen and dried samples, respectively. For the PDGI/PAAm gels, to make a quantitative comparison with the behavior of the bulk PAAm gels, the water content in relative to the PAAm gel layers, $C_{w,\mathrm{PAAm}}(\%)$, was calculated from the $C_w(\%)$,

$$C_{w,PAAm}(\%) = \frac{(1+A)C_w}{C_w/100 + A} \qquad (2)$$

Here, A is the mass ratio of PAAm to PDGI in the PDGI/PAAm gel. In the current study, A=3.82. The volume fraction ϕ of PAAm in PAAm gel or in PAAm gel layer of the PDGI/PAAm gel is calculated from,

$$\phi^{-1} = 1 + \left(\frac{C_w}{100 - C_w}\right)\frac{\rho_p}{\rho_w} \qquad (3)$$

Here, $C_w(\%)$ is the water content in the bulk PAAm gels or that in relative to the PAAm gel layers of the lamellar gels, $\rho_p = 1.437 \pm 0.2\, g/cm^3$ and $\rho_w = 1\, g/cm^3$ are densities of PAAm and water, respectively.[26]

4.1.2.4 DSC measurement

To elucidate the thermal property of water in the gels at different water content, differential scanning calorimeter (DSC X-7000) coupled with a cooling device was used. Samples were

hermetically sealed in aluminum pan, rapidly cooled to -80°C and heated to 500°C and then followed by cooling (500°C to -80°C) cycles, at a constant heating and cooling rate of 10°C/min. The temperature at which the water changes phase from solid to liquid was considered from the minima of corresponding endotherms. The amount of free water that freezes around 0°C was calculated according to the following expression;

$$W_{H_2O}(\%) = \frac{\Delta H_{m,gel}}{\Delta H_{m,H_2O}} x100\% \qquad (4)$$

Where, $W_{H_2O}(\%)$, $\Delta H_{m,gel}$ and $\Delta H_{m,H_2O}$ are free water content in relative to the total weight of the sample, melting enthalpy (J/g) of the gels calculated from area under the endotherm around 0°C, and the melting enthalpy of ice (334 *J*/g) as standard, respectively. Each data was measured for three times and the average was adopted.

4.1.2.5 Measurement of reflection spectrum

The structure color of PDGI/PAAm gels with different water content was characterized by the electromagnetic spectrum of light, using moveable angle reflection measurement optics (Hamamatsu Photonics KK, C10027A10687) coupled with photonic multichannel analyzer (Hamamatsu Photonics KK, C10027). White light from Xe source was used to irradiate the gel. Reflection spectrum was acquired by keeping both the angles of incident (Bragg's angle) and reflection at 60°. The wavelength at maximum reflection intensity, λ_{max}, was obtained from the reflection spectrum. The inter-lamellar distance (*d*) was estimated by using the Bragg's law of diffraction,

$$\lambda_{max} = 2nd\sin\theta \qquad (5)$$

Here *n* is the refractive index of water (1.33) and θ is the Bragg's angle (60°).[20]

4.1.2.6 Small angle X-ray diffraction (SAXD) measurements

SAXD measurements were performed at the BL40B2 of SPring-8 (JASRI, Japan). A substantially dehydrated PDGI/PAAm sample (diameter: 6 mm, thickness: 0.1 mm) was fixed horizontally and irradiated with 0.1 nm wavelength X-ray of 12.4 keV energy beam (horizontal 200 μm x vertical 200 μm) at room temperature for 2 s. The 2D diffraction pattern was recorded on an imaging intensifier coupled with imaging camera (camera length: 2.30 m).

The 2D diffraction image is converted to 1D data using Fit2D (V12.077) data analysis software.[27] From the q value of the 1st order peak the interlayer distance, d was calculated as $d = 2\pi/q$, where q is the scattering vector.

4.1.2.7 Measurement of mechanical properties

The dumb-bell shaped gel specimens, of standard dimension (gauge length, L = 12 mm width, W = 2 mm and thickness, T = at drying time), were cut out from the samples of different water content with a standard gel cutter (model JIS-K6251-7). The tensile tests were performed using tensile tester (Instron Anton Paar 5965) with deformation velocity 100 mm/min, corresponding to a strain rate 0.14 s^{-1}. The Young's modulus was calculated from the initial slope of the tensile stress-strain curves within 5% elongation. The results of tensile stress-strain curves are the average of three runs on each sample.

4.1.3 Results and Discussion

The as-prepared lamellar gels, 0.5 mm thick (T_0), were transparent. After immersing in water, the samples only swelled in thickness direction and reached a thickness 1.16~1.31 mm (T_{sw}), which slightly varied with the sample synthesis batches, at equilibrium swelling. The fully swollen PDGI/PAAm hydrogels had a water content of 94~96% in respect to the PAAm layer, exhibiting visible color with a λ_{max} peak at 556~673 nm in the optical reflection spectrum. From

the Bragg's law, the interlayer distance *d* is estimated as 230~278 nm. From the sample thickness and the interlayer distance *d*, the number of bilayers in the lamellar gels is estimated as *c.a.* 5000.

4.1.3.1 Anisotropic dehydration of bilayer hybrid gel

A series of the dehydrated PDGI/PAAm hydrogels was obtained by slow dehydration for several hundred hours. **Figure 4.1.3a** shows weight and dimension changes of the PDGI/PAAm hydrogels with their dehydration time. The weight (*W*) and thickness (*T*) of the samples decreased with the dehydration time while the lateral dimension (*D*) maintained constant. It should be noticed that the time profiles in **Figure 4.1.3a** do not reflect the drying kinetics at a constant humidity condition, given the drying protocol used in this study. **Figure 4.1.3b** shows the linear relationship between thickness and weight of the dehydrated PDGI/PAAm hydrogels, which confirms the perfect one dimension shrinkage upon dehydration. This perfect one-dimensional shrinkage suggests that the bilayers maintain the original layered structure even after dehydration. This suggestion has been also confirmed by SEM observation of the substantially dehydrated sample, which shows well-aligned and smooth layer structure (**Figure 4.1.4a**). The well-maintained structure is owing to the very slow dehydration process under the confined drying condition. The samples dehydrated in air without any confinement show a rough surface and undulation of the layered structure due to rapid dehydration (**Figure 4.1.4b**).

4.1.3.2 Probing anisotropic dehydration of confined gel layer

Consequently, the layered structure in the dehydrated PDGI/PAAm gels was analyzed. In concomitant with the anisotropic dehydration, the diffraction color of the gels shifted from orange to violet, and then to transparent as shown by the photographs of the samples and the corresponding reflection spectra (**Figure 4.1.5a**). The reflection peak wave length (λ_{max}) shifted

from ~560 nm to ~300 nm with the decreasing of water content $C_{w,\,PAAm}$ from 96% to 51%. Additionally, in order to characterize the structure for the highly-dehydrated sample that does not show structure color, the SAXD was performed on the sample of $C_{w,\,PAAm}$ = 14%. The 2D SAXD image shows a perfectly- anisotropic pattern (**Figure 4.1.5b**), and the scattering data show three clear peaks that can be assigned as the 1st order, 2nd order, and 3rd order reflections of lamellar layers of interlayer distance d =18.53 nm (**Figure 4.1.5b**). From the optical reflection and the SAXD spectra, we can quantitatively estimate the inter-bilayer spacing (d) of the gels. The d values are plotted against the relative sample thickness (T/T_0), where T_0 is the sample thickness at the as-prepared state. All the data, obtained from optical reflection experiment as well as SAXD measurement, fall on the same linear line, as shown in **Figure 4.1.5c**. This linear relationship confirms that the sample maintains the one-dimensional shrinkage even up to substantially dehydrated state.

4.1.3.3 Ductile-Brittle transition of bilayer hybrid gel

To decipher the effect of dehydration on the mechanical properties of PDGI/PAAm gels, the tensile tests were performed on the gels along the bilayer direction at various water contents. The water content of the gels was determined by TGA (**Figure 4.1.6a,b**). The samples used for the tensile test contains 94% of water in relative to the PAAm layers at the equilibrium swollen state, and photographs of the dumbbell-shaped samples at different water contents are shown in **Figure 4.1.6c**. The stress-strain curves of the PDGI/PAAm samples with varied water content in the PAAm gels layers are shown in **Figure 4.1.7**. For comparison, the results of bulk PAAm hydrogels are shown in **Figure 4.1.8**. The modulus, yield stress, fracture stress, and fracture strain, and toughness of these samples are summarized in **Figure 4.1.9a**,**b**,**c**,**d**,**e**, respectively.

First, we look at the behaviors of the bulk PAAm hydrogels. As shown in **Figure 4.1.8a**, the bulk PAAm gels showed a gradual increase of modulus, fracture stress, and fracture strain upon

dehydration until the water content was reduced to a value of 26%. Further dehydration to 22% water content induced an abrupt increase in modulus and a decrease in fracture strain, indicating the occurrence of ductile-brittle transition. At 12% water content, the sample became extremely rigid and brittle (modulus ~3 GPa, and fracture strain 0.03), as shown in **Figure 4.1.8b**.

The lamellar hydrogel also showed change of the mechanical properties, from soft/stretchable to rigid/brittle, upon dehydration (**Figure 4.1.7a, b**). The modulus and yield stress both increased with the dehydration (**Figure 4.1.9a**, **b**). However, the fracture stress kept almost constant until to 14% water content (**Figure 4.1.9c**). Another feature of the lamellar hydrogel is that the fracture strain monotonously decreased with the dehydration (**Figure 4.1.9d**). These behaviors are quite different from those of the pure PAAm gel that did not show yielding phenomenon but exhibited increase in fracture strain with the dehydration until the occurrence of the ductile-brittle transition at 22% water content (**Figure 4.1.8, Figure 4.1.9d)**. Compared with the high water content region (94%-61%), in the medium water content region (46%-22%), the lamellar sample exhibited rapid increase in the modulus and the yield stress and rapid decrease in the fracture strain upon the dehydration (**Figure 4.1.9a, b, d**). Moreover, the strain-hardening phenomenon disappears, instead, a pronounced necking phenomenon was observed. The necking became more obvious for the 22% water content sample. At the low water content (14%), the lamellar gel became very rigid and brittle (Modulus ~2 GPa, fracture stress ~50 MPa, fracture strain 0.03), almost the same as the rigid and brittle PAAm sample with 12% water content.

To better understand the tensile behaviors, the tensile data for the lamellar gels and PAAm gels are shown by the Mooney–Rivlin plots, respectively, in **Figure 4.1.7c** and **Figure 4.1.8c**. When the water content is above the critical values, 60% for lamellar gels and 22% for PAAm gels, the samples exhibited plateau regions at large elongation, which might correspond to ideal

rubbery-like behaviors from the PAAm hydrogels, as featured by strain-hardening at the extreme elongation before fracture due to finite extensibility effect.

The work of extension, W_{ext}, estimated from area under the tensile stress-strain curves of the gels, is summarized in **Figure 4.1.9e**. As W_{ext} is the energy density dissipated by the sample fracture (J/m^3), it is a measure of the soft material toughness. The PDGI/PAAm lamellar gels exhibited almost a constant W_{ext} around 2.5 MJ/m^3 upon dehydration, until the water content was decreased to 22%. The W_{ext} of PAAm samples were very low at high water content, and it increased upon dehydration reaching the same level of the lamellar gels, due to the increase of the fracture stress and fracture strain, as shown in **Figure 4.1.8**.

4.1.3.4 Enhanced quantity of bound water

The above results suggest that the ductile-brittle transition occurred around a water content as high as 60% in the lamellar gels and gels contain more non-mobile, bound water, in comparison to the PAAm gels. To verify such speculation, DSC was performed on PDGI/PAAm and PAAm gels of different water content, as shown in **Figure 4.1.10(a)** and **4.1.10(b)**, respectively. Therein the melting heat of water decreased by the dehydration of the gels. The melting peak of water in PDGI/PAAm was observed for the water content range of 94-61% while below 61%, no peak was observed [**Figure 4.1.10a,c,d**]. In comparison, PAAm gels showed melting peak of water up to 26% water content [**Figure 4.1.10b,c,d**]. From the DSC analysis, PDGI/PAAm gels contain more bound water than PAAm, which is well in agreement with their mechanical behaviors.

4.1.3.5 Probing Ductile-Brittle transition of confined gel layer

To analyze the modulus change of PAAm gel layers upon dehydration in the lamellar gels, we use a stratified layer structure model (**Figure 4.1.11a**).[28] The bulk modulus E of PDGI/PAAm

gels can then be correlated with the individual layer modulus of PDGI bilayer and PAAm hydrogel layer by the following equation.

$$E = \frac{(E_D h_D + E_A h_A)}{(h_D + h_A)} \qquad (6)$$

Where, E_D and h_D are the modulus and the thickness of single PDGI bilayer, respectively; E_A and h_A are the modulus and the thickness of single PAAm gel layer in PDGI/PAAm gel, respectively; $h_A + h_D = d$ is the inter-lamellar distance. According to previous literature, the modulus of PDGI bilayer, E_D, is 5 MPa.[18] We assume E_D is independent of water content of the gel since the PDGI bilayers in the lamellar gels maintained its layered structure even at low water content. The modulus of PAAm gel layer (E_A) in PDGI/PAAm gels at various water contents was calculated from the bulk modulus E of the hybrid gel shown in **Figure 4.1.9a** and **Figure 4.1.11a,b** using equation (6). In the calculation, the modulus (E_D) and thickness (h_D) of single PDGI bilayer were fixed as ~5 MPa and ~4.7 nm, respectively, according to literature.[29] The thickness of PAAm gel layer (h_A) was estimated from the inter-lamellar distance d, where d was determined from the reflection spectra or the SAXD result.

Figure 4.1.11c shows the log-log plot of the modulus of PAAm gel layer E_A and the PAAm volume fraction ϕ of the lamellar gels. Two power law regions were observed for the lamellar gels; that is, $E_A \sim \phi^{1.0}$ and $E_A \sim \phi^{10}$ for ϕ less and larger than 0.38 (Cw=58%), respectively. For the PAAm bulk gels, two power law regions were also observed as shown in **Figure 4.1.11c**; that is, $E \sim \phi^{0.90}$ and $E \sim \phi^{45}$ for ϕ less and larger than 0.66 (Cw=26%), respectively. The approximately linear correlation of E and ϕ in low ϕ range is in consistent with previous reports.[14,17] The low ϕ range and high ϕ range should correspond to the rubbery state and glassy

state of PAAm strands, respectively. It should be mentioned that linear dependence of modulus on the PAAm volume fraction is stronger than the theoretical value of $E \sim \phi^{-1/3}$ for swollen gels with Gaussian strands.[30]

The behaviors of the bulk PAAm and the PAAm gel layer have three remarkable differences. First, the PAAm gel layers in the lamellar gels showed a rubbery-glassy transition at a much lower polymer volume fraction, ϕ=0.38 (*Cw*=58%), than that of bulk PAAm gels, ϕ=0.66 (*Cw*=26%). Second, the modulus of PAAm gel layers in the rubbery state is about one order larger in magnitude than that of the bulk PAAm gels. Third, the modulus increase of the PAAm gel layers with dehydration in the glassy state is less abrupt in comparison with the bulk PAAm system.

For the first difference, the critical water contents, 58% for lamellar gels and *c.a.* 26% for bulk PAAm gels, for the rubbery-glassy transition determined from the behavior of modulus are very well in agreement with the results from DSC. The results indicate that the state of water strongly influences the dynamics and the mechanical behavior of the polymer network. For the bulk PAAm sample, the 26% water content corresponds to the molar composition of AAm: water=1:1.4, which means that when one AAm unit has 1.4 or less hydrated water molecules, the polymers lose mobility and become glassy-like. For the PDGI/PAAm sample, 58% water content in the PAAm gel layer corresponds to the molar composition AAm: DGI: water=20:1:130. Even if we assume that each hydrophilic head of the DGI molecules hydrates several water molecules, the number of hydrated water molecules per AAm is estimated as *c.a.* 6.5 (=130/20). This suggests that the polymers start to lose mobility and become glassy-like when the hydrated water is less than 6.5 molecules per AAm unit. This number is much larger than the bulk sample, indicating that PAAm gel layers confined between bilayers have very different structure of water from that of the bulk PAAm hydrogels. For the water content range

of 58% ~ 14%, the thickness of the PAAm gel layers is in the range of 52 nm ~ 14 nm. Although the phenomenon on confinement-induced ordering of water molecules have been reported, these ordering are in nano-scale.[31,32] Such long-range ordering of water in confined hydrogel layers in decades of *nano-scale* is firstly observed.

The second difference, the one order in magnitude high modulus E_A of the PAAm gel layers comparing to that of the bulk PAAm gels in the rubbery state, might attribute to a strong mechanical confinement effect of the PAAm gel layers between two bilayers. Previous studies have shown that the PDGI and PAAm are not covalently connected.[33] Furthermore, recent study has suggested that the PDGI bilayer and the PAAm hydrogel layer are connected by the physical adsorption of PAAm chains on the PDGI bilayer membranes via hydrogen bond formation.[24] It is reported that the polymer adsorption on a surface has a self-similar structure, and the concentration of adsorbed polymer layer decreases with the increase in the distance to the adsorbed surface.[34] This means that the PAAm concentration, and therefore the modulus, near the bilayer surface are higher than the average values while that in the middle region are less than the average values. This assumption can also explain the reason of the third difference, the less abrupt increase of the modulus of the PAAm gel layer than the bulk PAAm in the glassy state. Probably, the rubbery-glassy transition of the PAAm gel layer starts from the bilayer surface and then develops into the middle regions gradually upon dehydration. As a result, the PAAm gel layers shows a less abrupt rubbery-glassy transition at much higher water content in comparison with the bulk PAAm gels that have a homogeneous polymer structure. In summary, several experimental phenomena can be explained by this gradient polymer adsorption effect.

This gradient polymer adsorption effect can explain other phenomena of the PDGI/PAAm gels. The first phenomenon is the perfect one-dimensional shrinkage. It is expected that the bilayers experience biaxial tensile at swollen state ($T/T_0>1$) and compression at deswollen state ($T/T_0<1$).

The former destabilizes the bilayers and the latter has effect to induce buckling instability. The perfect one-dimensional dehydration suggests that the interfacial mismatching has been relaxed during the very slow dehydration process. If the adsorbed polymer chains are dynamic, the interfacial stress should be relaxed and isotropic shrinkage of the PAAm hydrogel layers should occur via the very slow dehydration process, which is not the case. This result suggests that the PAAm chains are strongly pinned to the bilayers to prevent the global isotropic shrinkage during the slow dehydration. Although we could not exclude the possibility of entanglement or trapping of the PAAm chains in the PDGI layers, the dominant pinning mechanism is probably due to the glassy state of the adsorption layer. The second phenomenon is the dramatic increase in the yield stress upon dehydration. The yielding of the lamellar gels at high water content could be related to the stress-induced flow of the bilayers that has a cloudy point at ~43°C, which is above the observation temperature.[35] The increase in the yield stress with the dehydration suggests that the stability of the bilayers is enhanced by dehydration (**Figure 4.1.9b**). Although the biaxial compression exerted on the bilayers by dehydration in the PAAm gel layers will increase bilayer stability, however, it is apparent that this mechanism alone could not explain the substantial increase in the yield stress at water content <60%. Again, the glassy state of the adsorption layer supports this substantial increase in the yield stress. It is conjected that, the yield stress at $C_{W,\ PAAm}$ <60% comes from the glassy state of PAAm. The third phenomenon is the decrease of the fracture strain with the increase of dehydration, which is opposite to the behavior of the PAAm bulk gels (**Figure 4.1.9d**). The self-similar adsorption mechanism would bring about more adsorption of the PAAm chains on the bilayer surface upon dehydration, which reduces the extensibility of the samples.

4.1.4 Conclusion

We show that the lamellar structure is well-maintained by a slow dehydration process, and with the progress of dehydration, the PAAm hydrogel layers shrink only in the thickness direction, and neither the delamination at the interface nor the buckling of the hard bilayers occurs. The PAAm gel layer in the lamellar hydrogels shows the rubbery-glassy transition at 58% water content, much higher than that of the bulk PAAm samples at 26% **(Figure 4.1.12).** At this transition point, the thickness of the hydrated PAAm gel layer was as high as ~52 nm. In accompany with such transition, the free water in the lamellar gels is found disappeared. These results indicate the long-range ordering of water in the lamellar hydrogels, which is observed for the first time.

4.1.5 References

[1] Y. C. Fung, *Biomechanics : Mechanical Properties of Living Tissues*; Springer-Verlage: New York, 1993.

[2] S. J. Ulijaszek, F. E. Johnston, M. A. Preece, *The Cambridge Encyclopedia of Human Growth and Development*; 1st ed.; Cambridge University Press, 1998.

[3] N. Koshoubu, H. Kanaya, K. Hara, S. Taki, E. Takushi, K. Matsushige, *Japanese Journal of Applied Physics* **1993**, *32*, 4038.

[4] M. Annaka, T. Matsuura, S. Maruoka, N. Ogata, *Soft Matter* **2012**, *8*, 8157.

[5] A. Nakamura, K. Hara, A. Matsumoto, N. Hiramatsu, *Japanese Journal of Applied Physics, Part 1: Regular Papers and Short Notes and Review Papers* **1998**, *37*, 4931.

[6] E. Takushi, L. Asato, T. Nakada, *Nature* **1990**, *345*, 298.

[7] J. P. Gong, Y. Katsuyama, T. Kurokawa, Y. Osada, *Advanced Materials* **2003**, *15*,

1155.

[8] T. L. Sun, T. Kurokawa, S. Kuroda, A. Bin Ihsan, T. Akasaki, K. Sato, M. A. Haque, T. Nakajima, J. P. Gong, *Nature Materials* **2013**, *12*, 932.

[9] Y. Zhao, T. Nakajima, J. J. Yang, T. Kurokawa, J. Liu, J. Lu, S. Mizumoto, K. Sugahara, N. Kitamura, K. Yasuda, A. U. D. Daniels, J. P. Gong, *Advanced Materials* **2014**, *26*, 436.

[10] H. J. Zhang, T. L. Sun, A. K. Zhang, Y. Ikura, T. Nakajima, T. Nonoyama, T. Kurokawa, O. Ito, H. Ishitobi, J. P. Gong, *Advanced Materials* **2016**, *28*, 4884.

[11] J.-Y. Sun, X. Zhao, W. R. K. Illeperuma, O. Chaudhuri, K. H. Oh, D. J. Mooney, J. J. Vlassak, Z. Suo, *Nature* **2012**, *489*, 133.

[12] M. A. Haque, T. Kurokawa, J. P. Gong, *Polymer* **2012**, *53*, 1805.

[13] M. J. Glassman, R. K. Avery, A. Khademhosseini, B. D. Olsen, *Biomacromolecules* **2016**, *17*, 415.

[14] K. Sato, T. Nakajima, T. Hisamatsu, T. Nonoyama, T. Kurokawa, J. P. Gong, *Advanced Materials* **2015**, *27*, 6990.

[15] T. Tominaga, K.-I. Sano, J. Kikuchi, H. Mitomo, K. Ijiro, Y. Osada, *ACS Macro Letters* **2012**, *1*, 432.

[16] T. Masuike, S. Taki, K. Hara, S. Kai, *Japanese Journal of Applied Physics* **1995**, *34*, *Part 1*, 4997.

[17] H. Itagaki, T. Kurokawa, H. Furukawa, T. Nakajima, Y. Katsumoto, J. P. Gong, *Macromolecules* **2010**, *43*, 9495.

[18] M. A. Haque, G. Kamita, T. Kurokawa, K. Tsujii, J. P. Gong, *Advanced Materials* **2010**, *22*, 5110.

[19] K. Mito, M. A. Haque, T. Nakajima, M. Uchiumi, T. Kurokawa, T. Nonoyama, J. P. Gong, *Polymer* **2017**, 1.

[20] T. Nakajima, C. Durand, X. F. Li, M. A. Haque, T. Kurokawa, J. P. Gong, *Soft matter* **2015**, *11*, 237.

[21] M. A. Haque, T. Kurokawa, G. Kamita, J. P. Gong, *Macromolecules* **2011**, *44*, 8916.

[22] Y. Yue, T. Kurokawa, M. A. Haque, T. Nakajima, T. Nonoyama, X. Li, I. Kajiwara, J. P. Gong, *Nature communications* **2014**, *5*, 4659.

[23] Y. F. Yue, M. A. Haque, T. Kurokawa, T. Nakajima, J. P. Gong, *Advanced Materials* **2013**, *25*, 3106.

[24] X. Li, T. Kurokawa, R. Takahashi, M. A. Haque, Y. Yue, T. Nakajima, J. P. Gong, *Macromolecules* **2015**, *48*, 2277.

[25] K. Naitoh, Y. Ishii, K. Tsujii, *Journal of Physical Chemistry* **1991**, *95*, 7915.

[26] T. Tominaga, V. R. Tirumala, S. Lee, E. K. Lin, J. P. Gong, W. L. Wu, *Journal of Physical Chemistry B* **2008**, *112*, 3903.

[27] A. Hammersley, *European Synchrotron Radiation Facility Internal Report ESRF97HA02T*; European Synchrotron Radiation Facility, 1997.

[28] M. A. Haque, J. P. Gong, *Reactive and Functional Polymers* **2013**, *73*, 929.

[29] M. A. Haque, T. Kurokawa, J. P. Gong, *Soft Matter* **2013**, *9*, 5223.

[30] M. Rubinstein, R. H. Colby, *Polymer physics.*; Oxford University Press, 2003.

[31] U. Raviv, J. Klein, *Science* **2002**, *297*.

[32] U. Raviv, P. Laurat, J. Klein, *Nature* **2001**, *413*, 51.

[33] J. Ozawa, G. Matsuo, N. Kamo, K. Tsujii, *Macromolecules* **2006**, *39*, 7998.

[34] P. G. de Gennes, *Macromolecules* **1981**, *14*, 1637.

[35] K. Tsujii, M. Hayakawa, T. Onda, T. Tanaka, *Macromolecules* **1997**, *30*, 7397.

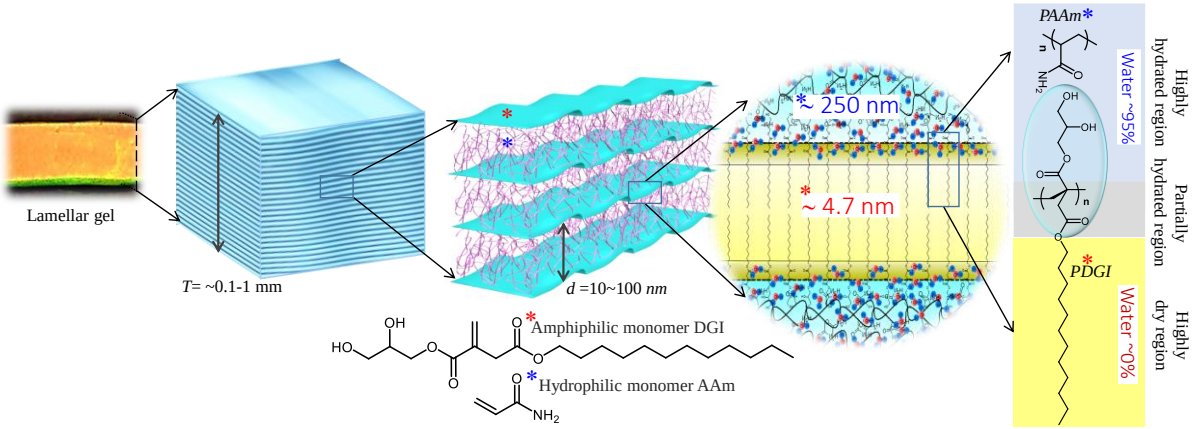

Figure 4.1.1 Schematic demonstration of anisotropic lamellar PDGI/PAAm gels, synthesized by a co-current homo-polymerization of the amphiphilic monomer dodecyl glyceryl itaconate (DGI) and hydrophilic monomer acrylamide (AAm).

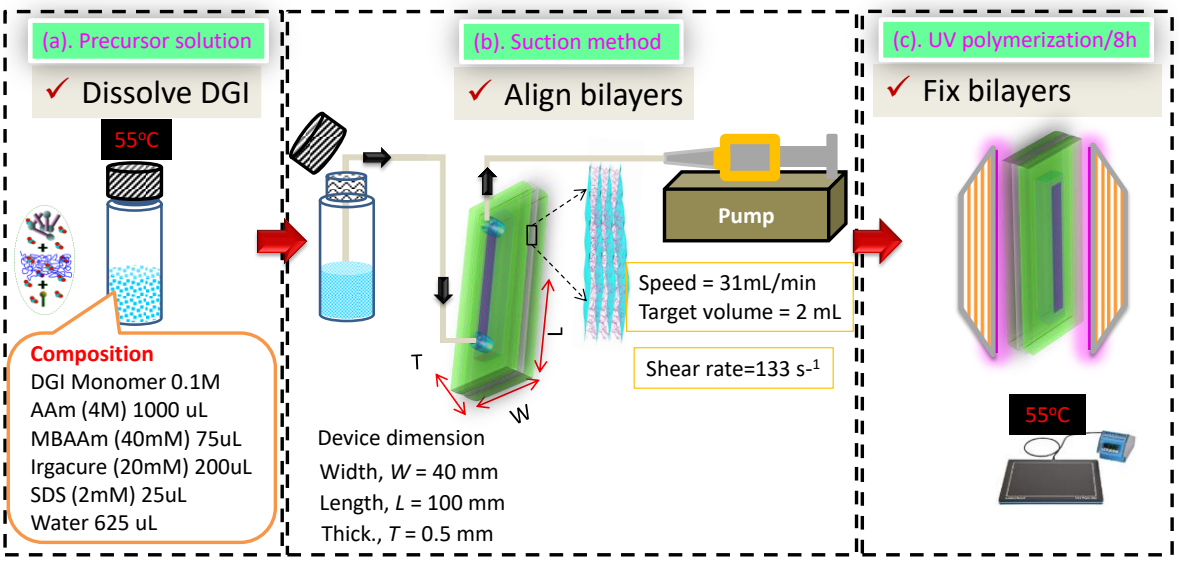

Figure 4.1.2 Schematics representation of anisotropic lamellar hydrogel. The method is comprise of three major steps. (a) Precursor solution preparation. (b) Applying suction to induce bilayer alignment by shear flow. (c) Polymerization by UV to start gelation for the bilayers fixing in hybrid gel. Temperature from solution to polymerization is constant.

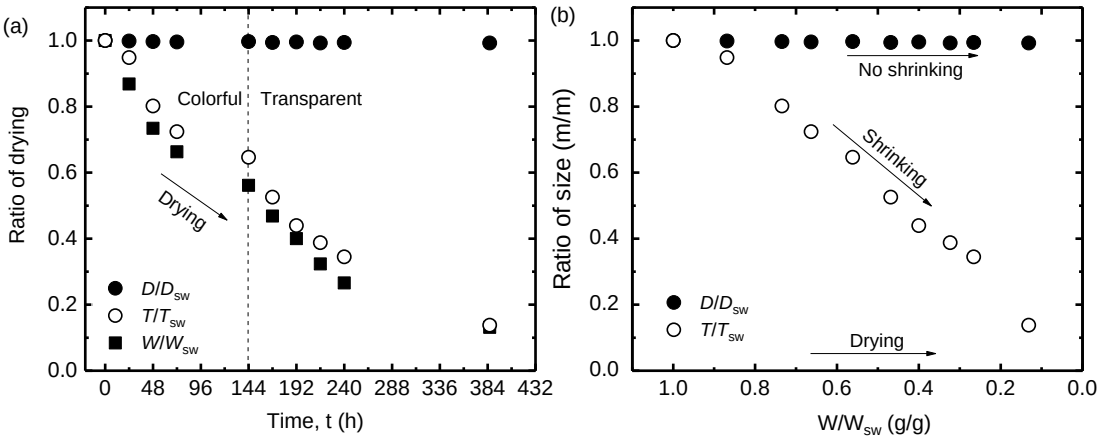

Figure 4.1.3 Confined drying generated size and weight changes of the sample. (a) Diameter *D*, thickness *T*, and weight *W* as a function of drying time. D_{sw}, T_{sw}, and W_{sw} are, respectively, the diameter, thickness, and weight of the sample at equilibrium swelling. (b) The correlation between the thickness and weight change.

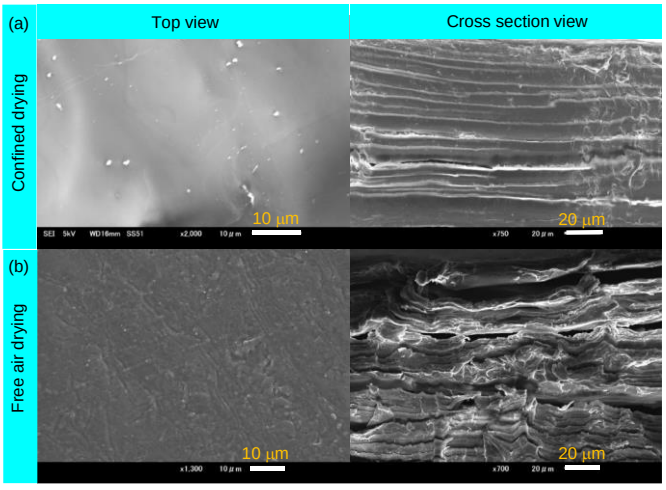

Figure 4.1.4 SEM micrographs of PDGI/PAAm gel (a) Confined dry and (b) Free air drying, respectively. Drying in confinement results in a relatively flat surface from top observation and uniform cross section, respectively. While open air drying causes the PAAm gel layer to

relax slightly faster as a result surface wrinkles and undulation of bilayer can be observe on top and cross section, respectively.

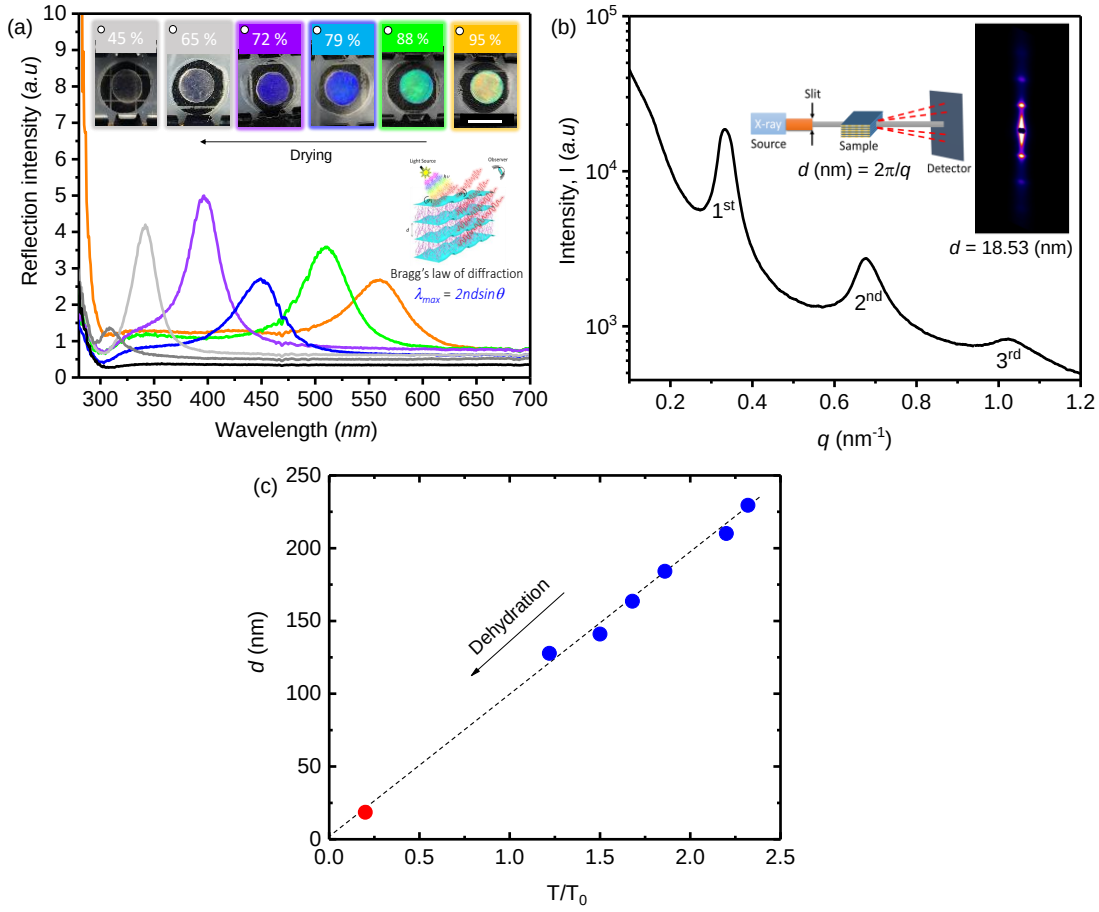

Figure 4.1.5 (a) Reflection spectra of PDGI/PAAm hydrogel as a function of wavelength, taken at different time intervals during confined dehydration. The visual color change can be perceived from the images given inside the graph. The scale bar is 1 cm. (b) SAXS measurement geometry for the substantially dehydrated sample and the 2D SAXS scattering image showing anisotropic pattern. Scattering data show three clear peaks, assigned as the 1st order, 2nd order, and 3rd order reflection peaks of lamellar layers of interlayer distance d=18.53 nm. (c) The d values obtained from optical reflection measurement and SAXS measurement against the sample thickness T. T_0 is the thickness of the sample at the as-prepared state.

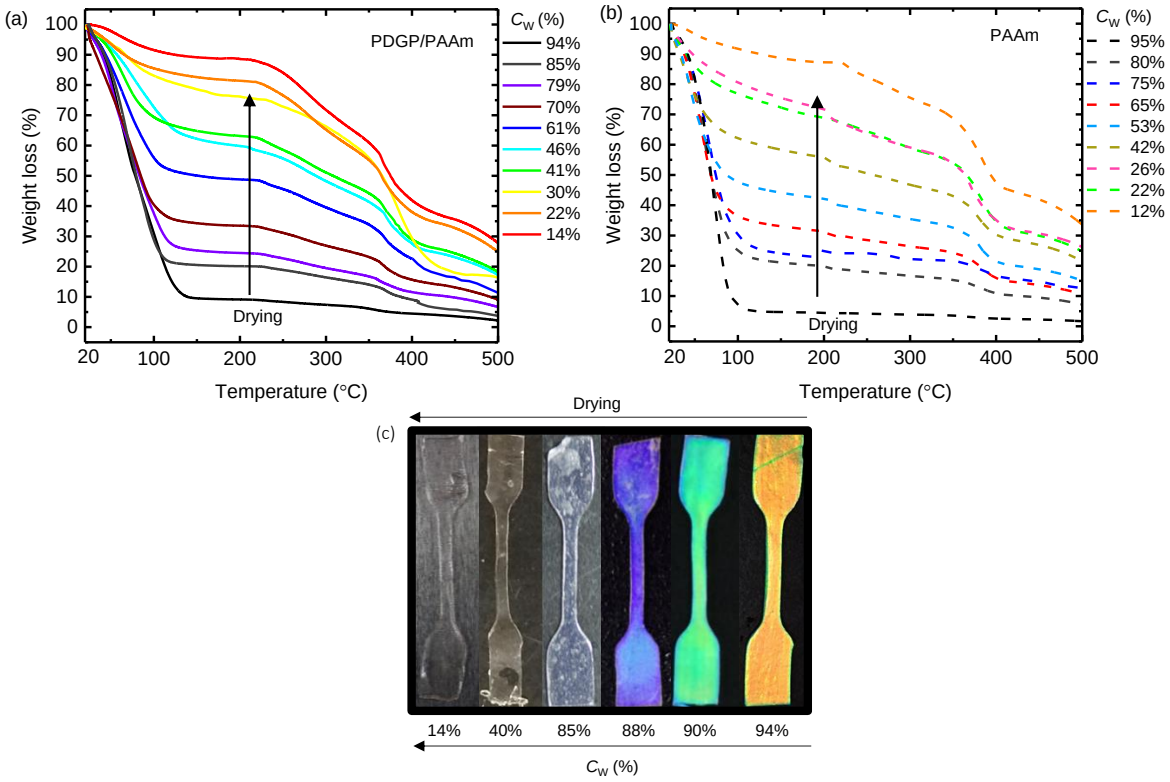

Figure 4.1.6 Weight loss % as a function of temperature at different water content gels obtained from Thermogravimetric analysis. (a) PDGI/PAAm gels (b) PAAm gels. Water content is calculated from the initial weight reduction at temperature range of 25- 200°C. (c) Photographs of standard dumbbell shaped tensile test specimens cut out from different water content of PAAm gel layer in PDGI/PAAm gels. The gauge length (l), width (w) and thickness (t) are 12 mm, 2 mm and thickness dependent on water content during drying, respectively.

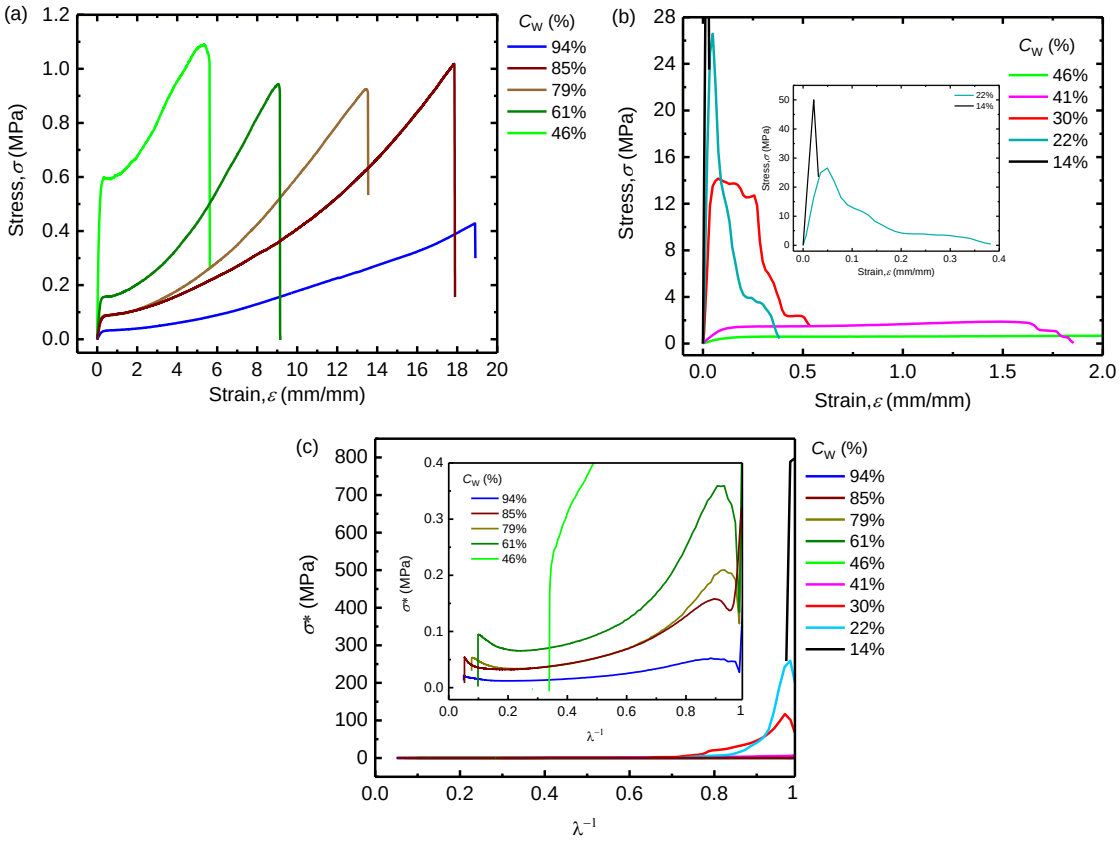

Figure 4.1.7 Stress-strain curves of anisotropic PDGI/PAAm gels at different water content obtained from uniaxial tension tests. (a) high water content region; (b) low water content region; (c) Mooney-Rivlin plot of the tensile result, where $\sigma^*=\sigma/(\lambda-\lambda^{-2})$ is the reduced stress and $\lambda=\varepsilon+1$ is the elongation ratio. The tests were performed for three times on each specimen, for clarity only the representative curves are shown. For clarity the transition region is enlarged and inserted in (b) and (c), respectively.

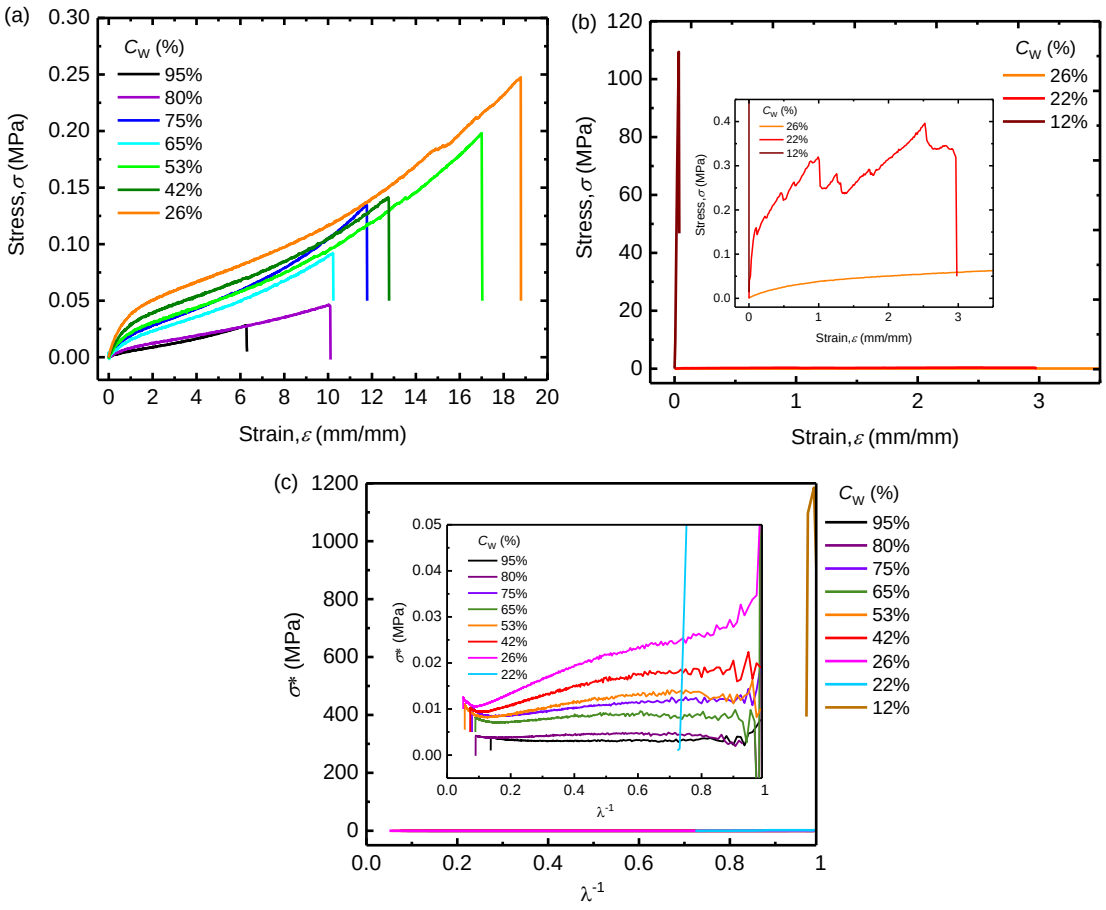

Figure 4.1.8 Stress-strain curves of isotropic PAAm gels at different water content obtained from uniaxial tension tests. (a) high water content region; (b) low water content regions; (c) Mooney-Rivlin plot of the tensile result, where $\sigma^*=\sigma/(\lambda-\lambda^{-2})$ is the reduced stress and $\lambda=\varepsilon+1$ is the elongation ratio. The tests were performed for three times on each specimen, for clarity only the representative curves are shown. For clarity the transition region is enlarged and inserted in (b) and (c), respectively.

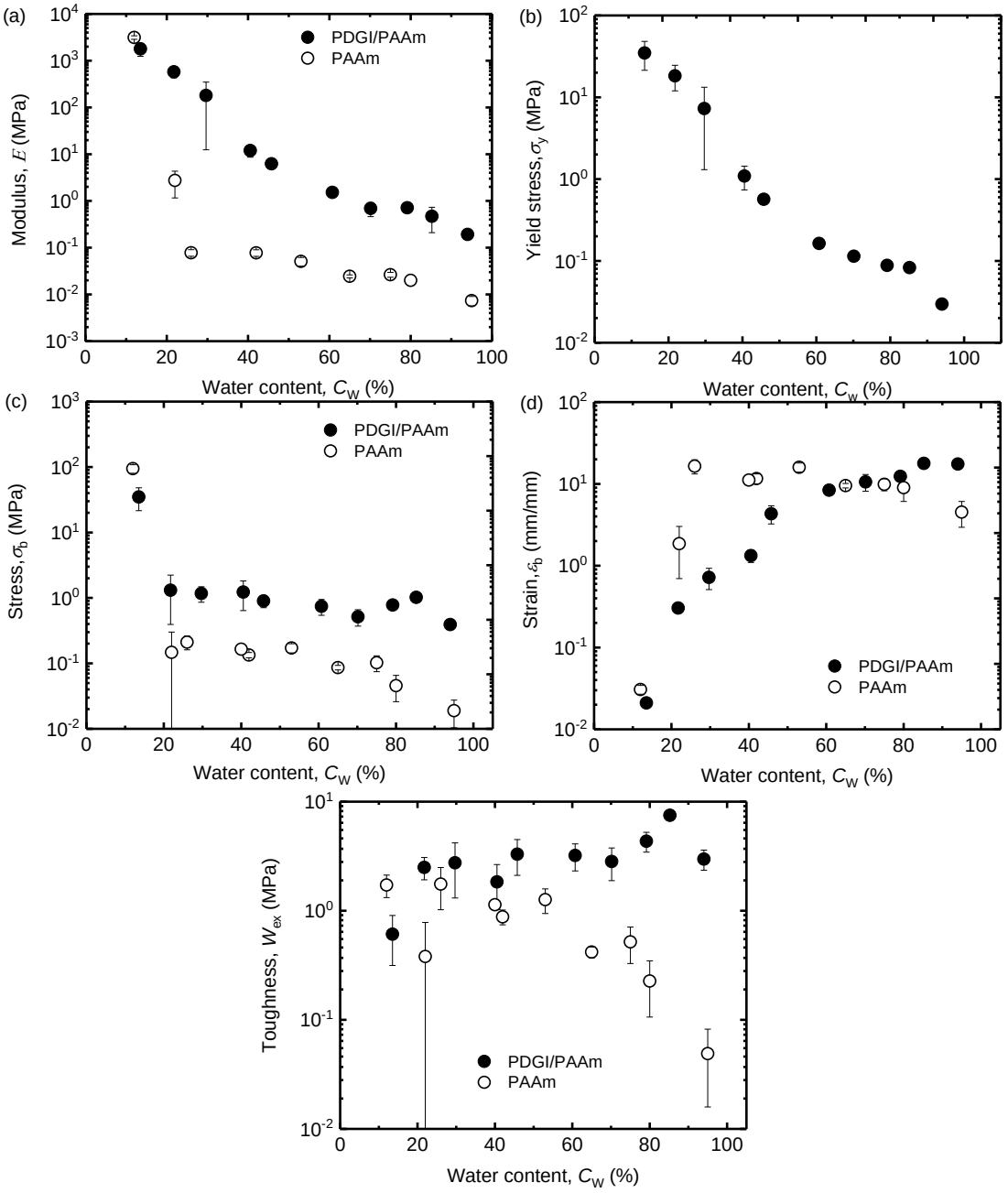

Figure 4.1.9 Summarized results of uniaxial tensile test as a function of water content. (a) Young's modulus, (b) Yielding stress; (c) Fracture stress; (d) Fracture strain; (e) Toughness. The water content shown here is, in relative to the PAAm gel layer for PDGI/PAAm specimens.

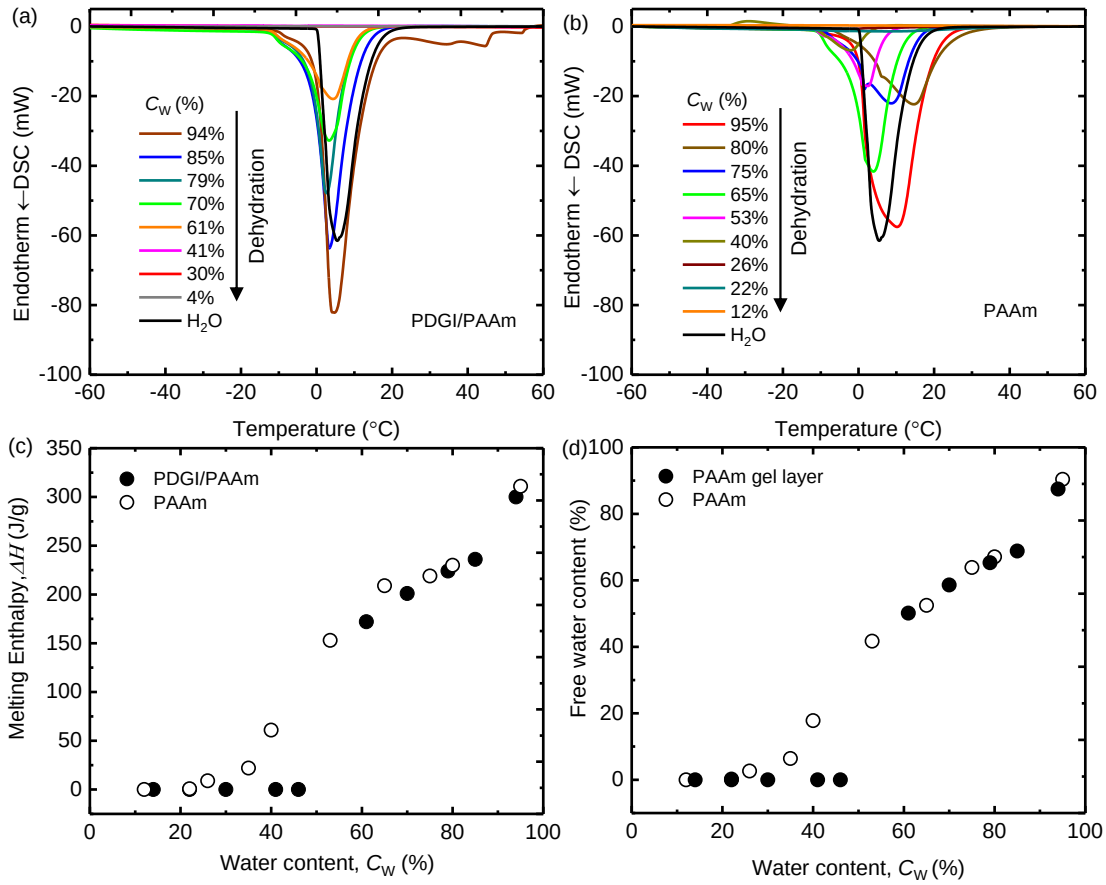

Figure 4.1.10 (a) PDGI/PAAm gels DSC as a function of temperature at different water content. (b) PAAm gels gels DSC as a function of temperature at different water content. (c) Melting enthalpy, *ΔH* (*J/g*) of water in PDGI/PAAm and bulk PAAm gels. The solid black and open circles represent hybrid PDGI/PAAm and PAAm bulk gels, respectively. The DSC was performed from -80°C to 500°C (heating rate = 10°C.min^{-1}). The representative curve is chosen for clarifying the corresponding melting peak of water. For correlation the melting enthalpy of PDGI/PAAm and bulk PAAm gel are plotted as a function of water in PAAm gel layer and bulk PAAm gel, respectively. It is worth noting that, below 60% PAAm gel layer water content the melting peak disappeared in DSc. (d) Comparison of water content C_w determined by TGA vs. free water content determined by DSC. For the PDGI/PAAm samples, water content in relative to the PAAm gel layer is shown.

.

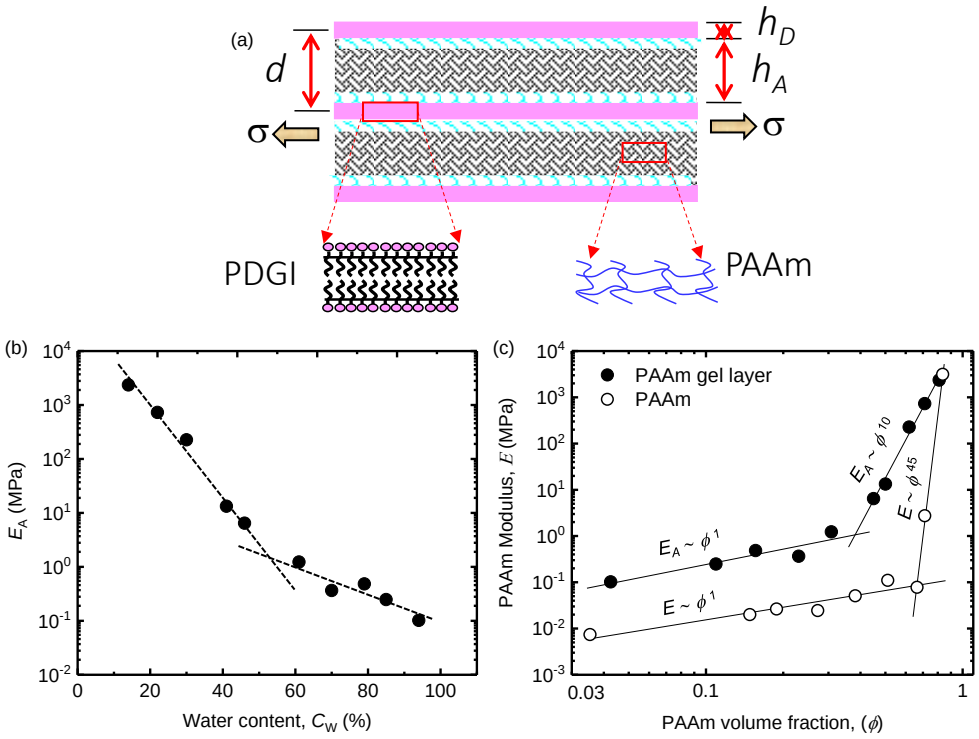

Figure 4.1.11 (a) Stratified layered structural model**.** Where, h_D and h_A and d, are single PDGI layer, single PAAm gel layer, and the distance between consecutively PDGI layers, respectively. (b) PAAm gel layer modulus obtained from the calculation of stratified layered structure model as a function of water content. (c) Correlations between the PAAm modulus and PAAm volume fraction, for bulk PAAm gel (E) and PAAm gel layer (E_A) in PDGI/PAAm gel, respectively.

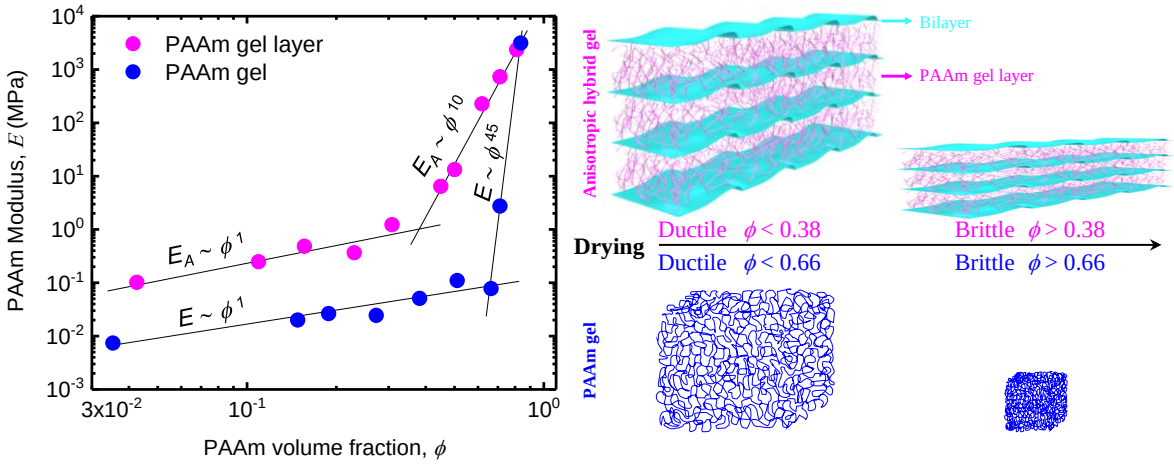

Figure 4.1.12 Representation of the rubbery to glassy transition of two kind of PAAm gels. Left side of figure is in term of PAAm modulus and PAAm volume fraction, for bulk PAAm gel (E) and PAAm gel layer (E_A) in PDGI/PAAm gel, respectively and right side is schematics.

CHAPTER 4

Structure and Properties Relationships

4.2 Ionic Liquid Bilayer Hybrid Gel Composite towards High Functional Materials

4.2.1 Introduction

Polymer hydrogels, consisting of three-dimensional cross-linked networks and a large amount of water (50–90%), are soft and wet materials. Due to the substantial progresses in the development of highly strong and tough hydrogels in recent decade, hydrogels become promising materials for various applications, especially as biomaterials such as cartilages.[1–8]

However, hydrogels are unstable in air because of the evaporation of water, which restricted the applicability of hydrogels to limited fields.[9–11] In contrast polymeric ion gels, comprise of three-dimensional crosslinked polymer strands and a large amount of ionic liquids, are promising soft materials.[12–18] Ionic liquid has many properties such as alternative solvent, air stable, non-volatile, non-flammable, antibacterial, thermally, chemically, and electrochemically stable, ionic conductive.[16,19,20] Therefore, the hybrid of ionic liquid with polymer retains all the characteristics of ionic liquid in a soft quasi solid state.[15] However, most of the ionic liquids are very expensive. On the other hand deep eutectic solvents (DESs), contains mixture of salts, or salts and H-bond donors, at a fix composition they form eutectic mixture.[21] DESs are interesting kind of ionic liquid because they have very low toxicity, are cheap, and preparation is easy.[22] Chloride/urea is simple DES which is prepared by the 1:2 mol/mol ratio of choline chloride: urea and heating at 70°C for 1h by slight modification of literature method.[21] Previous study have shown that amphiphilic molecules self-assemble in DES.[23,24] Recently, the study of ionic liquid based tough soft materials have been reported which are limited to isotropic single or double network polymers.[18,19,25] It is interesting to

understand the effect of ionic liquid on hydrogel that comprise of alternative hydrophilic and hydrophobic layers same as biological system.

Our group developed large area anisotropic bilayer-hybrid gel with 1D aligned lamellar structure along the sheet-shaped sample direction (**Figure 4.2.1**).[26–32] The anisotropic bilayer hybrid gel PDGI/PAAm contain repeating layers of 1D aligned amphiphilic poly(dodecyl glyceryl itaconate)(PDGI) polymeric bilayer membrane (4.7 nm thick) and the chemically or physically crosslinked polyacrylamide based (PAAm) gel layers (several hundred nm thick).[26,32] The bilayers are impermeable to the transport of water, rigid, stiff, while the PAAm gel layers are hydrophilic, soft and stretchable. The bilayer-hybrid gel displayed interesting properties, such as beautiful structure color, 1D swelling and diffusion[27], mechanical anisotropy, quasi-1D shrinkage upon uniaxial stretching[28], self-healing and high toughness.[29] Tunable structural color by small deformation, temperature, and pH.[30,31] The structural anisotropy of lamellar hydrogel closely resemble to that of soft biological tissues such as skin and muscles. Therefore, a model system to study functions of natural bio-tissues.

Herein, we report the effect of ionic liquid-water co-solvent on the structure and tensile properties of the PDGI/PAAm bilayer hybrid gels. The study of the interaction of polymer supported lipid bilayers with ionic liquid suggested that ionic liquid insert into the bilayers, perturb its self-assembled structure, as a result the bending elasticity reduces.[33,34] However, Some recent research has showed that both natural and synthetic amphiphilic molecules self-assemble in ionic liquid (DES) solvent.[34–37] Therefore, for deep understanding the study of ionic liquid-water co-solvent with anisotropic lamellar hydrogels is indispensable. In addition, given the water-impermeable nature of the bilayers and hydrophilic nature of the hydrogel layers, it is interesting to see the effect of ionic liquid on the interaction at the interface between the two components, which are expected to strongly influence the stability and mechanical

properties of the bilayer membranes. It is expected that the introduction of ionic liquid to hybrid gels the bilayer will be stabilized and tough iongels could be produced.

4.2.1.2 Experimental

4.2.1.2.1 Bilayer-hybrid gels synthesis

The multi-lamellar hydrogel, PDGI/PAAm, of large dimension (100×30×0.5 mm^3) was fabricated by modifying the method that described previously.[26] The precursor solution, composed of 0.1 M dodecyl glyceryl itaconate (DGI), 0.025 mol % sodium dodecyl sulfate (with respect to DGI monomer), 2.0 M acrylamide (AAm), 0.1 mol% *N*,*N*'-methylenebisacrylamide (MBAA) as chemical crosslinker of AAm, and 0.1 mol % Irgacure 2959 as initiator (both in relative to AAm monomers), was prepared in aqueous media. The aforementioned precursor solution was kept in a temperature controlled water bath for ~5 h at 55°C to dissolve monomeric DGI powders and stabilize lyotropic liquid crystalline phases of DGI.[38] Then the precursor solution was moved to a glove box purged with argon gas to eliminate the dissolved oxygen. Before polymerization, a reaction cell of 100 mm in length (L_0), 30 mm in width (W_0), and 0.5 mm in thickness (T_0) was prepared by sandwiching a 0.5 mm – thick silicone rubber spacer between two glass plates. In the previous method we applied a shear flow to induce bilayer orientation by injecting the precursor solution manually to the reaction cell.[26] In this work we used a suction method to apply the shear flow. One end of the reaction cell was connected to a suction pump (model Harvard PHD 4400 programmable), and through the other end, the precursor solution was suctioned vertically to the reaction cell against the gravity at a high suction rate to induce a strong shear flow (~133 s^{-1})**.** This method permitted us to obtain a uniform DGI lamellar phase, even with 3 times the sample area of the previous method, oriented uni-axially along the glass walls. This was followed by a co-current homo-polymerization of the DGI and AAm using UV light irradiation for 8 hours at 50°C. After the

polymerization, the gel was removed from the reaction cell and was immersed in a large amount of water for 7 days to reach equilibrium swelling state and to wash away the residual chemicals. PAAm hydrogels were synthesized by UV irradiation from a precursor solution containing 2.0 M AAm, 0.1 mol% MBAA, and 0.1 mol% Irgacure 2959 as initiator.

4.2.1.2.2 Ionic liquid synthesis

Ionic liquid known as deep eutectic solvent (DES) was synthesized by readily available reagents such as Urea CH_4N_2O (m.p 133°C) and choline chloride $C_5H_{14}ClNO$ (m.p 302°C), by slightly modifying the previous procedure[39]. Simply 2:1 mol ratio of urea and choline chloride was added to glass bottle along with magnetic bar and mixed well. Then an oil bath was preheated at 70°C temperature. By placing the bottle contain mixture of urea/choline chloride and heating after certain time the solid components turned to molten salt, then cooled down slowly to room temperature.

4.2.1.2.3 Preparation of co-solvent

The co-solvent of ionic liquid-water was prepared by blending different percentage ratio by weight of increasing ionic liquid content such as 0%, 10%, 15%, 25%, 30%, 40%, 50%. 60%, 70%, 80%, 100%, respectively. Then, water is removed in second set of experiment to obtain iongels. In the 3rd set of experiment bilayer hybrid gel was placed in bulk ionic liquid to create osmotic pressure that lead to shrinkage of gel.

4.2.1.2.4 Swelling ratio measurement

The equilibrium swollen gels in water were cut into a disc of diameter D_1 = 10 mm determined by imageJ software and polarized light microscope (POM). The samples were placed in co-solvents of ionic liquid-water 0-100 w/w% for 2 weeks to attain equilibrium condition. The samples length (L_2) diameter (D_2), and thickness (T_2) in co-solvents were measured, respectively, in the similar fashion. The reflection spectrum was also measured. After the measurements, the sample was returned back to the mixed solvent.

4.2.1.2.5 Measurement of reflection spectrum

The structure color of PDGI/PAAm gels with different ionic liquid content was characterized by the electromagnetic spectrum of light, using moveable angle reflection measurement optics (Hamamatsu Photonics KK, C10027A10687) coupled with photonic multichannel analyzer (Hamamatsu Photonics KK, C10027). White light from Xe source was used to irradiate the gel. Reflection spectrum was acquired by keeping both the angles of incident (Bragg's angle) and reflection at 60°. The wavelength at maximum reflection intensity, λ_{max}, was obtained from the reflection spectrum. The inter-lamellar distance (d) was estimated by using the Bragg's law of diffraction,

$$\lambda_{max} = 2nd\sin\theta \qquad (5)$$

Here n is the refractive index of water (1.33) and θ is the Bragg's angle (60°).[28]

4.2.1.2.6 Measurement of mechanical properties

The dumb-bell shaped gel samples, of standard dimension (gauge length, L = 12 mm width, W = 2 mm and thickness, T = at ionic liquid content), were cut out from the samples equilibrated with different ionic liquid content using standard gel cutter (model JIS-K6251-7). The tensile

tests were performed with a tensile tester (Instron Anton Paar 5965), at a same stretching velocity 100 mm/min, corresponding to a strain rate 0.14 s^{-1}. The Young's modulus was estimated from the initial slope of the uniaxial tensile stress-strain curves within 5% deformation regime. The results shown from tensile stress strain curve are the average of three tests on each gel specimen.

4.2.1.2.7 Polarized light microscopy (POM)

The water swollen and co-solvent equilibrated bilayer hybrid gels were cut into 1 cm long portion to observe the profile of the gel, and subsequently cut into 1 mm cross-sections for cross-sectional viewing on a conventional glass slide in air. Samples were then studied using POM (Eclipse LV100POL, Nicon, Co.). Next, they were analyzed between orthogonally oriented polarizers with and without a 530 nm tint plate. Birefringence were estimated using Berek compensator. The retardation values were noted at 0°,-45° and +45° from cross-section view of PDGI/PAAm gels.

4.2.3 Results and discussion

4.2.3.1 Effect of ionic liquid-water co-solvent

The as-prepared PDGI/PAAn gels, 0.5 mm thick (T_0), were transparent. After immersing in water, the samples only swelled in thickness direction and reached a thickness ~1.21 mm (T_1), at equilibrium swelling. The fully swollen PDGI/PAAm hydrogels exhibiting visible color with a λ_{max} peak at ~540 nm in the optical reflection spectrum. From the Bragg's law, the interlayer distance *d* is estimated as ~195 nm. From the sample thickness and the interlayer distance *d*, the number of bilayers in the lamellar gels is estimated as *c.a.* ~6000.

Then the effect of ionic liquid on dimension change was studied and the dimension change as compared to the swollen condition in deferent co-solvent are shown in **Figure 4.2.2a,b,c,d,**

respectively. The thickness (T_2/T_1), lateral dimension (D_2/D_1), overall volume (V_2/V_1) and surface area of the samples (S_2/S_1) decreased with increasing ionic liquid content. The gels shrinkage was gradually up to 50% ionic liquid content. Increasing further the ionic liquid the gel shrinkage was abrupt. This shrinkage suggests that the presence of ionic liquid in co-solvent increased osmotic pressure that shrink the PAAm gel layers. As a result the bilayer structure experienced biaxial compression. The ionic liquid perturb the layered morphology of the bilayer hybrid gels. This is also confirmed by SEM observation of the sample, which shows the formation of domains or clusters at the high ionic liquid content [**Figure 4.2.3 (cross-section view (g)**].

Afterward, the layered structure of hybrid gels at different ionic liquid-water co-solvent was observed. In concomitant with increasing ionic liquid content, the diffraction color of the gels shifted from greenish yellow to violet, and then to transparent as shown by the photographs of the gels and the corresponding reflection spectra (**Figure 4.2.4a**). The reflection peak wave length (λ_{max}) of original gel in water was ~540 nm (*d* 216 nm) containing ~6000 bilayers. When placed in co-solvent containing 10% ionic liquid λ_{max} slightly increased to 610 nm (*d* 244 nm), then further increasing ionic liquid concentration gradually decreased λ_{max} to ~550 nm (*d* 220 nm), at 50% ionic liquid content, and then a slightly sharp decrease happened in λ_{max} ~350 nm (*d* 140 nm), with the increasing of ionic liquid content $C_{IL,}$ from 50% to 100% (**Figure 4.2.4a, b, c**). Similar situation was observed to the change of full width at half maxima of the reflection peak, which represent the orientation order of bilayers in one dimension. The sharp increase and sharp decrease of full width half maxima and λ_{max} at critical ionic liquid concentration of 50% indicated the structural changes of bilayers in hybrid PDGI/PAAm gel (**Figure 4.2.4a, b, c**). Which is consistent to the SEM micrographs of the gels and dimension change of gels that showed cluster formations at higher ionic liquid content [**Figure 4.2.2, 4.2.3]**. However, the

overall gel in co-solvent exhibited adaptive structural color was observed as a result of change in the PAAm gel layer thickness *d* nm that reduced (216 nm, 244-350 nm) at increasing ionic liquid concentration induced osmotic pressure, diffracted different light waves in visible color range and became invisible (*d* 140 nm) similar to that of the structural color change of squid by reversible body fluid filling and releasing creating osmotic stress causes color tuning. The color tuning of squid or any marine organism is associated with the change of refractive index.

Polarized optical microscopy (POM) was used to understand the effect of increasing ionic liquid content on the orientation and refractive index change of bilayers in hybrid gels as shown in **[Figure 4.2.5]**. The cross section images of water swollen gels with tint plate and without tint plat as inset figure exhibited very intense yellow and bright interference images under POM at angles of +45°, respectively **[Figure 4.2.5a(i)-(viii)]** and **[Figure 4.2.5(f)]**. The gel bright homogenous birefringence, indicating the unidirectional alignment of the PDGI bilayers. The gels after soaking in different concentration of ionic liquid water co-solvent analyzed under POM by inserting compensator and observation angle of compensator 0°, -45°, and +45° are shown, respectively **[Figure 4.2.5 a(i)-(viii), b(i)-(viii), c(i)-(viii)]** and **[Figure 4.2.5(d)]**. The calculated value of birefringence for samples in increasing ionic liquid content are given in **[Figure 4.2.5(g)].** The result showed that, the birefringence value for water swollen gel was $\Delta n = 1.6 \times 10^{-4}$. However, in co-solvent the birefringence value decreased linearly with increasing ionic liquid content indicating anisotropy of the gel becomes weaker that showed weak birefringence. The possible reason for the negative birefringence might be the change of refractive index inside the PAAm gels layer. The water is replaced by ionic liquid-water mixed solvent that altered the refractive index. Another possible reason might be the interaction of bilayers with ionic liquid which changes the orientation pattern of bilayers.

To understand the effect of ionic liquid content on the mechanical properties of PDGI/PAAm bilayer hybrid gels, the tensile tests were performed on the gels sample along the bilayer direction at various ionic liquid contents in co-solvent. The tensile stress-strain curves of the PDGI/PAAm specimens with different ionic liquid content are shown in **Figure 4.2.6c**. The modulus, yield stress, fracture stress, and fracture strain of these samples are summarized in **Figure 4.2.7a**,**b**,**c**,**d**, respectively.

The tensile properties of the bulk PAAm gels in co-solvent is shown in **Figure 4.2.6a**, the bulk PAAm gels showed a gradual increase of fracture stress, fracture strain and toughness by increasing ionic liquid content in co-solvent until the ionic liquid content was increased to a value of 50%. Further increasing ionic liquid content induced decrease in fracture stress, fracture strain and toughness. However, the modulus of bulk PAAm gels were almost constant at any concentration of ionic liquid, indicates the soft and wet nature of the gels.

Similarly, the bilayers hybrid gels also showed change of the mechanical behavior, from soft/stretchable to stiff/tough, upon increasing ionic liquid content in co-solvent (**Figure 4.2.6**). The fracture stress remained almost same until 100% ionic liquid content (**Figure 4.2.7a**). However, the fracture strain slightly reduced up to 60% ionic liquid content, further increase showed abrupt decline in fracture strain (**Figure 4.2.7b**). The modulus and yield stress in co-solvent of the bilayer hybrid gels was different than the bulk PAAm gels, which showed constant modulus and lack of yielding (**Figure 4.2.7c**, **e**).

The uniaxial tensile stress-strain data for the bilayer hybrid gels and PAAm gels at different ionic liquid content are shown by the Mooney–Rivlin plots, respectively, in **Figure 4.2.6d** and **Figure 4.2.6b**. When the ionic liquid content is above the critical values, 60% for lamellar gels, the samples exhibited plateau regions at large elongation, which might correspond to ideal

rubbery-like behaviors from the PAAm hydrogels, as featured by strain-hardening at the extreme elongation before fracture due to finite extensibility effect.

The work of extension, W_{ext} is the energy density dissipated by the specimen fracture (J/m^3), it is a measure of the soft material toughness W_{ext}, estimated from area under the tensile stress-strain curves of the gels, is summarized in **Figure 4.2.7d**. As. The PDGI/PAAm bilayer hybrid gels showed almost a constant W_{ext} of 2.45 MJ/m^3 until the ionic liquid content was increased to 60%. In contrast, the W_{ext} of bulk PAAm gels were very low, that showed gradual increased until 50% ionic liquid content, further increase in ionic liquid content the PAAm toughness decreased as shown in **Figure 4.2.7d**.

The mechanical results indicated, that the soft-stiff transition occurred around ionic liquid content 60% in the bilayer hybrid gels because of possible interaction between ionic liquid-polymer. As a result the energy dissipation mechanism was enhanced. To prove such speculation fatigue tests were performed in the form of loading unloading curve. The area under hysteresis loop indicate the energy dissipation mechanism of gels. The cyclic stress-strain curve for loading-unloading cycle without waiting are shown in **Figure 4.2.8**. For clarity the 1^{st} and second loading-unloading cycles are shown separately **Figure 4.2.8a,b**. One can see that by increasing ionic liquid content (10-100%) the gels hysteresis loop increases for 1^{st} and 2^{nd} loading-unloading cycles, respectively as in **Figure 4.2.8a, b, c**. The ratio of hysteresis area (2^{nd} cycles/1^{st} cycle) as a function of ionic liquid content is shown in **Figure 4.2.8d.** The results suggested enhancement of hysteresis area ratio by increasing ionic liquid content (20-60%), indicating the energy dissipation was enhanced by the introduction of ionic liquid. The results are consistent with the tensile behavior that showed increased mechanical properties. To understand the mechanism of enhancement of energy dissipation, the molecular interaction was investigated by FTIR analysis of PAAm and PDGI/PAAm gels in various ionic liquid

concentration as shown in **Figure 4.2.9**. For that purpose the gels were soaked in different ionic liquid content and scan was performed in the wavenumber of 1000-4000 cm^{-1}. The functional groups absorbance located on polyacrylamide polymer chains such as amine bending 1300-1900 cm^{-1} and stretching vibration 2500-4000 cm^{-1} were located (**Figure 4.2.9a)**. However, in the case PDGI/PAAm in addition to carbonyl and amine, hydroxyl OH functional group was important to study **(Figure 4.2.9b)**. First we look at the results of pure PAAm in different ionic liquid content as shown in **Figure 4.2.10a**. It is obvious from the results that, the bending vibration 1300-1900 cm^{-1} shifted to lower value by increasing ionic liquid content. While the stretching vibration peaks 2500-4000 cm^{-1} of NH_2 increased by increasing ionic liquid content. In comparison, the bilayer hybrid gels stretching vibration 1300-1900 cm^{-1}, and bending vibration 2500-4000 cm^{-1} vibration peaks related to NH_2 linearly downshifted by increasing ionic liquid content **Figure 4.2.10b**. The additional hydroxyl peak -OH stretching vibration related to PDGI head group also showed downshift **Figure 4.2.10c**. The above results suggested that there is strong interaction not only between ionic liquid-polymers but also in polymer-polymer as well. The results of FTIR is in consistent with the mechanical data.

PDGI/PAAm gels showed pronounce increase of yielding and energy dissipation by increasing ionic liquid content. The PAAm gel modulus remained constant at all concentration of ionic liquid in co-solvent. The one order in magnitude high modulus of the PDGI/PAAm gels in comparison to that of the pure PAAm gels, might attribute to a strong interaction between bilayers-PAAm enhanced by ionic liquid effect. Previous study suggested that, PDGI and PAAm have no covalent bonds[40], and PAAm chains are physically adsorbed on the PDGI bilayer membranes by hydrogen bonding.[32] Our previous research on drying anisotropic lamellar gels suggested that the PAAm gel layers turns from soft-rigid at critical water content. The modulus of PAAm gels in between bilayers was increased to several decades of mega-

pascals due to the enhancement of adsorption of PAAm gels layers on PDGI layers. Here in the results of ionic liquid suggested that the PAAm layers experience 2D compression by osmotic de-swelling same as bulk PAAm gels. However, during this compression the bilayers were stabilized by increasing ionic liquid content in gels. The stability of bilayers enhanced yielding stress, energy dissipation mechanism, and modulus of PDGI/PAAm gels by increasing ionic liquid content in co-solvent.

Now we understand the mechanical properties in co-solvent. Another question arises that if we remove water from the gel equilibrated with co-solvent what will happen? Will the structural color be maintained by swelling the PAAm gel layer with ionic liquid? To support such speculation we have performed the experiment of removal of water from gel to obtain ionogels of PDGI/PAAm. Then at different concertation ionic liquid structure and mechanical properties were investigated.

4.2.3.2 Effect of water removal from co-solvent soaked gels

The adaptive structure color of gels soaked in different ionic liquid concentration in co-solvent is shown in **Figure 4.2.11a,b**. The gels showed pronounced blue shift by increasing the concentration of ionic liquid in co-solvent. The color changed from orange to green and then blue covering the entire visible spectrum of electromagnetic radiation of light by increasing ionic liquid content in co-solvent. Then the gels were subjected to drying for evaporation of water. The removal of water resulted in colorless transparent ion gel as shown in **Figures 4.2.11b.** The ionic liquid-bilayer hybrid gel produced unique iongel with alternating layer structure which is quite different from the literature study of iongels that are limited to hydrophilic single or double network polymeric systems. The iongels at different concentration of ionic liquid are visually transparent, the blue color background is easily observable. This step is reversible and can be repeated for many times without altering gel original structure in

swollen form. Simply adding co-solvent or swelling the ion gel is water will produced the original PDGI/PAAm gels without disturbing the internal morphology of bilayers. This step can also be achieved just by adding bulk ionic liquid on PDGI/PAAm gels which is also repeatable.

To understand the mechanical behavior of resultant PDGI/PAAm iongel with different concentration of ionic liquid, uniaxial tensile tests were performed on dumbbell shaped iongel specimens as shown in **Figure 4.2.12a**. The tensile stress-strain and Mooney-Rivlin curve are given in **Figure 4.2.12b,c**, respective. The result from stress-strain curve such as modulus, stress, strain and toughness are shown in **Figure 4.2.13a,b,c,d.**

The mechanical behavior of iongels are slightly different from that of the co-solvent gels, however the iongels showed soft/stretchable to stiff/tough with distinct enhancement in yielding, upon increasing ionic liquid content (**Figure 4.2.12a, b**). The modulus, stress and toughness of iongels initially 0-10% ionic liquid increased, gradual decrease at 10-80% ionic liquid, followed by a large increase 80-100% ionic liquid content, respectively **Figure 4.2.13a,b,d.**. However, the strain of iongel was gradually increased high upto 50% ionic liquid content, then gradually reduced at higher ionic liquid content **Figure 4.2.13c.**. The possible increase in the beginning of ionic liquid concentration might attribute to the higher stiffening of PAAm gel layers, as low amount of ionic liquid must remain after evaporation of water. The gradual decrease caused by the solvation of PAAm gel layers by ionic liquid that remained at relatively swollen state. The abrupt increase of the iongels mechanical behavior at higher ionic liquid content is associated with the huge osmotic drying effect and increased stiffness of PAAm strands.

4.2.3.3 Effect of bulk ionic liquid on gels

In this section, we study the effect of bulk ionic liquid on bilayer hybrid gel structure and mechanical properties. Briefly the osmotic drying is performed by soaking equilibrium water swollen PDGI/PAAm bilayers hybrid gel in bulk volume of ionic liquid. In this way the osmotic pressure is higher in ionic liquid than the water inside the PAAm gels layers. That causes the shrinkage of gels. The visual change of sample structural color by addition in ionic liquid is shown in **Figure 4.2.14a**. The gels absorbance as function of wavelength at different time interval in bulk ionic liquid is also shown in **Figure 4.2.14b**. The results indicated that the original red color PDGI/PAAm gel absorb light at λ_{max} 675 nm wavelength corresponding *d* 270 nm exhibited blue shift by addition of ionic liquid, the absorbance peak wavelength shifted to λ_{max} 650 nm (*d* 260 nm), λ_{max} 550 nm (*d* 220 nm), and λ_{max} 500 nm (*d* 200 nm), respectively with changing the gel color to green, blue and at last colorless with time **Figure 4.2.14a-f**. The structural color of the gel is tuned throughout the entire visible region of light waves. The color change is linearly tuning with time and thickness change, respectively. According to beer's lambert law absorbance is proportional to the thickness and concentration of path length.[41] Here the thickness plays important role. The process of structural color of the gel can be reversibly tuned to original color just by soaking in water again.[26] As shown in figure, green gel placed in a petri dish of black color, simply by adding bulk ionic liquid changed the gel to iongel that is transparent with no visible color **Figure 4.2.14f**. In turn by replacing ionic liquid with water the green gel color turned back. There reversible on-off switching is associated with solvent exchange without damage of the gel sample. The phenomena of color change by osmotic swelling-drying is same as marine organisms which tune their structural color by filling and emptying their order structure with fluid. In this the refractive contrast between the alternating layers give beautiful structure color.[42]

The polarized light microscopic images of gel in bulk ionic liquid are shown in **Figure 4.2.15**. The gel top surface view and cross-section were analyzed in cross polarizers using 532 nm tint plate at 0°, -45° and +45° angles to observation. The water swollen gel sample showed homogenous yellowish and blue interference colors at -45° and +45°, respectively. While no obvious color at an angle of 0°, indicating oriented bilayers in gels. However, as the ionic liquid is placed on gel the color pattern gradually changed with time. Until 30 min the sample showed completely different behavior. It seems that the ionic liquid induced huge osmotic pressure that generated the squeezing of water as a result the orientation of bilayers in gel changed to somewhat disordered or other direction. This was further supported by scanning electron microscopic images **Figure 4.2.16**. The sample after treatment with ionic liquid showed ordered orientation pattern from surface view. This indicated the ionic liquid greatly influenced the morphology of bilayer in hybrid gel. The optical images also indicated the gel shrinking in thickness direction with time. Which is consistent with the absorbance spectra results and shift of structural color.

In order to observe the effect of bulk ionic liquid on the mechanical properties of PDGI/PAAm gel and iongel, which was performed on standard bum-bell shaped specimens **Figure 4.2.17a**, the relative tensile stress-strain curve and results are shown in **Figure 4.2.17b,c**. The original gel showed large deformation of 11.20 mm/mm and strength 0.57 MPa. In comparison, the iongel stretched up to 0.55 mm/mm and stress was 0.07MPa. However, the modulus of iongel was much higher than the hydrogel sample. Therefore, just by solvent exchange readily changeable mechanical behavior of soft tough and stretchable to stiff and brittle one could be obtained within 60 min of duration. This mechanical property is reversible just by replacing ionic liquid with water. The mechanical properties are also in consistent with optical images

indicating the dis-ordered structure caused the decreased mechanical behavior of ionogels. Therefore, ionic liquid causes plasticizing effect in polymer chains.[17,43]

4.2.3.4 Effect of ionic liquid on precursor solution

Previous sections indicated that the structure and properties of PDGI/PAAm bilayer hybrid gels were moldable by ionic liquid either by co-solvent or bulk ionic liquid. Here in, the addition of ionic liquid to the standard precursor solution and its effect on the gel functionality are investigated. The hypothesis is whether adding ionic liquid at the time of precursor solution preparation could produce structure colored iongel and what kind of new functions are associated to the addition of ionic liquid. One possible expectation will be the perturbation of water and disordered structure of amphiphilic surfactant.[23,24,34,44,45] On purpose using the same experimental conditions for precursor solution as described in experimental section except at the last step of diluting precursor solution 1/1 % by volume water/ionic liquid were mixed **Figure 4.2.18a**. The mixed solvent of 600uL was added to precursor solution containing all reagents described above in experimental part. Another change in experimental condition was after heating precursor solution for 5h the gelation was performed in glass test tube diameter 10 mm without applying shear for 8h. As a reference the standard gel was also prepared using standard precursor solution **Figure 4.2.18b**.

After the completion of polymerization the as prepared PDGI/PAAm iongel and hydrogel are shown in **Figure 4.2.18c,d.** The PDGI/PAAm iongel was transparent showing no structural color while the standard gel showed greenish blue structural color even without applying strong shear flow.

The polarized optical study of iongel at 0°, -45° and +45° angles to observation either from top side or cross-section revealed non-uniform birefringence color in crossed polarizer or with 532

nm tint plate **Figure 4.2.19a,b,c.** The effect of water removal or aging on iongel was observed to change birefringence probably due to drying effect **Figure 4.2.19a(ii-iv),b(ii-iv),c(ii-iv)**. However, the optical study indicated the internal isotropic structure of bilayers in hybrid iongel system. It is obvious because shear was not applied to the precursor solution and gelation was performed in test tube of large diameter. Ionic liquid might have perturb the structure of water that caused the slight distortion of bilayer orientation.[33,46] Despite of isotropic structure, amphiphilic molecules are known for their dynamic bonds because they are rich in hydrophobic sites and OH functional groups.[4,32] Utilizing the multiple interaction of hydrogen bonding and Vander walls interaction, it is possible to obtain superfast supramolecular self-healing iongel that show self-healing to damage or rupture.[2,47–51] The results of as prepared, aged and solvent induced self-healing Behavior of iongel are shown in **Figure 4.2.20a,b,c**. The as prepared ion gel was cut by conventional gel cutter, then hold the cute pieces together for 5s, and stretch as shown in **Figure 4.2.20a(i-vi)**. Interestingly, the ion gel showed self-healing and the connected part was not detaching even for large deformation. The self-healing behavior was becoming much robust and faster by aging the sample in air or evaporation of water [**4.2.20b (i-iii)]**. The possible mechanism of such ultrafast self-healing behavior might be the multiple interactions such as Vander wall, hydrogen bonding prompted by the incorporation of small quantity of ionic liquid. This result also indicate the isotropic structure are indispensable for further study. The benefits associated with such study was that air stable and self-healing soft tough iongel can be prepared that show efficient self-healing property. Then the effect of different organic solvents polar protic (ethanol, propanol) and polar aprotic (DMSO, DMF, Acetone) do not participate in hydrogen bonding but on the self-healing behavior of iongel was investigated.[52] Briefly, the as prepared or aged iongels were soaked in different organic solvent as shown in **Figure 4.2.20c** for 24h. Then the solvent soaked iongel were cut in two pieces by gel cutter,

held the cut pieces together for 5s, and applied uniaxial deformation. The iongel soaked in protic solvents 2-propanol and aprotic solvent acetone showed self-healing behavior while other were either dissolved (DMSO), not able to self-heal (DMF) or became solid dry polymer (ethanol). The reason behind the self-healing behavior in propanol and acetone is because of their participation and promotion of hydrogen bonding.[53] It is assumed that the DES ionic liquids in polymer chains are present as rich source of dynamic hydrogen bond especially hydrogen bond acceptor carbonyl of urea pairs.[21,22,51] Once the gel is cut into two pieces, the restricted mobile sites which were formed become disturbed. By addition of acetone or propanol the ionic liquid polymer interaction lose order, strength and moved towards the edge of the iongel. The interaction of solvent lead to the rearrangement of these physical crosslinked site that also initiated favorable polymer entanglements essential for the promotion of self-healing of iongel. At the last stage the the van der Waals interactions and hydrogen bonding initiated the formation of ultrafast reversible dynamic active, non-covalent interaction sites leading to robust self-healing.

4.2.4 Conclusion

The bilayer hybrid gels showed unique adaptive structural color somewhat similar to marine organism like squid, by shrinking in various concentration of ionic liquid-water co-solvent, throughout the entire visible spectrum of light. The mechanical properties was found to enhance by increased ionic liquid content that enhanced the energy dissipation mechanism of bilayers hybrid gels. The addition of co-solvent acted as filler that enhanced the intermolecular interaction of PDGI/PAAm and PAAm gels, respectively. The removal of water from co-solvent produced air stable soft tough iongel based on bilayers. The iongel has the characteristic property of conductivity (application chapter in detail) might be useful for using as stretchable electronics skin or batteries or as a barrier coating. Moreover, the addition of ionic liquid to

bilayer hybrid gel recipe perturb the structure of bilayers lead to the formation of ultrafast robust air stable self-healing soft iongel.

4.2.5 References

[1] J. P. Gong, Y. Katsuyama, T. Kurokawa, Y. Osada, *Advanced Materials* **2003**, *15*, 1155.

[2] T. L. Sun, T. Kurokawa, S. Kuroda, A. Bin Ihsan, T. Akasaki, K. Sato, M. A. Haque, T. Nakajima, J. P. Gong, *Nature Materials* **2013**, *12*, 932.

[3] Y. Zhao, T. Nakajima, J. J. Yang, T. Kurokawa, J. Liu, J. Lu, S. Mizumoto, K. Sugahara, N. Kitamura, K. Yasuda, A. U. D. Daniels, J. P. Gong, *Advanced Materials* **2014**, *26*, 436.

[4] H. J. Zhang, T. L. Sun, A. K. Zhang, Y. Ikura, T. Nakajima, T. Nonoyama, T. Kurokawa, O. Ito, H. Ishitobi, J. P. Gong, *Advanced Materials* **2016**, *28*, 4884.

[5] J.-Y. Sun, X. Zhao, W. R. K. Illeperuma, O. Chaudhuri, K. H. Oh, D. J. Mooney, J. J. Vlassak, Z. Suo, *Nature* **2012**, *489*, 133.

[6] M. A. Haque, T. Kurokawa, J. P. Gong, *Polymer* **2012**, *53*, 1805.

[7] M. J. Glassman, R. K. Avery, A. Khademhosseini, B. D. Olsen, *Biomacromolecules* **2016**, *17*, 415.

[8] K. Sato, T. Nakajima, T. Hisamatsu, T. Nonoyama, T. Kurokawa, J. P. Gong, *Advanced Materials* **2015**, *27*, 6990.

[9] N. a Peppas, In *Biomaterials Science: An Introduction to Materials in Medicine*; 2012; pp. 35–42.

[10] K. Hara, Y. Sueyoshi, M. Sugiyama, T. Fukunaga, *Ferroelectrics* **2007**, *348*, 166.

[11] W. Hong, X. Zhao, Z. Suo, *Journal of Applied Physics* **2008**, *104*.

[12] T. Ueki, M. Watanabe, *Bulletin of the Chemical Society of Japan* **2012**, *85*, 33.

[13] S. Kasahara, E. Kamio, T. Ishigami, H. Matsuyama, *Chemical Communications* **2012**, *48*, 6903.

[14] A. Rehman, X. Zeng, *RSC Adv.* **2015**, *5*, 58371.

[15] J. Le Bideau, L. Viau, A. Vioux, *Chem. Soc. Rev.* **2011**, *40*, 907.

[16] X. Liu, Z. Wen, D. Wu, H. Wang, J. Yang, Q. Wang, *Journal of Materials Chemistry A* **2014**, *2*, 11569.

[17] S. Y. Choi, H. Rodríguez, A. Mirjafari, D. F. Gilpin, S. McGrath, K. R. Malcolm, M. M. Tunney, R. D. Rogers, T. McNally, *Green Chemistry* **2011**, *13*, 1527.

[18] E. Kamio, T. Yasui, Y. Iida, J. P. Gong, H. Matsuyama, *Advanced Materials* **2017**, *1704118*, 1.

[19] F. Ranjbaran, E. Kamio, H. Matsuyama, *Journal of Membrane Science* **2017**, *544*.

[20] M. P. Scott, M. Rahman, C. S. Brazel, *European Polymer Journal* **2003**, *39*, 1947.

[21] A. P. Abbott, D. Boothby, G. Capper, D. L. Davies, R. Rasheed, *J. Am. Chem. Soc* **2004**, *126*, 9142.

[22] Q. Zhang, K. De Oliveira Vigier, S. Royer, F. Jérôme, *Chemical Society Reviews* **2012**, *41*, 7108.

[23] M. Pal, R. Rai, A. Yadav, R. Khanna, G. A. Baker, S. Pandey, *Langmuir* **2014**, *30*, 13191.

[24] T. Arnold, A. J. Jackson, A. Sanchez-Fernandez, D. Magnone, A. E. Terry, K. J. Edler, *Langmuir* **2015**, *31*, 12894.

[25] F. Moghadam, E. Kamio, T. Yoshioka, H. Matsuyama, *Journal of Membrane Science* **2017**, *530*.

[26] M. A. Haque, G. Kamita, T. Kurokawa, K. Tsujii, J. P. Gong, *Advanced Materials* **2010**, *22*, 5110.

[27] K. Mito, M. A. Haque, T. Nakajima, M. Uchiumi, T. Kurokawa, T. Nonoyama, J. P. Gong, *Polymer* **2017**, 1.

[28] T. Nakajima, C. Durand, X. F. Li, M. A. Haque, T. Kurokawa, J. P. Gong, *Soft matter* **2015**, *11*, 237.

[29] M. A. Haque, T. Kurokawa, G. Kamita, J. P. Gong, *Macromolecules* **2011**, *44*, 8916.

[30] Y. Yue, T. Kurokawa, M. A. Haque, T. Nakajima, T. Nonoyama, X. Li, I. Kajiwara, J. P. Gong, *Nature communications* **2014**, *5*, 4659.

[31] Y. F. Yue, M. A. Haque, T. Kurokawa, T. Nakajima, J. P. Gong, *Advanced Materials* **2013**, *25*, 3106.

[32] X. Li, T. Kurokawa, R. Takahashi, M. A. Haque, Y. Yue, T. Nakajima, J. P. Gong, *Macromolecules* **2015**, *48*, 2277.

[33] B. Jing, N. Lan, J. Qiu, Y. Zhu, *Journal of Physical Chemistry B* **2016**, *120*, 2781.

[34] S. J. Bryant, K. Wood, R. Atkin, G. G. Warr, *SOFT MATTER* **2017**, *13*, 1364.

[35] F. Gayet, J. D. Marty, A. Brûlet, N. L. De Viguerie, *Langmuir* **2011**, *27*, 9706.

[36] C. R. López-Barrón, D. Li, L. Derita, M. G. Basavaraj, N. J. Wagner, *Journal of the*

American Chemical Society **2012**, *134*, 20728.

[37] M. Pal, R. Rai, A. Yadav, R. Khanna, G. a Baker, S. Pandey, *Langmuir : the ACS journal of surfaces and colloids* **2014**, *30*, 13191.

[38] K. Naitoh, Y. Ishii, K. Tsujii, *Journal of Physical Chemistry* **1991**, *95*, 7915.

[39] A. P. Abbott, G. Capper, D. L. Davies, R. K. Rasheed, V. Tambyrajah, *Chemical Communications* **2003**, 70.

[40] J. Ozawa, G. Matsuo, N. Kamo, K. Tsujii, *Macromolecules* **2006**, *39*, 7998.

[41] D. F. Swinehart, *Journal of Chemical Education* **1962**, *39*, 333.

[42] D. G. DeMartini, D. V. Krogstad, D. E. Morse, *Proceedings of the National Academy of Sciences* **2013**, *110*, 2552.

[43] M. P. Scott, C. S. Brazel, M. G. Benton, J. W. Mays, J. D. Holbrey, R. D. Rogers, *Chemical Communications* **2002**, 1370.

[44] M. A. Haque, T. Kurokawa, J. P. Gong, *Soft Matter* **2013**, *9*, 5223.

[45] R. Hayes, S. Imberti, G. G. Warr, R. Atkin, *Angewandte Chemie - International Edition* **2012**, *51*, 7468.

[46] B. Yoo, Y. Zhu, E. J. Maginn, *Langmuir* **2016**, *32*, 5403.

[47] Z. Wei, J. H. Yang, J. Zhou, F. Xu, M. Zrínyi, P. H. Dussault, Y. Osada, Y. M. Chen, *Chemical Society reviews* **2014**, *43*, 8114.

[48] E. D. Elia, S. Eslava, M. Miranda, T. K. Georgiou, E. Saiz, *Nature Publishing Group* **2016**, 1.

[49] H. Ying, Y. Zhang, J. Cheng, *Nature communications* **2014**, *5*, 3218.

[50] A. Phadke, C. Zhang, B. Arman, C.-C. Hsu, R. a Mashelkar, A. K. Lele, M. J. Tauber, G. Arya, S. Varghese, *Proceedings of the National Academy of Sciences of the United States of America* **2012**, *109*, 4383.

[51] P. Cordier, F. Tournilhac, C. Soulié-Ziakovic, L. Leibler, *Nature* **2008**, *451*, 977.

[52] M. Sharma, D. Mondal, C. Mukesh, K. Prasad, **2013**, *364002*, 5.

[53] Y. Katsumoto, T. Tanaka, K. Ihara, M. Koyama, Y. Ozaki, *Journal of Physical Chemistry B* **2007**, *111*, 12730.

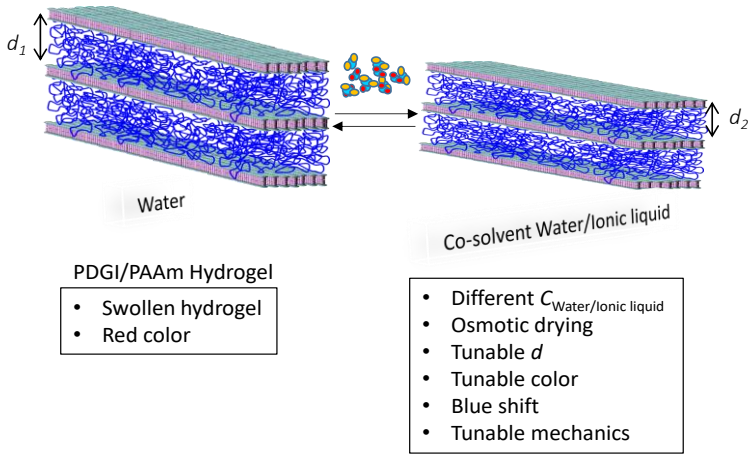

Figure 4.2.1. Schematic representation of anisotropic lamellar PDGI/PAAm gels, synthesized by a co-current homo-polymerization of the amphiphilic dodecyl glyceryl itaconate (DGI) and hydrophilic acrylamide (AAm). Addition of gel in water-ionic liquid co-solvent and proposed changes in the gel properties.

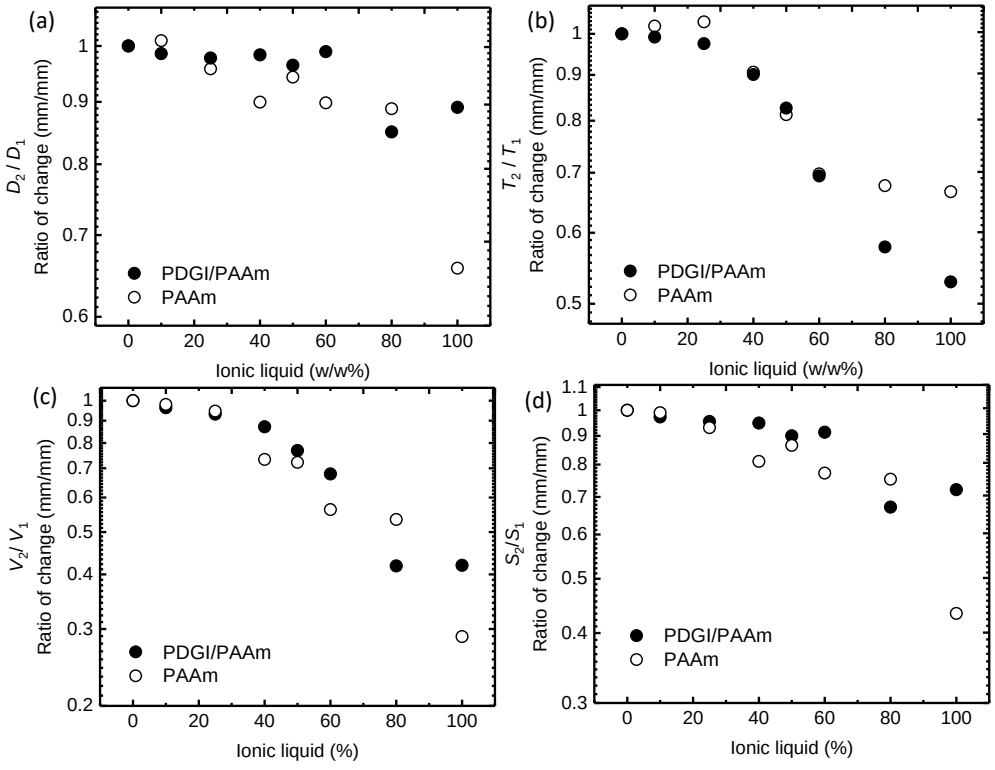

Figure 4.2.2 Ionic liquid/water co-solvency induced ratio of size change. (a) Diameter (D_2/D_1), thickness (T_2/T_1), volume (V_2/V_1), and surface area (S_2/S_1) as a function of concentration of

ionic liquid in co-solvent. D_2, T_2, V_2 and S_2 are, respectively, the diameter, thickness, volume and surface area of the sample at equilibrium swelling in water ionic liquid co-solvent. D_1, T_1, V_1 and S_1 are, respectively, the diameter, thickness, volume and surface area of the sample at equilibrium swelling in water as reference condition.

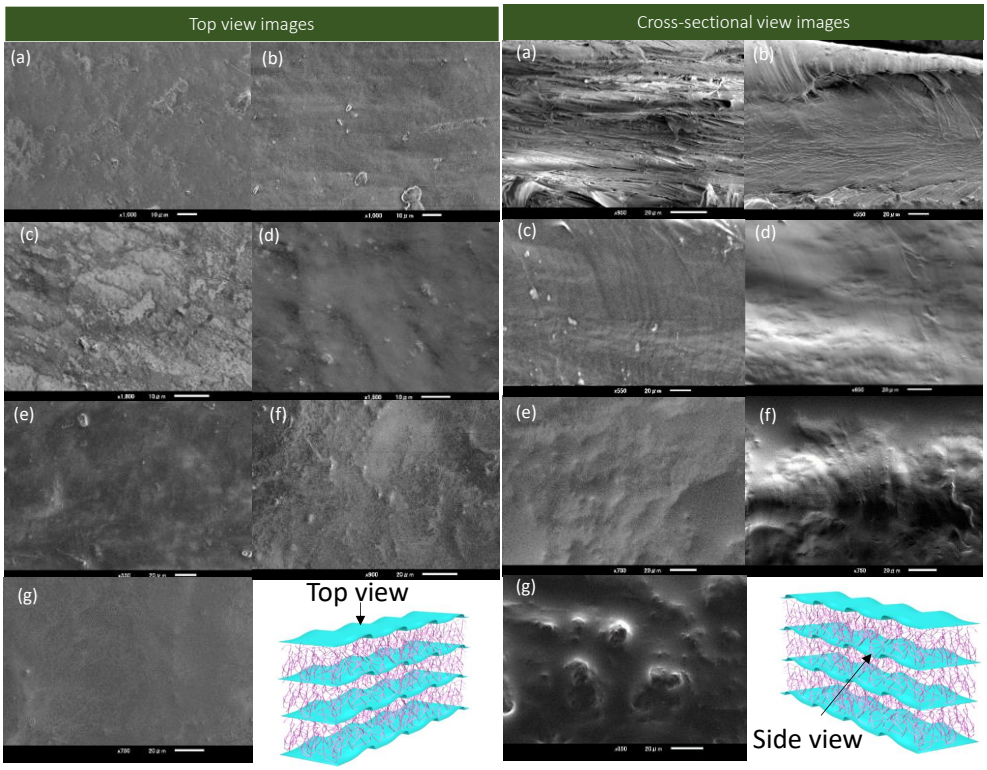

Figure 4.2.3 (a)-(g) left side are **the** top view images **while** (a)-(g)right side are the cross-section view images of PDGI/PAAm under SEM. **Among these images** (a) and (b) are the top view image and cross-section corresponds to the original PDGI/PAAm bilayer hydrid gel. (b)-(g) in top view images and cross-section view SEM micrographs are increasing concentration of ionic liquid in co-solvent such as 0-100%, respective. The scale bar is 10 μm for the (a)-(d) and 20 μm (e)-(g) in top view images, respectively. The scale for cross-section view images (a)-(g) is 20 μm, respectively. For as a clarification the layer structure images indicates the top view and cross-section view of gels under observation.

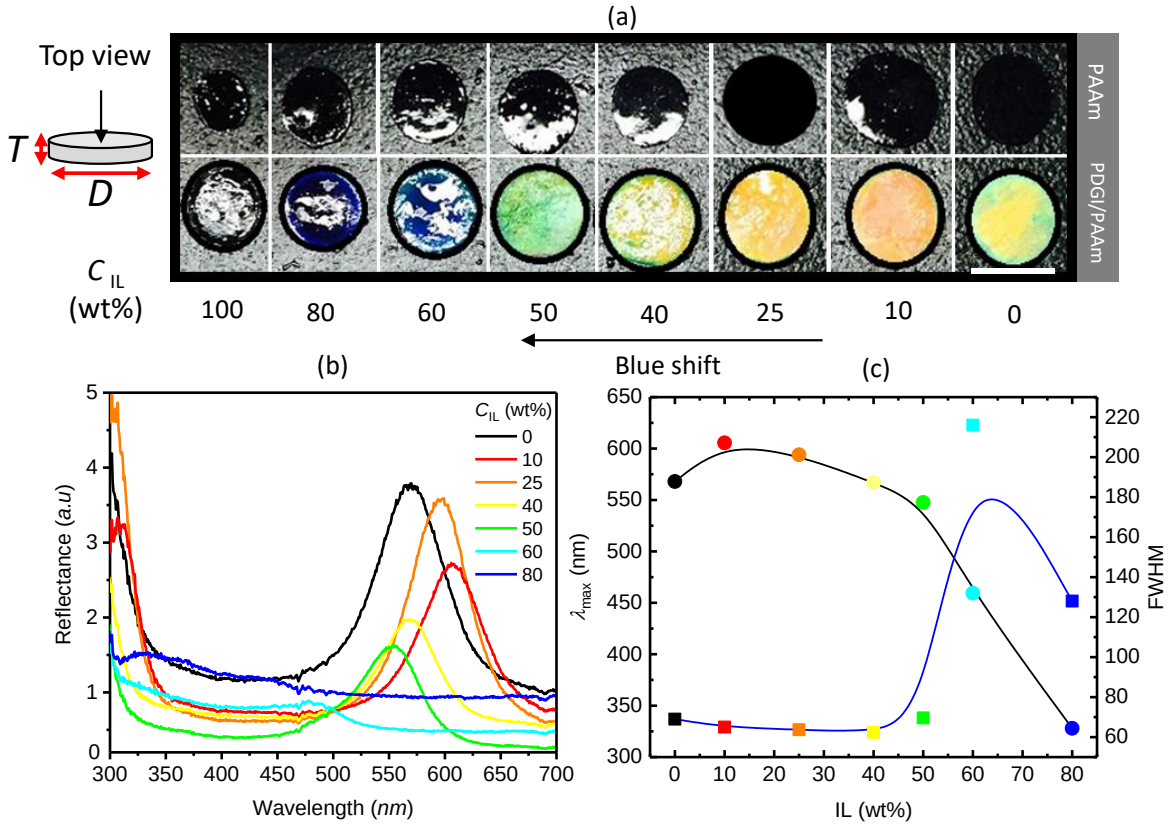

Figure 4.2.4 (a) Images of pure PAAm and PDGI/PAAm gels in different concentration of ionic liquid. Where *T* and *D* represent thickness and diameter of specimens in mm. The scale bar is 1 cm (b) Reflection spectra as a function of wavelength that represent color profile at different ionic liquid concentration in co-solvent. (c) The effect of ionic liquid content on maximum wavelength λ_{max} nm and Full-width at half maxima of the reflection peak that roughly represent the orientation order of bilayers in one dimension.

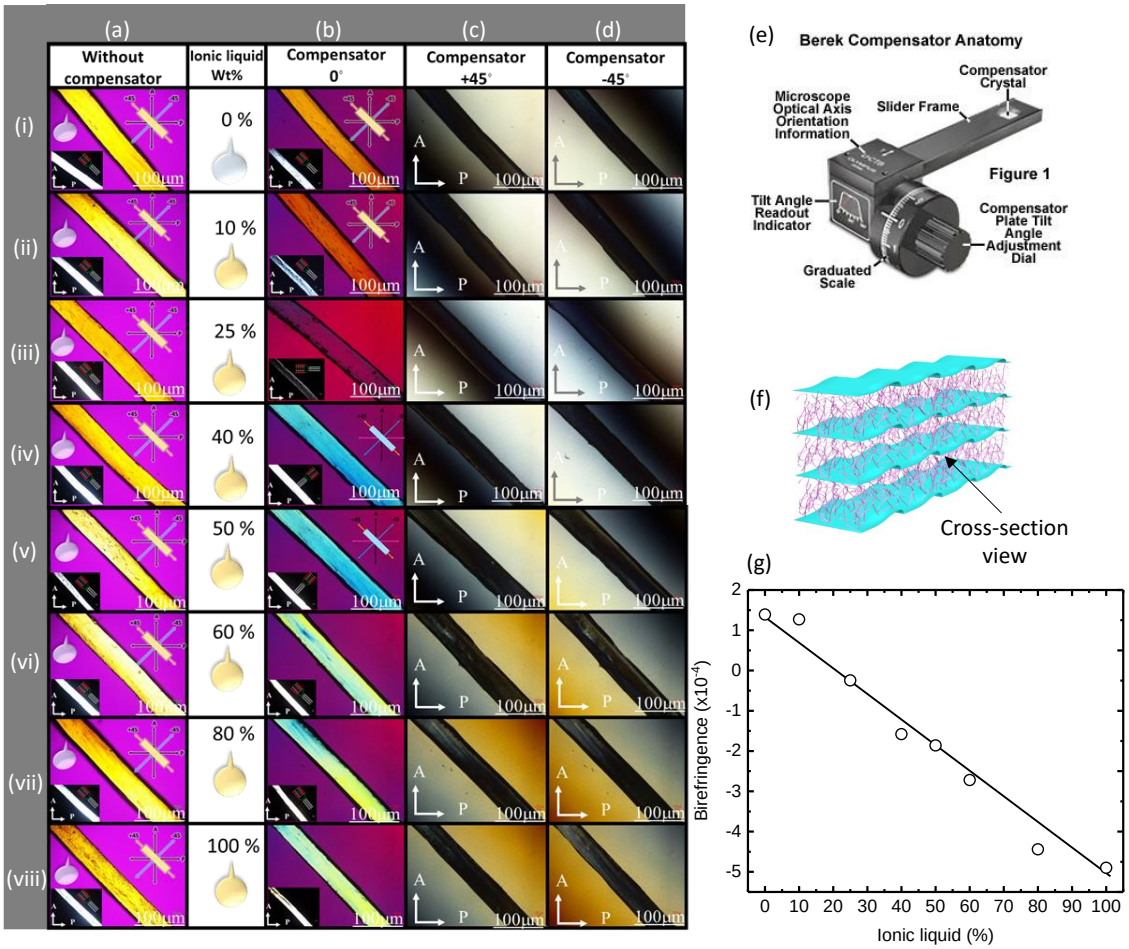

Figure 4.2.5 (a) Original PDGI/PAAm gels in water under polarized light microscope at +45° in cross polarizers at 532 nm quarter wave plate dark yellow color, and without wave plate as inset figure showing bright birefringence. (b) The inserted Berek compensator at 0° rest. (c) and (d) The Berek compensator was dialed until dark extinction appeared. (e) A typical berek compensator. (f) The sample analysis was performed from cross-section. (g) The calculated Birefringence as a function of ionic liquid content. Where, a(i-viii), b(i) and c(i) are the gels in water, and b(ii-viii) and c(ii-viii) increasing ionic liquid 10-100% in co-solvent.

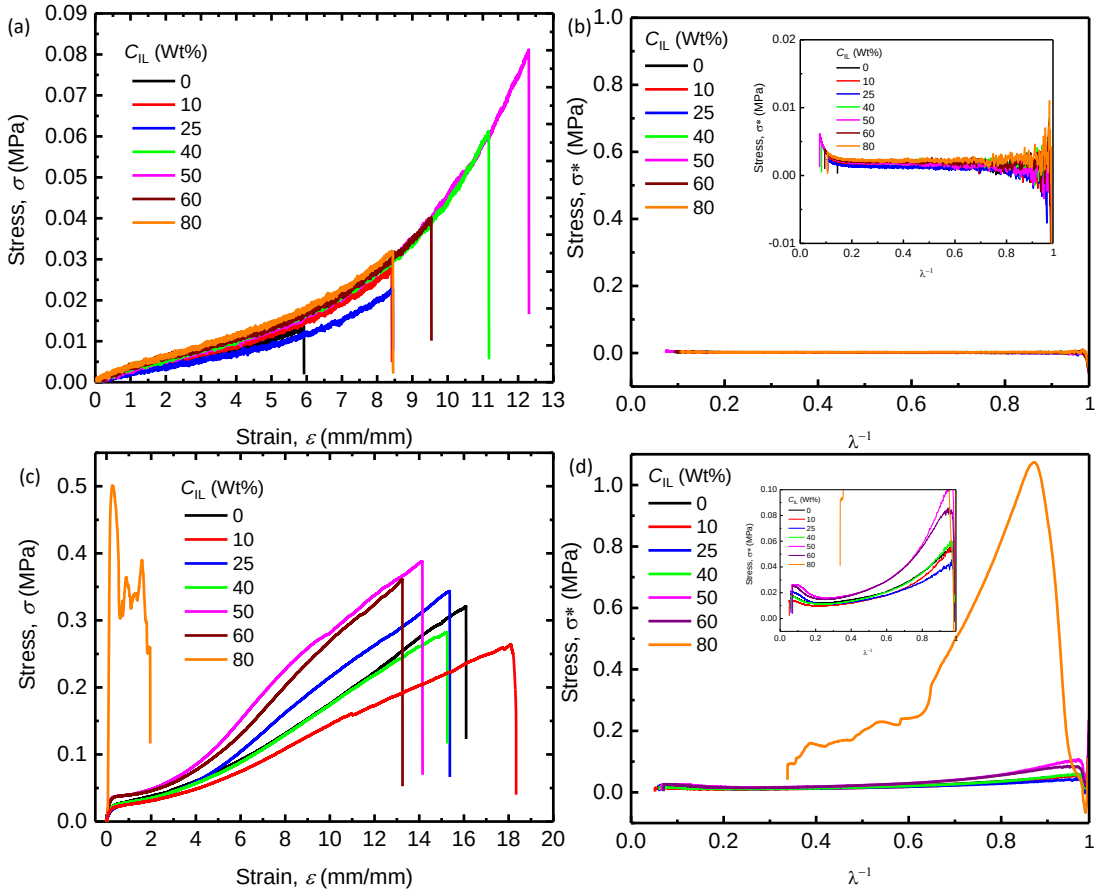

Figure 4.2.6 (a) Stress-strain curves of PAAm gels at different ionic liquid content obtained from uniaxial tension tests. (b) Mooney Rivlin plot of the PAAm tensile result; (c) Stress-strain curves of PDGI/PAAm gels at different ionic liquid content obtained from uniaxial tension tests; (d) Mooney-Rivlin plot of the PDGI/PAAm tensile result, where $\sigma^*=\sigma/(\lambda-\lambda^{-2})$ is the reduced stress and $\lambda=\varepsilon+1$ is the elongation ratio. The tests were performed for three times on each specimen, for clarity only the representative curves are shown. For clarity the transition region is enlarged and inserted in (b) and (d), respectively.

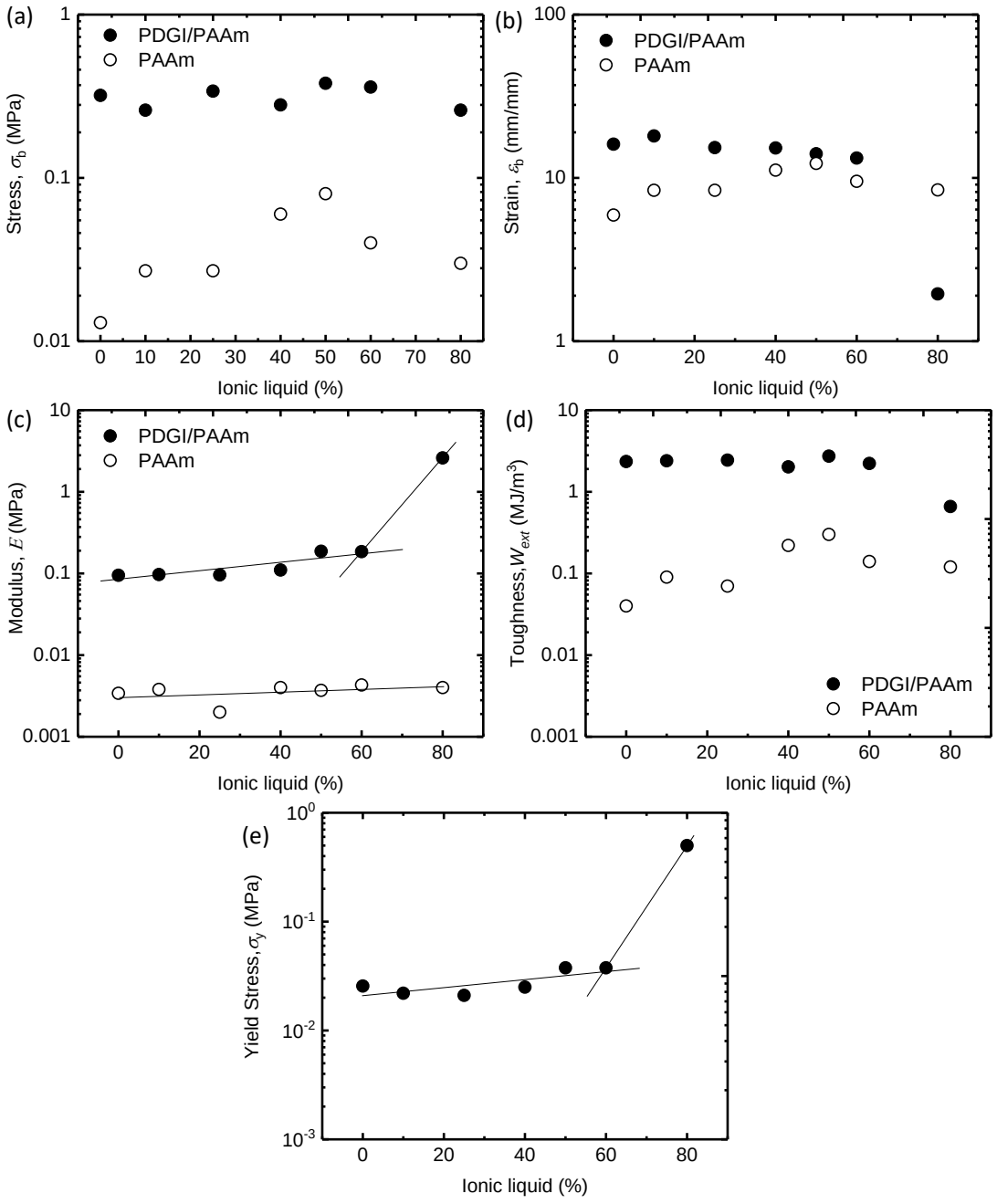

Figure 4.2.7 Summary of uniaxial tensile test results as a function of ionic liquid content. (a) Fracture stress; (b) Fracture strain; (c) Young's modulus; (d) Toughness; (e) Yield stress of PDGI/PAAm gel.

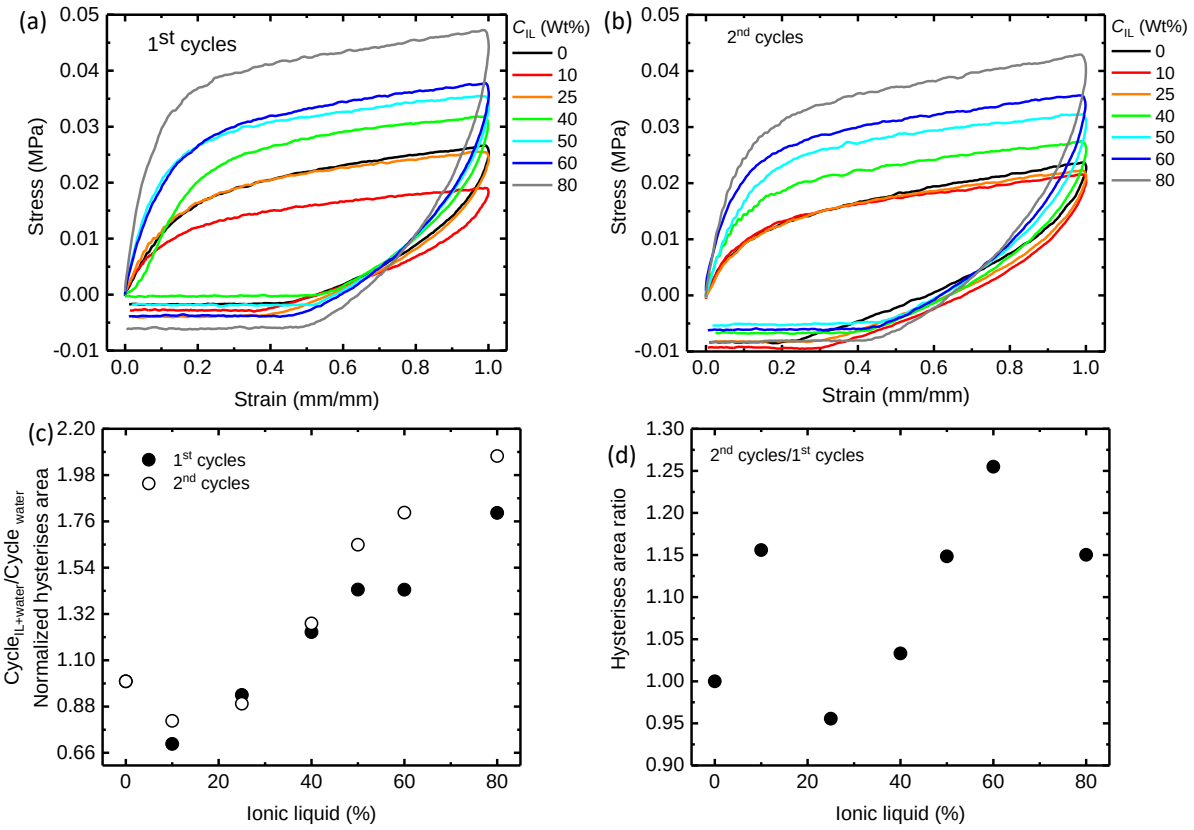

Figure 4.2.8 (a) 1st cyclic loading-unloading curve (b) 2nd cyclic loading-unloading curves of PDGI/PAAm gels in water as well as increasing ionic liquid concertation in co-solvent, respectively. The area/loop under cyclic loading-unloading curve represent the energy dissipation of soft matter also known as hysteresis energy. (c) For clarity, the normalized hysteresis area of the 1st cycle and 2nd cycles, respectively. Normalization is performed by the value of original gel sample as a reference state. (d) The hysteresis area ratio 2nd /1st cycles.

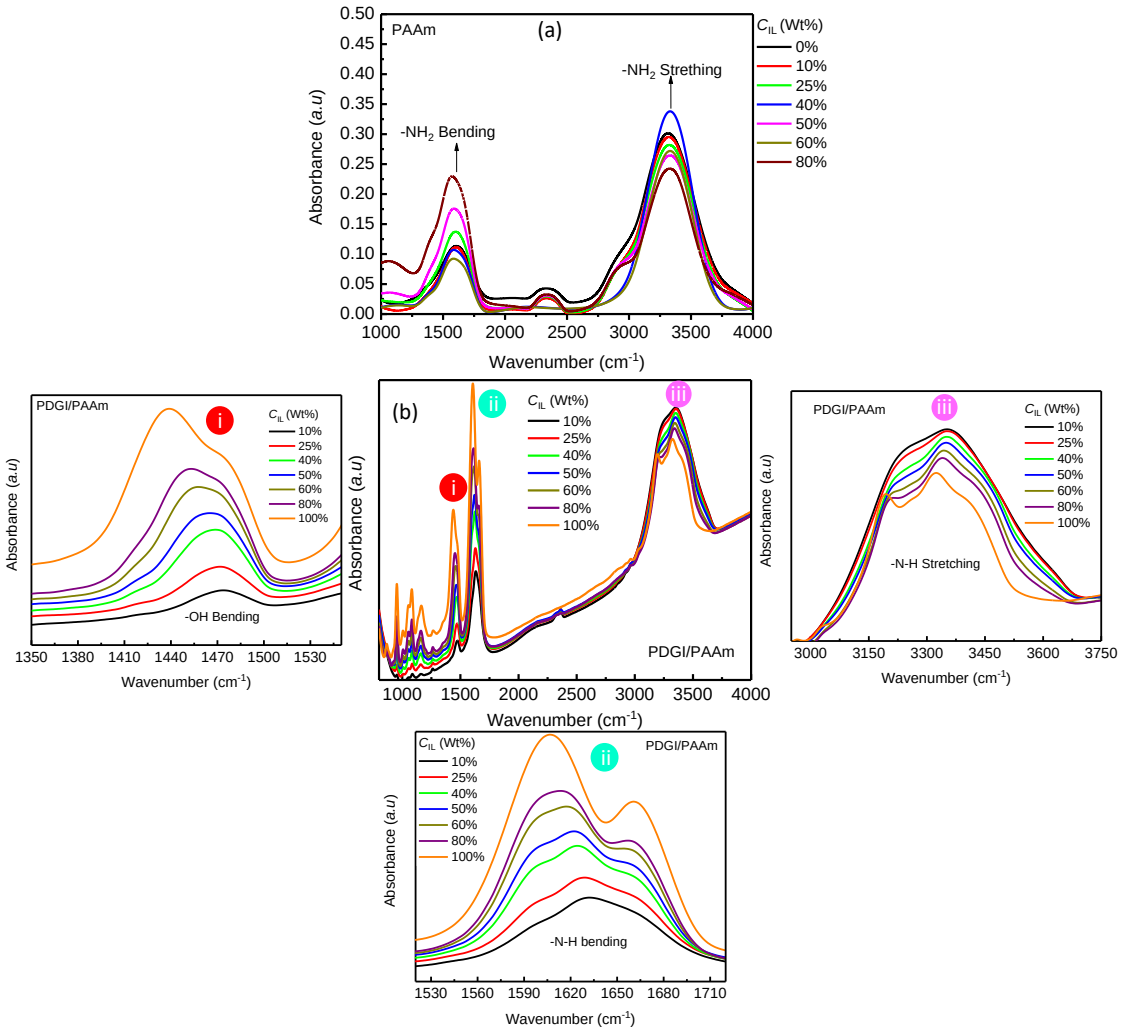

Figure 4.2.9 FTIR absorbance as a function of wavenumber 1000-4000 cm^{-1} at increasing ionic liquid concentration in co-solvent. (a) PAAm**;** (b) PDGI/PAAm. For clarity the PDGI/PAAm FTIR regions of interest are shown as an enlarged view (i)-(iii), respectively.

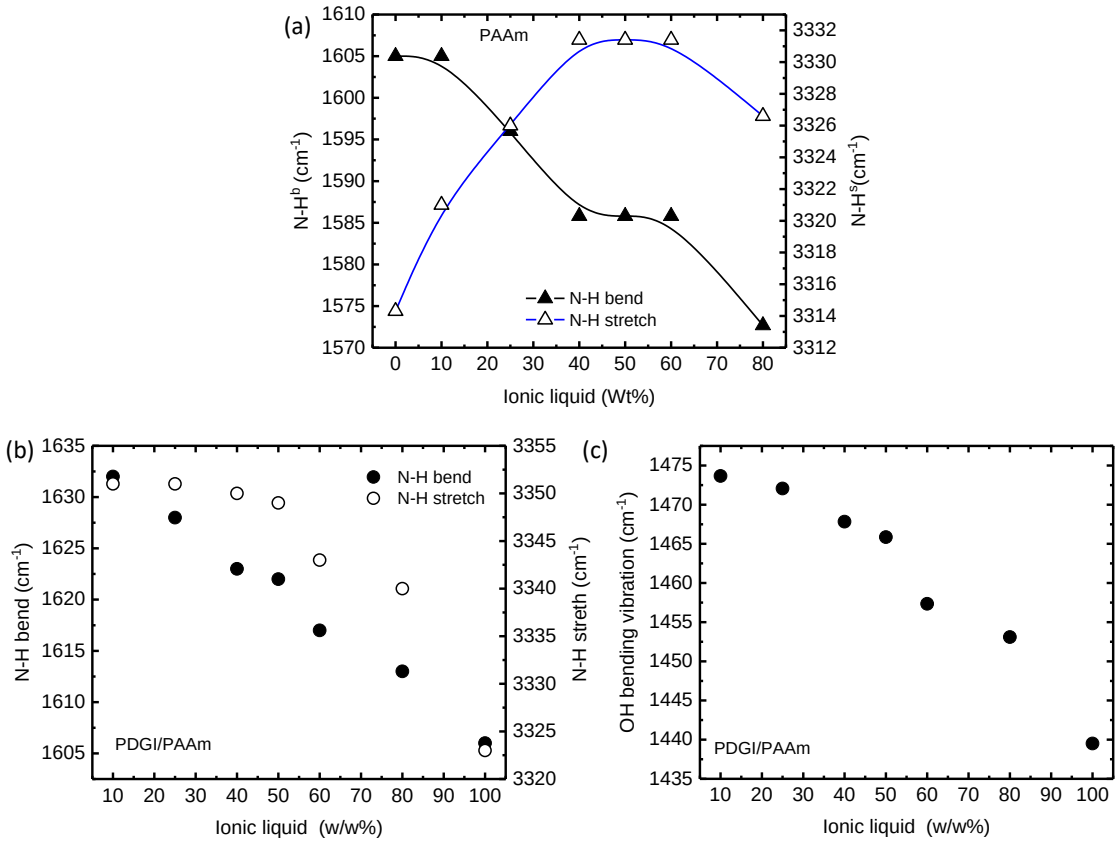

Figure 4.2.10 FTIR absorbance as a function of wavenumber 1000-4000 cm^{-1} at increasing ionic liquid concentration in co-solvent. (a) PAAm**;** (b) PDGI/PAAm. For clarity the PDGI/PAAm FTIR regions of interest are shown as an enlarged view (i)-(iii), respectively.

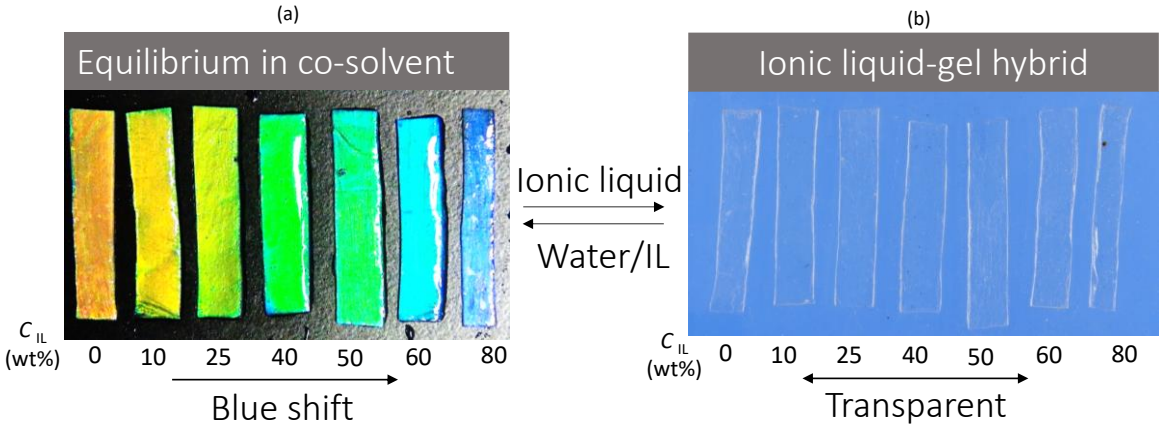

Figure 4.2.11 (a) PDGI/PAAm gels in co-solvent**.** (b) PDGI/PAAm iongels containing different ionic liquid content produced just by drying of water from co-solvent soaked gels.

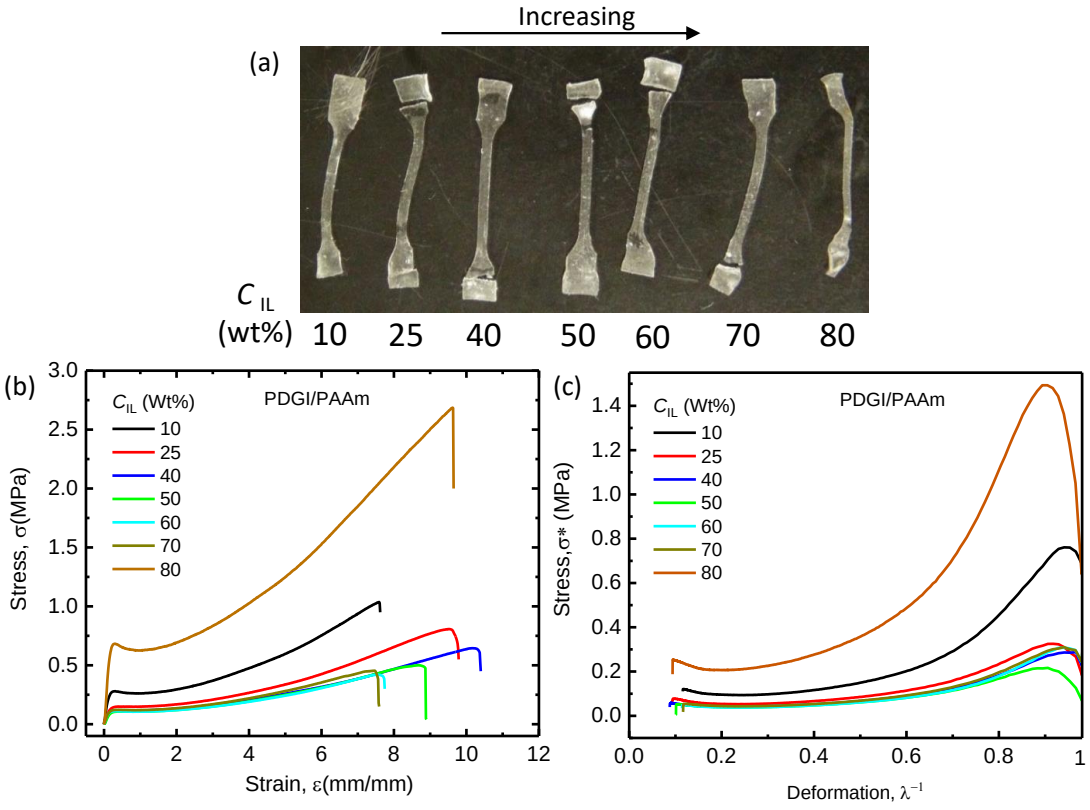

Figure 4.2.12 (a) Dumb-bell shaped PDGI/PAAm iongels. (b) Stress-strain curves of PDGI/PAAm iongels at different ionic liquid content obtained from uniaxial tension tests; (c)

Mooney-Rivlin plot of the PDGI/PAAm tensile result, where $\sigma^*=\sigma/(\lambda-\lambda^{-2})$ is the reduced stress and $\lambda=\varepsilon+1$ is the deformation ratio.

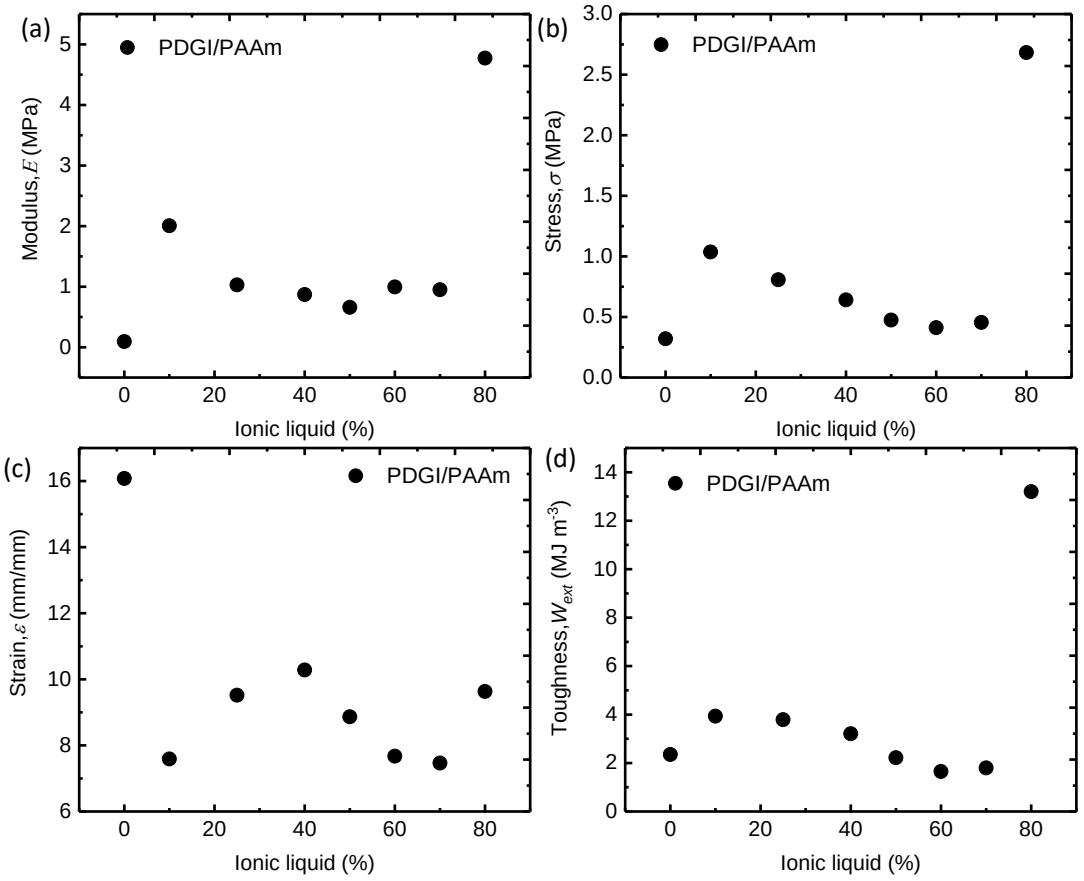

Figure 4.2.13 Summary of uniaxial tensile test results as a function of ionic liquid content. (a) Young's modulus; (b) Fracture stress; (c) Fracture strain; (d) Toughness of PDGI/PAAm gel.

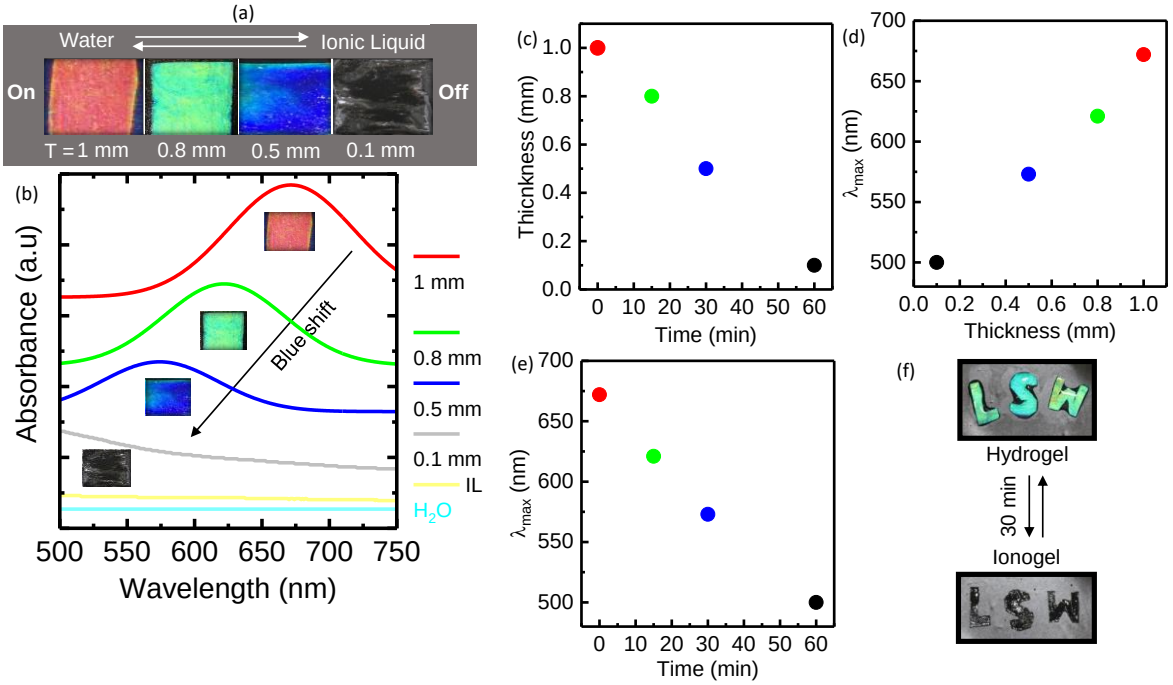

Figure 4.2.14 (a) Easy conversion of gel to iongel by adding bulk ionic or water, respectively. (b) Reflection spectra as a function of wavelength at different time after adding bulk ionic liquid on sample. (c) Thickness change with time. (d) λ_{max} nm change with thickness. (e) λ_{max} nm change with times. (f) Reversible color change of LSW by addition of bulk ionic liquid or water.

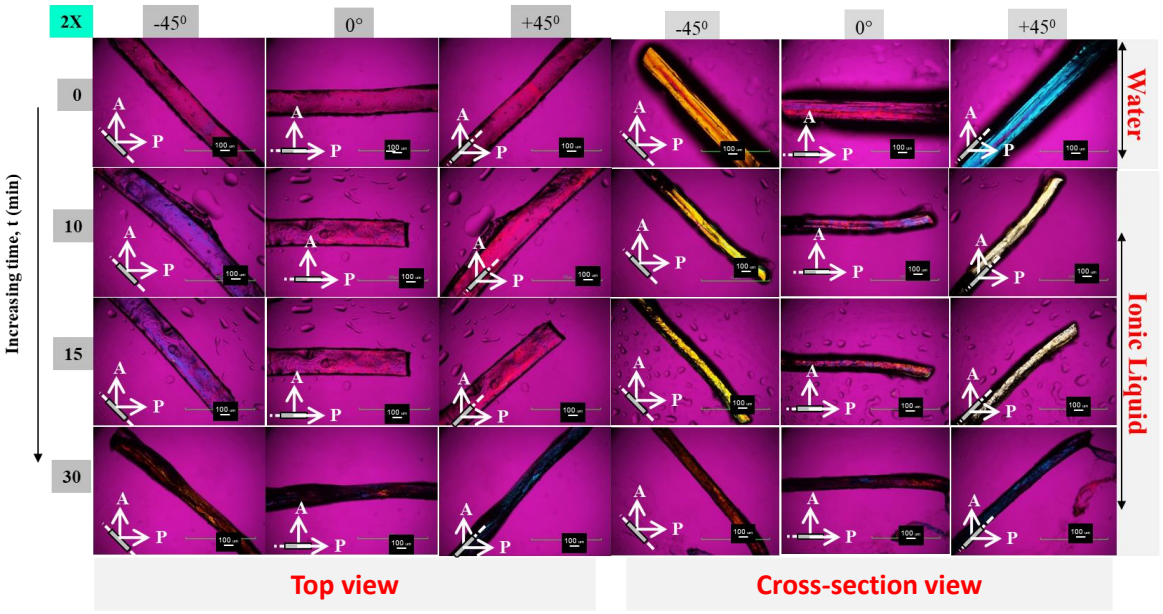

Figure 4.2.15 Polarized optical images of PDGI/PAAm gel in water and addition of bulk ionic liquid at different time from reference gel state to complete iongel formation. The left top view images parallel to the orientation of bilayers. Right cross-section view images perpendicular to the orientation axis of PDGI bilayers head groups. The observation was performed at three angles such as 0°, -45° and +45°, respectively. The pink colored background is 532 nm tint plate as reference for interference colors as a result of change in orientation. The scale for all images is 100 μm.

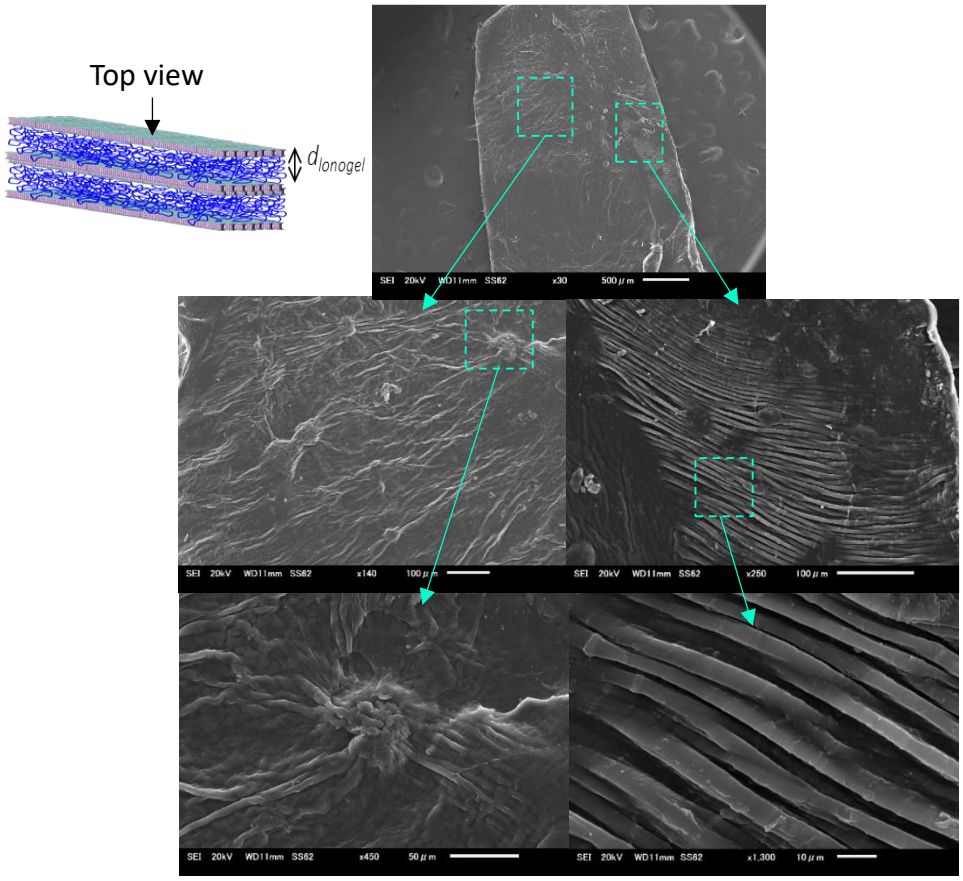

Figure 4.2.16 Top view scanning electron microscopic images of PDGI/PAAm iongel. The regions of interest are denoted by dotted lines. The arrow lines follow the different magnification images of region of interest to clarify the pattern appeared on surface of iongel.

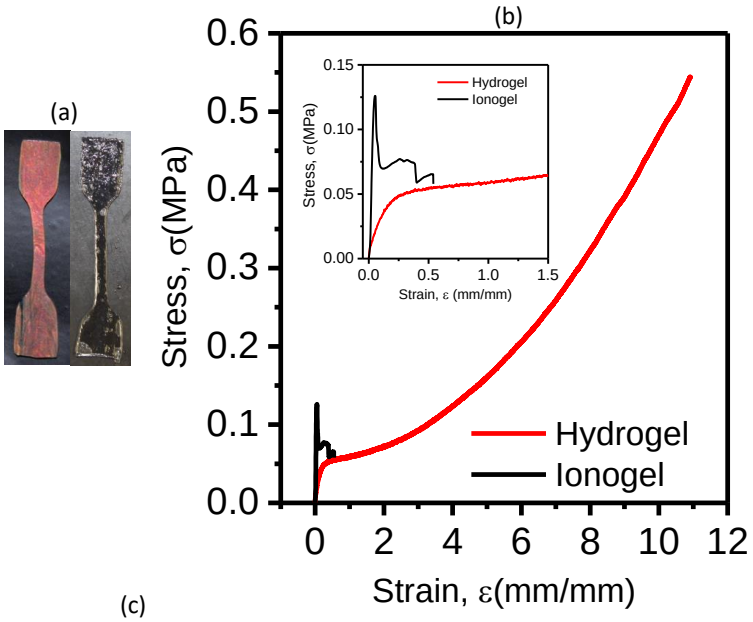

(c)

Sample code	σ (MPa)	ε(mm/mm)	E (MPa)
Hydrogel	0.57	11.20	0.24
Ionogel	0.07	0.55	4.00

Figure 4.2.17 (a) Dumb-bell shaped specimens of PDGI/PAAm gel and iongel, respectively. The dimension 12 mm gauge length, 2 mm width and thickness dependent on condition of sample (b) Tensile stress-strain curve of PDGI/PAAm gel and iongel, respectively. (c) Results from the tensile stress-strain curves. The tensile testing speed was 100 mm/min corresponds to the tensile testing strain rate of 0.14^{-s}.

code (a)	AAm Monomer [M]	DGI Monomer [M]	MBAAm Cross linker [mol%]	Irgacure Initiator [mol%]	SDS Co-surfactant [mol%]	Solvent [mL]
3	2	0.1	0.1 wrt AAm	0.1 wrt AAm	0.025	IL
4	2	0.1	0.1 wrt AAm	0.1 wrt AAm	0.025	W
Cond	Heat for 5h	55^0 C temp	Test tube	Inert Ar atm	Polymerization time	8h

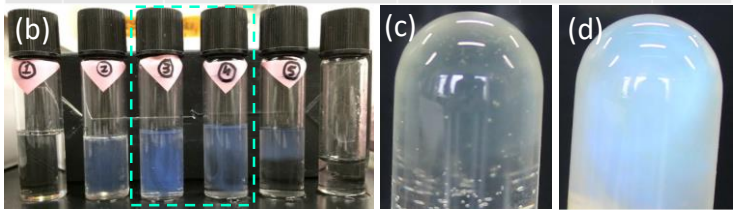

Figure 4.2.18 (a) Table of PDGI/PAAm iongel and gel precursor solution composition. (b) Left to right is AAm solution in ionic liquid ;DGI in ionic liquid with no SDS ;Standard precursor solution in water; Precursor solution in co solvent 1/1 volume ratio ionic liquid/water; Standard precursor solution in ionic liquid and pure ionic liquid. (c) PDGI/PAAm as prepared iongel. (d) PDGI/PAAm standard bilayer hybrid gel.

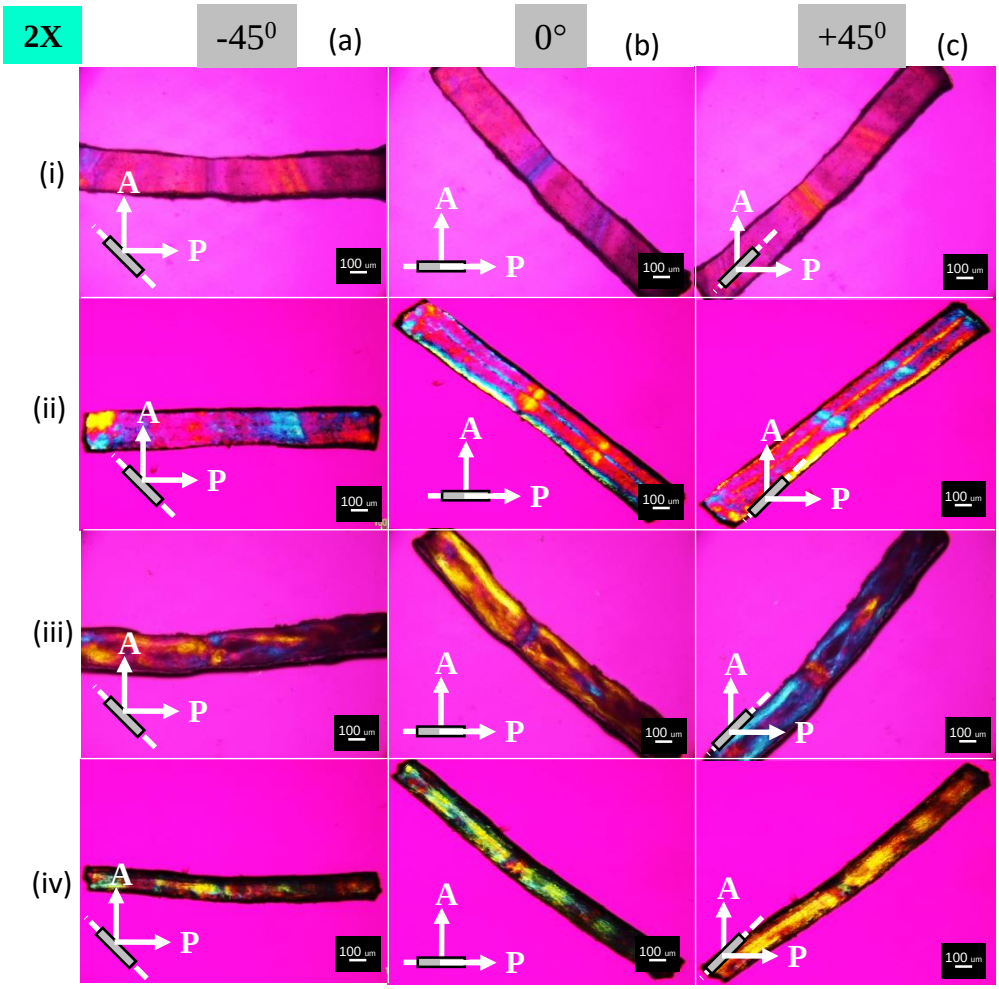

Figure 4.2.19 POM images of PDGI/PAAm iongel taken under 532 nm quarter waveplate. (a) Images at -45 °. (b) Images at 0 °. (c) Images at +45 °. Where a(i), b(i), c(i) are the top view images of as prepared iongel. Also a(ii-iv), b(ii-iv), c(ii-iv), respectively are the cross-section view images of as preparation condition iongel. This also represent aging induced orientation of bilayers in iongel.

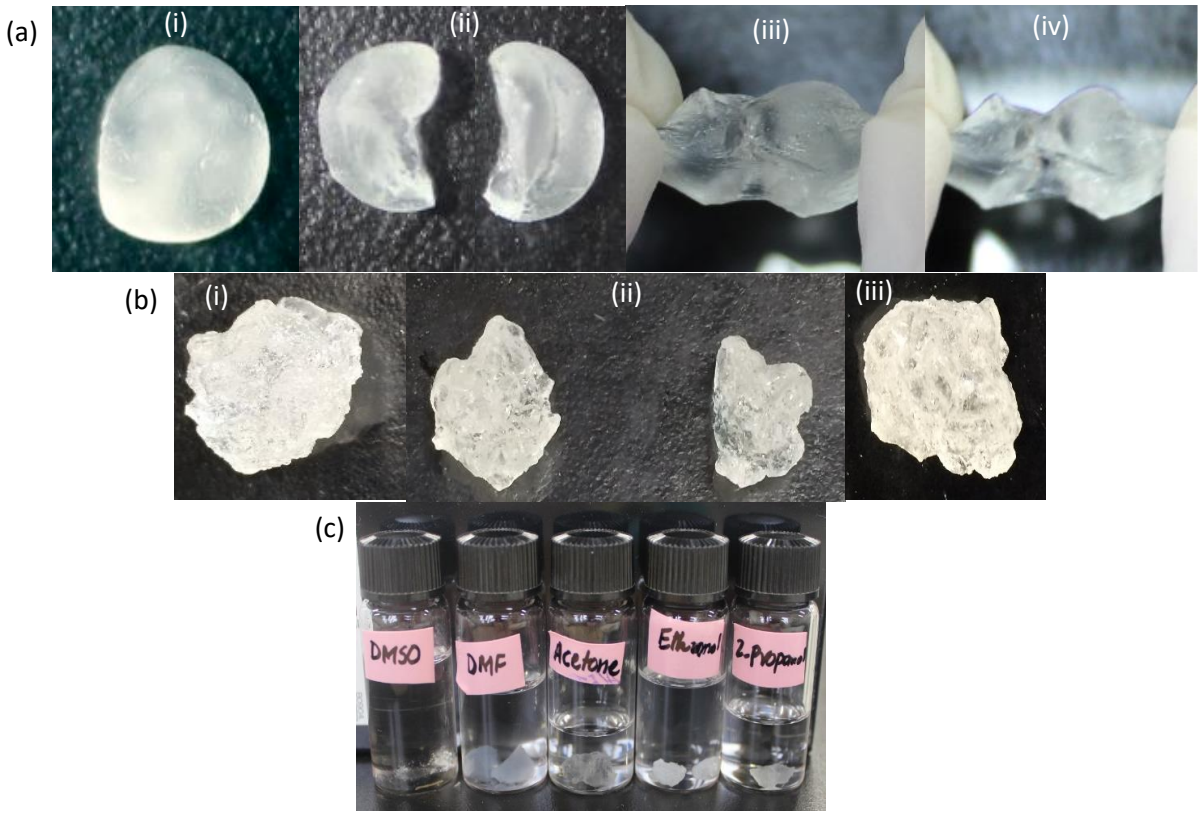

Figure 4.2.20 (a) PDGI/PAAm iongel self-healing behavior in as prepared condition. Where, a(i)-(iv) are respectively, the original sample, bisected in two pieces, the two pieces contacted together for 5s, and deformed uni-axially. (b) PDGI/PAAm iongel self-healing behavior in aged state. Where, b(i)-(iii) are respectively, the original aged specimen, cut in two pieces, the two pieces contacted together were healed already. (c) PDGI/PAAm iongel self-healing behavior in organic solvents as shown by labels on bottles. The iongel self-healed in Aceton and slightly in 2-propanol. Other solvent either dissolved the iongel (DMSO), or not healed (DMF), or became dry (ethanol).

CHAPTER 4

Structure and Properties Relationships

4.3 The Effect of Configuration Change on the Structure and Properties of Large Area Bilayer Hybrid gel

4.3.1 Introduction

Hydrogel is, a novel soft and wet, hybrid system of polymer and water. Polymer component in hydrogels remains undissolved, swollen form with a significant fraction of water within its molecular structure.[1,2] Hydrogel dominates, any other synthetic biomaterial because, of its similar physical properties to biological tissues.[3] The holding capacity of large quantity of water and their soft, wet and elastic stability pave hydrogel as potential biomaterial such as artificial bio-tissues for example artificial human skin and cartilage substitutes etc.[3–5] To fulfill the requirement of biological tissues, synthetic hydrogels must have additional functions such as bio-tissues like chiral hierarchical self-assembled structure with well define morphology.[6–10] Therefore, long range ordered chiral nanostructure, arising from the self-assembly of bio-macromolecules, is gaining great attention due to its relation to the natural biological structures and possible emergent functions in the field of sensing, well controlled drug delivery, catalysis, chiroptical switching, template for self-assembly, and tool for designing tough soft photonic materials.[7,11–14] Some recent research imprinted chirality in hydrogels which is limited to template based self-assembly of bio-macromolecules such as virus to induce chirality in hydrogel.[15] For potential application such kind of method is not acceptable and often uncontrolled. Therefore, imparting bio-systems like chiral hierarchical order structure in hydrogels, arranged at long range centimeter scale is a pressing task. Amphiphilic chiral and racemic molecules, *S*-DGI, *R*-DGI, contains hydrophilic glycerol and hydrophobic dodecyl

head groups self-assemble in aqueous solution as bilayer membranes similar to natural lipid bilayer structure was first introduced by Tsuji et al.[16–19] Their results suggested that, the configuration change has influence on the packing of bilayer membranes, therefore showing different iridescence color in solution. The chiral structure was found well packed than racemic one.[16] The racemic DGI monomer by polymerization produced partially anisotropic structure in the presence of polyacrylamide gel. Until recently, our group developed a method to incorporate racemic *R*-DGI molecules into amorphous hydrogels, on macro-scale bilayer hybrid hydrogels (PDGI/PAAm).[20] The gels displayed exceptional functions, such as structure color, high mechanical toughness, and response to stimuli.[21–26] This promises great potential of the bilayer-based hydrogels for wide range of applied research. The study of synthesis large area bilayer-hybrid hydrogels with the supramolecular self-assembled chiral structure is indispensable for the future application. Herein in this section, the synthesis and functions of racemic and chiral amphiphilic monomers and their orientation in solution as well as arrangement on centimeter scale inside large area bilayer hydrogel are discussed. The effect of changing their configuration is expected to tune the structure and mechanical behavior of PDGI/PAAm bilayer hybrid gel. Inducing chiral membrane structures into isotropic hydrogels to create chiral-bilayer-hybrid-gel is expected to show innovative functions.

4.3.2 Experimental

4.3.2.1 Materials and method

Amphiphilic racemic and chiral DGI monomers of different configuration; was synthesized according to the procedure reported by Tsuji *et al*.[13] Briefly, the crude product after the synthesis was purified by passing on packed column of silica-gel followed by elution utilizing mix-solvent of ethyl acetate-hexane keeping 1:1 volume-ratio. The separately portion of eluent contained DGI, is subjected to the process of re-crystallization on hexane-acetone mixture-

solvent 1:1 weight-ratio. The melting and recrystallization temperature of DGI monomer were 63°C and 32°C, respectively confirmed by Differential scanning calorimetry DSC. *N*,*N*′-methylenebisacrylamide MBAA (Wako Pure Chemical Industries, Ltd., Japan) was recrystallized from ethanol, acrylamide AAm (Junsei Chemical Co., Ltd., Japan) was recrystallized from chloroform, Irgacure 2959 (BASF SE, Germany), and sodium dodecyl sulfate SDS (MP Biomedicals Inc., USA) were of commercial grade. Millipore deionized water was used for the reparation of monomer solutions and equilibrium swelling of gel.

4.3.2.2 Solution preparation of *R*-*S* Amphiphilic DGI

Step 1. The precursor solution, composed of 0.1 M dodecyl glyceryl itaconate (DGI), 0.025 mol % sodium dodecyl sulfate SDS (with respect to DGI monomer), 2.0 M acrylamide (AAm), 0.1 mol% *N*,*N*'-methylenebisacrylamide (MBAA) as chemical crosslinker of AAm, and 0.1 mol % Irgacure 2959 as initiator (both in relative to AAm monomers), were mixed in aqueous media and flush with Ar gas for 1 min.

Step 2. The aforementioned precursor solution was incubated in a temperature controlled water bath for ~5 h at 55°C since the krafft temperature of DGI monomer is 43°C, to dissolve amphiphilic monomer DGI powders and stabilize lyotropic liquid crystalline phases of DGI[27], it is worth to mention that after 15 min incubation the precursor solution was shake well to avoid the self-aggregation of DGI liquid crystalline domains, then at each 30 min interval the precursor solution was sheared by shake and flow for 50 times. This method allow the domains of amphiphilic molecules to self-assemble at the micrometer length scale.

4.3.2.3 Inducing *R*-*S* Amphiphilic DGI into hydrogels

Step 3. Before polymerization, two reaction cells of 100-200 mm in length (*L*), 30-60 mm in width (*W*), and 0.05-0.5 mm in thickness (*T*) were prepared by sandwiching a 0.5 mm–thickness

of silicone rubber spacer embedded between two pre-cleaned glass plates (NaOH/Ethanol 200g/6L). The glass plates cleaning is essential step to get hydrophilic glass surface which is good for the orientation of amphiphilic domains.

Step 4. In previous method, the shear flow was applied manually to induce racemic bilayer orientation by injecting the manual injection of precursor solution to the reaction cell inside glove box.[20] In current method, automatic suction method is used to apply the constant and strong shear flow under the controlled incubation temperature using incubator with temperature console (model EYELA NTI 400E). This step is very crucial for the lyotropic liquid crystals of racemic and chiral (*R*-DGI and *S*-DGI) amphiphilic domains because their gel to liquid crystalline phase transition temperature is ~43°C. Briefly, in separate batches inside incubator one end of the preheated reaction cell was connected to a suction pump (model Harvard PHD 4400 programmable), and through the other end, the precursor solution containing amphiphilic racemic and chiral domains was suctioned vertically to the reaction cell against the gravity at a high suction rate for a strong shear flow (~133 s^{-1}) at 50°C that induced the alignment of racemic and chiral DGI domains between glass plates at controlled temperature inside incubator, respectively**.** This method permitted us to obtain a uniform chiral and racemic DGI lamellar phase, even with 3 times the sample area of the previous method, oriented uni-axially along the glass walls.

4.3.2.4 Gelation induced fixing *R*-*S* Amphiphilic DGI into hydrogels

Step 5. This was followed by a co-current homo-polymerization of the DGI and AAm using UV light irradiation for 8 hours at 50°C inside incubator. This step is very important to fix the already oriented racemic and chiral domains in conventional polymer matrix. In case of delayed UV irradiation the gel might have un-oriented domains.

4.3.2.5 Hydrogels swelling containing *R*-*S* amphiphilic PDGI

Step 6. After the polymerization, the gel was removed from the reaction cell either by peeling from glass plate or soaking in water in the case of thin gel. Then immersed in a large amount of water for 7 days to reach equilibrium swelling state and to wash away the residual chemicals. PAAm hydrogels were synthesized by UV irradiation from a precursor solution containing 2.0 M AAm, 0.1 mol% MBAA, and 0.1 mol% Irgacure 2959 as initiator using the same technique.

4.3.3 Characterization

4.3.3.1 Polarized optical microscopy (POM)

The bilayer hybrid gels were swollen in water for at least 1 week and cut into 1 cm long pieces. The thickness of gel in as prepared T_0 and water swollen T were measured by polarized optical microscopy (POM). The orientation of bilayers in hybrid system is confirmed.

4.3.3.2 Measurement of mechanical properties

The dumb-bell shaped gel specimens, standard dimension (length, L = 12 mm width, W = 2 mm and thickness of swollen gel, T) were cut with commercial standard gel cutter (model JIS-K6251-7). The uniaxial tensile and cyclic tests were performed using commercial tensile tester (Instron Anton Paar 5965) with tensile velocity 100 $mm.min^{-1}$ & stretching rate 0.14 s^{-1}. The modulus (stiffness) was calculated from the initial slope of the tensile stress-stretch curves

within 5% deformation. The tensile tests were performed three times and average values with error bar were adopted.

4.3.3.3 Measurement of reflection spectrum

The structure color of racemic and chiral DGI monomer contained precursor solution and their PDGI/PAAm gels was characterized by the electromagnetic spectrum of light, using moveable angle reflection measurement optics (Hamamatsu Photonics KK, C10027A10687) coupled with photonic multichannel analyzer (Hamamatsu Photonics KK, C10027). White light from Xe source was used to irradiate the gel. Reflection spectrum was acquired by keeping both the angles of incident (Bragg's angle) and reflection at 60°. The wavelength at maximum reflection intensity, λ_{max}, was obtained from the reflection spectrum. The inter-lamellar distance (d) was estimated by using the Bragg's law of diffraction,

$$\lambda_{max} = 2nd\sin\theta \qquad (5)$$

Here n is the refractive index of water (1.33) and θ is the Bragg's angle (60°).

4.3.4 Results and discussion

4.3.4.1 Iridescence color shift in solution

The precursor solution containing racemic and chiral monomer of same 0.1M concentration are shown in **Figure 4.3.1a,b,c,d**. The results indicated that before heating and shaking the domains self-aggregated at local regions without obvious iridescence and opaque color appeared. The phases separation can be observed visually [**Figure 4.3.1a(i),(ii)]**. In case of leaving at this state for longer time without shaking/mixing the onion like structure will stabilize that alters the structure color of the final gel. Therefore, after heating solution and gradual mixing/shaking the solution for 5h at 55°C above the krafft temperature[28,29] of DGI monomer are shown in **Figure**

4.3.1b, sufficiently dissolved amphiphilic racemic and chiral DGI monomers, the solution appeared as green and blue iridescent colors, respectively for chiral and racemic [**Figure 4.3.1b(i),(ii)]**. The self-assembly of monomeric domains arrange at large scale inside the precursor solution give beautiful homogenous structural color by satisfying the Braggs law of diffraction as shown from different angles [**Figure 4.3.1b(i),(ii)],** [**Figure 4.3.1c(i),(ii)] and** [**Figure 4.3.1d(i),(ii)].** Previous research suggested that, the structural color arises as a result of interlayered distance of the ordered structure even in solution of lamellar phases with a red shift of 4 nm between the racemic and chiral DGI molecules.[16] Therefore, the corresponding color of the solution of racemic and chiral DGI is quantified using reflection spectrometer, the spectra and results are shown in [**Figure 4.3.2a, c].** The results suggested that, the chiral DGI showed red shift in solution as compared to the racemic DGI. The values of maximum wavelength of reflection (λ_{max} 466 nm), the distance between consecutive chiral bilayers (*d* 269 nm) and full width at half maxima (FWHM 66 nm) of reflection peaks were quite higher than that of the racemic DGI solution (λ_{max} 430 nm, *d* 248 nm, FWHM 26 nm) indicating slight red shift in solution [**Figure 4.3.2a, c]**. This is also consistent with the visual color of the solution as chiral solution appears intense green than that of racemic blue color solution. The distance between repeating chiral bilayers is ~20 nm higher than racemic as in **Figure 4.3.2c.** This value is much higher than the reported literature that showed 4 nm difference of *d* value.[16] One possible reason might be the difference between concentrations of precursor solution of DGI monomer, here we used 0.1M concentration to prepare chiral and racemic monomers precursor solutions. However, the full width at half maxima of the racemic reflection peak (26 nm) is lower than the chiral (66 nm), representing the good packing of racemic DGI molecules in the precursor solution. Now we showed that the precursor solution containing racemic and chiral amphiphilic monomer displayed beautiful iridescence structural color in the presence of acrylamide

monomer along with crosslinked and initiators. The next question arises weather the configuration of racemic and chiral amphiphilic lamellar phases will maintain after gelation of precursor solution.

4.3.4.2 Iridescence color after gelation

Although the conversion and rate of polymerization has been reported in the literature.[16] To date no study has been devoted to the reinforcement of chiral bilayers arranged at long distance in centimeter scale in hydrogels. The aforementioned precursor solution after strong shear flow by automatic pump, polymerization and swelling the resultant racemic and chiral gels in water, the reflection spectra and their comparison of results is shown in [**Figure 4.3.2b, d**]. Interestingly, after polymerization the chiral bilayers inside the gel behavior is very different from its monomeric bilayers in solution state. The peak wavelength was found intense narrow (λ_{max} 503 nm) with the distance between consecutive chiral bilayers slightly increased (*d* 270.5 nm) and full width at half maxima reduced (FWHM 38 nm). Similarly the racemic DGI after gelation showed slight red shift compared to its solution condition. The racemic solution showing blue color was changed to green gel (λ_{max} 483 nm), with slight increase in distance between racemic bilayers (*d* 230 nm), the value of full width half maxima (FWHM 62 nm) increased as compared to solution indicating slight red shift in gel state [**Figure 4.3.2a, c]**. However, the chiral PDGI/PAAm gels again showed red shift in gel condition in comparison to racemic PDGI/PAAm gel. Another interesting results is the increase *d* value which is related to the reduction of surface area of bilayers after polymerization that would bring the DGI molecules much closer to each other by self-assembly.[16] The reduced value of full width at half maxima of chiral PDGI also represent closed packed PDGI molecules. This is obvious because the steric configuration of chiral molecules are of similar that prefer to reduce the surface area of aligned bilayers membrane. The reduction of surface area of chiral PDGI

bilayers causes to increase the distance between the alternating chiral PDGI bilayers. As a consequent, the polymerization of chiral DGI showed red shift in gel condition. The racemic bilayers FWHM lower than the chiral molecules also indicated that the packing density of racemic molecules is not as good as that of the chiral. However, in solution form the racemic DGI molecules were of good packing with blue color and distance between racemic bilayer was lower than that of racemic gel condition. After polymerization the racemic PDGI bilayers were of slightly poor packing because of the different steric configuration in racemic molecules. Now we understand the packing difference between racemic and chiral molecules in gel form. Next the optical study was performed to understand the microscopic difference between the two types of configuration and their influence on birefringence of the overall gel.

4.3.4.3 Enhancement of birefringence

The equilibrium swollen racemic and chiral PDGI/PAAm gels (N ~4000) polarized optical microscopic images are shown in **Figure 4.3.3a,b.** The observation of specimens were performed at three angles such as 0°, -45°, +45° from top and cross-section side of gels using 532 nm quarter wave plate as well as cross polarizers, respectively. The racemic and chiral PDGI/PAAm gels top view images at any angle either with tint plate or cross-polarizer were without birefringence, indicating the head group of racemic and chiral molecules aligned well that do not deviate the propagation of light waves **Figure 4.3.3a (i),(ii) and 4.3.3b(i),(ii).** However, the cross-section of gels with tint plate exhibited yellow and blue colored interference that were bright white under cross-polarizers at viewing angle of -45° and +45°, respectively. The obvious difference was at a viewing angel of 0°, where the racemic gel still showed some orientation colors which was absent in chiral gel. Another difference was the bright and homogenous birefringent of chiral gels indicating well packed and alignment of chiral bilayers in PDGI/PAAm gel as compared to that of the racemic bilayers in racemic PDGI/PAAm gel.

The reason of high bright and intense colored chiral PDGI/PAAm gel is also attributed to the well and dense packing of chiral PDGI molecules. The equilibrium swelling ratio in thickness direction (T/T_0) for racemic and chiral PDGI/PAAm gels are shown in **Figure 4.3.3c.,** where the T and T_0 are respectively the thickness value of equilibrium water swollen gels and as prepared gels. The swelling behavior is related to the permeability difference between the PDGI molecular layers and PAAm chains. The PDGI layers because of their dodecyl groups are impermeable to water either from surface or side wise. However, the water loving polyacrylamide chain are solvated/dry by water molecules entering or evaporation causes the thickness of gels to increase or decrease. Another interesting fact is that the PAAm layers are strongly pinned to the PDGI surfaces by weak hydrogen bonding. Therefore, the thickness wise ratio of gel must be increase. It is expected that, the change of configuration would have influence on the packing of PDGI molecules that must show different swelling ratio in water. Being higher thickness ratio for dense packed as compared to the less dense packing of bilayers molecules. The results indicated that thickness ratio of chiral gel is higher than that of the racemic gel which is well in agreement with the assumption. This also in agreement with the higher *d* value obtained from relation spectra.

4.3.4.4 Enhancement of energy dissipation

In this section the effect of contrasting molecular structure on the gel mechanical properties is given. Some previous literature suggest that changing configuration can alter the rigidity of amphiphilic bio-macromolecules that contains hydrophilic and hydrophobic sites.[7,30,31] For examples amino acids of racemic and chiral structure reported in literature showed changed of the rigidity in their hydrogel formation.[32] To understand the effect change of racemic and chiral configuration on the bilayers hybrid gel mechanical properties of PDGI/PAAm gels. Therefore uniaxial tensile test along the bilayer packing direction was performed. The stress-

strain curves of the PDGI/PAAm samples of different configuration are shown in **Figure 4.3.4(a).** The comparison of their results such as modulus, fracture strain, fracture stress, toughness and yield stress are summarized in **Figure 4.3.4c**, respectively. The Mooney-Rivlin plot of stress strain data is also given in **Figure 4.3.4(b).**

According to the results from tensile tests, the racemic and chiral bilayers reinforce hydrogels showed almost similar level of tensile deformation 12 mm/mm. The tensile strength 0.38 MPa of racemic gel was slightly higher than that of the chiral gel 0.28 MPa. The toughness related to the energy density of soft materials is higher for racemic gel 1.85 than chiral gel 1.6 $MJ.m^{-3}$. However, the modulus of chiral gel was quite higher than racemic gel, indicating the stiffness and rigidity of chiral bilayers whose molecules are arranged densely at long range in the form of membrane inside the gel that enhanced the stiffness of bilayers as a result of same steric site groups. Another important feature of bilayer is its sacrificial behavior. The previous research on membrane embed hydrogels suggested that bilayers act as reversible sacrificial bonds that dissipates energy by applying deformation either by flow behavior or rupture.[33,34] The sacrificial behavior is well related to the phenomena of yielding or necking.[35–37] Therefore, the comparison of yielding stress from tensile stress strain curve between racemic and chiral hydrogel is worth to study. The yielding of chiral gel is higher than that of the racemic gel. Again this indicated the well packed dense structure of chiral molecules in bilayers. This yielding is followed by the transfer of deformation to the matrix gel PAAm with a pronounce strain hardening just before fracture failure of gels. Therefore, the configuration of amphiphilic molecules has pronounce effect on the gel mechanical properties. By tuning the configuration one can tune the gel mechanics.

For better comparison of the tensile behaviors at different configuration, the tensile data for the lamellar racemic and chiral gels is shown by the Mooney–Rivlin plots in **Figure 4.3.4b**. The

racemic gel exhibited nearly a plateau regions at large elongation, which might correspond to ideal rubbery-like behaviors as featured by pronounce strain-hardening at the extreme elongation before fracture due to the effect of finite extensibility. The initial low deformation ratio the reduce stress of chiral gel is higher than racemic gel.

4.3.5 Conclusion

In conclusion, we succeeded to synthesized amphiphilic molecules of different configuration. Systematically the effect of racemic and chiral configuration on the structural color of precursor solution was studied. Then a method was developed to induce racemic and chiral bilayers in PAAm gels matrix and synthesized large area bilayer-hybrid photonic gel with alternating racemic and chiral layered structures. The gels showed nicely arranged one dimensional chiral bilayers that enhanced the structural color, birefringence as well the yielding behavior of bilayer hybrid gel. This method might open new ways to explore various novel function of chiral bilayer hybrid gels in biomedical application.

4.3.6 References

[1] N. A. Peppas, B. V. Slaughter, M. A. Kanzelberger, In *Polymer Science: A Comprehensive Reference, 10 Volume Set*; Elsevier, 2012; Vol. 9, pp. 385–395.

[2] Y. Tamai, H. Tanaka, K. Nakanishi, *Macromolecules* **1996**, *29*, 6761.

[3] J. P. Gong, Y. Osada, Springer Berlin Heidelberg, 2010; pp. 203–246.

[4] J. P. Gong, Y. Katsuyama, T. Kurokawa, Y. Osada, *Advanced Materials* **2003**, *15*, 1155.

[5] H. Shin, B. D. Olsen, A. Khademhosseini, *Biomaterials* **2012**, *33*, 3143.

[6] M. Inaki, J. Liu, K. Matsuno, *Philosophical Transactions of the Royal Society B:*

Biological Sciences **2016**, *371*, 20150403.

[7] J. I. Takahashi, H. Shinojima, M. Seyama, Y. Ueno, T. Kaneko, K. Kobayashi, H. Mita, M. Adachi, M. Hosaka, M. Katoh, *International Journal of Molecular Sciences* **2009**, *10*, 3044.

[8] A. D. Rey, *Soft Matter* **2010**, *6*, 3402.

[9] J. W. Goodby, *Proceedings of the Royal Society A: Mathematical, Physical and Engineering Sciences* **2012**, *468*, 1521.

[10] F. Rolf M., *Journal of Chemical Information and Modeling* **2013**, *53*, 1689.

[11] P. Xie, X. Liu, R. Cheng, Y. Wu, J. Deng, *Industrial and Engineering Chemistry Research* **2014**, *53*, 8069.

[12] P. Yin, Z. M. Zhang, H. Lv, T. Li, F. Haso, L. Hu, B. Zhang, J. Bacsa, Y. Wei, Y. Gao, Y. Hou, Y. G. Li, C. L. Hill, E. B. Wang, T. Liu, *Nature Communications* **2015**, *6*, 1.

[13] L. Zhang, L. Qin, X. Wang, H. Cao, M. Liu, *Advanced Materials* **2014**, *26*, 6959.

[14] P. Duan, L. Qin, X. Zhu, M. Liu, *Chemistry - A European Journal* **2011**, *17*, 6389.

[15] X. Pei, T. Zan, H. Li, Y. Chen, L. Shi, Z. Zhang, *ACS Macro Letters* **2015**, 1215.

[16] X. Chen, G. Matsuo, B. Ohtani, K. Tsujii, *Journal of Polymer Science Part A: Polymer Chemistry* **2007**, *45*, 4891.

[17] J. Ozawa, G. Matsuo, N. Kamo, K. Tsujii, *Macromolecules* **2006**, *39*, 7998.

[18] K. Naitoh, Y. Ishii, K. Tsujii, *The Journal of Physical Chemistry* **1991**, *95*, 7915.

[19] M. Hayakawa, T. Onda, T. Tanaka, K. Tsujii, *Langmuir* **1997**, *7463*, 3595.

[20] M. A. Haque, G. Kamita, T. Kurokawa, K. Tsujii, J. P. Gong, *Advanced Materials* **2010**, *22*, 5110.

[21] M. A. Haque, J. P. Gong, *Reactive and Functional Polymers* **2013**, *73*, 929.

[22] Y. F. Yue, M. A. Haque, T. Kurokawa, T. Nakajima, J. P. Gong, *Advanced Materials* **2013**, *25*, 3106.

[23] Y. Yue, T. Kurokawa, M. A. Haque, T. Nakajima, T. Nonoyama, X. Li, I. Kajiwara, J. P. Gong, *Nature communications* **2014**, *5*, 4659.

[24] T. Nakajima, C. Durand, X. F. Li, M. A. Haque, T. Kurokawa, J. P. Gong, *Soft matter* **2015**, *11*, 237.

[25] K. Mito, M. A. Haque, T. Nakajima, M. Uchiumi, T. Kurokawa, T. Nonoyama, J. P. Gong, *Polymer* **2017**, 1.

[26] M. Ilyas, M. A. Haque, Y. Yue, T. Kurokawa, T. Nakajima, T. Nonoyama, J. P. Gong, *Macromolecules* **2017**, acs. macromol.7b01438.

[27] K. Naitoh, Y. Ishii, K. Tsujii, *Journal of Physical Chemistry* **1991**, *95*, 7915.

[28] K. Corporation, **1983**, *10*.

[29] H. Kunleda, T. Krafft, E. Section, **1976**, *80*, 2468.

[30] Z. Shen, T. Wang, M. Liu, *Langmuir* **2014**, *30*, 10772.

[31] T. Gibaud, E. Barry, M. J. Zakhary, M. Henglin, A. Ward, Y. Yang, C. Berciu, R. Oldenbourg, M. F. Hagan, D. Nicastro, R. B. Meyer, Z. Dogic, *Nature* **2012**, *481*, 348.

[32] K. J. Nagy, M. C. Giano, A. Jin, D. J. Pochan, J. P. Schneider, *Journal of the American Chemical Society* **2011**, *133*, 14975.

[33] M. A. Haque, T. Kurokawa, G. Kamita, J. P. Gong, *Macromolecules* **2011**, *44*, 8916.

[34] X. Li, T. Kurokawa, R. Takahashi, M. A. Haque, Y. Yue, T. Nakajima, J. P. Gong, *Macromolecules* **2015**, *48*, 2277.

[35] J. P. Gong, Why are double network hydrogels so tough? *Soft Matter* **2010**, *6*, 2583.

[36] K. H. Nitta, M. Takayanagi, *Polymer Journal* **2006**, *38*, 757.

[37] Y. Tanaka, Y. Kawauchi, T. Kurokawa, H. Furukawa, T. Okajima, J. P. Gong, *Macromolecular Rapid Communications* **2008**, *29*, 1514.

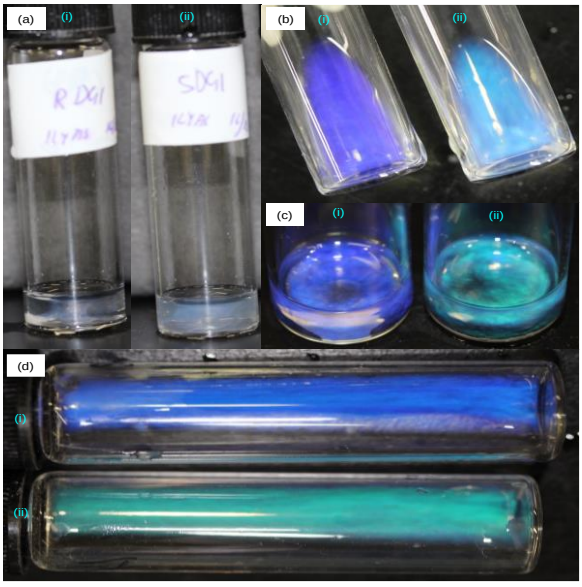

Figure 4.3.1 Photographs of precursor solution. (a) At 55°C temperature for 15 min in incubator before shaking and mixing. (b), (c) and (d) are respectively precursor solution after 5h at 55°C shaking and mixing. The images were taken from different viewing angles, respectively. Where, a-c(i), a-c(ii) are racemic *R* DGI and chiral *S* DGI monomers in precursor solution. The DGI monomers concentration was same 0.1M.

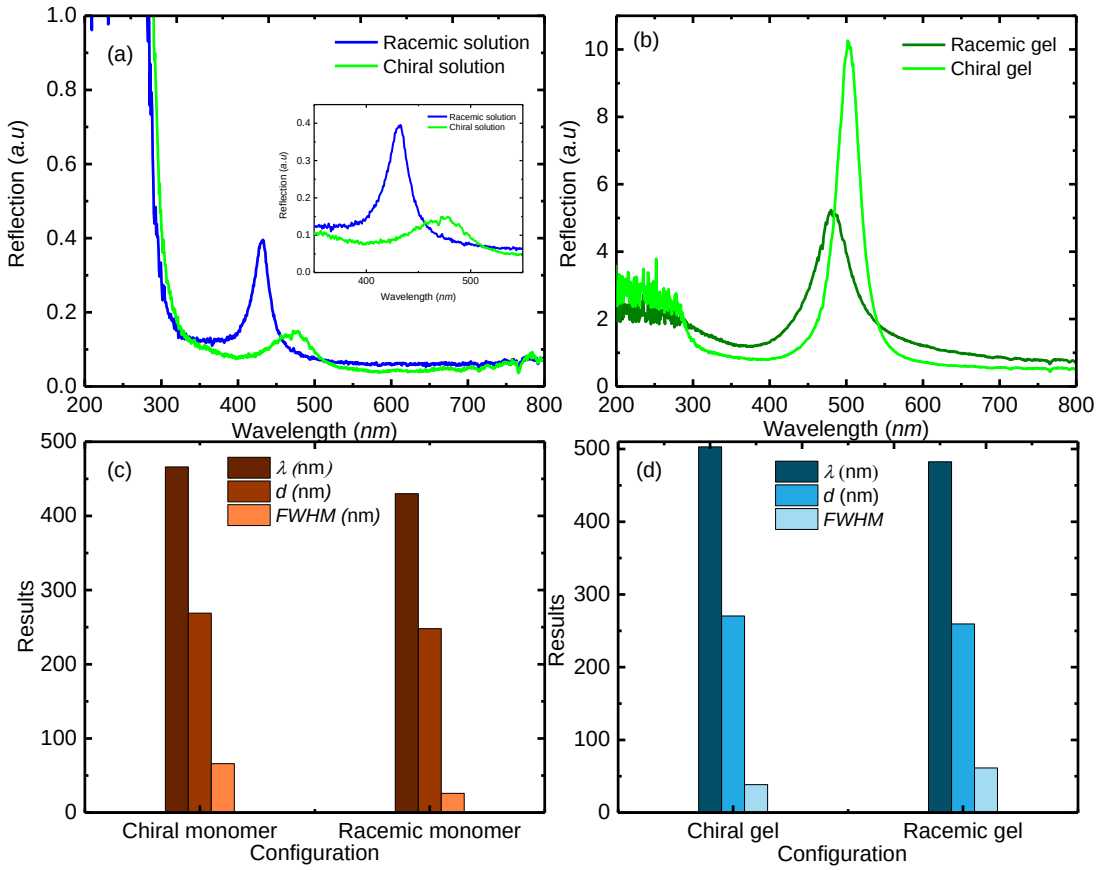

Figure 4.3.2 (a) Reflection spectra of racemic (blue line) and chiral (green line) DGI precursor solution. For clarity the figure is enlarged as inserted figure. (b) Reflection spectra of PDGI/PAAm gels contain racemic (dark green line) and chiral PDGI. (c) Results from reflection spectra of monomers. (d) Results from the reflection spectra of gels. Where, λ nm. *d* nm, *FWHM*, are respectively the maximum wavelength, distance between bilayers and Full-width-half-maxima.

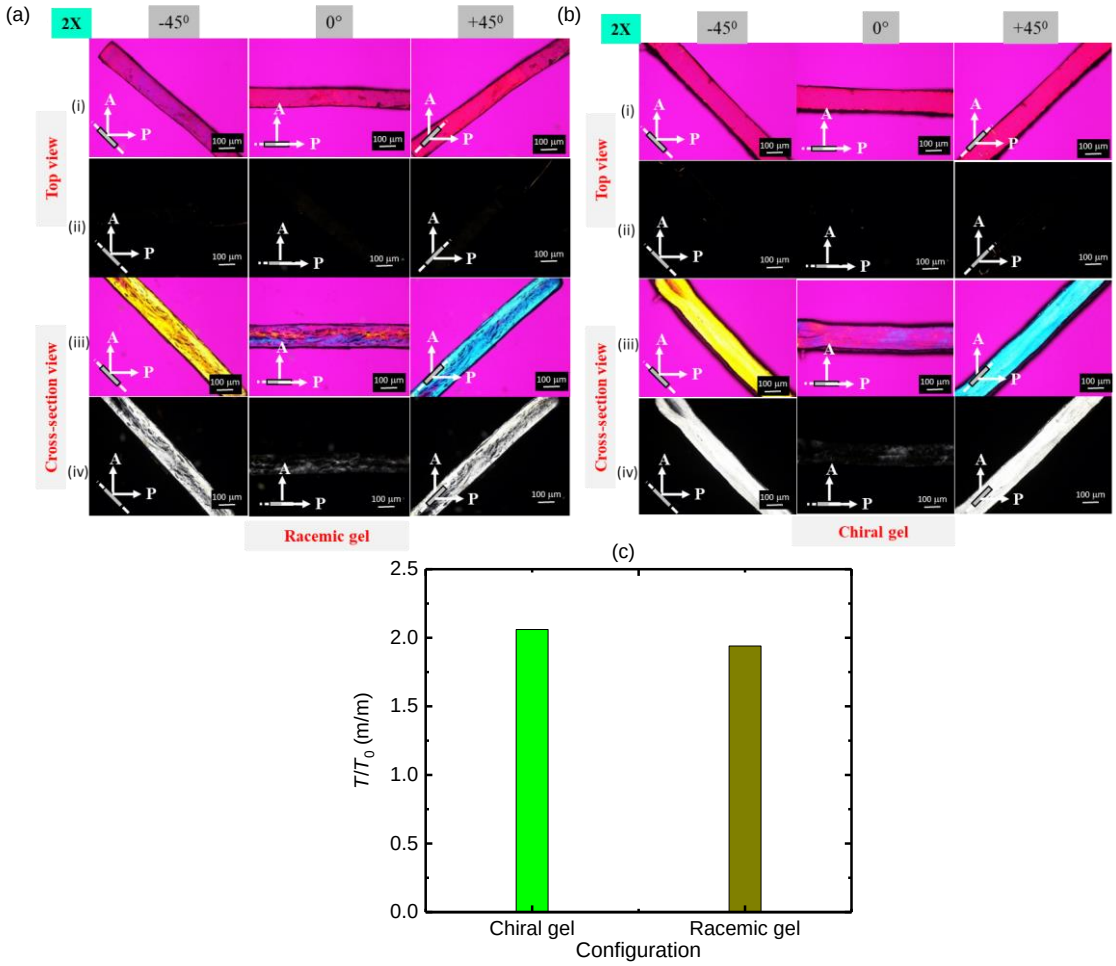

Figure 4.3.3 (a) POM images of racemic PDGI/PAAm gel. (b) POM images of chiral PDGI/PAAm gel. (c) Ratio of change in thickness (T/T_0) for racemic and chiral PDGI/PAAm gels, receptively. Where, T is the water equilibrium swollen thickness and T_0 is the thickness of as synthesis condition.

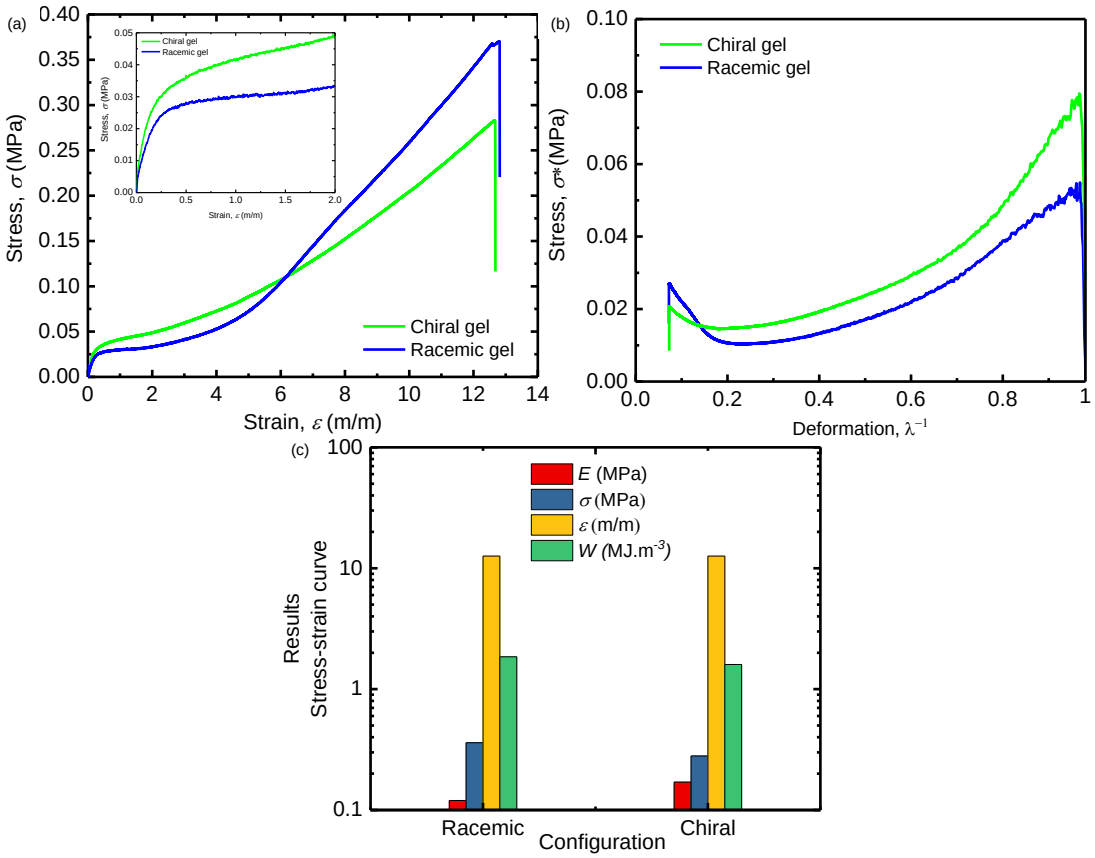

Figure 4.3.4 (a) Tensile stress-strain curves of racemic and chiral PDGI/PAAm gels. (b) Mooney-Rivlin curve fitting of the tensile stress-strain curve in term of reduced stress as a function of deformation ratio. Where $\sigma^*=\sigma/(\lambda-\lambda^{-2})$ is the reduced stress and $\lambda=\varepsilon+1$ is the elongation ratio. (c) Results from stress-strain curve of racemic and chiral PDGI/PAAm gels. Where, E,σ, ε and W, are Young's modulus, fracture stress, fracture strain and toughness, respectively.

CHAPTER 5

Drying Induced Functions of Bilayer Hybrid Gel

5.1 Introduction

In nature, the process of drying is often associated with fascinating functions such as the dry scales, wings, and feathers of certain organisms shows reversible color change upon exposure to water, act as photonic display devices for communication.[1–7] The dry nacre in addition to iridescence metallic luster is known for high strength & toughness.[8–10] All these functions are due to the presence of self-assembled sophisticated microstructure.[11–14] Therefore, gaining tremendous attention and are model system for the fabrication of biomimetic materials that shows directional intake/release of water and structural materials in the field of materials science and technology. On the contrary, polymer hydrogels are soft and wet materials.[15] There are very limited functions associated with the drying of conventional hydrogels because of their isotropic structure.[16,17] Considering that the natural hybrid materials have anisotropic, ordered microstructure of multicomponent, it is important to study the drying induced functions of hydrogels possessing ordered microstructures from hydrophobic and hydrophilic components.

Recent research on bilayers reinforced hydrogels greatly improved the applicability of ordinary PAAm hydrogel. The system contains 1D aligned multilayered structure along the rectangular direction.[18–24] with repeating layers of uniaxially oriented poly(dodecyl glyceryl itaconate)(PDGI) bilayer membrane (4.7 nm thick) and the chemically crosslinked or non-crosslinked polyacrylamide (PAAm) hydrogel layer (several hundred nm thick).[18,24] The bilayers are rigid, impermeable to water, while the PAAm hydrogel layers are soft and stretchable. The hybrid gel exhibited various functions such as color, one dimensional

drying/swelling[19,25], mechanical anisotropy, quasi-unidirectional shrinkage upon uniaxial stretching and confined drying[20,25], high toughness and self-healing.[21] The structure color of the gels respond to external stimuli such as by small stress/strain, temperature, and pH.[22,23] Because of anisotropic structure, lamellar hydrogel closely resemble to that of natural hybrid materials. Therefore, a model system to mimic the various functions of natural anisotropic materials.[18,20,22,23,26]

Here in we investigate the effect of various kind of drying on the structure and functions of anisotropic lamellar hydrogels.[21,24] Previous study showed that in addition to anisotropic function bilayers serve as a physical barrier to the transport of water and promote 1D permeability.[27] Therefore, given the water-impermeable nature of the bilayers and hydrophilic nature of the PAAm hydrogel layers, it is interesting to see the effect of water intake/release on the swelling/drying of overall gel which are expected to strongly influence the functionality and properties of the bilayer membranes.

This chapter is organized as follows. First free air drying and restricted drying of lamellar gel is given. Then drying of lamellar gel on flat substrate to understand the effect of water intake and release on the PAAm hydrogel layers confined between the bilayers, which effect the structural color of the overall gel. The effect of water on surface and rewriting photonic displaying behavior is studied. Then drying the lamellar gel on patterned substrate to understand the adaptive behavior of gel by directional drying. Then studying the effect of stress and light exposure to the substantially dried samples. Additional drying is performed using ionic liquid just for comparison. The specific functions and mechanical behaviors of the PDGI/PAAm multi-lamellar hydrogel are analyzed and discussed.

It is expected that the PAAm layers are permeable to water and mainly responsible for water intake/release behavior of gel while the rigid PDGI layers are impermeable to water. The change in spacing distance (*d*) between PDGI lamellae by controlling the water content of PAAm gel layer as PDGI layer thickness remain unchanged. When *d* meets to satisfy the Braggs law for diffraction of visible light wavelength band, the material appears as the corresponding color. The wavelength band of the material can be tuned over the entire UV-visible spectral range and even far below the UV region (visibly transparent) by maintaining *d* with regulating water content in PAAm matrix.

5.2 Experimental

5.2.1 Materials and method

Functional monomer DGI (Dodecyl Glyceryl Itaconate) was synthesized according to previously method.[28] Acrylamide (AAm) (Junsei Chemical Co., Ltd., Japan), N,N'-methylenebis(acrylamide) (MBAA) (Wako Pure Chemical In- dustries, Ltd., Japan), Irgacure 2959 (BASF SE, Germany) and sodium dodecyl sulfate (SDS) (MP Biomedicals Inc., USA are of commercial grades.

5.2.2 Hybrid gel fabrication

All the multi-lamellar hybrid PDGI/PAAm gels were synthesized by slightly modification of the previously method.[29] Briefly, 0.1M DGI, 0.025 mM SDS, 2 M AAm, 2.1 mM MBAA(as a cross- linker of AAm), and 2 mM Irgacure 2959 (as a UV initiator) were dissolved in water. This precursor solution was poured into a 10 ml glass bottle and placed in a water bath at 55 °C for approximately 5 h, until stable lamellar DGI bilayers formed. The solution was then suctioned into a rectangular glass mold separated by silicone rubber (inner thickness: ~100 μm-0.5 mm, length: ~ 20 cm, width: ~6 cm) using a 10 mL plastic syringe under Ar by automatic

pump method. The flowrate of the sample solution was kept as high as possible (roughly 3 cm s^{-1}, shear rate of 133 s^{-1}) to orient bilayers along the glass surface. Co-current polymerization of DGI and AAm was performed using 365 nm UV light irradiation in the glass mold for 8 h at 50 °C under inert Ar atmosphere. The polymerized thin hybrid PDGI/PAAm gel was removed from the surface of glass plate by soaking in water without being damaging the surface due to thickness effect. The neat PAAm gels were also prepared as a reference by using 2 M AAm, 2.1 mM MBAA, and 2 mM Irgacure 2959 aqueous solutions using the same technique.

5.3 Characterization

5.3.1 Optimizing drying conditions

PDGI/PAAm hybrid gels were swollen in water for at least 1 week. Four types of drying was performed such as drying in open air, drying in confinement [25], drying by desiccant using different RH% and drying by solvent ionic liquid, respectively.

For the open air drying the gel of diameter 1 mm and thickness 1.30 mm respectively is placed under polarized optical microscope in reflection mode in bright field fluorescence view. The light is incident normal to plane and images of drying samples were taken each 5 second intervals. The still images are converted to movie using windows movie maker software. The frame rate is 25fps. The confined drying is performed according to our previous method.[25] Briefly the gels of different diameters *D* 4 mm, 6 mm, 8 mm and same thickness *T* 1.30 mm were placed in plastic zipper bags for the homogenous drying and color stimulation. The gels were taken after certain time of drying the samples were taken out from the zipper bag, and its weight *W,* diameter *D,* and thickness *T* were measured using a digital balance (Shimazu Co., Kyoto, Japan) and a digital caliper. After measurement of dimensions the samples were placed back in confined condition. For the drying on different RH% aqueous salt solution were prepared in air tight chamber using KBr, NaCl, $Mg(NO_3)_2$, K_2CO_3, $MgCl_2$, and LiCl that created

85%, 75%, 55%, 45%, 33%, 11%, relative humidity. The gel samples were placed inside chamber and after certain time of drying on RH% images were taken. Drying by ionic liquid was performed on soaking gel in co-solvent of water-ionic liquid and removal of water part from the gel that produced iongel.

For the study of rewriting photonic sheet the large area lamellar sheet is placed on black substrate to dry under confinement. Separately the large lamellar gel is dried for the artificial nacre (flat and hexagonal patterned substrate) and luminescence study.

The large area sheet like rewriting iongel paper was also obtained by mix solvent of ionic liquid water and subsequent evaporation of water. The large sheet like iongel was also tested for conductivity.

5.3.2 Measurement of reflection spectrum

In order to quantify the wavelength of reflecting colors at different types of drying and re-swelling of gels with water, moveable angle reflection measurement was performed. An optical device (Hamamatsu Photonics KK, C10027A10687) coupled with photonic multichannel analyzer (Hamamatsu Photonics KK, C10027) is used by exposing the gel with white light (Xe source). Reflection spectrum was attained by observance both the angles of incident (Bragg's angle) and reflection at 60°. The wavelength maxima, λmax, was acquired from the reflection spectrum.

5.3.3 Luminescence measurement

The absorbance and emission spectrum were recorded using spectrofluorometric instrument by illumination high intensity white light originating from xenon lamp on the highly dehydrated lamellar sample.

5.3.4 Scanning Electron Microscopy

The sample after air drying, confine drying on flat substrate and drying on pattern substrate are observed under Scanning electron Microscope model JOEL JSM, JAPAN. The specimens were Pt-Pd sputtered for better conduction, mounted on Cu grid and placed on stage under vacuum for further analysis.

5.3.5 Laser Light Transmission (LLT)

Light source of commercially available laser pointer is used to observe what kind of pattern is there on the surface of sample. Simply, the sample is illuminated via ordinary laser light (λ 600 nm) and the transmitted light is focused over a black background.

5.3.6 Conductivity measurement

Laboratory scale voltmeter was used for the conductivity measurement of PDGI/PAAAm large iongel paper. The current flow from sample was detected using LED. One part of LED was connected by alligator wire to equipment and another with alligator wire that connected to sample.

5.4 Results and discussion

The as-synthesized hybrid gels of 0.5 mm thickness T_0, were immersed in distilled water, the gels only swollen in thickness and reached a thickness T_{sw} of 1.23 mm at equilibrium condition. The equilibrium swollen PDGI/PAAm hydrogels had a water content of 92% displaying visible color with a λ_{max} peak at 608 nm for open air drying and 555-590 nm for confine drying samples, respectively in the optical reflection spectrum. From the Bragg's law, the interlayer distance *d* is estimated as 252 nm for open air drying sample and 231-243 nm for confine drying gels, respectively.

5.4.1 Free air drying

5.4.1.1 Concentric Patterning

The behavior of free air drying of swollen PDGI/PAAm anisotropic lamellar gel on ambient conditions (RH 45%, 25°C, 1 atm.) is shown in **Figure 5.1**. The change of radius of the gel with drying time is also shown **Figure 5.1a**, along with the photographs of sample taken during free air drying. Where, *R* is radius of gel and *r* is the position/radius of structural color ring appeared on gel surface by drying. The radius *R* of the gel slightly decreased with drying time while the radius *r* of color started to appear from edge of sample because of the fast evaporation of water from periphery of gel as a result of contraction of PAAm gel layer, the color ring moving inward to the center of the gel uniformly with time. As a result the mixture of all the visible color of the electromagnetic spectrum of light in the form of rainbow pattern can be observed on the gel surface (**Figure 5.1a**). However, at critical time of 120 min the surface of the gel shows complete rainbow like colored ring pattern. Above this critical time the individual color ring started to appear. Below this critical drying time the colored ring disappeared one by one starting from red-violet. The reflection of color arises from the layered structure and the position in the visible light wave range is quantified as in **Figure 5.1b, c, d**. Focusing on the first order reflection peak wavelength of the original gel color λ_{max} 608 nm [**Figure 5.1b (inserted)]**, initially the peak wavelength intensity was gradually decreased with drying time (90 min) along with the position of color ring radius that gradually moved inward. The gel central color turned slightly yellowish (120 min), then green (250 min), cyan (310 min), blue (375 min), violet (410 min) and then transparent with drying time, respectively. The shifting of color indicated the faster one dimensional drying process accompanying swelling mismatch and buckling of the sample surface. This color pattern suggested that there is non-homogenous distribution of water content in the PAAm gel layers *d* that resulted in the gradient in the thickness of sample from

edge to center.[30] This rainbow pattern also explains that the gel shows swelling mismatch and fast relaxation PAAm gel layers embedded between bilayers resulted in the wrinkles in the complete dry sample.[31] The FWHM is an indicator of the packing parameter of the oriented structure is shown in **Figure 5.1d**. The value of full width at half maxima of the reflation peak initially increased followed by decrease. This also indicated the faster relaxation of PAAm gel layers by drying perturb the internal structure of aligned PDGI from order to disorder resulting on the complicated type patterns on gel surface. This result suggested that, though the free air drying is faster but internal layered structure was perturb.

5.4.2 RH% drying

The PDGI/PAAm swollen gels drying on different RH% created by aqueous salt solution inside chamber is shown in **Figure 5.2a,b,c.** The water swollen PDGI/PAAm gels exhibited visual green color iridescence, the gels were of 1 cm dimeter and 1.10 mm thickness, respectively **(Figure 5.2a**). The gels were placed in a chamber that is saturated with different level of humidity 85%, 75%, 55%, 45%, 33%, 11% using aqueous salt solutions of KBr, NaCl, $Mg(NO_3)_2$, K_2CO_3, $MgCl_2$, and LiCl, respectively.[32] After 5h of drying, the gels showed humidity dependent drying pattern in the form of different colors **(Figure 5.2b**). The drying induced color patterns indicating the different level shrinking of PAAm gel layers by removing water by osmotic pressure. The sequence of drying was much slower for high humidity condition and gradually decreasing humidity the gel drying became faster. However, the slower drying of sample over a high humidity of 85%, little visual shrinkage in dimeter and flat surface was observed **(Figure 5.2a,b,c**). In comparison, low humidity 11% caused severe desiccation that force dried the sample as a results of faster drying wrinkles and crease type white color appeared on surface of sample **(Figure 5.2a,b,c)**. The sample in equilibrium swollen state and force dried 11% humidity along with their POM observation along the orientation of bilayers

(top view) at +45° with cross-polarizer along with 532 nm quarter wave plate and open polarizer are shown in **Figure 5.3a.** The neat gel that showed beautiful orange structural color under POM revealed no sign of birefringence and the gel sample was homogenous **Figure 5.3a(i-ii)**. However, on 11% RH the force dried sample that showed visual silvery like luster exhibited desiccation and severe force drying induced shrinking crease patterns inside POM **Figure 5.3b(i-iv)**. Again this result indicating the structure of the gel upon drying over humidity is also perturbed.

5.4.3 Confined drying

5.4.3.1 Homogenous color stimulation

For comparison the constrained air drying is performed on swollen gel sample of different diameters and same thickness, the photographs are shown in the inset of **Figure 5.4a,b** and **Figure 5.5a,b**. The results suggested that, the weight and thickness of samples changed for the different diameter samples as a function of drying time. The structural color is uniformly tuned for several hundreds of hour by drying in confinement. In brief, the weight W and thickness T of the samples decreased faster for the sample of small diameter with drying time while much slower for the large diameter gel. While the diameter of the samples remains unchanged, which confirms the perfect 1D contraction of PAAm gel layers upon drying. This perfect one-dimensional contraction is an indication that the bilayers retain the original layered structure even after drying. The well-maintained structure is due to the very slow drying under confinement. During anisotropic drying, the diffraction color of the gels shifted from orange to violet, and then to transparent as shown by the photographs of the samples and the corresponding reflection spectra (**Figure 5.5a,b,c**). The (λ_{max}) for small diameter sample exhibited sharp blue shifted from orange (~570 nm), green (~495 nm), blue (~374), violet (~312

nm) and then to transparent. The medium dimeter sample showed intermediate color change from orange (~554 nm), green (~509 nm), blue (~445), violet (~393 nm), far violet (~338 nm-302 nm) and then to transparent. The reflection peak wave length (λ_{max}) shif of large diameter sample was quite slow and covered the entire visible spectrum of electromagnetic radiation of light waves. The sequence of color shift during drying was near orange-red (~590 nm), yellow (~555 nm), dark green (~523 nm), light green (~486 nm), cyan (~455 nm), blue (~415), violet (~380 nm), far violet (~350 nm-302 nm) and then to transparent, respectively. The blue shift is size dependent being early for sample of smaller size because of faster drying and delayed for larger one. The change of ratio of diameter, ratio of thickness, color change and thickness of *d* was linear with drying time and their slope as a function of gel diameter also follows linear line indicating perfect one dimension drying and color change during drying under constrained conditions. This result suggested that, though the constrained air drying is very slow but internal layered structure was unperturbed.

5.4.3.2 Shape memory & Nacre mimetic optical iridescence

After the understanding of PDGI/PAAm bilayer hybrid gel drying. It is interesting to explore some novel function related to drying of photonic gel. The study of natural organism suggested that, their surface layered have ordered morphology some of which like nacre shows silver like metallic luster that arises from the ordered nanocomposite structure.[1,4,33] The structure is comprise of alternating hard crystals and soft polymer.[34] This contrasting refractive index give nacre silver like metallic luster.[35] The PDGI/PAAm gel is also a nanocomposite of hard PDGI layers and soft PAAm layer in swollen form but our previous results suggested that the PDGI layers become soft and PAAm layers hard by drying.[25] Therefore, it is important to study the dry PDGI/PAAm sample. For that purpose, the water swollen gel exhibited striking orange structural color was subjected to confine drying **[Figure 5.6a,d]**. With simple air drying, blue

shift of the gel's color is realized, which covers the entire visible spectra and turns transparent **[Figure 5.6b,e],** due to the smaller lamellar spacing (~20 nm) corresponding to the lower wavelength of light (~50 nm) that is far below the visible spectral range. Although, the sample appears as dry, hard, and stiff at this transparent stage but still exhibits sufficient flexibility upon bending, twisting, and stretching **(Movie S1**). Apparently, the flexibility of the PDGI/PAAm bilayer hybrid gel is attributed to the presence of alternating layered structures even at low water content (~12%). This is because the multilayered structure restricts water in the form of bound water, adapt an equilibrium dry state with 12% water content at room temperature 25°C and humidity 90% similar to the amphiphilic behavior of skin that retains sufficient amount of bound water.[25,36] Despite flexibility, unique crease patterns are noticed when the PDGI/PAAm gel is subjected to a complete folding **(Movie-1).** Each crease appeared as nontransparent metallic silver-like luster. Upon huge crushing or pressing by hand, the metallic luster is formed over the entire sample which makes it nontransparent **[Movie-1, Figure 5.6c,f].** The turbid crease pattern has characteristic silvery mirror like metallic luster in accordance with the iridescence of sea shell, abalone and nacre.[37] These unique behaviors are in contrast to the dried PAAm gel of similar level of water content which shows lack of flexibility and fractures upon crushing **[Movie-1, PAAm].** The origin of crease pattern is due to the stress induced delamination, buckling and de-bonding at the interface between PDGI and PAAm that results the non-homogeneous distribution of PDGI domains which are confirmed by SEM images **[Figure 5.7c,d].** In contrast, the surface morphology of the transparent gel is not evident for such nonhomogeneous domains an maintain the layered structure in dry condition **[Figure 5.7a,b]**. Furthermore, when the sample with such metallic luster is immersed in water the structural color of the gel reappeared within an hour and after several hours the sample regains the original structural color **[Figure 5.7c,d].** This indicated a new concept of

shape and internal structure memory behavior which was perturbed by pressing or crushing. After re-swelling in water regain the original structure. Interestingly, this process can be repeatable for many cycles just by drying and re-swelling. The appearance and erasing of crease pattern can be repeated for several subsequent cycles.

5.4.3.3 Birds feather mimetic structural color

Most of the organism not only show ordered structure arranged alternating manner but also comprise of surface patterns for example the moth eyes, the bouligand structure on beetle surface cuticles, the skin of chameleon that has patterned made of guanine crystal etc not only show many novel functions.[6,38,39] Therefore, in this section the study of the equilibrium swollen gel placed over a pattern surface and drying induced function is given. The original PDGI/PAAm gel is placed over a PDMS sheet that has hexagonal pattern and allowed to dry under confined condition. The lamellar morphology of PDGI/PAAm promoted water lose from periphery of gel that triggered one dimensional contraction of PAAm layers. In this way the drying triggered self-assembled hexagonal patterns were sketched on the surface of PDGI/PAAm. The dried sample is simply detached from the substrate as **Figure 5.8a**. The conventional dry sample previously showed no color but transparent hybrid polymers of PDGI/PAAm. In contrast drying the sample on pattern substrate revealed visual iridescence structural coloration by shining light over the surface of sample or by changing the sample [**Figure 5.8b (i),(ii)]**, indicating angle dependent structure coloration. The iridescence color appearance is in close resemblance to that of bird's feathers and butterfly wings that act as light filters due to the presence of ordered microstructure. The iridescent color can be tuned through the entire spectrum of light by changing the angle of incident and reflected light beams, respectively (**Figure 5.9a,b,c**). The color shifting is very fast and revel red shift mimicking the changing coloration in natural display devices such as butterfly wings, beetles cuticles and birds

feathers (**Figure 5.9c**). To understand the texture and surface morphology of the sample, polarized light microscopic image is shown in **Figure 5.10a**. The sample observation under transmission mode of optical microscope revealed rough morphology with some ordered microstructure structure that is below the magnification of optical microscope. Furthermore, by the illumination of laser light on the surface of PDGI/PAAm dry patterned sample, the texture transmit hexagonal pattern that support the presence of well-ordered hexagon type surface microstructure (**Figure 5.10b,d**). The light without presence of sample reveled just a single spot focused on black background (**Figure 5.10c**). This was further supported by analysis the sample top and cross-sectional view under scanning electron microscope at different magnifications shown in [**Figure 5.11a(i-vi) ,b(i-ii)]**. The results of SEM indicated well defined surface micro patterning that has ordered hexagonal array like texture. The arrays are as a result of drying induced self-assembly of PDGI/PAAm internal structure printed by the substrate. The cross section images shows that the patterning is limited to the surface that contacted the substrate with several nm layers [**Figure 5.11b(ii)**]. The calculated size of each spheres is 1.5 μm and the distance between two spheres is 150 nm. The distance satisfy the Braggs law of diffraction that is why diffract iridescence structural coloration even in dry state similar to that of the diffraction colors in natural organism.[40] This result suggest the exploration of function relevant to security purposes or holographic display devices just by allowing the sample to dry on pattern message or hologram. Interestingly the print texture can be removed by swelling in water and is repeatable.

5.4.3.4 Color stimulation by water rewriting

In addition to water triggered shape memory behavior, water rewritable photonic paper based on lamellar bilayer hydrogels is designed (**Figure 5.12**). A transparent photonic paper (100×40×0.01 mm^3) was fabricated simply by drying the rectangular sheet gel on a black substrate [**Figure 5.12 top right**]. To write or sketch, water was used as an ink because it is environmental friendly, non-hazardous and abundantly available solvent. A simple butterfly shape was sketched on sponge stamp using professional laser cutter (model PLS4.75) [**Figure 5.12 top left**]. The butterfly sketched surface of the stamp was dipped in petri dish contained water. After absorption of sufficient amount of water, the stamp was gently pressed on the surface of the photonic paper for a while and then removed [**Figure 5.12(i), (ii)**]. As water touch the photonic paper, sample intakes water and butterfly sketch appears as visible color gradually [**Figure 5.12(iii)**]. With progress of time, the color of butterfly shift from blue to green [**Figure 5.12(iii-v)]**. The color contrast can be observed clearly between swollen (high water content) and non-swollen gel (low water content) region. The photonic sheet is regenerated to the original one by simply erasing the printed butterfly image keeping the sample in air for several minutes (25°C, 1 atm, and ~50% RH) [**Figure 5.12 (vi-x)**]. Reflection spectra were taken during writing and erasing (**Figure 5.12b**). Initially, the dried photonic paper (blank sheet) appears visibly no color and thereby the reflection peak is appeared at UV wavelength of ~250 nm corresponding to a *d*-spacing of ~95 nm. The dry PAAm matrix absorbs water and undergoes fast swelling that increases the *d*-spacing. As a result, reflection peak shift from UV to greenish-blue wavelength band with time. The reverse shift (erasing) in reflection peak observed gradually from green to blue by simple air drying and finally the reflection peak for regaining the original colorless (blank sheet) state of the sample. Upon drying, evaporation of water from the PAAm matrix leaves the photonic paper of reduced *d*-spacing and thereby blue shift of

reflection peak. The writing/erasing by water intake/release can be repeated for many cycles (**Figure 5.12c**). That means the photonic sheet absorb sufficient amount of water through PAAm layer and the thickness increases in such a way to reach the visible wavelength of electromagnetic spectrum. Therefore the photonic sheet recover the original structural coloration. The Transmission electron Microscopic images revealed that the sample contains well oriented bilayers in PAAm matrix (**Figure 5.12d**). The bright and dark stripes pattern in TEM images represent PDGI lamellae reinforced into PAAm matrix, respectively. However, the literature study showed much smaller layered morphology of the PDGI 5 nm and PAAm layers 200-300 nm.[18] In our observation it is speculated that during PDGI/PAAm sample preparation for TEM study slight increase in the bilayers might have occurred. Furthermore, the wettability of the photonic paper was observed by using contact angle measurement. The contact angle of the sample at the initial stage is high suggests that the surface is hydrophobic (~110) but decreases gradually with time and turn out to be hydrophilic (~12).

5.4.3.5 Photoluminescence induced by drying

Luminescence polymers are gaining tremendous attention as tunable lasers, displays, medical diagnostics, solar energy conversion, amplifiers for optical communication and sensing.[41] Most of the luminescence polymers are based on conjugated organic molecules/fluorophores[42] and non-conjugated/sub-fluorophore.[43] The former are purely organic molecules of conjugated units that promote emission, utilizing the principle of aggregation induced emission (AIE), while the later contain functional groups C=O, N=O, C=N usually are weak fluorescence. Polymers composed of non-conjugated fluorophores are environmental friendly, low cost and easy to impart fluorescence phenomena as compared to conjugated polymers. Therefore, some strategies are available that causes non conjugated sub-fluorophores as strong emissive and dominating the conjugated fluorophores, such as by chemical crosslinking and immobilization,

treatment hydrothermally, physically and self-assembly[44]. To our knowledge, limited literature is available on fluorescence polymers because most of the authors reported this phenomena in polymers dots.[44] We have investigated fluorescence phenomena in completely dried condition of composite hydrogel containing self-assembled non-ionic surfactant polymer poly-(dodecyl glyceryl itaconate) PDGI sandwiched between polyacrylamide PAAm.[18]

In detail, two kind of PDGI/PAAm gels such as physical and chemically crosslinked gels were dried in constrained condition. The PDGI/PAAm dry sample 0.1 mm thickness was transparent as shown in **Figure 5.13(a)**. For the visual study of photoluminescence, white light from Xe lamp was shined on the surface of samples in dark condition and then switched off. The sample absorbed certain wavelength of light waves, interestingly exhibited blue light emission [**Figure 5.13(b)]**. The detailed investigation was performed using spectrofluorometric analyses of the two types of specimens. First, the behavior of physical sample was studied. The optimization for the excitation of fluorophores at different emission wavelength was determined as shown in **Figure 5.13c**. Similarly the emission intensity as a function of emission wavelength at different excitation was performed for optimization (**Figure 5.13d**). The results are summarized in [**Figure 5.13(e),(f**)]. The results indicated that the photoluminescence emission intensity decreased linearly by increasing excitation wavelength. Also the peak position shifted to higher value linearly by increasing excitation wavelength. This results suggested that the absorbing fluorophores have specific sites that absorb light waves at specific wavelength range. Increasing the excitation wavelength of light causes passivation of the absorbing fluorophore leading to reduction in light emission. For comparison the optimization of excitation spectra of chemical samples at different emission wavelength is shown in **Figure 5.14a**. The emission spectra optimization at different excitation wavelength is also given **Figure 5.14b**. The results of chemical sample is shown in **Figure 5.14c,d**. The results indicated that increasing the excitation

wavelength from 260-320 nm. The chemical sample photoluminescence intensity increases with almost same emission peak wavelength. However, further increasing the excitation wavelength 320-340 nm, the light emitting intensity and wavelength reduced. Additional increase of the excitation 340-350 nm again increased the emission intensity as well wavelength position became higher. In nutshell, though the sample absorbing light was not stable but the intensity of the emission was higher compared to that of the physical sample. This indicate another phenomena such as the crosslinking enhances rigidity of the sample that enhanced the photoluminescence emission intensity.[44–47] The resultant optimized excitation wavelength position at which the sample absorb maximum wavelength of light and emission wavelengths for high intensity light emission is shown in spectra as in **Figure 5.15a**. The light emission time and decay behavior is also given in **Figure 5.15b**. It is obvious that, the sample absorb ultra-violet light at 345 nm by n-π* electronic transition (3.5 eV) and emits blue light in the visible range 435 nm (2.8 eV), exhibited highly photoluminescence property with 0.78 photoluminescence relative quantum yield. The orgini of such behavior in hybrid polymer is the presence of carbonyl >C=O and Amine -NH_2 chromophores, in dry state showed high photoluminescence phenomena. The hybrid system is good candidate as an energy harvesting material and screening hazardous ultraviolet radiations.

5.4.4 Solvent drying

5.4.4.1 Conductive properties

Ionic liquid based hybrid soft and dry materials has the characteristic properties of air stability, ion conductivity, and electrochemical stability.[48–50] The potential application are the stretchable electronics skin, batteries, humidity sensor, separation media and so on.[48,51,52] On the other hand hydrogels are water swollen soft wet materials.[53,54] The drying of water reduces the functionality of conventional hydrogels.[17,55–57] Therefore, some strategies are available to

replace the water of hydrogels by ionic liquid and impart functionality.[58,59] These studies are mostly limited to isotropic hydrogels of single and double network structure.[50,58,60,61] It is interesting to study the effect of ionic liquid on the hydrogels containing anisotropic structure of alternating amphiphilic and hydrophilic layers. Previous study on the composite hydrogel containing self-assembled non-ionic surfactant polymer poly(dodecyl glyceryl itaconate) PDGI inserted between poly(acrylamide) PAAm has showed various function in the drying from the water. In this portion the gels were dried using ionic liquid water co-solvent. The bilayer hybrid gels were soaked in different concentration w/w% of the co-solvent of ionic liquid (Urea: choline chloride) and water. The gel after equilibrium swelling in co-solvent was subjected to drying on black PAAm substrate. The water dried from the sample, produced ionic liquid hybrid gel with bilayer structure that was stable at ambient condition as soft and stretchable matter (**Figure 5.16a**). The border lines in the images indicate the area (*T* 10 cm x W 6 cm) occupied by ion gel membrane on PMMA substrate **(5.16a,b,c).** Then, the ion gel membrane was checked for the conductivity property using AC voltmeter. One side of the ion gel is connected to the positive electrode of equipment and other side with the LED light. The AC current originating from instrument passed LED light, when touched the substrate that was unable to switch the lights on because of its non-conductive property (**Figure 5.16b)**. In case of iongel the current successfully passed and migrated towards the positive electrode. Interestingly the ion gel was able to conduct electricity and the LED light connected to the opposite electrode was switched-on (**Figure 5.16c**). The reason behind the conductivity is the abundance of Cl^{-1} ions[62] that has the characteristic properties of electron rich source available for the free migration inside the iongel. The iongel could have application as stretchable electronics like skin, batteries, gas barrier coating and so on.

5.4.4.2 Stable photonic sheet

In addition to electricity conductivity the iongel also exhibited as display device based on water writing and erasing. The ion gel contains ionic liquid in the PAAm gel layer is stable in air and transparent [**Figure 5.17 (0s)**]. The transparency is due to the decrease PAAm gel layer *d* that diffract light-waves beyond the perception of human eyes at invisible range of spectrum of light wavelengths. The sponge contained water was used as writing tool on iongel photonic sheet. As the water contacted the surface of iongel membrane, the word LSW was printed in the form of visible structural color because of the increased in the PAAm gel layer that satisfying the Braggs law of diffraction of light waves. The iongel absorb sufficient amount of water appears as blue and then green (0.67s-15s). After the color saturation the evaporation of water help in erasing the water mark or printed sketch. The color of the iongel started to gradually disappear from green, blue and then become transparent same as original condition (15s-60s). In this way the water writing and erasing is repeatable for many cycles.

5.5 Conclusion

By controlling the internal structure of anisotropic gel just by different types of drying approaches, we obtained various biomimetic functionality. The gel showed adaptive structural color such as rainbow like color stimulation by free or humidity air drying. The structural color is homogenously tuned by restricted drying throughout the entire visible spectrum of electromagnetic radiation of light. At high water content, the gel behaves as soft/elastic colorful skin same as certain marine organism, whereas at low water content transparent photonic sheet act as an active water triggered display device same as beetle cuticle, novel shape memory simply by maintaining the amount of water intake/release, stress induced nacre like metallic luster, birds feather mimetic iridescence color, and jelly-fish like blue light emission. In addition drying of gel pre-soaked in water-ion liquid co-solvent resulted into an air stable iongel

membrane photonic sheet that showed high conductivity and exhibited rewriting photonic paper properties. The switchable color of the hybrid PDGI/PAAm induced by water could act as a visual indicator of moisture content with novel shape memory behavior for diversified applications such as soft and stretchable electronic skin, batteries, or barriers coating, or gas separation membrane. Moreover, the material is deliberated as a rewritable photonic paper which can be printed simply using water as ink.

5.6 References

[1] C. Campos-Fernández, D. E. Azofeifa, M. Hernández-Jiménez, A. Ruiz-Ruiz, W. E. Vargas, *Optical Materials Express* **2011**, *1*, 85.

[2] M. Rassart, J.-F. Colomer, T. Tabarrant, J. P. Vigneron, *New Journal of Physics* **2008**, *10*, 33014.

[3] M. Rassart, P. Simonis, A. Bay, O. Deparis, J. P. Vigneron, *Physical review. E, Statistical, nonlinear, and soft matter physics* **2009**, *80*, 31910.

[4] C. M. Eliason, M. D. Shawkey, *Optics express* **2010**, *18*, 21284.

[5] F. Liu, B. Q. Dong, X. H. Liu, Y. M. Zheng, J. Zi, *Optics express* **2009**, *17*, 16183.

[6] J. Teyssier, S. V Saenko, D. van der Marel, M. C. Milinkovitch, *Nature communications* **2015**, *6*, 6368.

[7] S. R. Mouchet, E. Van Hooijdonk, V. L. Welch, P. Louette, J.-F. Colomer, B.-L. Su, O. Deparis, *Scientific reports* **2016**, *6*, 19322.

[8] K. Okumura, P. G. De Gennes, *European Physical Journal E* **2001**, *4*, 121.

[9] H. Kakisawa, T. Sumitomo, *Science and Technology of Advanced Materials* **2012**, *12*, 64710.

[10] K. Okumura, *MRS Bulletin* **2015**, *40*, 333.

[11] J. Sun, B. Bhushan, J. Tong, *RSC Advances* **2013**, *3*, 14862.

[12] P. Fratzl, R. Weinkamer, *Progress in Materials Science* **2007**, *52*, 1263.

[13] W. Yang, V. R. Sherman, B. Gludovatz, E. Schaible, P. Stewart, R. O. Ritchie, M. A. Meyers, *Nature Communications* **2015**, *6*, 1.

[14] E. Munch, M. E. Launey, D. H. Alsem, E. Saiz, A. P. Tomsia, R. O. Ritchie, *Science (New York, N.Y.)* **2008**, *322*, 1516.

[15] J. P. Gong, Y. Osada, Springer Berlin Heidelberg, 2010; pp. 203–246.

[16] J. Itagaki, Hiroko.; Kurokawa, Takayki.; Furukawa, Hidemitsu.; Nakajima, Tasuku.; Katsumoto, Yukitru and Gong, *Macromolecules* **2010**, 9495.

[17] W. Hong, X. Zhao, Z. Suo, *Journal of Applied Physics* **2008**, *104*.

[18] M. A. Haque, G. Kamita, T. Kurokawa, K. Tsujii, J. P. Gong, *Advanced Materials* **2010**, *22*, 5110.

[19] K. Mito, M. A. Haque, T. Nakajima, M. Uchiumi, T. Kurokawa, T. Nonoyama, J. P. Gong, *Polymer* **2017**, 1.

[20] T. Nakajima, C. Durand, X. F. Li, M. A. Haque, T. Kurokawa, J. P. Gong, *Soft matter* **2015**, *11*, 237.

[21] M. A. Haque, T. Kurokawa, G. Kamita, J. P. Gong, *Macromolecules* **2011**, *44*, 8916.

[22] Y. Yue, T. Kurokawa, M. A. Haque, T. Nakajima, T. Nonoyama, X. Li, I. Kajiwara, J. P. Gong, *Nature communications* **2014**, *5*, 4659.

[23] Y. F. Yue, M. A. Haque, T. Kurokawa, T. Nakajima, J. P. Gong, *Advanced Materials*

2013, *25*, 3106.

[24] X. Li, T. Kurokawa, R. Takahashi, M. A. Haque, Y. Yue, T. Nakajima, J. P. Gong, *Macromolecules* **2015**, *48*, 2277.

[25] M. Ilyas, M. A. Haque, Y. Yue, T. Kurokawa, T. Nakajima, T. Nonoyama, J. P. Gong, *Macromolecules* **2017**, acs. macromol.7b01438.

[26] M. A. Haque, T. Kurokawa, J. P. Gong, *Soft Matter* **2012**, *8*, 8008.

[27] M. A. Haque, J. P. Gong, *Reactive and Functional Polymers* **2013**, *73*, 929.

[28] K. Tsujii, N. Saito, T. Takeuchi, **1980**, 2287.

[29] K. Tsujii, M. Hayakawa, T. Onda, T. Tanaka, *Macromolecules* **1997**, *30*, 7397.

[30] W. Lee, J. Yoon, E. L. Thomas, H. Lee, *Macromolecules* **2013**, *46*, 6528.

[31] P. G. De Gennes, M. Delaye, **2003**, *865*, 2002.

[32] F. E. M. O'Brien, *Journal of Scientific Instruments* **1948**, *25*, 73.

[33] P. U. P. A. Gilbert, R. A. Metzler, D. Zhou, A. Scholl, A. Doran, A. Young, M. Kunz, N. Tamura, S. N. Coppersmith, *Journal of the American Chemical Society* **2008**, *130*, 17519.

[34] M. Meyers, P. Chen, A. Lin, Y. Seki, *PROGRESS IN MATERIALS SCIENCE* **2008**, *53*, 1.

[35] T. M. Jordan, J. C. Partridge, N. W. Roberts, *Journal of the Royal Society, Interface* **2014**, *11*, 20140948.

[36] J. M. Waller, H. I. Maibach, *Skin research and technology : official journal of International Society for Bioengineering and the Skin (ISBS) [and] International*

Society for Digital Imaging of Skin (ISDIS) [and] International Society for Skin Imaging (ISSI) **2006**, *12*, 145.

[37] J.-P. Cuif, M. Burghammer, V. Chamard, Y. Dauphin, P. Godard, G. Moullac, G. Nehrke, A. Perez-Huerta, *Minerals* **2014**, *4*, 815.

[38] A. R. Parker, C. R. Lawrence, *Nature* **2001**, *414*, 33.

[39] M. Duvert, Y. Bouligand, C. Salat, *Tissue and Cell* **1984**, *16*, 469.

[40] A. R. Parker, R. C. McPhedran, D. R. McKenzie, L. C. Botten, N.-A. P. Nicorovici, *Nature* **2001**, *409*, 36.

[41] H. Lu, L. Feng, S. Li, J. Zhang, H. Lu, S. Feng, *Macromolecules* **2015**, *48*, 476.

[42] J. Mei, N. L. C. Leung, R. T. K. Kwok, J. W. Y. Lam, B. Z. Tang, *Chemical Reviews* **2015**, 151022123319003.

[43] S. Zhu, L. Wang, N. Zhou, X. Zhao, Y. Song, S. Maharjan, J. Zhang, L. Lu, H. Wang, B. Yang, *Chemical communications (Cambridge, England)* **2014**, *50*, 13845.

[44] S. Zhu, Y. Song, J. Shao, X. Zhao, B. Yang, *Angewandte Chemie (International ed. in English)* **2015**.

[45] K.-P. Tung, C.-C. Chen, P. Lee, Y.-W. Liu, T.-M. Hong, K. C. Hwang, J. H. Hsu, J. D. White, A. C.-M. Yang, *ACS nano* **2011**, *5*, 7296.

[46] Y. Deng, W. Yuan, Z. Jia, G. Liu, .

[47] Y. Ren, J. W. Y. Lam, Y. Dong, B. Z. Tang, K. S. Wong, *J. Phys. Chem. B* **2005**, 1135.

[48] J. Le Bideau, L. Viau, A. Vioux, *Chem. Soc. Rev.* **2011**, *40*, 907.

[49] P. G. De Gennes, K. Okumura, M. Shahinpoor, K. J. Kim, *Europhysics Letters (EPL)*

2007, *50*, 513.

[50] E. Kamio, T. Yasui, Y. Iida, J. P. Gong, H. Matsuyama, *Advanced Materials* **2017**, *1704118*, 1.

[51] D. Y. Choi, M. H. Kim, Y. S. Oh, S.-H. Jung, J. H. Jung, H. J. Sung, H. W. Lee, H. M. Lee, *ACS Applied Materials & Interfaces* **2017**, *9*, 1770.

[52] F. Ranjbaran, E. Kamio, H. Matsuyama, *Journal of Membrane Science* **2017**, *544*.

[53] J. Ruiz, A. Mantecón, V. Cádiz, *Journal of Polymer Science, Part B: Polymer Physics* **2003**, *41*, 1462.

[54] N. A. Peppas, B. V. Slaughter, M. A. Kanzelberger, In *Polymer Science: A Comprehensive Reference, 10 Volume Set*; Elsevier, 2012; Vol. 9, pp. 385–395.

[55] J. Y. Chung, I. Regev, L. Mahadevan, *Soft Matter* **2016**, *12*, 7855.

[56] H. Itagaki, T. Kurokawa, H. Furukawa, T. Nakajima, Y. Katsumoto, J. P. Gong, *Macromolecules* **2010**, *43*, 9495.

[57] P. A. Mahanawar, B. N. Thorat, **2005**, *22*, 209.

[58] F. Moghadam, E. Kamio, T. Yoshioka, H. Matsuyama, *Journal of Membrane Science* **2017**, *530*.

[59] S. Kasahara, E. Kamio, a Yoshizumi, H. Matsuyama, *Chemical communications (Cambridge, England)* **2014**, *50*, 2996.

[60] X. Liu, Z. Wen, D. Wu, H. Wang, J. Yang, Q. Wang, *Journal of Materials Chemistry A* **2014**, *2*, 11569.

[61] J. Bandomir, A. Schulz, S. Taguchi, L. Schmitt, H. Ohno, K. Sternberg, K. P. Schmitz,

U. Kragl, *Macromolecular Chemistry and Physics* **2014**, *215*, 716.

[62] A. P. Abbott, D. Boothby, G. Capper, D. L. Davies, R. Rasheed, *J. Am. Chem. Soc* **2004**, *126*, 9142.

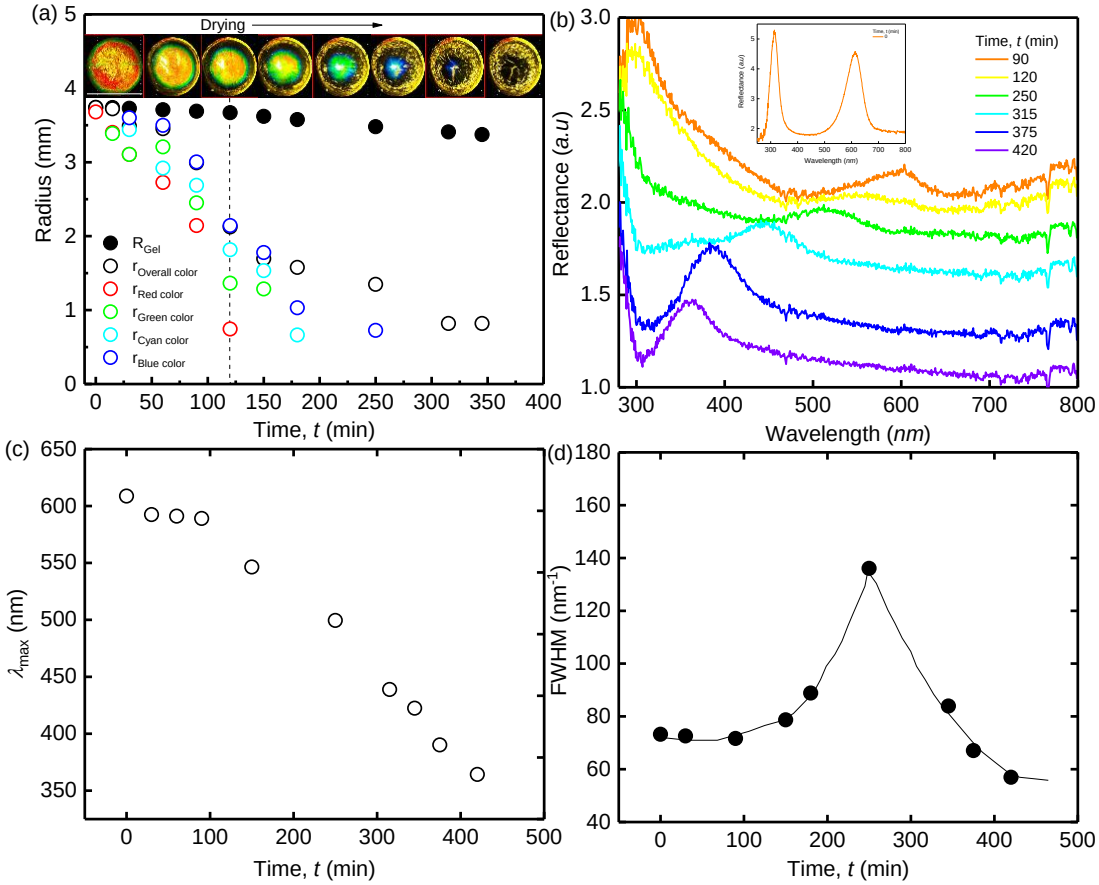

Figure 5.1 (a) PDGI/PAAm gel free air drying radius change vs time. *R* and *r*, respectively are the radius of gel and radius of each color position that appeared during free air drying on gel surface. The photographs of gel at time of free air drying are given as inset. (b) Reflection spectra of gel obtained during free air drying. For clear comparison the spectra is translated vertically. (c) The position of color λ_{max} (nm) as a function of drying time *t* (min). (d) Full-width-half-maxima from peaks of reflection spectra vs free air drying time.

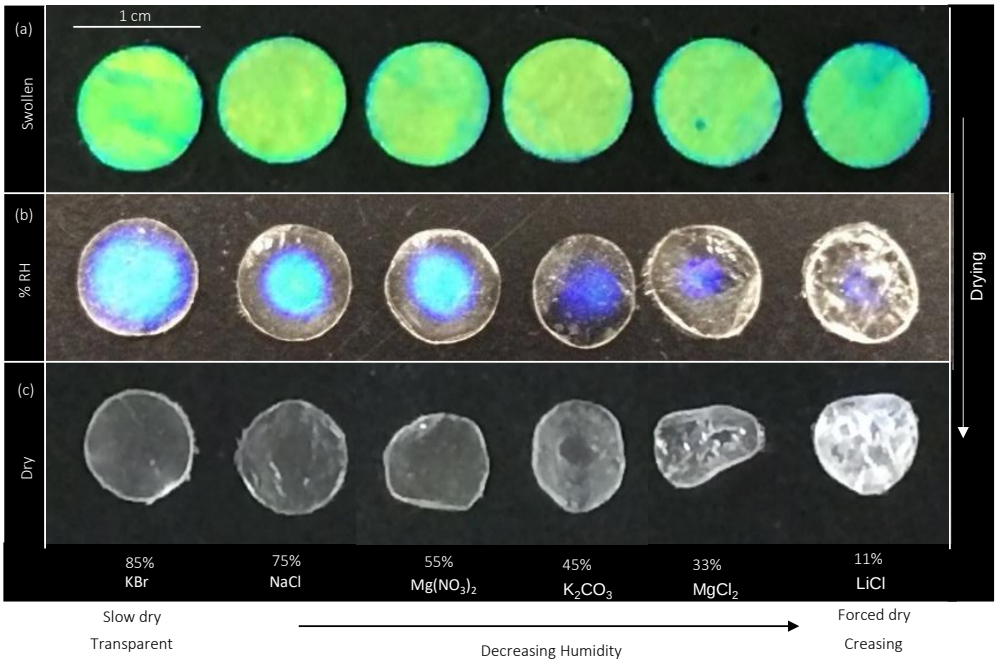

Figure 5.2 (a) Water swollen PDGI/PAAm gels exhibiting green colored iridescence. (b) Gels were placed on decreasing RH 85-11% using desiccant salt solution and appearance samples colors after 5h. (c) Completion of drying on different RH%. Left to right the osmotic stress increases by decreasing RH from 85-11% using aqueous salt solutions.

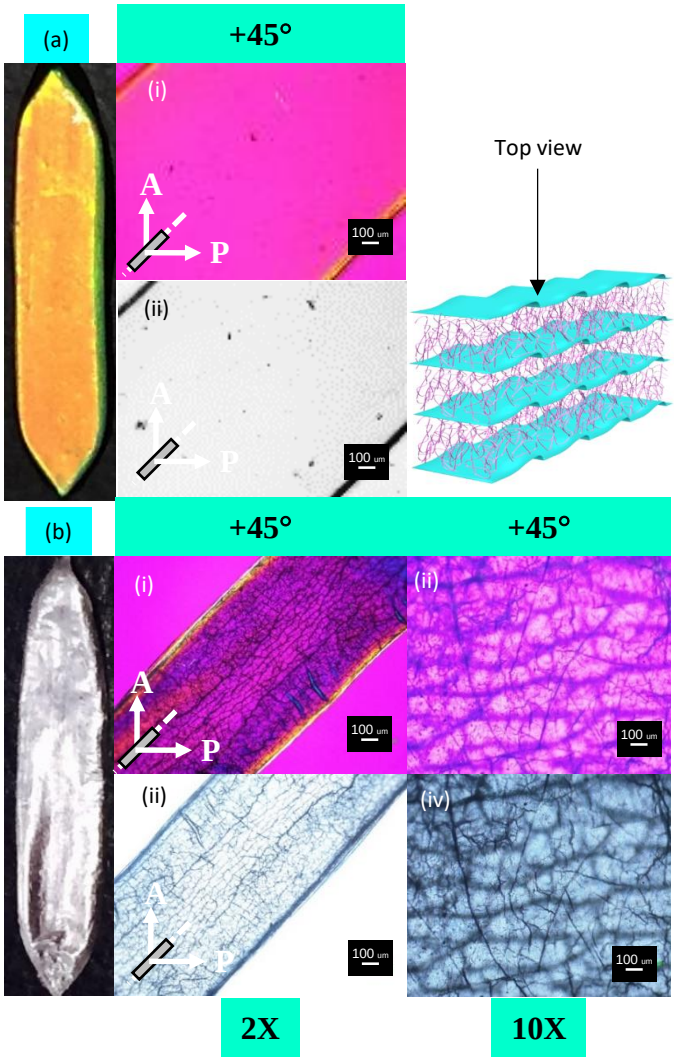

Figure 5.3 (a) Water swollen PDGI/PAAm gels exhibiting orange colored iridescence. The gel was observed under polarized light microscope with 532 nm tint plate between cross polarizer a(i) and open polarizer a(ii). (b) PDGI/PAAm dried on 11% RH shows white metallic luster. The gel was observed under polarized light microscope with 532 nm tint plate between cross polarizer b(i) and open polarizer b(ii). For clarity the magnification was increased b(iii) and b(vi). All observation was performed from the surface of sample perpendicular to the shear direction or parallel to the orientation of PDGI bilayers.

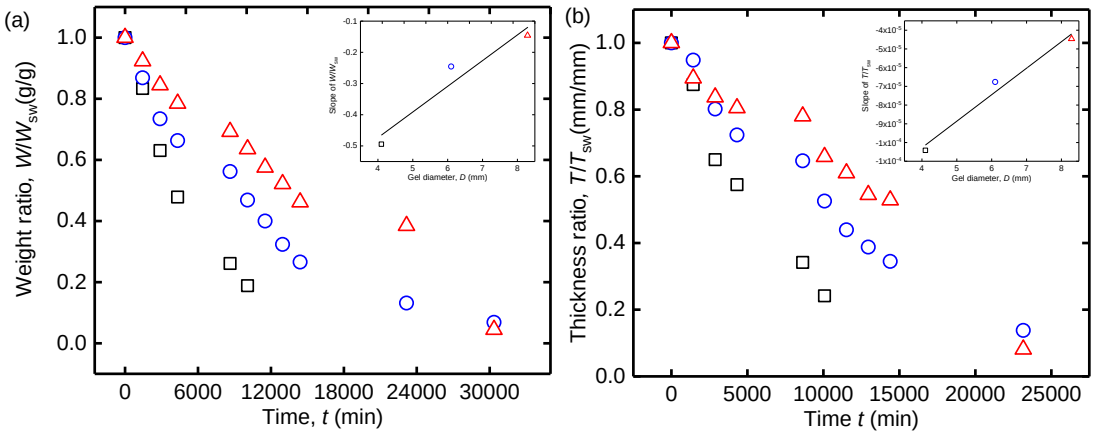

Figure 5.4 (a) PDGI/PAAm gel weight ratio vs confined drying time. The inserted figure is the slope obtained from change of weight vs time and plotted against the gel diameter. The slope vs diameter follow straight line. (b) PDGI/PAAm gel thickness ratio vs confined drying time. The inserted figure is the slope obtained from change of thickness ratio vs time and plotted against the gel diameter. The slope of thickness vs diameter follow straight line. Where, W, T, W_s, T_s are Weight of gel at different drying time, thickness of gels at the time of drying, weight of initial swollen gel and thickness of initial swollen gel, respectively.

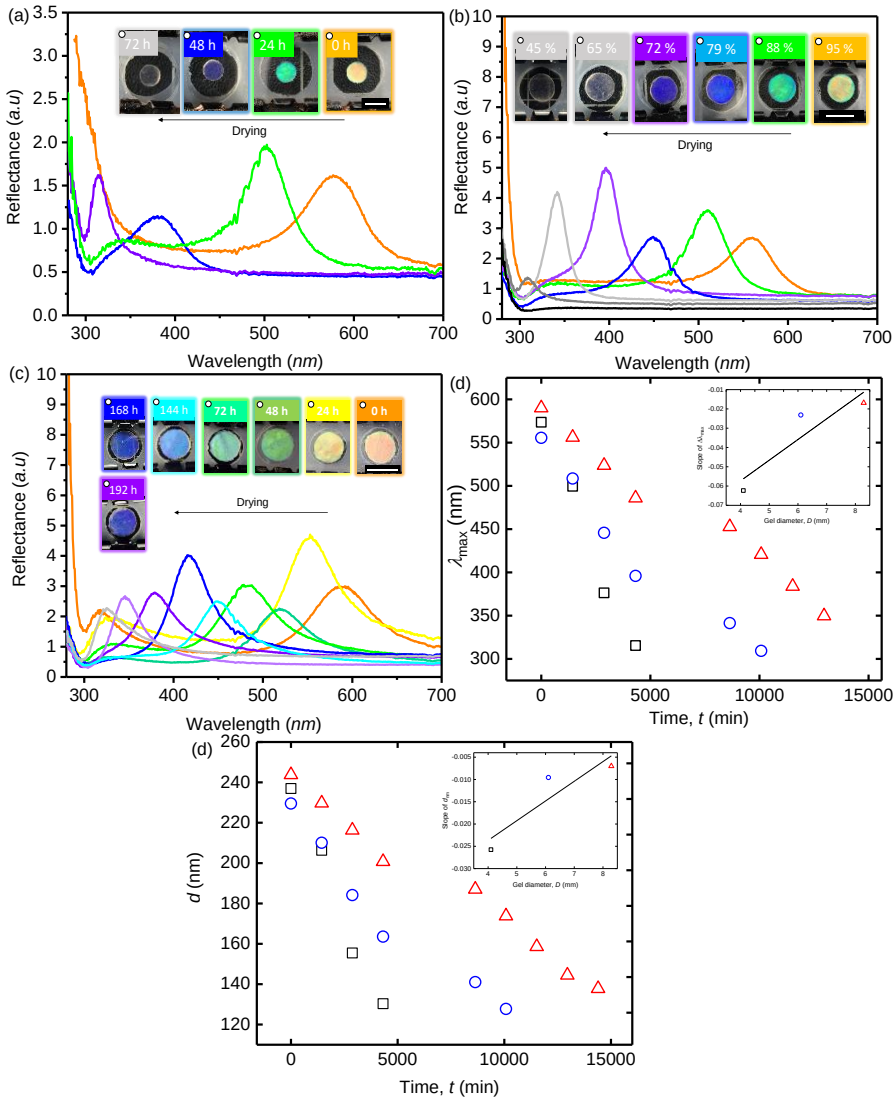

Figure 5.5 PDGI/PAAm gel different diameter under constrained air drying as a function of time shown as inset photographs**.** (a) Reflection spectra of small diameter sample. (b) Reflection spectra of medium diameter sample. (c) Reflection spectra of large diameter sample. (d) The position of color λ_{max} nm as a function of drying time *t* (min). (e) The distance between bilayers *d* nm vs time of drying *t* min. for clarity the inset figures in (d) and (e) shows the slope of different dimeter gels drying vs diameter.

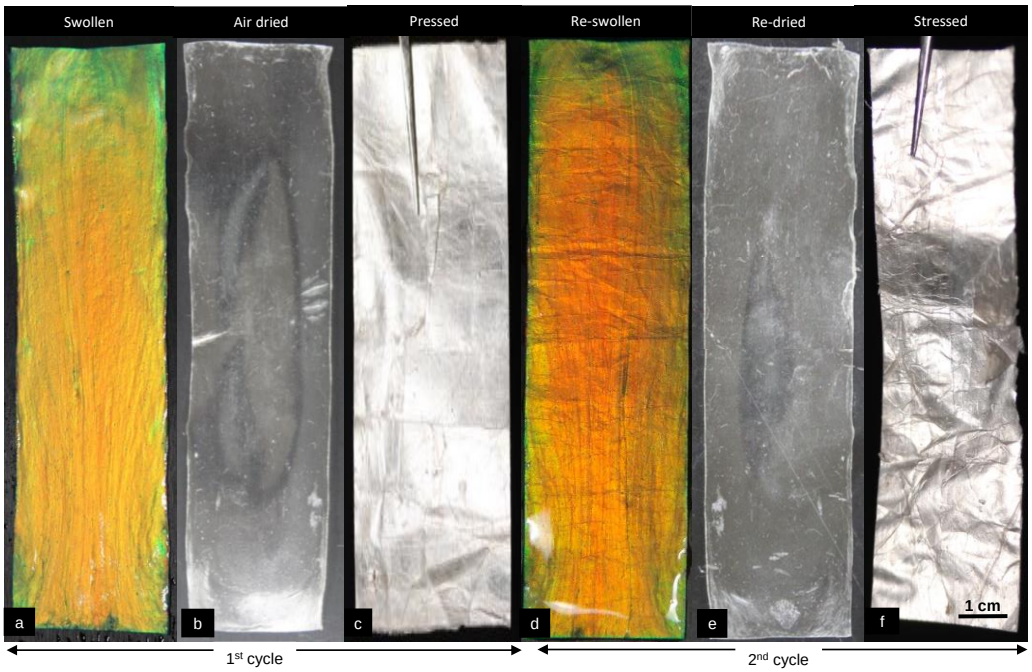

Figure 5.6 (a) PDGI/PAAm gel at equilibrium swollen condition. Thickness *T*, length *L*, and width *W*, are respectively 1.23 mm, 40 mm, and 100 mm. Orange Iridescence structural color arises from multilayered morphology by satisfying the Braggs law of diffraction. (b) PDGI/PAAm sample after confined air drying. Thickness *T*, length *L*, and width *W*, are respectively 0.1 mm, 39 mm, and 99.95 mm. The sample appeared transparent and is far below the visible range of electromagnetic spectrum of light. (c) After applying random stress on complete confined dry PDGI/PAAm sample. The sample appeared opalescence/nacre and silver like metallic luster. (d) PDGI/PAAm gel by re-swelling in water, remember original internal nanostructure/shape and reappears as structural color. (e) Re-drying the re-swollen sample under confinement become transparent again. (f) The random crushed on sample after re-drying re-appears metallic silver-like white/opalescence**.** This a unique shape/nanostructure memory phenomena in soft matter indicated by structure color. All the images are from top view of samples. The scale bar is 1 cm for all images, respectively.

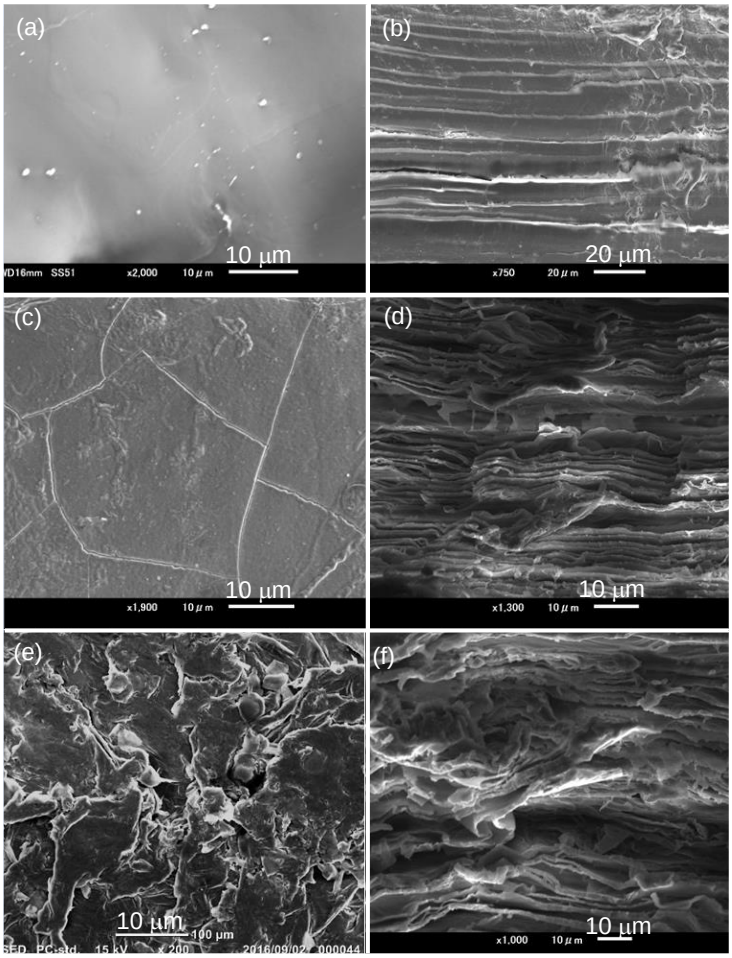

Figure 5.7 SEM micrographs of PDGI/PAAm samples. (a) & (b) Top view and cross-sectional view images of constrained air dry sample. (c) & (d) Top view and cross-sectional view images of sample pressed after drying. (e) & (f) PDGI/PAAm sample after applying random stress.

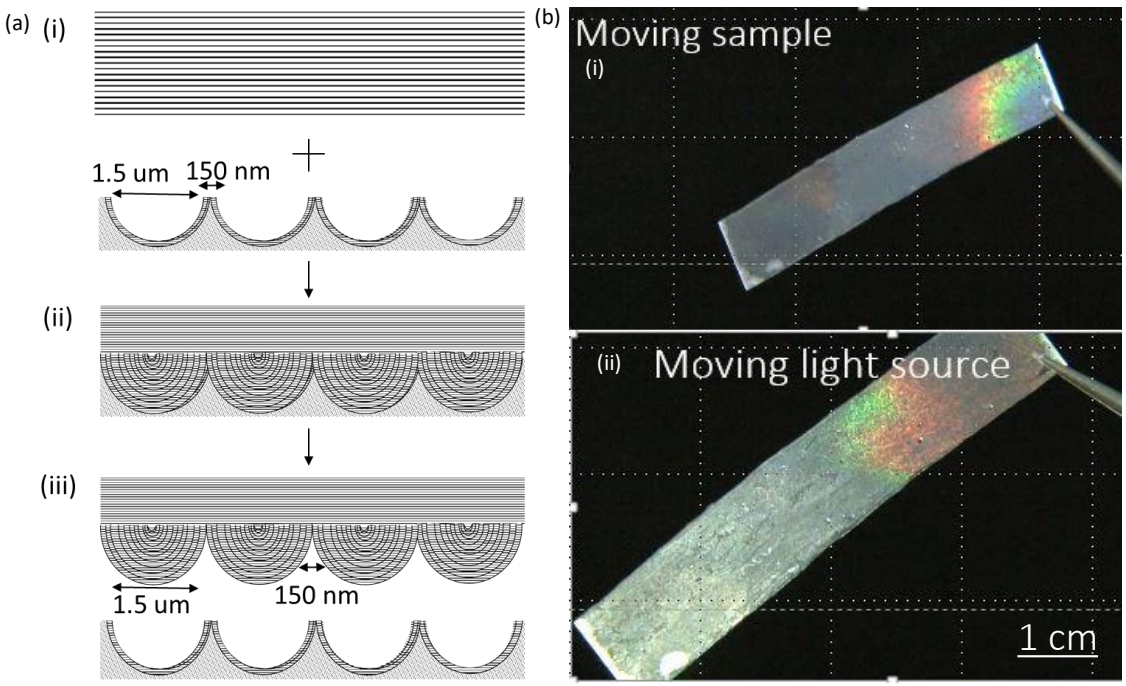

Figure 5.8 (a) Schematic representation of printing the surface patterns on PDGI/PAAm gel. Where, a(i) top is swollen gel and bottom a substrate with 1.5 μm pores, the distance between pores is 150 nm. a(ii) drying gel on substrate. a(iii) detachment of dried PDGI/PAAm sample from substrate. (b) Surface patterned dry PDGI/PAAm visual iridescence by shining light on surface and moving sample. (c) The light source movement on surface of dry sample.

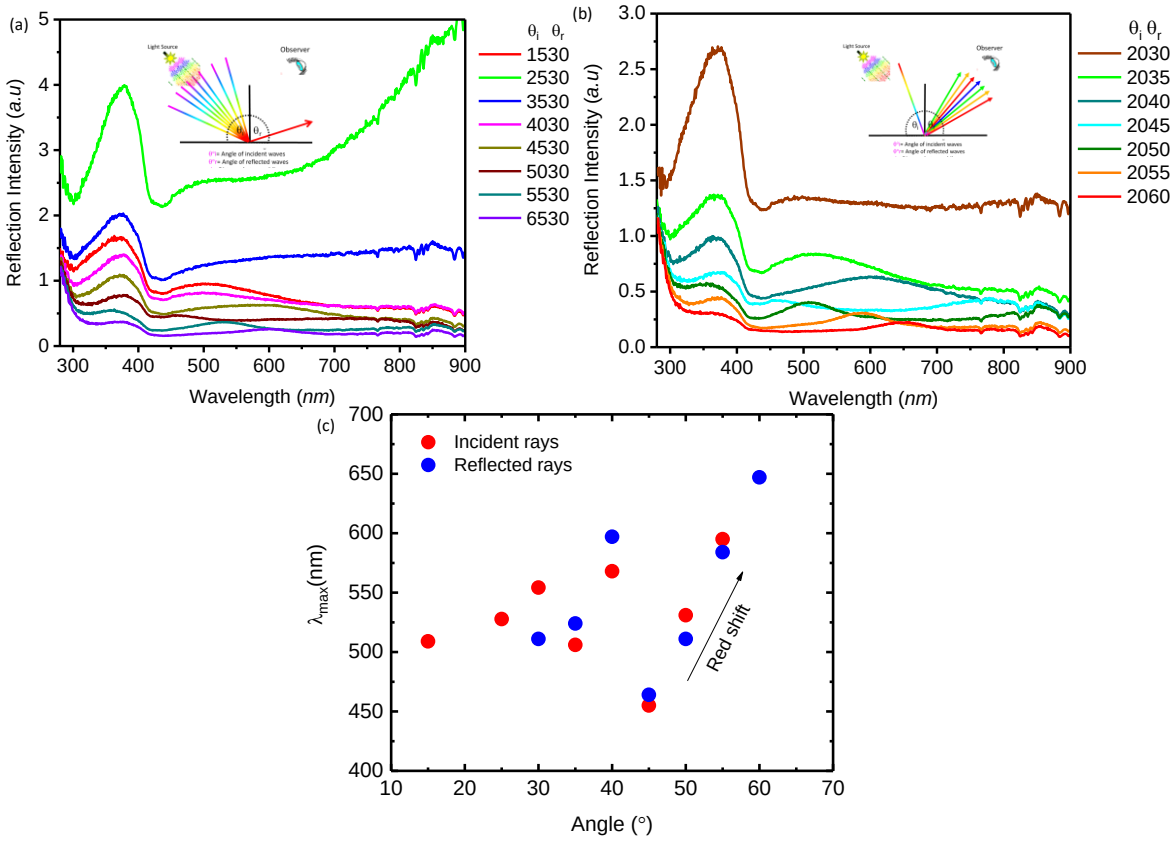

Figure 5.9 (a) Reflection spectra of PDGI/PAAm dry patterned sample at different angle of incident of light waves at constant viewing angle 30°. (b) Reflection spectra of PDGI/PAAm dry specimen at different angle of viewing angle at fix incident angle 20°. (c) Color tuning λ_{max} as a function of changing angle of incident and reflection.

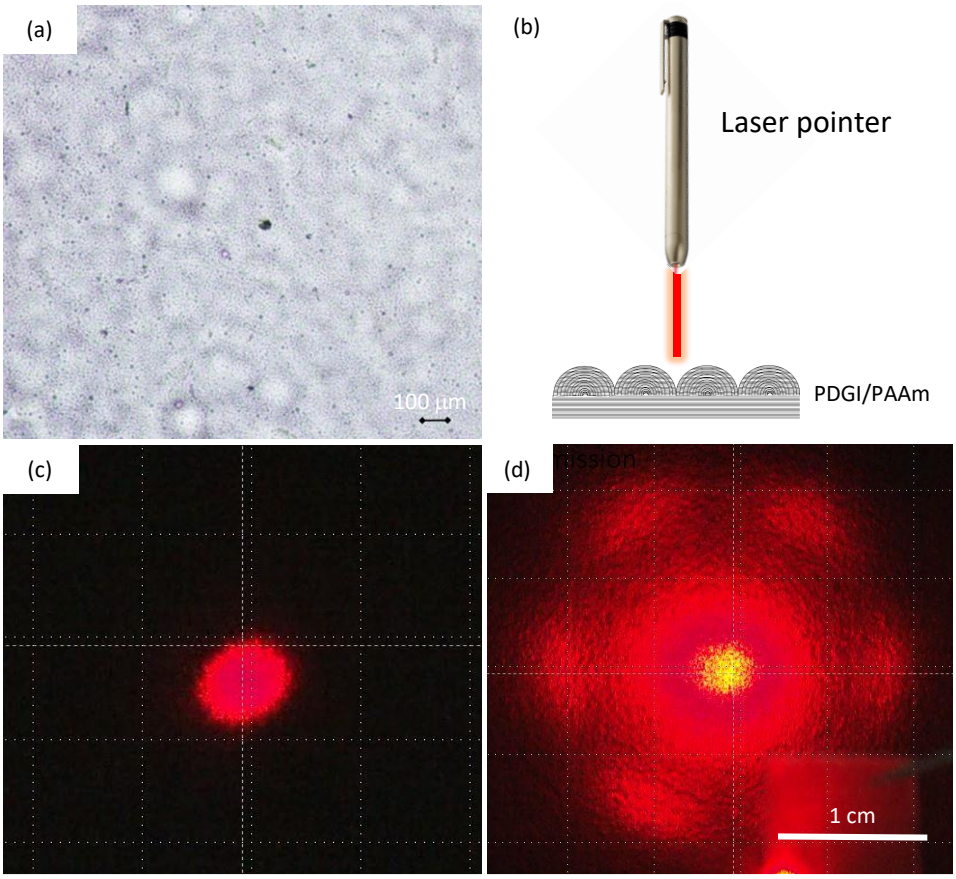

Figure 5.10 (a) Transmission view of dry PDGI/PAAm under POM. The scale bar is 100 µm. (b) Demonstration of laser light transmission (λ_{max} 635 nm) from PDGI/PAAm dry patterned specimen at angle 90° to the surface texture. (c) The oval shaped spot of laser beam on black substrate in the absence of sample. (d) The hexagonal diffraction pattern of laser beam by dry patterned PDGI/PAAm. The sable bar is 1 cm.

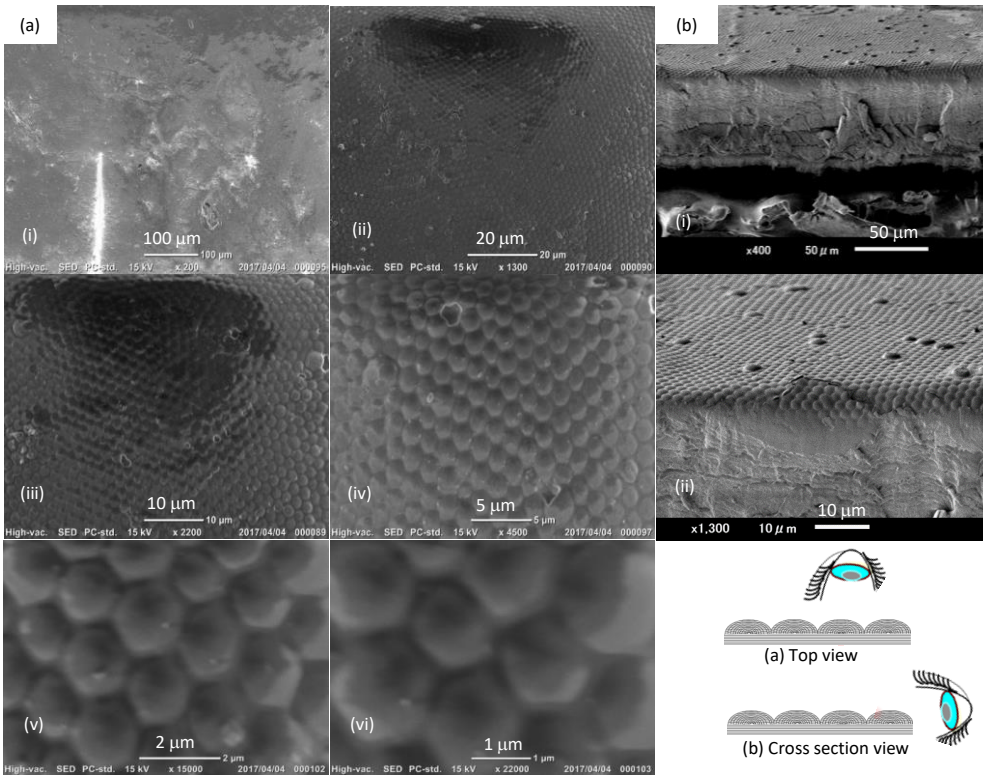

Figure 5.11 (a) PDGI/PAAm dry patterned sample top view SEM images at different magnification and scale bars a(i)-(vi) 100 µm-1 µm. (b) observation from cross-section of sample.

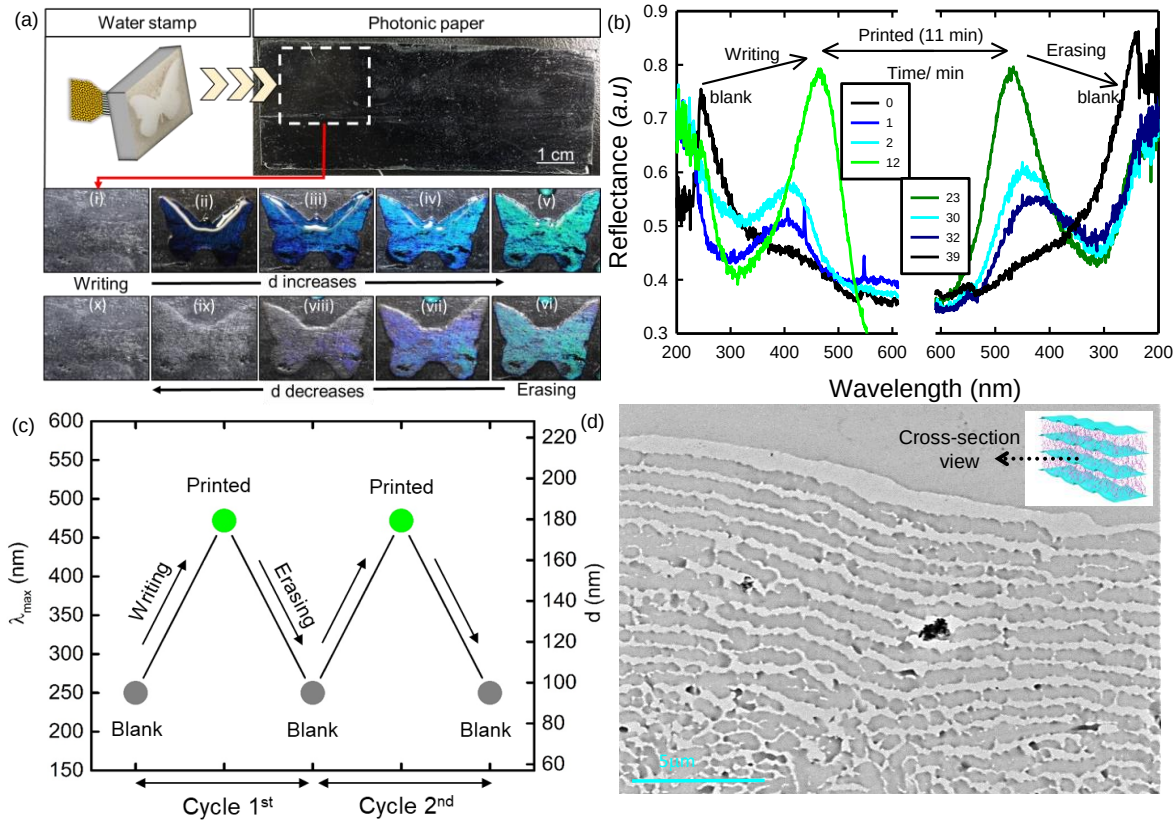

Figure 5.12 (a) PDGI/PAAm gel sheet on black substrate as reusable photonic paper that can be written-in with water ink and erased-off by drying (top right) by a water stamp made from water-soaked sponge engraved with butterfly pattern (top left). When the stamp was pressed gently on the photonic paper (i), water with the butterfly pattern was squeezed on the photonic paper to deep blue immediately (ii). With progress of time, the color of butterfly pattern changed from blue to green (iii–v). The printed green color remains unchanged for several minutes depending on the amount of water squeezed from the stamp. The green color was then erased gradually upon normal drying in air (vi–x). The appearance of color is due to the increase of lamellar *d*-spacing by absorbing water in PAAm layers and *vice versa*. (b) Shift in reflection peak during water intake (writing) and drying (erasing) of photonic paper. (c) Cyclic writing and erasing of the photonic paper. (d) TEM image from cross-section side shows multilayered morphology. The scale bar is 5 μm.

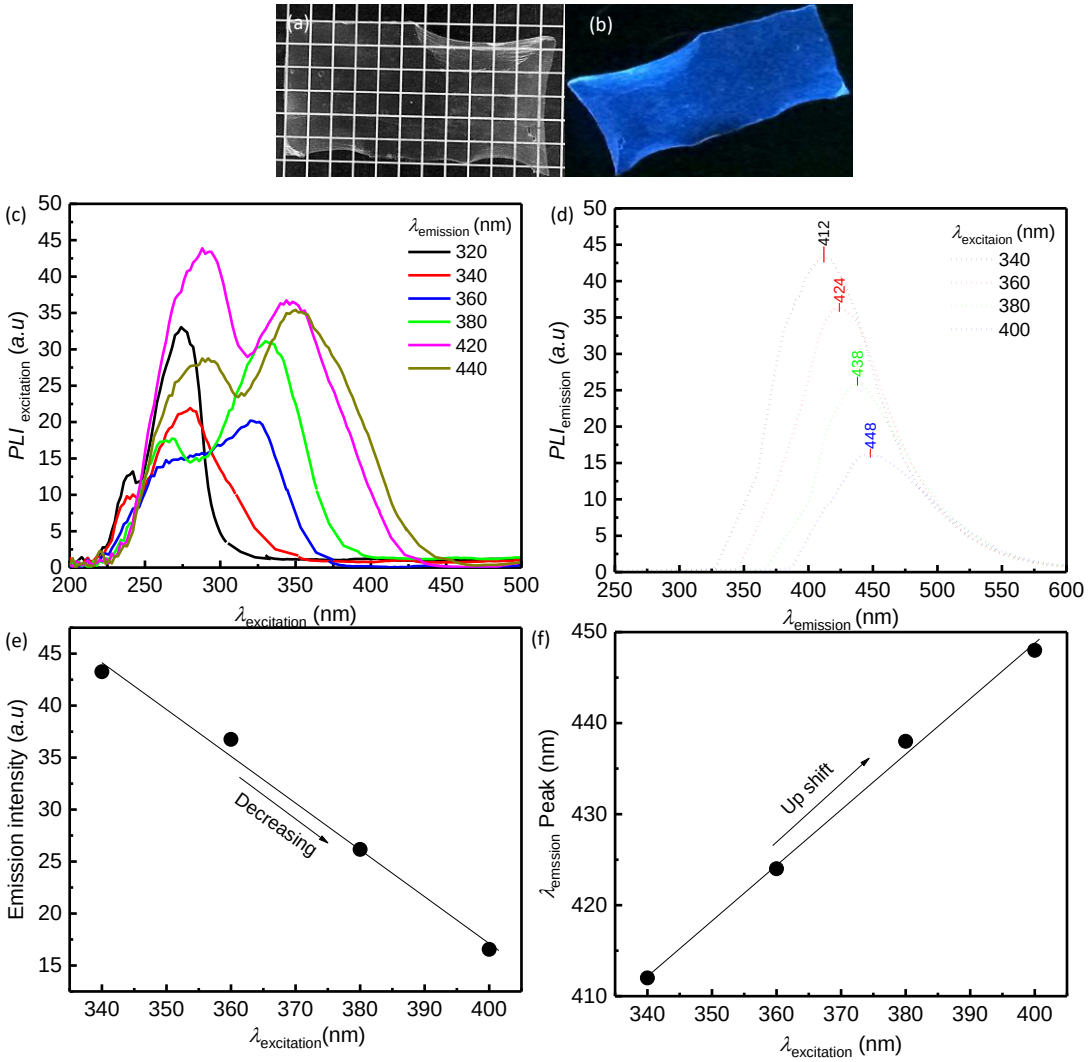

Figure 5.13 (a) PDGI/PAAm dried sheet on grid paper indicating transparency and large area. (b) The scenario of emission of blue light in dark after shining high intensity white light originated from Xe lamp. (c) Optimization of excitation wavelength and intensity at different emission wavelength range. (d) Optimization of emission wavelength and intensity at different excitation wavelength range. (e) Light emission intensity vs excitation wavelength. (f) Position of wavelength in spectra as a function of excitation wavelength.

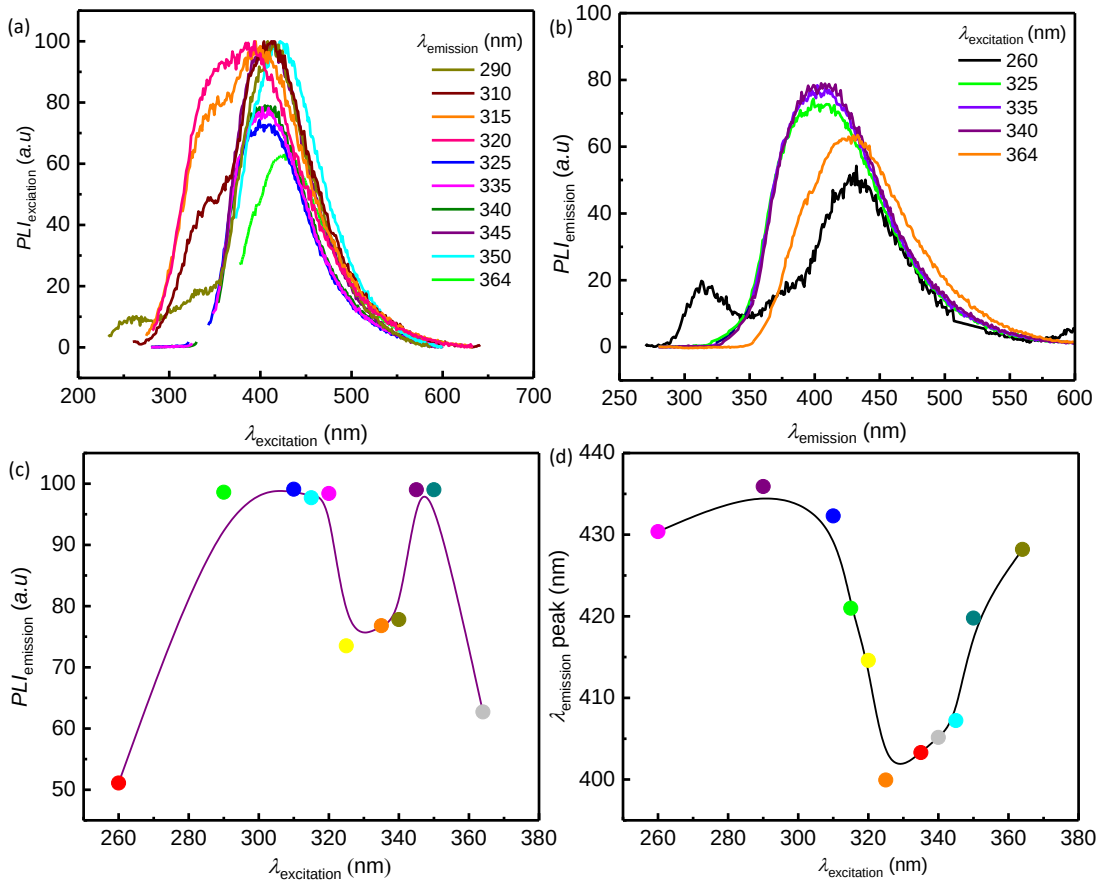

Figure 5.14 (a) Chemical crosslinked PDGI/PAAm optimization of excitation wavelength and intensity at different emission wavelength range. (d) Chemical crosslinked PDGI/PAAm sample optimization of emission wavelength and intensity at different excitation wavelength range. (e) Chemically cross-linked sample light emission intensity vs excitation wavelength. (f) Chemically crosslinked sample position of wavelength in spectra as a function of excitation wavelength.

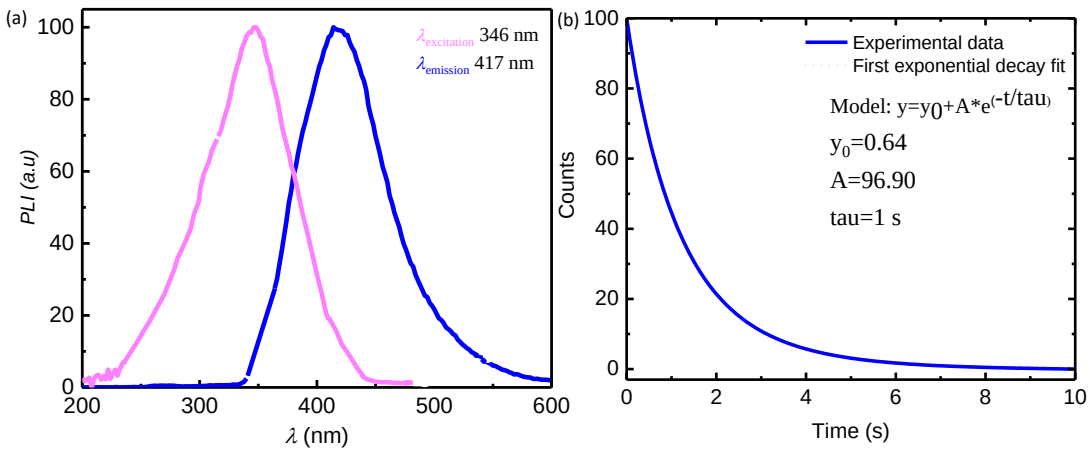

Figure 5.15 (a) Optimized absorption or excitation wavelength 345 nm of ultraviolet light necessary for the blue light emission 417 nm wavelength. (b) The decay profile of experimental data follows the first exponent decay fit. The life time for light to be remain emitted is 1s.

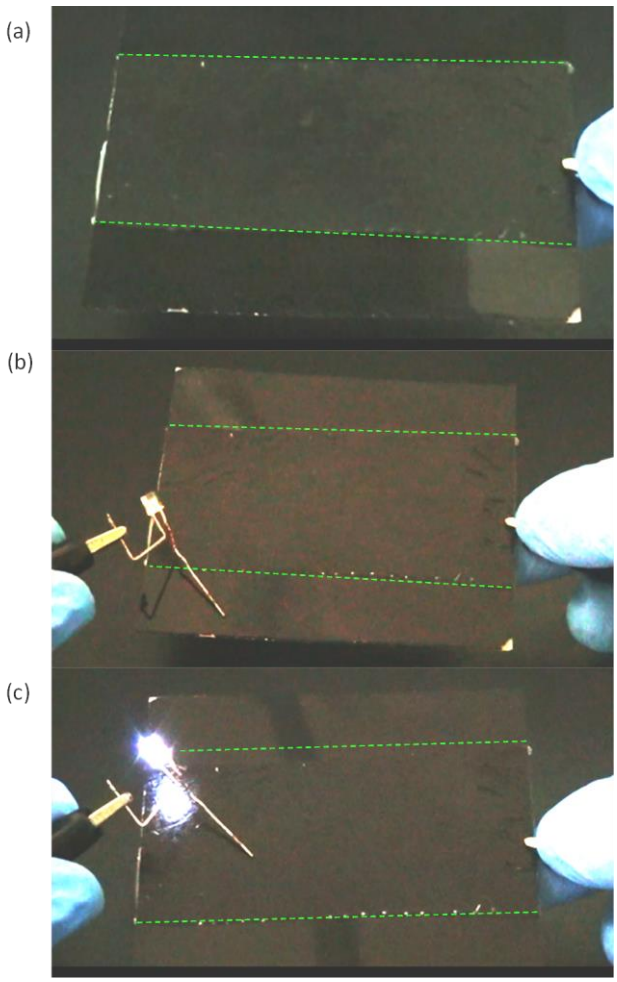

Figure 5.16 (a) Large area thin hybrid PDGI/PAAm iongel on black PMMA substrate. (b) For clarity the substrate does not show conductivity and current cannot pass the LED that showed off state. (c) However, the iongel is highly conductive obvious from LED lights on. The alligator wires are connected to equipment for AC current flow. The border lines represent the area (*L* 10 cm x *W* 6 cm) occupied by thin iongel membrane.

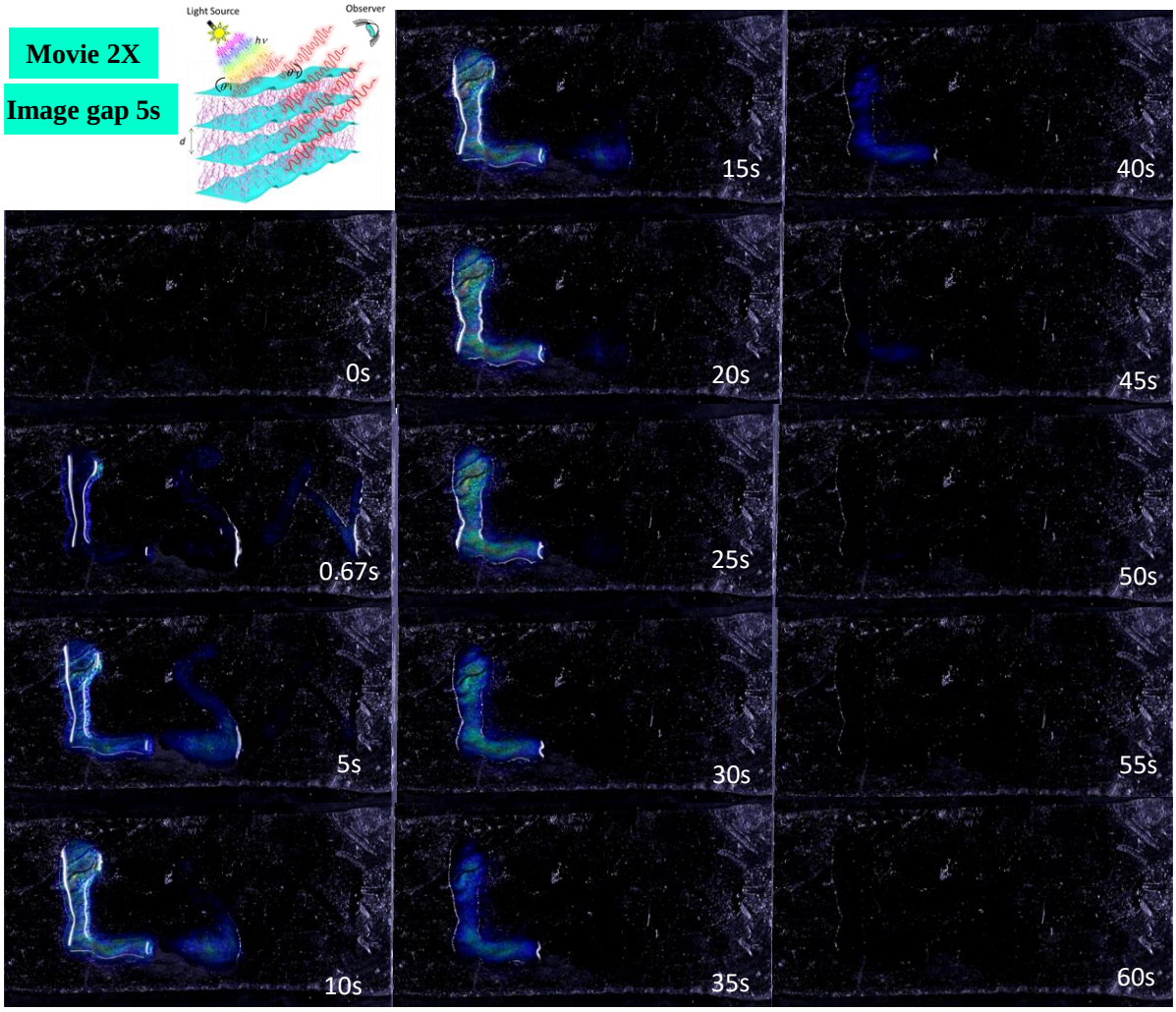

Figure 5.17 Large area thin hybrid PDGI/PAAm iongel on black PMMA substrate as water re-writing photonic paper. The images were taken after each 5s (0-60s) from the movies that has speed of 2x. The time of 0s indicate original iongel sheet. The word LSW was sketch by writing with water sponge (0.67s) and gradually the water allow the PAAm iongel layers to swell from colorless to blue and then green (0.67-15s) satisfying the Braggs law of diffraction of light. After the time of 15s the sketch started to erase by evaporation of water in free air drying (15s-60s). The PAAm gel layers shrink that cases the color shift from visible to invisible range of wavelength. The process of writing and erasing is repeatable.

CHAPTER 6

Solvent Free Fabrication of Soft Liquid Crystalline Elastomers Based on Amphiphilic Polymers

6.1 Introduction

Liquid crystalline elastomers, are rubbery networks of long, physically/chemically crosslinked chains of polymeric liquid crystal phases such as nematic or smectic.[1] The properties of such elastomers are deformation, moldable, birefringence, order, and exhibited response to external stimuli.[2–9] Because of these characteristics, liquid crystalline elastomers can simulate various functions of biological tissues, are gaining great attention to create artificial muscles.[10–14] However, to gain muscle like functions, tough elastomers are required.

Previous research suggested that, polymerizing amphiphilic monomer, DGI, contains hydrophilic glycerol and lipophilic dodecyl head groups form lyotropic liquid crystalline multi-lamellar vesicles, and shear induced orientation in the form of bilayer membranes just like lipid bilayer.[15] In hydrogels condition as hybrid of PDGI/PAAm, the polymerized PDGI amphiphilic polymer imparted exceptional biomimetic functions, such as marine organism skin like structure color, muscles-like mechanical toughness, and response to stimuli.[16,17] However, the detail investigation related to the properties of PDGI alone has been not been investigated. The next challenge is to unveil the structure and functions of amphiphilic PDGI liquid crystalline elastomer. The synthesis of large area amphiphilic liquid crystalline polymers PDGI with the supramolecular self-assembled structure is indispensable for the future application.

According to the reported research, the LCEs are capable of large, anisotropic deformations similar to that of many biological tissues.[18,19] The deformation of liquid crystal elastomers along the alignment direction exhibited a classical elastic response. However, by deformation

orthogonally to the orientation direction showed ‘soft’ elastic response. This phenomenon in LCEs is commonly called ‘soft elasticity’ and attributed to the reorientation of the LCE to align along the direction of the stretch.[20] Therefore, the deformation of PDGI liquid crystal elastomer by roll pressing and structure orientation along the shear direction is expected to change the alignment of domain chain and expected to enhance the birefringence of LCE.

6. 2 Experimental

6.2.1 Materials and method

Amphiphilic DGI monomers; was synthesized according to the procedure.[21] Briefly, the crude product after the synthesis was purified on a column packed with silica-gel, then elution by mix-solvent of ethyleacetate-hexane (1:1 volume-ratio). Separate volume of eluent from column contained DGI was collected in vial bottles, then was subjected to the re-crystallization using 1:1 weight-ratio mixture-solvent hexane-acetone. The last step was performed to insure the high purified DGI monomer. Therefore again two times DGI was subjected to re-crystallization from hexane/acetone mix-solvent that has 1:1 weight ratio. The melting and recrystallization temperature of DGI monomer were 63°C and 32°C, respectively confirmed by Differential scanning calorimetry DSC (**Figure**). *N*,*N*′-methylenebisacrylamide MBAA (Wako Pure Chemical Industries, Ltd., Japan) was recrystallized from ethanol, acrylamide AAm (Junsei Chemical Co., Ltd., Japan) was recrystallized from chloroform, Irgacure 2959 (BASF SE, Germany), and sodium dodecyl sulfate SDS (MP Biomedicals Inc., USA) were of commercial grade. Millipore deionized water was used for the reparation of monomer solutions and equilibrium swelling of gel.

6.2.2 Melt polymerization of DGI

In air tight glass vial, the measured weight of solid crystals of dodecyl glyceryl itaconate (DGI) monomer and 0.1 wt % Irgacure 2959 as initiator were mixed. The solid crystal to liquid crystal transition temperature of DGI monomer is 32°C, Kraft temperature is 43°C and melting temperature is 63°C. The mixture was heated at 70°C inside temperature controlled incubator. Within 5 min the monomer melt was obtained as a transparent liquid. The molten monomer was stirred for 30 min to ensure the dissolution of initiator.

Before polymerization, two reaction cells of 100-200 mm in length (*L*), 30-60 mm in width (*W*), and 0.05-0.5 mm in thickness (*T*) were prepared by sandwiching a 0.5 mm–thickness of silicone rubber spacer embedded between two pre-cleaned glass plates (NaOH/Ethanol 200g/6L). The precursor mixture of monomer melt contain initiator was injection casted on polymerization mold. This was followed by a co-current homo-polymerization of the molten DGI using UV light irradiation for 8 hours at 50°C inside incubator. After the completion of polymerization, the PDGI liquid crystalline elastomer (PDGILCE) was removed from the reaction cell.

For comparison the standard PDGI/PAAm hydrogel was also prepared according to previous reported method. The swollen PDGI/PAAm gel was stretched 4x of its initial length, fixed with adhesive tape and allowed to dry in air.

6.3 Characterization

6.3.1 Roll pressing of PDGILCE

The as prepared LCE sample was sheared in one direction by using metal bar applying roll pressed approach. The sample thickness *T* before and after roll pressing was measured by digital caliper.

6.3.2 Polarized optical microscopy (POM)

Before and after roll pressing, the PDGI liquid crystalline elastomer was analyzed under polarized optical microscope (POM). The self-assembly and shear induced orientation of amphiphilic molecules were analyzed. For comparison the water swollen and stretch dry PDGI/PAAm were also observed under POM.

6.3.3 Measurement of mechanical properties

The dumb-bell shaped LCE specimens, standard dimension (length, L = 12 mm width, W = 2 mm and T= 0.5 mm) were cut with commercial standard gel cutter (*model JIS-K6251-7*). The uniaxial tensile tests were performed using commercial tensile tester (Instron Anton Paar 5965) with tensile velocity 100 $mm.min^{-1}$ & stretching rate 0.14 s^{-1}. The modulus (stiffness) was calculated from the initial slope of the tensile stress-stretch curves within 5% deformation. Using the same condition except the dimensions the stretch dry PDGI/PAAm was also tested.

6.4 Results and discussion

6.4.1 Soft elasticity by roll pressing

The as prepared 0.5 mm thickness, poly-dodecyl-glyceryl-itaconate (PDGI) liquid crystalline elastomer was visually opaque/turbid. It is obvious because the melt viscosity was higher and shear flow was not applied to the amphiphilic melt. The roll pressing was performed by placing the elastomer on glass slide substrate, metallic rod was used to roll the sample using hand as shown in **Figure 6.1a(i)**. After roll pressing the sample elongated along the direction of roll pressing [**Figure 6.1a(ii)**]. This reduced the thickness of the elastomer to 45μm. The roll pressed induced flow of the elastomer that caused the dimension of sample to change. This phenomena is also related to the soft elasticity of the sample. By applying stress the direction of amphiphilic molecules changes towards the direction of applied stress showing malleability.

For comparison the pre-stretched air dried PDGI/PAAm hybrid is also shown in **Figure 6.1b.** The stretched dry sample maintained its length that was pre-stretched four times to initial length and do not show relaxation after release from fixation. However, the gel transformed from colorful to slightly turbid colorless hybrid dry PDGI/PAAm [**Figure 6.1b(i-iii)].**

6.4.2 Enhancement of birefringence

In order to understand the orientation of PDGI LCE before and after roll press, PDGI/PAAm stretch dry and PDGI/PAAm gel polarized optical microscopic analysis and SEM analysis were performed. The results obtained from POM are shown in **Figure 6.2** and **Figure 6.3**. For clarity the SEM images are shown in **Figure 6.4**.

First we look at the as prepared and roll pressed liquid crystal PDGI elastomer polarized optical microscopic images which as are shown in **Figure 6.2a,b.** The observation of specimens were performed at three angles such as 0°, -45°, +45° from top and cross-section side of gels using 532 nm quarter wave plate as well as cross polarizers, respectively. In the as preparation conditions of PDGILCE, the POM top view images under the cross-polarizer indicated mild birefringence in the presence of quarter wave plate, that appeared slightly white in cross-polarizers without quarter wave plate. Specially at the angle of 0° the sample also exhibited birefringence indicating the random self-assembly of amphiphilic domains **Figure 6.2a(i-vi)**. This is reasonable because shear flow was not applied to the melt of PDGI monomer before polymerization. However, after applying the roll press using metallic bar on PDGI LCE sample to align these amphiphilic domains, with tint plate the roll pressed sample exhibited blue and yellow colored interference that were bright white under cross-polarizers at viewing angle of -45° and +45°, respectively **Figure 6.2b(i-vi)**. However, at a viewing angel of 0°, no birefringence were observable either in the presence of absence of quarter wave plate. The observation of this results suggest that the application of roll pressing has influenced the

alignment of amphiphilic liquid crystal PDGI elastomer. This alignment was confirmed by SEM analysis as shown in **Figure 6.4a,b**. The SEM results confirmed that the PDGILCE sample before roll press exhibited rough surface and no obvious alignment from cross-sectional view **[Figure 6.4a(i-ii)]**. However, after roll presence the sample top view SEM images have wrinkled oriented patterns [**Figure 6.4b(i-ii)]**. The cross-section also indicated some ordered structure. That is why the POM images showed high birefringence by roll pressing. This could also be explained by stress induced birefringence of aligned polymer chains. Additionally, the retardation value for the roll pressed PDGILCE was also determined using Berek compensator.

The sample was oriented -45° from extinction between crossed polarizers. The compensator is inserted into the light path in such a way to make the slow axis parallel to the polarizer transmission direction. Then, the knob of compensator drum is rotated until an intensity minimum is observed very close to extinction. From the approximation of low retardation, the angle deviation of the compensator from its extinction position allows the calculation of the sample retardation. Then the birefringence are calculated from the division of the retardation value by sample thickness. The values of birefringence was $109x10^{-4}$ which is greater than that of the calculated birefringence of PDGI/PAAm gel as $1.6x10^{-4}$. This also indicated the birefringence in PDGIPAAm arises from PDGI orientation. However, the orientation of PDGI bilayer is not as good as that of PDGILCE by roll press.

In order to understand this behavior in hybrid PDGI/PAAm system the POM images of gel as well as stretch dry PDGI/PAAm are shown in **Figure 6.3a,b.** The results showed that in gel condition the bright interference colors between cross-polarizer in the presence and absence of quarter wave plate, are opposite as compared to the roll pressed PDGILCE [**Figure 6.3a(i-vi)]**. However, pre-stretch dry sample exhibited the same orientation pattern as that of the LCE system, indicating the roll pressing or stretching allowed the orientation of amphiphilic domains

that has soft elasticity towards the stretch direction either by manual stretching in uniaxial direction or roll pressing, respectively **[Figure 6.3b(i-vi)**]. The SEM images of stretched samples showed bridging of fibrous alignment towards the elongation direction **[Figure 6.4c**]. These results are reasonable for the enhancement of birefringence from top view of the samples. This similar behavior indicated another phenomena that there is a strong interaction between the bilayers of PDGI and PAAm layers.

6.4.3 Enhancement of mechanical property

The self-assembled and oriented structure in nature are famous for their enhanced mechanical behavior and are inspiring systems to create highly tough synthetic materials for example biological tissues such as skin that consist of lipid bilayers. Some silk moth adapted to orient silk by rolling-weaving its head that help spinning and pulling silk for orientation. The spider that produce highly oriented fiber by precipitously dropping down along the dragline. Natural biopolymers are also known for their highly oriented structure with enhanced mechanical behavior. The recent study of hybrid PDGI amphiphilic polymer with PAAm gel such PDGI/PAAm showed high toughness with pronounce yielding. The yielding was attributed to the structure re-organization of PDGI bilayers at low strain regime that contributed to the energy dissipation of bulk PDGI/PAAm gel. Therefore, to related current study of PDGILCE, the tensile mechanical properties of non-oriented PDGILCE, dry stretch oriented PDGI/PAAm, PDGI/PAAm incubated at RH 97%, standard PDGI/PAAm and PAAm gels are shown in **Figure 6.5,** for clarity the yielding region are enlarged and shown below the main figure. The results from stress-strain curve such as modulus, stress, strain and toughness in term of work of extension are shown in **Figure 6.6a,b,c,d.** The tensile behavior indicated that, the neat PAAm gel was soft/wet/ductile extremely low level of load bearing property (modulus ~0.006 MPa, and fracture strain 8 m/m), as shown in **Figure 6.5** and **Figure 6.6a,b,c,d**. The neat

PDGI/PAAm gel was soft/wet and tough exhibited two times high elongation at breakage compared to neat PAAm gel (modulus ~0.14 MPa, and fracture strain 16 m/m), with pronounce yielding **Figure 6.5** and **Figure 6.6a,b,c,d**. Moreover, in comparison to neat PAAm and PDGI/PAAm gels, the PDGI LCE showed high strength (stress at break ~3.5 MPa but slightly low level of tensile deformation 0.76 m/m) indicating highly stiffness (~45 MPa) in addition to toughness (~2.5 $MJ.m^{-3}$) that surpassed the mechanical behavior of both neat PDGI/PAAm and PAAm gels **Figure 6.5** and **Figure 6.6a,b,c,d**. Another interesting behavior is the long yielding behavior of PDGILCE sample. Although the sample was not oriented by shear flow or by roll pressing but still exhibited distinct yielding behavior indicating the yielding PDGI/PAAm neat gel definitely because of the PDGI/PAAm bilayers. However, the modulus reported for the bilayers is much lower than the bulk sample. This might be due to the thickness effect because bilayers are 5 nm thick while the bulk PDGILCE is 0.6 mm thick. For further understanding, the tensile behavior of stretch dry PDGI/PAAm or PDGI/PAAm soaked on RH 97% must have some relationship with PDGILCE. In the dry sample after stretching the PAAm polymer chains are also freezes by elongation. However, for the RH97% the bilayers might have stabilized that would contribute in mechanical property of sample. First we look at the tensile behavior of stretch dry PDGI/PAAm sample, shown in **Figure 6.5** and **Figure 6.6a,b,c,d.** The pre-stretch and dried PDGI/PAAm exhibited very high stiffness and toughness (E ~78 MPa, $W_{ext.}$ 12 $MJ.m^{-3}$) with 5 times higher stretch than that of the PDGILCE. In this case the high stiffness is probably due to the glassy state of PAAm chains and formation of fibrous structure by elongation that freezes by drying. Therefore, the tensile behavior of sample soaked on RH97% must be considered to have good relation with that of PDGILCE. The tensile results of PDGI/PAAm RH97% showed almost not exactly the same but nearly same level of stiffness

(~25MPa), strain at break (~2.3 m/m), stress at break (~2.7 MPa), and toughness (~5.5MPa), respectively **Figure 6.5** and **Figure 6.6a,b,c,d**.

6.5 Conclusion

In conclusion, we succeeded to synthesize and investigate the properties of amphiphilic PDGI liquid crystalline elastomer. The PDGILCE showed high toughness, stiffness, malleability by roll pressing, with enhanced birefringence. This method might open new ways to explore various novel function of PDGILCE for creation of artificial muscles.

6.6 References

[1] M. Warner, E. M. Terentjev, Liquid Crystal Elastomers. *Book* **2003**, 423.

[2] N. Torras, K. E. Zinoviev, C. J. Camargo, E. M. Campo, H. Campanella, J. Esteve, J. E. Marshall, E. M. Terentjev, M. Omastová, I. Krupa, P. Teplický, B. Mamojka, P. Bruns, B. Roeder, M. Vallribera, R. Malet, S. Zuffanelli, V. Soler, J. Roig, N. Walker, D. Wenn, F. Vossen, F. M. H. Crompvoets, *Sensors and Actuators, A: Physical* **2014**, *208*, 104.

[3] V. Shibaev, *Cross-linked Liquid Crystalline Systems : From Rigid Polymer Networks to Elastomers*; 2011; Vol. 20.

[4] H. Kim, J. M. Boothby, S. Ramachandran, C. D. Lee, T. H. Ware, *Macromolecules* **2017**, *50*, 4267.

[5] T. Kato, K. Tanabe, *Chemistry Letters* **2009**, *38*, 634.

[6] A. Sengupta, U. Tkalec, M. Ravnik, J. M. Yeomans, C. Bahr, S. Herminghaus, *Physical Review Letters* **2013**, *110*.

[7] J. S. Moore, S. I. Stupp, *Macromolecules* **1988**, *21*, 1217.

[8] O. Yaroshchuk, Y. Reznikov, *J. Mater. Chem.* **2012**, *22*, 286.

[9] T. J. White, D. J. Broer, Programmable and adaptive mechanics with liquid crystal polymer networks and elastomers. *Nature Materials* **2015**, *14*, 1087–1098.

[10] D. L. Thomsen, P. Keller, J. Naciri, R. Pink, H. Jeon, D. Shenoy, B. R. Ratna, *Macromolecules* **2001**, *34*, 5868.

[11] Y. Ji, J. E. Marshall, E. M. Terentjev, Nanoparticle-liquid crystalline elastomer composites. *Polymers* **2012**, *4*, 316–340.

[12] M.-H. Li, P. Keller, *Philosophical transactions. Series A, Mathematical, physical, and engineering sciences* **2006**, *364*, 2763.

[13] P.-G. De Gennes, M. Hébert, R. Kant, *Macromolecular Symposia* **1997**, *113*, 39.

[14] D. K. Shenoy, D. Laurence Thomsen, A. Srinivasan, P. Keller, B. R. Ratna, *Sensors and Actuators, A: Physical* **2002**, *96*, 184.

[15] K. Tsujii, M. Hayakawa, T. Onda, T. Tanaka, *Macromolecules* **1997**, *30*, 7397.

[16] M. A. Haque, J. P. Gong, *Reactive and Functional Polymers* **2013**, *73*, 929.

[17] Y. Yue, T. Kurokawa, M. A. Haque, T. Nakajima, T. Nonoyama, X. Li, I. Kajiwara, J. P. Gong, *Nature communications* **2014**, *5*, 4659.

[18] D. P. Knight, F. Vollrath, *Philosophical Transactions of the Royal Society B: Biological Sciences* **2002**, *357*, 155.

[19] R. Ishige, K. Osada, H. Tagawa, H. Niwano, M. Tokita, J. Watanabe, *Macromolecules* **2008**, *41*, 7566.

[20] T. H. Ware, J. S. Biggins, A. F. Shick, M. Warner, T. J. White, *Nature*

Communications **2016**, *7*, 10781.

[21] K. Tsujii, N. Saito, T. Takeuchi, **1980**, 2287.

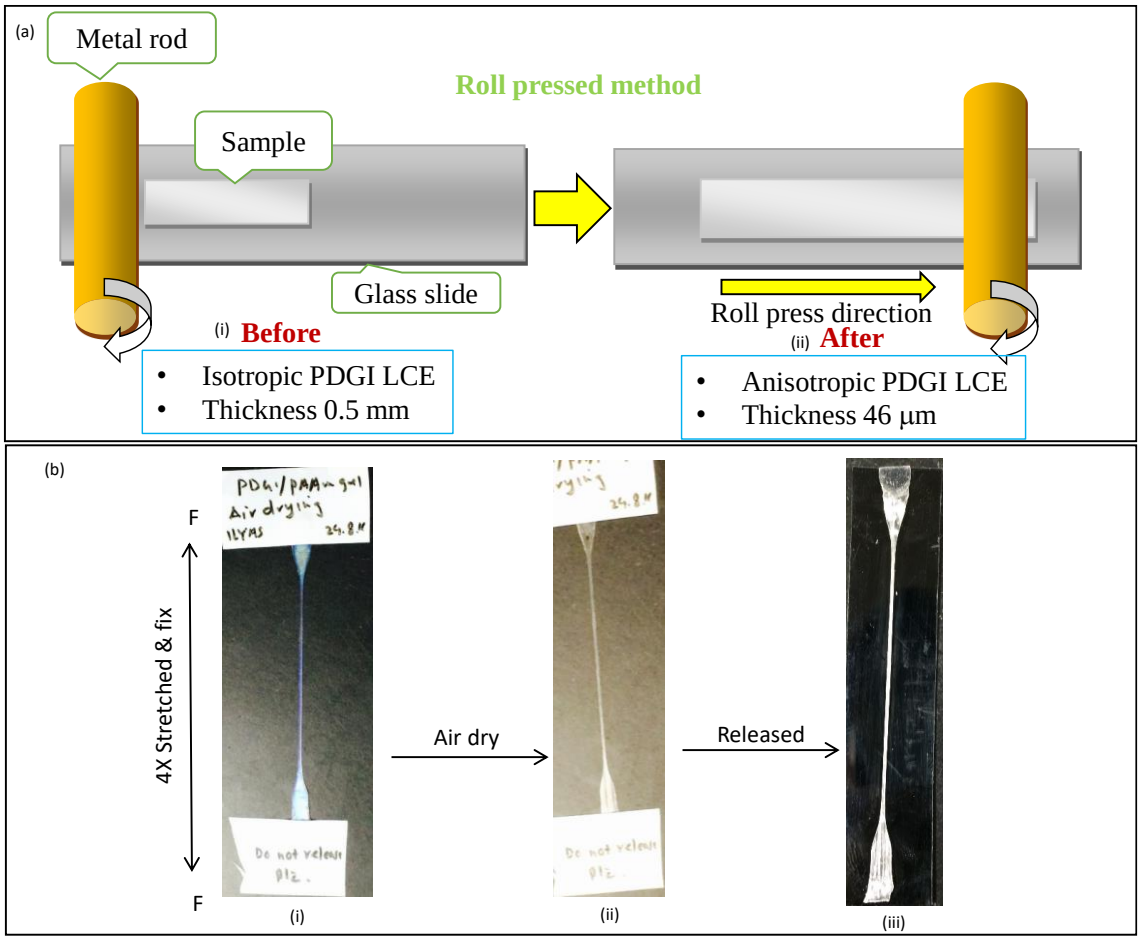

Figure 6.1 (a) Roll pressing of as prepared PDGI liquid crystal elastomer. The T_0 and T was respectively 0.5 mm and 45 μm. (b) For comparison, the pre-stretch air drying of PDGI/PAAm gel. Where, (i), (ii) and (iii) are respectively, the four times length to initial length prestretched PDGI/PAAm gel sample, (ii) the pre-stretched air dried PDGI/PAAm sample after 24h and, (iii) release of PDGI/PAAm dried sample from fixation.

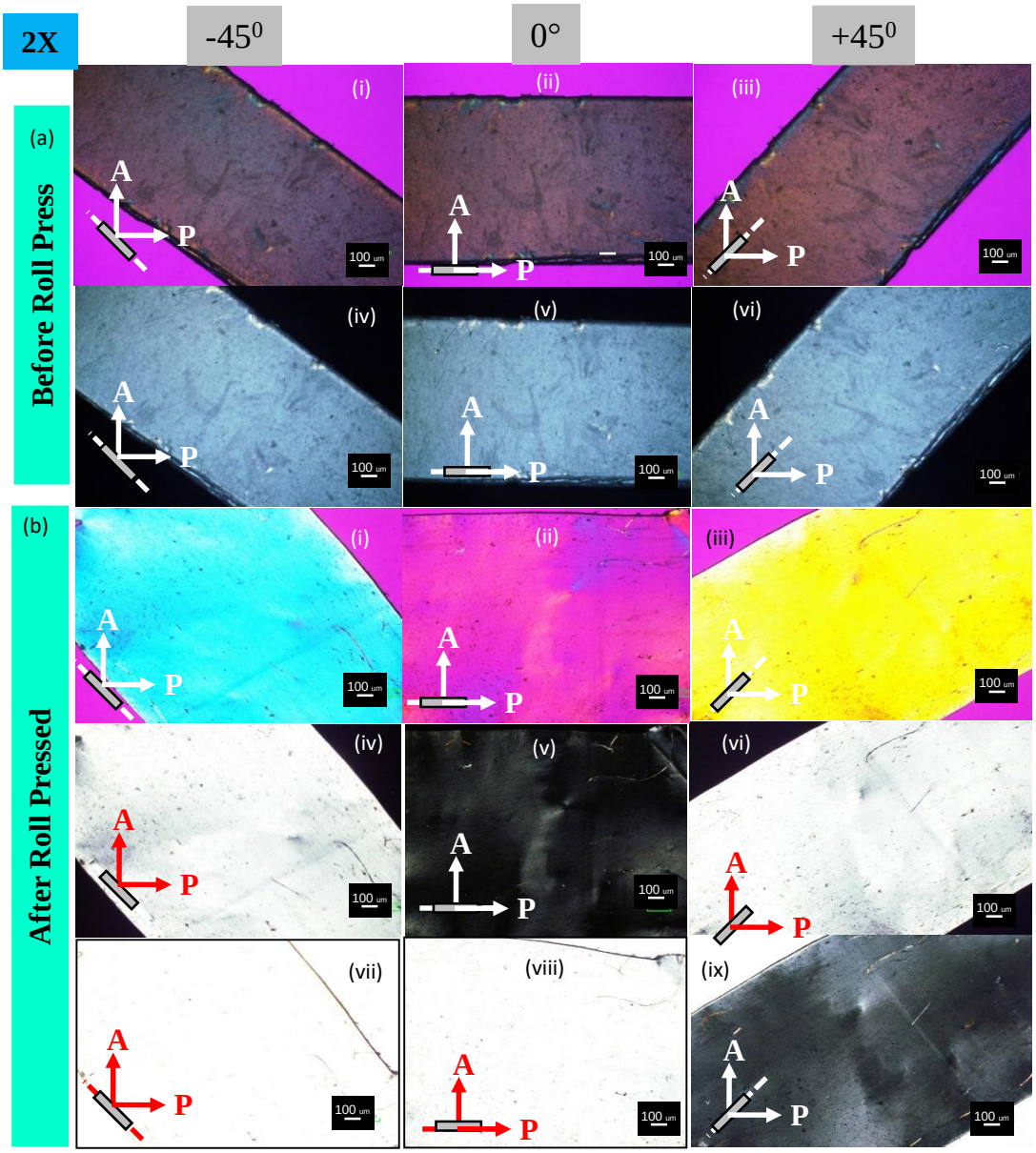

Figure 6.2 Top view POM images of PDGI liquid crystalline elastomers. (a) As prepared conditions before applying roll press in the presence of cross-polarizers with tint plate (i-iii) and without tint plate (iv-vi). (b) Observation of PDGI LCE after applying roll press between cross-polarizers in the presence (i-iii), and absence of tint plate (iv-vi) as well as open polarizer (vii-ix) view, respectively. All the observation were performed at same scale bar of 100 μm at three viewing angles such as -45°, 0° and +45°.

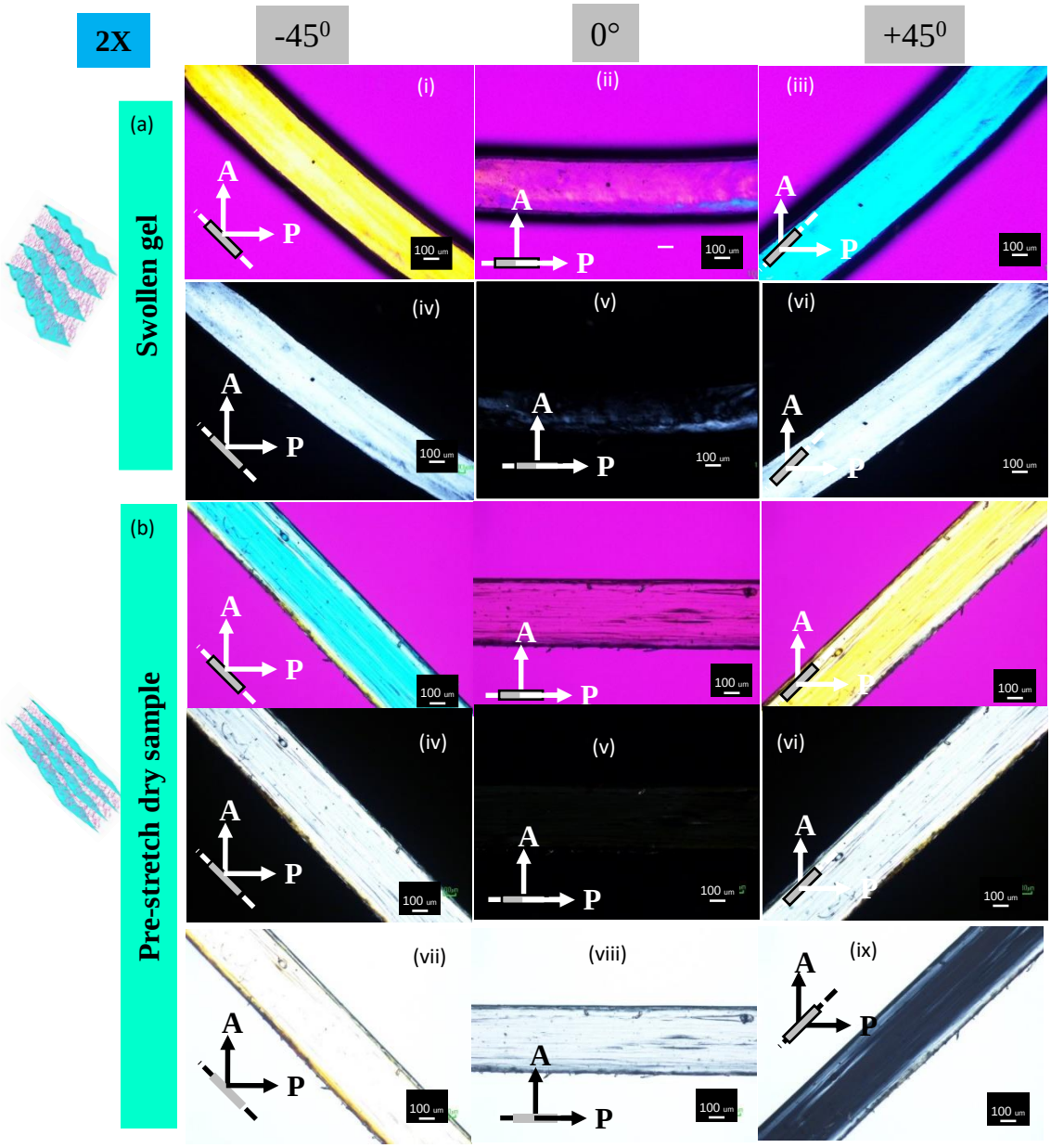

Figure 6.3 (a) Cross-sectional view POM images of PDGI/PAAm. (a) Equilibrium swollen condition in the presence of cross-polarizers with tint plate (i-iii) and without tint plate (iv-vi). (b) The pre-stretched dried PDGI/PAAm sample between cross-polarizers in the presence (i-iii), and absence of tint plate (iv-vi) as well as open polarizer (vii-ix) view, respectively. All the observation were performed at same scale bar of 100 μm at three viewing angles such as -45°, 0° and +45°.

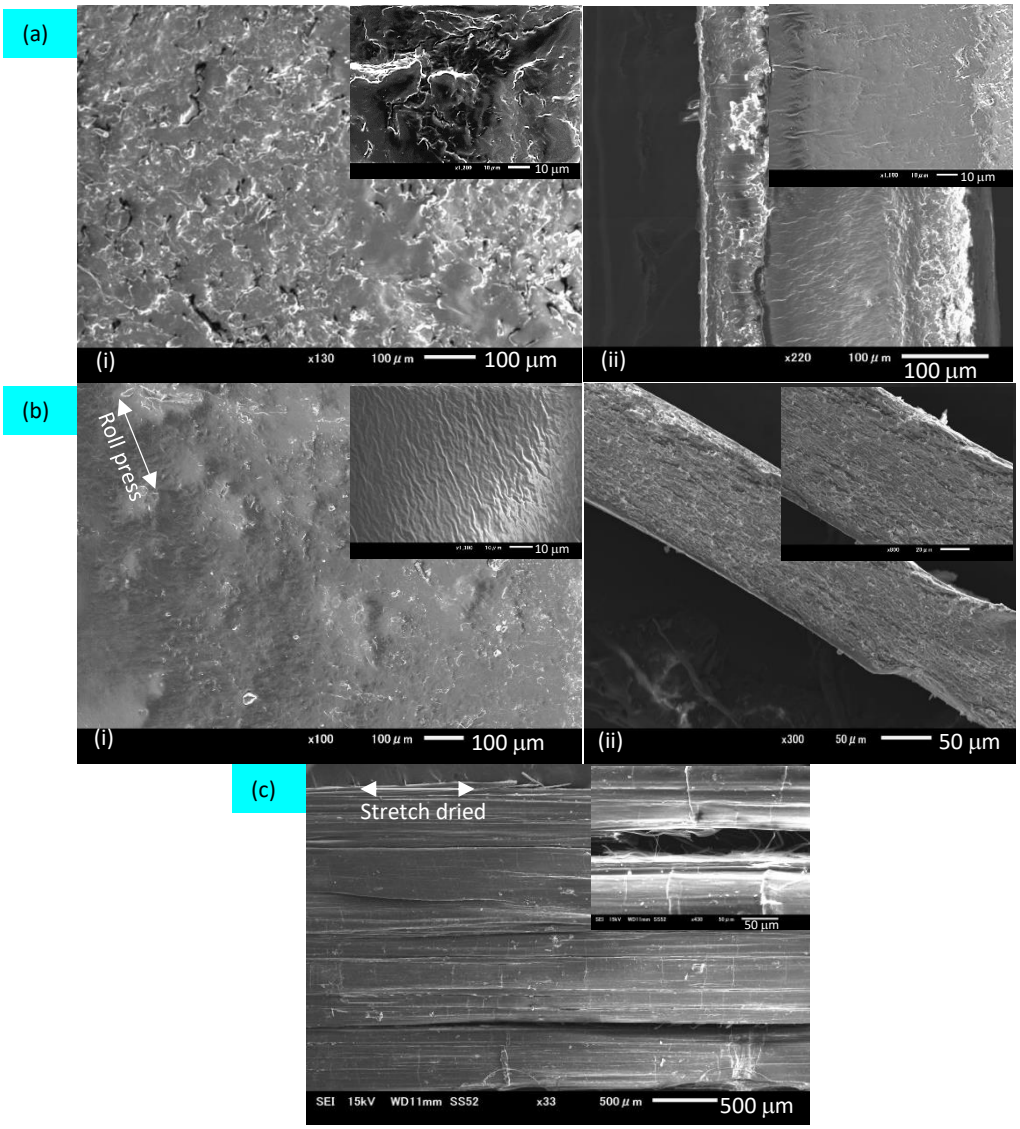

Figure 6.4 SEM images of (a) As prepared PDGI/PAAm LCE, (i) top view and (ii) Cross-sectional view. (b) After applying roll pressing on PDGI/PAAm LCE, (i) Top view and (ii) cross-section view. (c) Top view SEM image of PDGI/PAAm pre-stretched air dried sample.

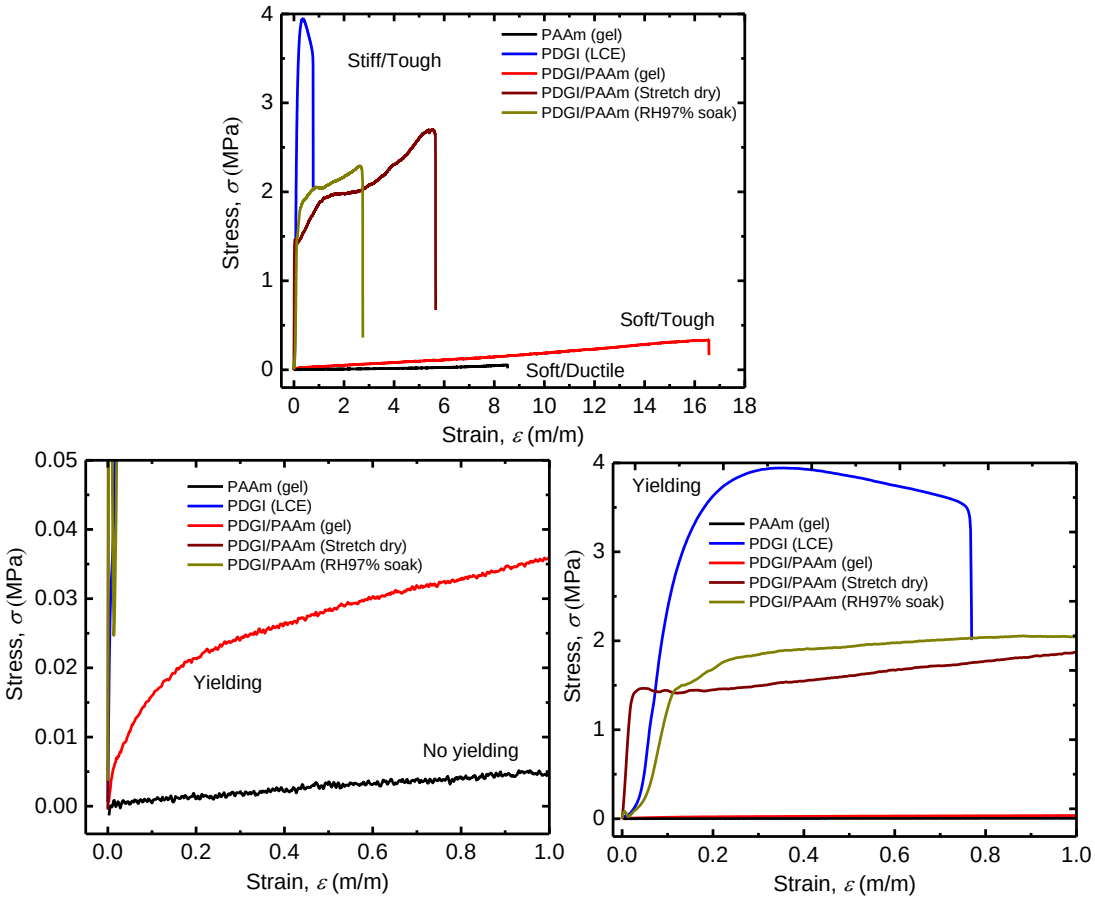

Figure 6.5 Tensile stress-strain cure of PAAm (gel), PDGI/PAAm (gel), PDGI/PAAm (LCE), PDGI/PAAm (stretch dry) and PDGI/PAAm (soaked on RH97%), respectively. The cross-head speed was 100 mm/mm that corresponds to the strain rate of $0.14s^{-1}$. For clarity, the yielding regions are shown as in enlarge view.

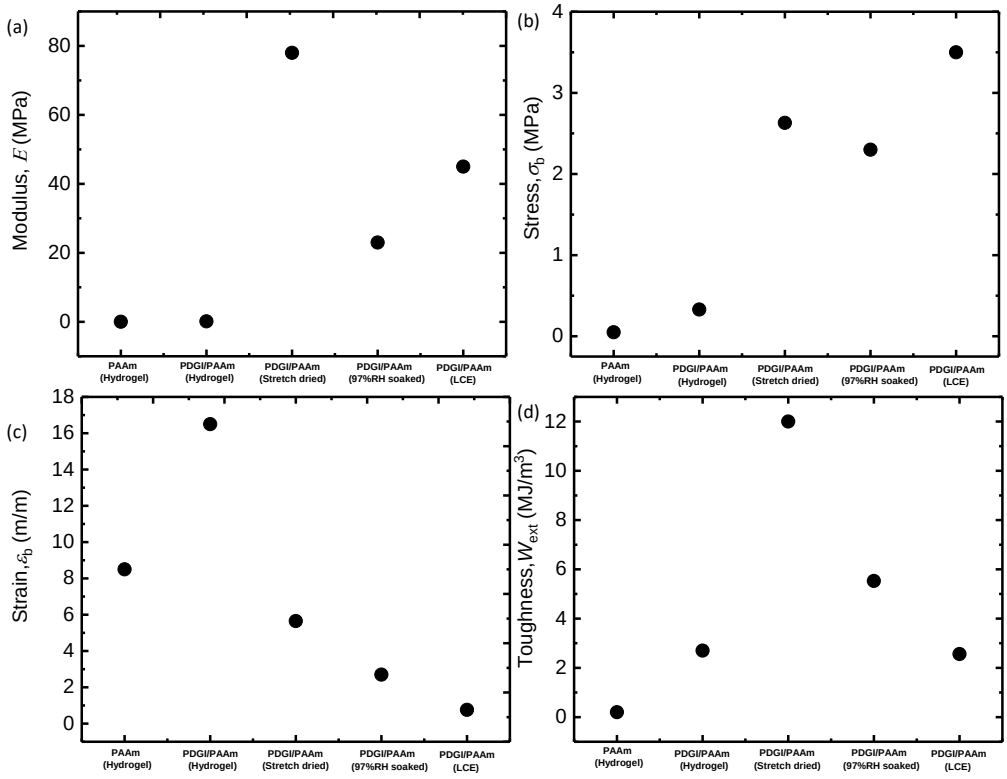

Figure 6.6 Results from tensile stress-strain cure of PAAm (gel), PDGI/PAAm (gel), PDGI/PAAm (LCE), PDGI/PAAm (stretch dry) and PDGI/PAAm (soaked on RH97%), respectively. The cross-head speed was 100 mm/mm that corresponds to the strain rate of 0.14s^{-1}. For clarity, the yielding regions are shown as in enlarge view. (a) Modulus; (b) Stress; (c) Strain; and (d) Toughness of aforementioned samples, respectively.

CHAPTER 7

Glucose sensing DN photonic Hydrogels

7.1 Introduction

Glucose is an essential fuel for the normal activity of biological tissues of human being. The deviating of glucose level from optimum concentration is associated with various health hazards including the risk of diabetes.[1] Diabetes is detrimental for human health in which pancreas cannot secrete insulin and usually damaged by high glucose level.[2] Therefore, there is an increasing demand for the hand on, readily available, non-invasive and patient friendly glucose monitoring devices.[3]

Hydrogel, are soft and wet matter imbibed in large amount of water have many potential application as biomaterial.[4] As a hybrid of solid polymer strands and fluid components, hydrogels are highly permeability to water containing small molecules and experience reversible volume change by intake and release of water.[5,6] However, due to the lack of specific recognition sites for the detection of external stimuli or small molecules, conventional hydrogels remains dormant and do not respond to important stimuli, such as light, temperature, pH, ionic strength, and chemical reactions.[7] Recent research on hydrogels that contains glucose recognition sites phenyl-boronic-acid are gaining tremendous attention as glucose monitoring soft devices but the problem associated with them is non-homogenous color indication.[8] Therefore, there is a need of soft and wet devices for a common person to understand the clearly glucose recognition by uniform visual color change or naked eyes.

To fulfill the requirement of visual color indication in response to glucose, the hydrogels must exhibit anisotropic structure that interfere constructively with the visible wavelength of lights.[9]

Recent study of the bilayer hybrid gel, containing alternating liquid crystalline amphiphilic polymer PDGI (bilayer) and aquaphilic polymer PAAm showed various stimuli responsive structural color change such as stress-strain, one-dimensional re-swelling, one-dimensional stretching, one-dimensional release of small molecules, one-dimensional drying, hydrolysis induced color change to pH, temperature, and small deformation.[10–15]

According to the literature study, usually two major factors affect the swelling behavior of hydrogels with functionality sites as they come in contact with medium consist of analytes. Firstly, the osmotic pressure term caused by Donnan-potential (ion) as a result of the concentration variances of analyte ions between inside and outside the hydrogel with bound receptors. Secondly, enthalpy of mixing term (mix) between aqueous media and hydrogel from the Flory–Huggins solubility parameters point of view.[16] The ionic and mixing terms are balanced with the osmotic pressure related to elastic restoring force (el) of the fully swollen hydrogel and is written as following;

$$-\Pi\text{elastic} = \Pi\text{ionic} + \Pi\text{mixing} \qquad (1)$$

For the chemical sensing of specific analyte recognition, ionic term must be increased.

Here in, the current chapter is related to the incorporate of glucose recognition unit phenyl-boronic-acid unit to create interpenetrating double network glucose responsive photonic hydrogel using concept of double network hydrogel. It is envisioned that the structure coloration of hydrogel is to be tuned in the presence of phenyl-boronic-acid group. It is expected that the structure color of the hybrid PDGI/PAAm-PPBA gel will tune in the visible range of electromagnetic spectrum of light in response to glucose, pH and small deformation, respective by satisfying the Braggs law of diffraction.

7. 2 Experimental

7.2.1 Materials and method

7.2.1.1 Synthesis of Functional DGI monomer

Amphiphilic DGI monomers; was synthesized according to the procedure.[21] Briefly, the crude product after the synthesis was purified on a column packed with silica-gel, then elution by mix-solvent of ethyleacetate-hexane (1:1 volume-ratio). Separate volume of eluent from column contained DGI was collected in vial bottles, then was subjected to the re-crystallization using 1:1 weight-ratio mixture-solvent hexane-acetone. The last step was performed to insure the high purified DGI monomer. Therefore again two times DGI was subjected to re-crystallization from hexane/acetone mix-solvent that has 1:1 weight ratio. The melting and recrystallization temperature of DGI monomer were 63°C and 32°C, respectively confirmed by Differential scanning calorimetry DSC. *N,N′*-methylene-bis-acrylamide MBAA (Wako Pure Chemical Industries, Ltd., Japan) was recrystallized from ethanol, acrylamide AAm (Junsei Chemical Co., Ltd., Japan) was recrystallized from chloroform, Irgacure 2959 (BASF SE, Germany), and sodium dodecyl sulfate SDS (MP Biomedicals Inc., USA) were of commercial grade. Millipore deionized water was used for the reparation of monomer solutions and equilibrium swelling of gel. For the glucose recognition unit 3-(Acrylamido)phenylboronic acid monomer was purchased by Sigma-Aldrich.

7.2.1.2 Preparation of PDGI/PAAm bilayer hybrid gel

PDGI/PAAm gel was synthesized by slightly modification of the previously method.[18] Briefly, 0.13M DGI, 0.0325 mM SDS, 2 M AAm, 2.1 mM MBAA(as a cross- linker of AAm), and 2 mM Irgacure 2959 (as a UV initiator) were dissolved in water. The aforementioned precursor solution was poured into a 10 ml glass vial and placed in a water bath at 55 °C for approximately

5 h, until stable lamellar DGI bilayers formed. The solution was then suctioned into a rectangular glass mold separated by silicone rubber (inner thickness: ~0.5 mm, length: ~ 20 cm, width: ~6 cm) using a 10 mL plastic syringe under inert Argon atmosphere using automatic pump method. The flowrate of the sample solution was kept as high as possible (roughly 3 cm s^{-1}, shear rate of 133 s^{-1}) to orient bilayers along the glass surface. Co-current polymerization of DGI and AAm was performed using 365 nm UV light irradiation in the glass mold for 8 h at 50 °C under inert Ar atmosphere. The polymerized as prepared hybrid PDGI/PAAm gel was removed from the surface of glass plate and soaked in water for one week for equilibrium swelling.

7.2.1.3 Preparation of double network photonic hydrogel

Second precursor solution in 9:1 volume ratio DMSO:water was prepared by adding 1M 3APBA, 0.1 mol% *N*,*N*′-methylene-bis-acrylamide MBAA (cross-linker for 3ABPA), 0.1 mol% irgacure 2959 (photo-initiator for 3ABPA). The equilibrium swollen PDGI/PAAm gel was soaked in aforementioned solution for 24h in order to diffuse the monomer solution inside the PAAm matrix. UV free radical polymerization was initiated by UV irradiation for 8h. After the completion of polymerization the interpenetrating PDGI/PAAm-PPBA double network hydrogel was obtained. For the sensing of glucose PDGI/PAAm-PAPBA was first immersed in NaOH 1 min, the boronic group becomes charged and activates for sensing of glucose. The whole scheme of preparation to sensing of glucose is shown in **Figure 7.1**.

7.3 Characterization

7.3.1 Measurement of dimension

The swelling/shrinking sample dimensions such as thickness, width and length before T_0, W_0, L_0 and after exposure T, W, L to different stimuli such as glucose, pH and stress was measured by digital caliper.

7.3.2 Measurement of Reflection spectra

The structure color of PDGI/PAAm-PPBA in response to pH or glucose was characterized by the electromagnetic spectrum of light, using moveable angle reflection measurement optics (Hamamatsu Photonics KK, C10027A10687) coupled with photonic multichannel analyzer (Hamamatsu Photonics KK, C10027). White light from Xe source was used to irradiate the hybrid gel. Reflection spectrum was acquired by keeping both the angles of incident (Bragg's angle) and reflection at 60°. The wavelength at maximum reflection intensity, λ_{max}, was obtained from the reflection spectrum. The inter-lamellar distance (d) was estimated by using the Bragg's law of diffraction,

$$\lambda_{max} = 2nd\sin\theta \qquad (5)$$

Here n is the refractive index of water (1.33) and θ is the Bragg's angle (60°).

7.4 Results and discussion

7.4.1 Ratio of change

7.4.1.1 PDGI/PAAm SN gel- 1D swelling

The as-prepared PDGI/PAAn gels, 0.5 mm thick (T_0), gels was transparent. After immersing in water, the samples only swelled in thickness direction and reached a thickness ~1.20 mm (T_1), at equilibrium swelling. The equilibrium swollen PDGI/PAAm hydrogel exhibiting visible color with a λ_{max} peak at ~400 nm in the optical reflection spectrum. From the Bragg's law, the interlayer distance d is estimated as ~160 nm. From the sample thickness and the interlayer distance d, the number of bilayers in the lamellar gels is estimated as *c.a.* ~7500 The study of dimension change of equilibrium swollen PDGI/PAAm (with respect to as prepared), double network PDGI/PAAm-PAPBA (with respect to swollen) and double network photonic gel in

glucose condition are shown in **Figure 7.2** respectively. First we look at the swelling behavior of PDGI/PAAm as compared to as prepared condition. The change of thickness (T_1/T_0), and lateral dimensions such as width (W_1/W_0), and (L_1/L_0) of pure PDGI/PAAm showed that the thickness ratio increased much more as compared to the lateral dimension indicated that the PDGI/PAAm gel after swelling in water exhibited 1*D* swelling. This also indicated the perfect orientation of bilayers in PDGI/PAAm hybrid gel. Here, T_0, W_0, L_0 and T_1, W_1, L_1 are respectively the dimension of as prepared and equilibrium swollen PDGI/PAAm gels in water.

7.4.1.2 PDGI/PAAm-PAPBA DN gel- Shrinking/Swelling

As shown in **Figure 7.2**, by introducing second polymer PAPBA inside PAAm gel layers of PDGI/PAAm. The resultant DN photonic gel thickness ratio (T_2/T_1) decreased, in lateral dimensions only length ratio (L_2/L_1) slightly increased. This showed gel shrunk in thickness direction and expanded in length by swelling in water as second polymer was introduced. Here, T_1, W_1, L_1 and T_2, W_2, L_2 are respectively the dimension of PDGI/PAAm single network and PDGI/PAAm-PAPBA double network gels in water. Then the by activation of the DN photonic sensor and adding to glucose, the gel thickness ratio (T_3/T_2) as well as the lateral dimension such as width ratio (W_3/W_2) and length ratio (L_3/L_2) were gradually increased with increasing soaking time (**Figure 7.1)**, suggesting the isotropic swelling of sensor in glucose solution. Here, T_2, W_2, L_2 and T_3, W_3, L_3, are respectively the dimension of double network PDGI/PAAm-PAPBA in water and in glucose solution. It is worth to mention that the activated sample remain dormant at pH 7 neutral condition in the absence of glucose. However, by addition of 100 mM glucose the gel color and dimensional gradually increased.

The overall results of swelling ratio suggested that the pure PDGI/PAAm was blue in color. After incorporation of second network PBA no swelling was observed as the PBA network shrunk the DN photonic hydrogel. This shrinking is probably because of the multiple inter and

intramolecular interaction of boronic groups itself and PAAm polymer chains.[8] After the addition of 0.1M NaOH for 1 min the PBA becomes charged with excessive hydroxyl groups -OH group.[19] The sensor in aqueous glucose solution at pH 7 created huge osmotic pressure as a result the PDGI/PAAm-PBA hydrogel swollen isotopically.[20] The swelling in thickness direction is more compared to length and width thus leading to the tuning of structural coloration from blue to red with a pronounced red shift. The results indicated that the bilayers by huge osmotic pressure are broken to discontinue bilayers domains.[21] The non-continuous lamellar domains are also important for the rapid response of sensor that allow the media contains analyte to permeate easily into the gel. This behavior was also observed by some recent research on the stimuli responsive hydrogels photonic sensor.[11]

7.4.2 Probing glucose recognition

Afterward, the layered structure of hybrid gels at different condition-such as PDGI/PAAm SN, PDGI/PAAm-PAPBA DN in water and glucose solution was observed **Figure 7.3**. In concomitant with increasing time in glucose, the diffraction color of the gels shifted from ultraviolet to red, as shown by the photographs of the gels and the corresponding reflection spectra (**Figure 7.3a,b**). The reflection peak wave length (λ_{max}) of original PDGI/PAAm gel in water was ~400 nm (*d* 160 nm) containing ~7500 bilayers. When incorporated the second network PAPBA the λ_{max} slightly decreased to 374 nm (*d* 143 nm) exhibited ultraviolet color, indicated blue shift, this also supported the shrinking ratio of gel by addition of second network of polymer (**Figure 7.3a,b** and **Figure 7.2**). Then DN photonic sensor after activation and placing in glucose solution red shift was observed. The structure color of the DN photonic sensor gradually changed with time from ultraviolet 374 nm (*d* 143 nm) to blue 414 nm (*d* 159 nm), cyan 462 nm (*d* 185 nm), green 491 nm (*d* 188 nm), yellow 505 nm (*d* 194 nm), orange 520 nm (*d* 208 nm), and then red 542 nm (*d* 208 nm), that covered all the entire wavelength of

the visible region of the electromagnetic spectrum of light (**Figure 7.3a,b,c**). This also suggested that the sensor is efficiently responding to the glucose stimuli which is attributed to the presence of highly hydrophilic poly(3-acrylamide)phenylboronic acid functional group as the second interpenetrating network. The second network created the osmotic pressure because the free energy of mixing for boronate ion is high (**Figure 7.1(iii-iv)**.

Such color tuning is similar to the mechanism of color tuning in marine organism such as squid that utilizes the osmotic stress stimulated by organic chemical like acetylcholine responsible for the arrangement of order structure to shrink or swell reversible, tuning the color throughout the entire visible spectrum of electromagnetic radiation of light.[22] Therefore, because of this biomimetic color tuning the bilayer based DN gel photonic sensor hold dominancy over conventional particles based sensor.[23] The caveats related to particle based photonic glucose sensor is there poor color quality with non-uniform structural color and their stimuli responsive color changing ability covers a narrow wavelength band. However, the photonic gel based on bilayers are responding homogenously throughout the entire visibly spectrum of electromagnetic radiation of light. The gel can be used for many cycles without damaging and can be returned back to original color by washing away glucose from the sensor using bi-distilled water for reusing.

7.4.3 Probing deformation

In addition to glucose sensor, The PDGI/PAAm-PABPA double network photonic gel also responded to tensile stretching (**Figure 7.4**). The original gel at the relax form with tensile strain of 0% showed bright orange visible structural color λ_{max} 502 nm (*d* 208 nm) **[Figure 7.4(i)],** as the gel was deformed (26%) in parallel to the plane of bilayers the color changed to hybrid of orange-green **[Figure 7.4(ii)]**. Further increase of tensile stretching (45%) the gel color changed to homogenous green color λ_{max} 491 nm (*d* 188 nm) **[Figure 7.4(ii-v)]**. The color tuning is

reversible, such as the gel color tune upon applied tensile stress/strain and then returns to original color and dimensions after relaxation from the tensile stress/strain. The λ_{max} of the reflection spectrum reduced by increasing of the tensile strain. In this way the gel thickness decreases and in turn, *d*, decreases by tensile deformation. That results to the change of visible structural color in form of reflection in the lower wavelength range causes blue shift of visual structural color. The color change is repeating just by relaxation and deformation, the gel act like a synthetic chameleon skin changing color by deformation.

7.5 Conclusion

In conclusion, taking the advantage of structural color from anisotropic lamellar gel, active functionality of poly-(3-Acrylamido)phenyl-boronic-acid, and universal approach of double network concept we have succeeded to synthesized multiple responsive hydrogel. The PDGI/AAm-PBA DN photonic hydrogel is highly responsive to glucose and minute deformation, actively changes structural color in the visible wavelength range. Will have possible application as a soft-wet glucose and deformation sensitive hydrogel.

7.6 References

[1] Department of Human Services, Institute, Diabetes. *State government of victoria* **2013**.

[2] A. Dey, K. Swaminathan, Hyperglycemia-induced mitochondrial alterations in liver. *Life Sciences* **2010**, *87*, 197–214.

[3] M. E. Wilinska, R. Hovorka, *Clinical Chemistry* **2014**, *60*, 1500.

[4] J. P. Gong, Y. Osada, Springer Berlin Heidelberg, 2010; pp. 203–246.

[5] N. A. Peppas, B. V. Slaughter, M. A. Kanzelberger, In *Polymer Science: A Comprehensive Reference, 10 Volume Set*; Elsevier, 2012; Vol. 9, pp. 385–395.

[6] T. Bertrand, J. Peixinho, S. Mukhopadhyay, C. W. MacMinn, **2016**.

[7] M. Y. Kizilay, O. Okay, *Polymer* **2004**, *45*, 2567.

[8] Y. Guan, Y. Zhang, *Chemical Society reviews* **2013**, *42*, 8106.

[9] Y. Zhao, Z. Xie, H. Gu, C. Zhu, Z. Gu, *Chemical Society reviews* **2012**, *41*, 3297.

[10] M. A. Haque, T. Kurokawa, J. P. Gong, *Soft Matter* **2012**, *8*, 8008.

[11] Y. Yue, T. Kurokawa, M. A. Haque, T. Nakajima, T. Nonoyama, X. Li, I. Kajiwara, J. P. Gong, *Nature communications* **2014**, *5*, 4659.

[12] M. Ilyas, M. A. Haque, Y. Yue, T. Kurokawa, T. Nakajima, T. Nonoyama, J. P. Gong, *Macromolecules* **2017**, acs. macromol.7b01438.

[13] K. Mito, M. A. Haque, T. Nakajima, M. Uchiumi, T. Kurokawa, T. Nonoyama, J. P. Gong, *Polymer* **2017**, 1.

[14] Y. F. Yue, M. A. Haque, T. Kurokawa, T. Nakajima, J. P. Gong, *Advanced Materials* **2013**, *25*, 3106.

[15] T. Nakajima, C. Durand, X. F. Li, M. A. Haque, T. Kurokawa, J. P. Gong, *Soft matter* **2015**, *11*, 237.

[16] X. Xu, A. V. Goponenko, S. A. Asher, *Journal of the American Chemical Society* **2008**, *130*, 3113.

[17] K. Tsujii, N. Saito, T. Takeuchi, **1980**, 2287.

[18] K. Tsujii, M. Hayakawa, T. Onda, T. Tanaka, *Macromolecules* **1997**, *30*, 7397.

[19] V. L. Alexeev, A. C. Sharma, A. V. Goponenko, S. Das, I. K. Lednev, C. S. Wilcox, D. N. Finegold, S. a. Asher, *Analytical Chemistry* **2003**, *75*, 2316.

[20] D. Morales, E. Palleau, M. D. Dickey, O. D. Velev, **2014**, *10*, 1235.

[21] M. A. Haque, T. Kurokawa, J. P. Gong, *Soft Matter* **2013**, *9*, 5223.

[22] D. G. DeMartini, D. V. Krogstad, D. E. Morse, *Proceedings of the National Academy of Sciences* **2013**, *110*, 2552.

[23] M. Ben-Moshe, V. L. Alexeev, S. A. Asher, *Analytical chemistry* **2006**, *78*, 5149.

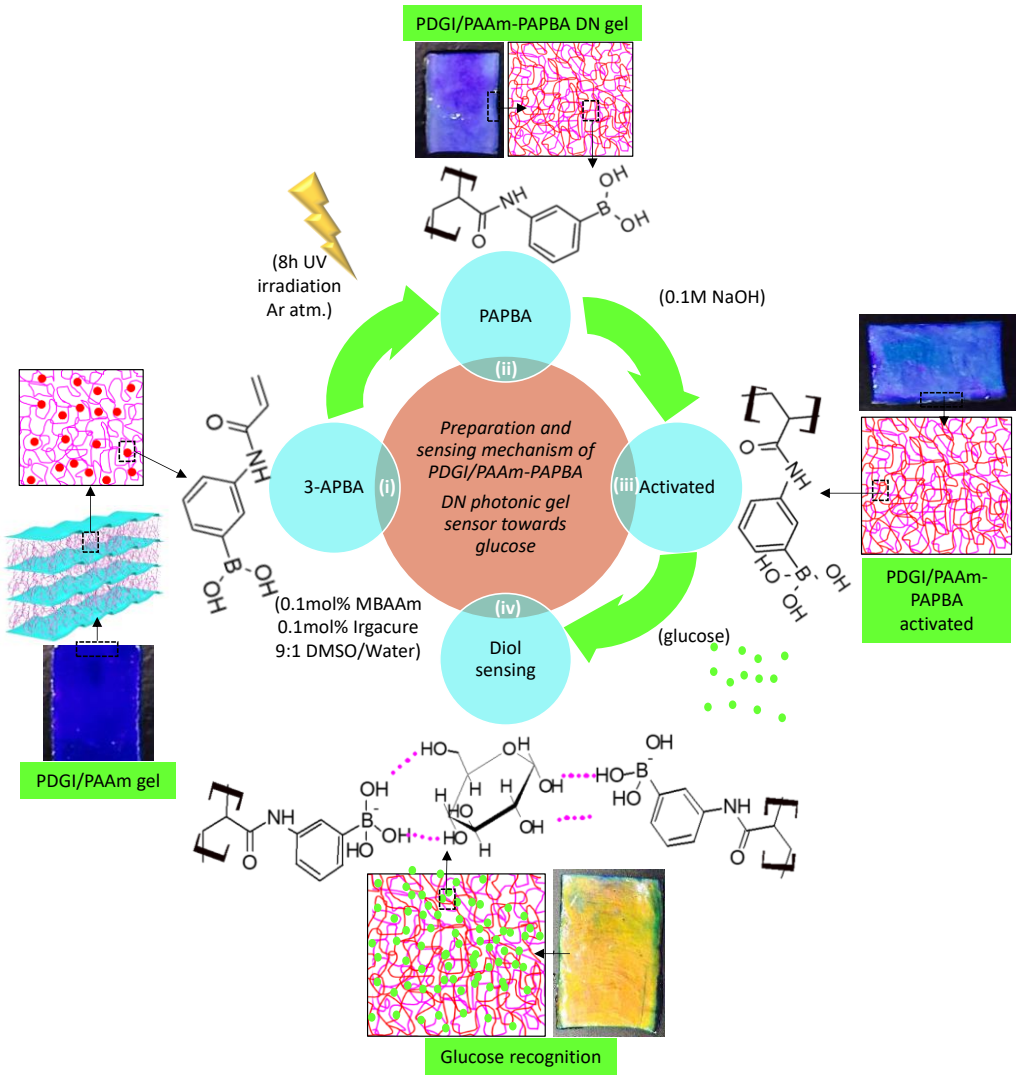

Figure 7.1 Schematics for the preparation of PDGI/PAAm-PAPBA DN photonic sensor. (i) Soaking PDGI/PAAm gel for 24h in monomer of 3-APBA solution. The monomer diffuse inside the PAAm gel layers. Then polymerization for 8h in inert argon atmosphere. (ii) After polymerization the PDGI/PAAm-PAPBA interpenetrating double network as prepared gel contains glucose recognition unit. (iii) Activating the gel for glucose sensing by placing in 0.1 M basic solution for 1 min without heating. (vi) Glucose sensing mechanism of the gel. Step vi to ii is reversible just by washing the sensor with distilled water.

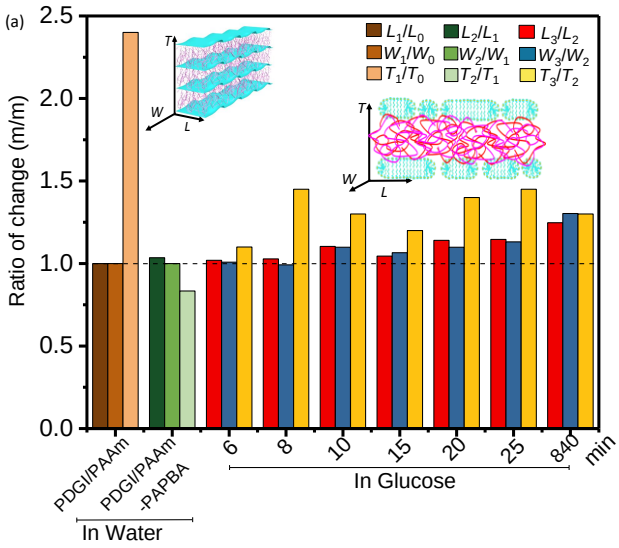

Figure 7.2 Swelling behavior of PDGI/PAAm as compared to as prepared condition. The change of thickness (T_1/T_0), and lateral dimensions such as width (W_1/W_0), and (L_1/L_0) of pure PDGI/PAAm showed that the thickness ratio increased much more as compared to the lateral dimension indicated that the PDGI/PAAm gel after swelling in water exhibited 1*D* swelling. This also indicated the perfect orientation of bilayers in PDGI/PAAm hybrid gel. Here, T_0, W_0, L_0 and T_1, W_1, L_1 are respectively the dimension of as prepared and equilibrium swollen PDGI/PAAm gels in water. DN photonic gel thickness ratio (T_2/T_1) decreased, in lateral dimensions only length ratio (L_2/L_1) slightly increased. This showed gel shrunk in thickness direction and expanded in length by swelling in water as second polymer was introduced. Here, T_1, W_1, L_1 and T_2, W_2, L_2 are respectively the dimension of PDGI/PAAm single network and PDGI/PAAm-PAPBA double network gels in water. Activation of the DN photonic sensor and adding to glucose, the gel thickness ratio (T_3/T_2) as well as the lateral dimension such as width ratio (W_3/W_2) and length ratio (L_3/L_2) were gradually increased with increasing soaking time, suggesting the isotropic swelling of sensor in glucose solution. Here, T_2, W_2, L_2 and T_3, W_3, L_3, are respectively the dimension of double network PDGI/PAAm-PAPBA in water and in glucose solution.

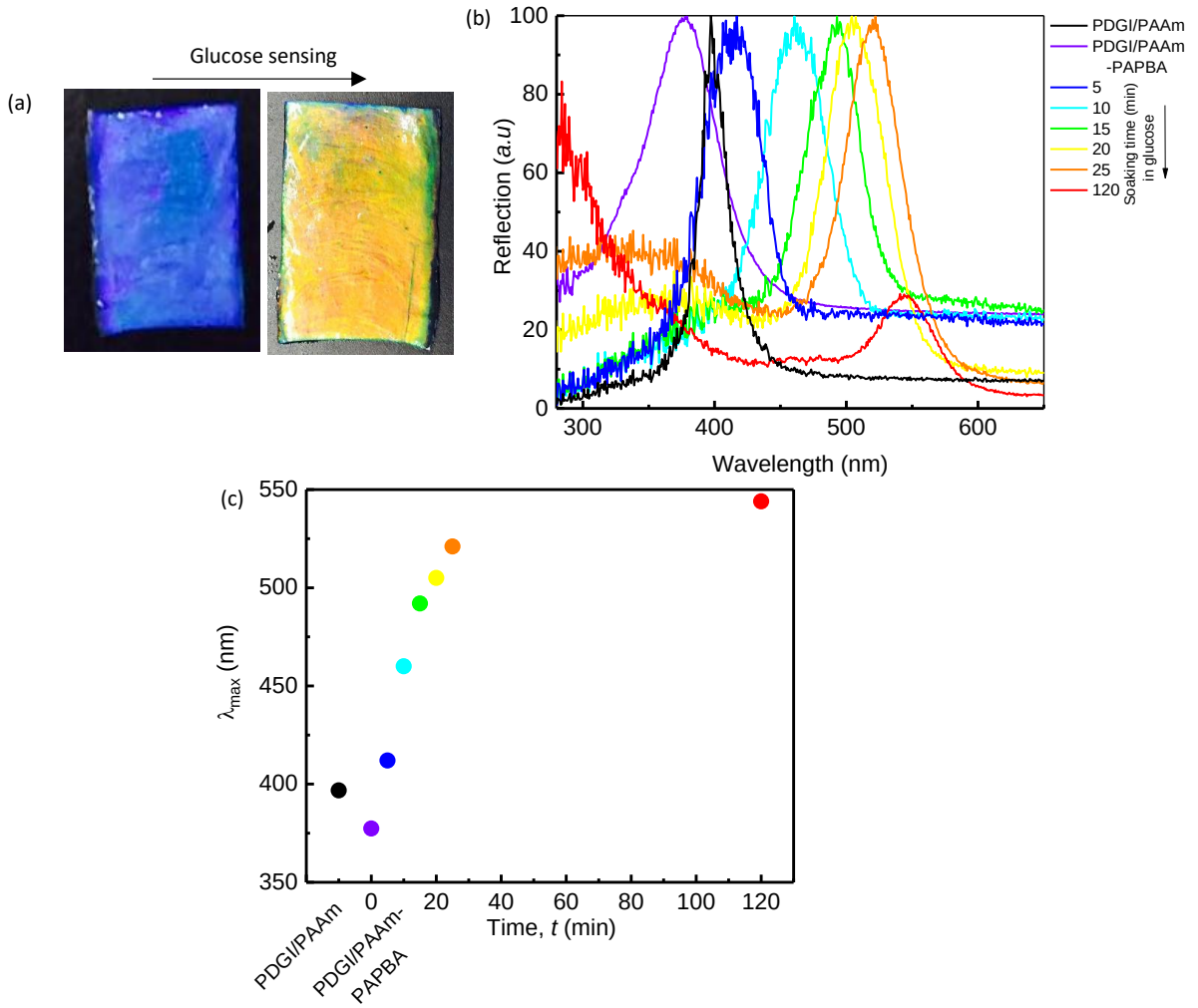

Figure 7.3 (a) Top view images of PDGI/PAAm-PAPBA gel sensor before and after sensing 100 mM glucose. (b) The reflection spectra probing the structural color of the gel during sensing glucose as a function of time. The black peak represents the original PDGI/PAAm gel that showed blue shift by shrinking after incorporation of second network PAPBA polymer. After that the ultraviolet to red peak represent sensing of glucose. (c) The maximum reflection peak wavelength λ_{max} as a function of time indicating red shift of the gel color in glucose.

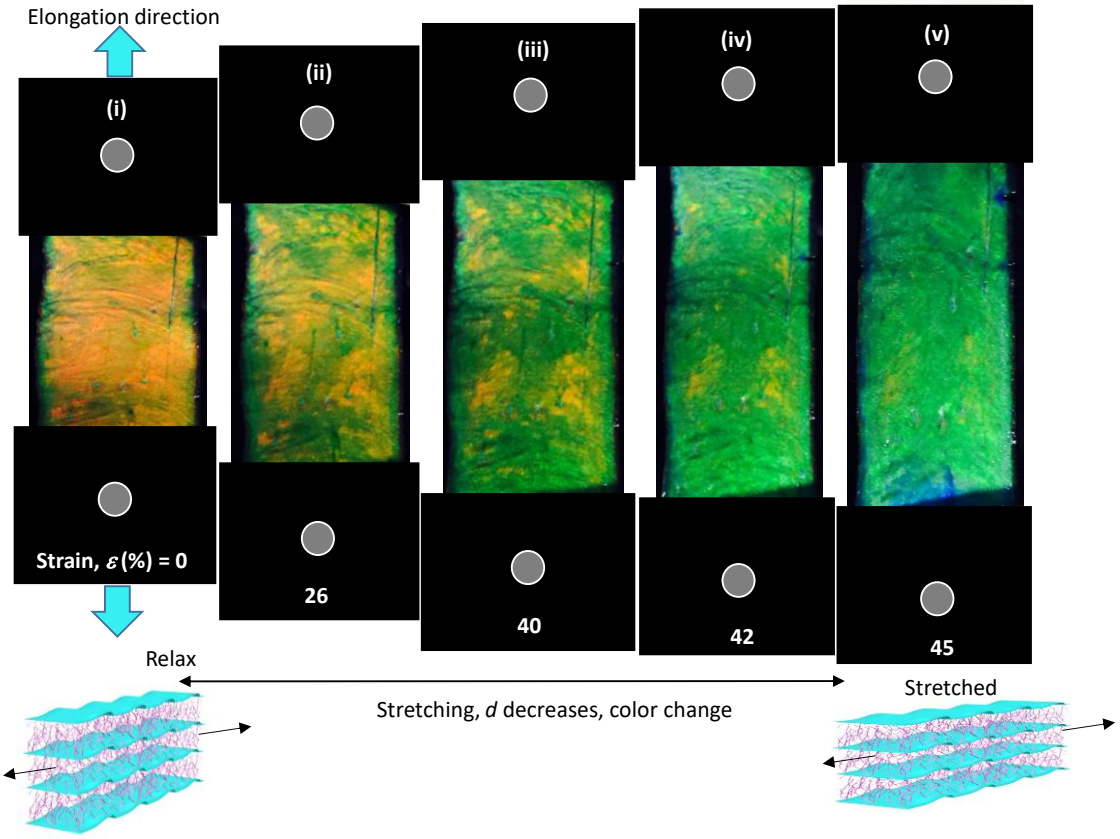

Figure 7.4 Top view images of PDGI/PAAm-PAPBA gel sensor before and after uniaxial stretching. (i) The original gel at the relax form with tensile strain of 0% showed bright orange visible structural color λ_{max} 502 nm (*d* 208 nm), (ii) as the gel was deformed (26%) in parallel to the plane of bilayers the color changed to hybrid of orange-green.(iii)-(v) Further increase of tensile stretching (45%) the gel color changed to homogenous green color λ_{max} 491 nm (*d* 188 nm). The color tuning is reversible, such as the gel color tune upon applied tensile stress/strain and then returns to original color and dimensions after relaxation from the tensile stress/strain. The λ_{max} of the reflection spectrum reduced by increasing of the tensile strain. In this way the gel thickness decreases and in turn, *d*, decreases by tensile deformation. That results to the change of visible structural color in form of reflection in the lower wavelength range causes blue shift of visual structural color.

CHAPTER 8

Conclusions

The dissertation clarifies in depth understanding of combining isotropic and anisotropic structures of contrasting properties into a novel hybrid soft and wet matter. The arrangement of centimeter scale supramolecular self-assembled anisotropic structure, in depth understanding and novel functions associated with such structures in bulk soft matter.

In Chapter 3, we successfully developed a method to induce bilayers in PAAm gels matrix and synthesized large area bilayer-hybrid photonic gel with alternating layered structure. The parameters such as shear flow and temperature of incubation were found to affect the orientation behavior of bilayers that largely impact the quality of bilayer-hybrid gels. Under optimized condition gels repeatability was observed and hybrid gels regarding dimension and thickness were obtained. The thin gel and thick gels contained few hundreds (~700) to few thousand (~6000) of well oriented bilayers, showed visible structural coloration. In addition to high toughness, stiffness, strength and stretchability, and the release of small molecules was observed to be tuned by changing dimensions of gels. This method might open new ways to explore various novel function of bilayer hybrid gels where large dimension are necessary.

In Chapter 4.1, the detailed investigation of the effect of water content, temperature, solvent, configuration of monomers, on the structure and properties of bilayer-hybrid gels are explored. It is concluded that by slowly reducing water content the layered microstructure is unperturbed, and ductile-brittle transition of the PAAm gel layers occurs at much higher water content (58 wt%) as compared to the water content (26 wt%) of bulk PAAm hydrogels. At this transition point, the thickness of PAAm gel layers is 52 nm, much higher than the reported literature of

water confined at several nanometer length scale. Accompanied with such a transition, the free water in the lamellar gels disappeared. These results indicate the long-range ordering of water in the lamellar hydrogels, which is observed for the first time.

In Chapter 4.2, the effect of co-solvent, on the adaptive mechanical behavior of gels at various concentration is studied. Drying water from co-solvent produced air stable, soft, tough and stretchable ion gel based on bilayers. The hybrid gel synthesized by adding small amount of ionic liquid that perturb the structure of water shows self-healing. The ion gel exhibited an ultra-fast self-healing behavior due to multiple reversible interactions.

In Chapter 4.3, we succeeded to synthesized amphiphilic molecules of different configuration. Systematically the effect of racemic and chiral configuration on the structural color of precursor solution was studied. Then a method was developed to induce racemic and chiral bilayers in PAAm gels matrix and synthesized large area bilayer-hybrid photonic gel with alternating racemic and chiral layered structures. The gels showed nicely arranged one dimensional chiral bilayers that enhanced the structural color, birefringence as well the yielding behavior of bilayer hybrid gel. This method might open new ways to explore various novel function of chiral bilayer hybrid gels in biomedical application.

In Chapter 5 explained that, controlling the internal structure of anisotropic gel just by different types of drying approaches, we obtained various biomimetic functionality. The gel showed adaptive structural color such as rainbow like color stimulation by free or humidity air drying. The structural color is homogenously tuned by restricted drying throughout the entire visible spectrum of electromagnetic radiation of light. At high water content, the gel behaves as soft/elastic colorful skin same as certain marine organism, whereas at low water content transparent photonic sheet act as an active water triggered display device same as beetle cuticle, novel shape memory simply by maintaining the amount of water intake/release, stress induced

nacre like metallic luster, birds feather mimetic iridescence color, and jelly-fish like blue light emission. In addition drying of gel pre-soaked in water-ion liquid co-solvent resulted into an air stable iongel membrane photonic sheet that showed high conductivity and exhibited rewriting photonic paper properties. The switchable color of the hybrid PDGI/PAAm induced by water could act as a visual indicator of moisture content with novel shape memory behavior for diversified applications such as soft and stretchable electronic skin, batteries, or barriers coating, or gas separation membrane. Moreover, the material is deliberated as a rewritable photonic paper which can be printed simply using water as ink.

In Chapter 6, we succeeded to synthesize and investigate the properties of amphiphilic PDGI liquid crystalline elastomer. The PDGILCE showed high toughness, stiffness, malleability by roll pressing, with enhanced birefringence. This method might open new ways to explore various novel function of PDGILCE for creation of artificial muscles.

In Chapter 7, we showed that, by taking the advantage of structural color from anisotropic lamellar gel, active functionality of poly-(3-Acrylamido)phenyl-boronic-acid, and universal approach of double network concept we have succeeded to synthesized multiple responsive hydrogel. The PDGI/AAm-PBA DN photonic hydrogel is highly responsive to glucose and minute deformation, actively changes structural color in the visible wavelength range. Will have possible application as a soft-wet glucose and deformation sensitive hydrogel.

This dissertation explained the establishment of method of fabrication high quality bilayer-based hydrogels with supramolecular self-assembled structure, properties and novel functions. We believe this research is helpful to design biomimetic advanced functional soft and wet devices for diverse application regardless dimension.

List of Publications

1. Muhammad Ilyas, Md-Anamul Haque, Youfeng Yue, Takayuki Kurokawa, Tasuku Nakajima, Takayuki Nonoyama and Jian Ping Gong. Water-Triggered Ductile-Brittle Transition of Anisotropic Lamellar Hydrogels and Effect of Confinement on Polymer Dynamics. *Macromolecules*, **2017**, 50, 1869-1877.

2. Md-Anamul Haque, Youfeng Yue, Takayuki Kurokawa, Tasuku Nakajima, Takayuki Nonoyama, Muhammad Ilyas and Jian Ping Gong. Tough and Variable-Band-Gap Photonic Hydrogel Displaying Programmed Angle-Dependent Colors. *ACS Omega*, **2018**, 3, 55-62.

3. Muhammad Ilyas, Takayuki Kurokawa, Tasuku Nakajima, Takayuki Nonoyama and Jian Ping Gong. Glucose Sensing DN-photonic Hydrogels. (In preparation)

Presentations and Published Abstracts in Scientific Meetings

1. Ilyas Muhammad, Md-Anamul Haque, Youfeng Yue, Takayuki Kurokawa, Tasuku Nakajima, Takayuki Nonoyama and Jian Ping Gong, "Probing the Water Triggered Ductile-Brittle Transition of Anisotropic Lamellar Hydrogels and Confinement Effect on Polymer Dynamics," 5th International Life Science Symposium for Younf Scientists ILSS, October 27, 2017 Hokkaido University, Japan 平成 29 年 10 月 27 日 Oral
2. Ilyas Muhammad, Md-Anamul Haque, Youfeng Yue, Takayuki Kurokawa, Tasuku Nakajima, Takayuki Nonoyama and Jian Ping Gong, "Water Triggered Ductile-Brittle Transition of Anisotropic Lamellar Hydrogels," 66th Symposium on Macromolecules, SPSJ, September 20-22, 2017 Ehime University Johoku Campus (Bunkyo-cho 3, Matsuyama, Ehime 790-8577)、平成 29 年 9 月 22 日 Oral
3. Ilyas Muhammad, Md-Anamul Haque, Youfeng Yue, Mito Kei, Takayuki Kurokawa, Tasuku Nakajima, Takayuki Nonoyama and Jian Ping Gong, "Biomimetic Multilayered Hydrogels Towards High Functional Materials ," The 4th International Life-Science Symposium for young Scientists 2016, Hokkaido University, JAPAN、平成 28 年 11 月 18 日 Oral
4. Ilyas Muhammad, Takayuki Kurokawa, Tasuku Nakajima, Takayuki Nonoyama, Jian Ping Gong, "Functional design of Lipid Bilayer Hydrogel: A Dehydration Induced Dynamic Optical and Mechanical properties," The First International Symposium On Advanced Soft Matter 2016, Hokkaido University JAPAN、平成 28 年 06 月 13-15 日 Poster
5. Ilyas Muhammad, Md-Anamul Haque, Takayuki Kurokawa, Tasuku Nakajima, Takayuki Nonoyama and Jian Ping Gong, "Tough Functional Hybrid Gel Thin Film,"Gel Workshop at Matsuyama, Ehime, JAPAN, Nigitatsu Kaikan (118-2 Dogo Himetsuka, Matsuyama, Ehime 790-0858) (Sep 22-24, 2017).平成 29 年 9 月 23 日 Poster

6. Ilyas Muhammad, Md-Anamul Haque, Takayuki Kurokawa, Tasuku Nakajima, Takayuki Nonoyama and Jian Ping Gong, "Ultra-thin Tough Functional hydrogel Based on Bilayers, “International Symposium on Advanced Soft Matter: From Single Molecule To Tough Polymers@ International Soft Matter Summer School in Hokkaido 2017, JAPAN.、平成 29 年 8 月 8 日 Poster
7. Ilyas Muhammad, Md-Anamul Haque, Takayuki Kurokawa, Tasuku Nakajima, Takayuki Nonoyama and Jian Ping Gong, "Ultra-thin Tough Functional hydrogel Based on Bilayers," International Soft Matter Summer School in Hokkaido 2017 for Young Researchers, JAPAN、平成 29 年 7 月 31 日 Poster
8. Ilyas Muhammad, Takayuki Kurokawa, Tasuku Nakajima, Takayuki Nonoyama, Jian Ping Gong, "The origin of photoluminescence from hybrid Multilayered Thin Film," The 3rd International Life Science symposium for young scientists 2015, Hokkaido University, JAPAN、平成 27 年 11 月 26 日 Poster
9. Ilyas Muhammad, Takayuki Kurokawa, Tasuku Nakajima, Takayuki Nonoyama, Jian Ping Gong, "Solid State Photo-luminescence Multi-layered Thin Film with High Quantum Efficiency,"30th Summer University in Hokkaido & 2015 Young Researchers Group Meeting sponsored by SPSJ Hokkaido Branch, JAPAN. 平成 27 年 8 月 28 日～29 日 Poster
10. Muhammad Ilyas, Takayuki Kurokawa, Tasuku Nakajima, Takayuki Nonoyama, Jian Ping Gong,「Solvent mediated on/off switching of photonic hybrid gel」、化学系学協会北海道支部 2015 年冬季研究発表会、北海道大学フロンティア応用科学研究棟（札幌市）、27 年 1 月 27-28 日 Poster
11. Muhammad Ilyas, Takayuki Kurokawa, Tasuku Nakajima, Takayuki Nonoyama, Jian Ping Gong,「Solvent induced photonic on/off switching in lamellar bilayer hydrogel」、高分子学会 2014 年度北海道支部冬季研究発表会、北海道大学学術交流会館（札幌市北区）、平成 27 年 1 月 26 日（月）Poster

12. Ilyas Muhammad, Takayuki Kurokawa, Tasuku Nakajima, Takayuki Nonoyama, Jian Ping Gong, "Chemo-responsive multi-laminated bilayer hydrogel ," The 2nd International Life Science symposium for young scientists 2014, Hokkaido University, JAPAN、平成 26 年 10 月 23 日 Poster
13. Muhammad Ilyas, Takayuki Kurokawa, Tasuku Nakajima, Takayuki Nonoyama, Jian Ping Gong、「Synthesis of CDME/Urea eutectic mixture and its polymerization」、29th Summer University in Hokkaido・2014 年度北海道高分子若手研究会、定山渓ビューホテル（札幌市南区）、26 年 8 月 29 日 Poster

List of Collaborative work and others

14. Md-Anamul Haque, Ilyas Muhammad, Takayuki Kurokawa and Jian Ping Gong. "Fabrication of Nacre-like Strong and tough Composite from both Organic Components, “Hokkaido University-ImPACT Joint Symposium @ International Soft Matter Summer School in Hokkaido 2017.、平成 29 年 8 月 8 日 Poster
15. Md-Anamul Haque, Ilyas Muhammad, Takayuki Kurokawa and Jian Ping Gong. "Fabrication of Nacre-like Strong and tough Composite from both Organic Components," The 2017 Polymers Gordon Research Conference (GRC)@South Hadley, MA.、平成 29 年 6 月 Poster
16. Md-Anamul Haque, Ilyas Muhammad, Kei Mito, Takayuki Kurokawa, Tasuku Nakajima, Takayuki Nonoyama and Jian Ping Gong, "Lamellar Hydrogel to Fabricate Nacre like Strong Composite ," The 66th Annual SPSJ meeting (Monday, May 29th.,2017 ～ Wednesday, May 31th.,2017) 2017、平成 29 年 05 月 31 日 Oral talk
17. Ilyas Muhammad (left side), Yiwan Huang(Right side) performing manual tearing test of one of the toughest gel in the world to CNN at LSW, Hokkaido University, JAPAN. http://edition.cnn.com/2017/06/13/tech/hydrogel-steel-japan/index.html
18. M.Ilyas, I.Peroni, S. Agnelli, F. Bignotti, F. Baldi. Preparation and Characterization of Tough Polyacrylamide Hydrogels. European Polymer Congress EPF-2013, Pisa Italy June 2013.
19. Chairperson at the, 3rd International Life Science Symposium 2015, 平成 27 年 11 月 26 日

Acknowledgements

The research work reported here in this dissertation has been carried out in Laboratory of Soft and Wet Matter (LSW), Graduate School of Life Science, Hokkaido University, Japan during 2013-2017, under the supervision of distinguished Professor Dr. Jian Ping Gong.

I would like to express my cordial and sincere appreciation to my respected supervisor Professor **Dr. Jian Ping Gong** for her scholastic supervision, precious suggestions and thoughtful discussion during my research work. I gratefully acknowledge her diligent effort, perseverance, enthusiasm, and kindness for giving long time to write paper and finish my dissertation. I have learnt from her the passionate attitude for research about polymer and gel science. Prof. Gong always used to instigate me to enjoy the life in Japan and its importance to become an excellent researcher. I am privileged to have been influenced by her approach to research, which embodies all the best of collegiality and the true spirit of scientific endeavor. I honestly owe to her for providing me the opportunity to work in close association with her at the Laboratory of Soft and Wet Matter, LSW.

I also would like to express my sincere thanks to Professor **Takayuki Kurokawa**, Assistant Professor **Tasuku Nakajima**, and Assistant Professor **Takayuki Nonoyama** for their valuable comments, fruitful suggestions, and technical supports related to research.

I would like to express my appreciations to administrative secretary Mrs. **Eiko Hasegawa**, **Yuki Ookubo**, and technical staff **Hane Yukiku**, Dr. **Katsuyama Yoshinori** for their administration, technical and daily life related assistant and help.

I would like also express my gratitude to all the members in LSW, the Japanese and International students, for their kind experimental supports and sacrificial help, especially Dr. **Md. Anamul Haque** for his fruitful discussion, collaboration and help.

Finally I wish to express my earnest appreciations to my parents (especially late father), brothers especially Muhammad Riaz (who helped me a lot during my academic journey), sisters, my relatives and my friends for their love, support, advice, and spiritual encouragement. Specially, bundles of thanks to my beloved wife, **Faiza Ilyas**, who always supports me for daily life and encourages me all the time being and sacrifices her times for me. I would like to dedicate this dissertation to them.

At last but not the least I express my gratitude to the Ministry of Education, Culture, Sports, Science and Technology of Japan for supporting this study under the JSPS KAKENHI Grant Number JP17H06376 and 17H06144. I also express gratitude to the International Graduate Program (IGP) of Hokkaido University and their committee for support during doctoral studies.

MUHAMMAD ILYAS

March 2018

Laboratory of Soft & Wet Matter (LSW),

Divisions of Biological Sciences,

Graduate School of Science,

Hokkaido University Sapporo, Japan.